Screening and discovery of symbiotic and antagonistic microbial networks using microwell recovery arrays

by

Niloy Barua

B.S., Bangladesh University of Engineering and Technology, 2016

AN ABSTRACT OF A DISSERTATION

submitted in partial fulfillment of the requirements for the degree

DOCTOR OF PHILOSOPHY

Tim Taylor Department of Chemical Engineering
Carl R. Ice College of Engineering

KANSAS STATE UNIVERSITY
Manhattan, Kansas

2021

Abstract

Understanding the dynamic interactions among soil and plant rhizosphere microbiomes is critical for predicting community function and developing improved probiotic and biocontrol agents for plant growth, biofuel production, and human health. However, uncovering these interactions is a grand challenge in microbiology due to the lack of experimental tools suitable for discovery and characterization. This research develops high throughput microwell recovery arrays (MRA) combined with advanced bioinformatics techniques to screen and detect microbial interactions across soil/root microbial communities to uncover bacteria species with an important function.

The first part of this thesis describes developing a novel, light-responsive, step-polymerized poly(ethylene glycol) hydrogel membrane to retrieve cells from MRAs with a high degree of spatial control. The utility of microwell arrays, particularly in screening applications, could be significantly expanded if cells of interest could be removed from individual wells for subsequent genetic and phenotypic characterizations. The photodegradability of the membrane permits exchange of nutrients and waste products and seals motile bacteria within microwells and enables individual wells of interest to be opened using a patterned UV light for selective release and retrieval.

The second part of the thesis demonstrates the unique application of the MRA platform to discover multi-membered consortia that generate emergent outcomes. The platform was initially developed to discover dual-species co-culture and interactions between two well-characterized interaction pairs, *Agrobacterium tumefaciens* and *Pseudomonas aeruginosa*. After investigating the on-chip co-culture using this pair, *Populus trichocarpa* rhizosphere microbiome was screened for strains affecting the growth of *Pantoea* sp. YR343, an indole-3-acetic acid (IAA) producing, plant growth-promoting bacteria isolated from *Populus deltoides* rhizosphere.

The third chapter of the thesis uses this approach for enhancing the survival and colonization of commercial nitrogen-fixing, plant growth-promoting bacteria, *Azospirillum brasilense*, into maize roots to improve crop

yield. Diazotrophs such as *Azospirillum brasilense* function as biofertilizers by colonizing plant roots and enhancing plant productivity through symbiotic interactions within the rhizosphere. Using the MRAs, new isolates showing that promote *A. brasilense* growth were extracted and identified by 16S sequencing as *Serratia mercescens*, *Serratia nematodiphila*, *Serratia urelytica*, *Pantoea agglomerans*, *Enterobacter tabaci*, and *Acinetobacter bereziniae*, and the interactions were validated off-chip in 96 well plate reader. Also, the growth enhancement and the improvement of the survival and colonization of *A. brasilense* in *Zea mays* roots were validated in plant growth chamber experiments, demonstrating the potential to apply the interactions found *in vitro* towards *in vivo* systems of agricultural relevance.

In the final chapter of the thesis, the screening capabilities using MRAs were further extended towards screening non-pathogenic *Agrobacterium* isolates for the growth inhibition of pathogenic *A. tumefaciens*, which is a key plant biotechnology tool and also the causative agent of Crown Gall disease. MRAs were used to combine fluorescently labeled *A. tumefaciens* sp.15955 with non-pathogenic *Agrobacterium* isolates collected from native plant roots at the Konza Prairie Biological Station (Manhattan, KS) to uncover several candidates for inhibiting *A.tumefaciens* sp. 15955 growth. The discovery of such growth-inhibiting isolates will help improve plant productivity by using them as reliable biocontrol agents that prevent Crown Gall disease, and further demonstrates the unique capability of the MRA platform to screen natural isolate collections to discover bacteria capable of inhibiting pathogens.

Screening and discovery of symbiotic and antagonistic microbial networks using microwell recovery arrays

by

Niloy Barua

B.S., Bangladesh University of Engineering and Technology, 2016

A DISSERTATION
submitted in partial fulfillment of the requirements for the degree

DOCTOR OF PHILOSOPHY

Tim Taylor Department of Chemical Engineering
Carl R. Ice College of Engineering

KANSAS STATE UNIVERSITY
Manhattan, Kansas

2021

Approved by:

Co-Major Professor
Ryan R. Hansen

Approved by:

Co-Major Professor
Thomas G. Platt

Abstract

Understanding the dynamic interactions among soil and plant rhizosphere microbiomes is critical for predicting community function and developing improved probiotic and biocontrol agents for plant growth, biofuel production, and human health. However, uncovering these interactions is a grand challenge in microbiology due to the lack of experimental tools suitable for discovery and characterization. This research develops high throughput microwell recovery arrays (MRA) combined with advanced bioinformatics techniques to screen and detect microbial interactions across soil/root microbial communities to uncover bacteria species with an important function.

The first part of this thesis describes developing a novel, light-responsive, step-polymerized poly(ethylene glycol) hydrogel membrane to retrieve cells from MRAs with a high degree of spatial control. The utility of microwell arrays, particularly in screening applications, could be significantly expanded if cells of interest could be removed from individual wells for subsequent genetic and phenotypic characterizations. The photodegradability of the membrane permits exchange of nutrients and waste products and seals motile bacteria within microwells and enables individual wells of interest to be opened using a patterned UV light for selective release and retrieval.

The second part of the thesis demonstrates the unique application of the MRA platform to discover multi-membered consortia that generate emergent outcomes. The platform was initially developed to discover dual-species co-culture and interactions between two well-characterized interaction pairs, *Agrobacterium tumefaciens* and *Pseudomonas aeruginosa*. After investigating the on-chip co-culture using this pair, *Populus trichocarpa* rhizosphere microbiome was screened for strains affecting the growth of *Pantoea* sp. YR343, an indole-3-acetic acid (IAA) producing, plant growth-promoting bacteria isolated from *Populus deltoides* rhizosphere.

The third chapter of the thesis uses this approach for enhancing the survival and colonization of commercial nitrogen-fixing, plant growth-promoting bacteria, *Azospirillum brasilense*, into maize roots to improve crop

yield. Diazotrophs such as *Azospirillum brasilense* function as biofertilizers by colonizing plant roots and enhancing plant productivity through symbiotic interactions within the rhizosphere. Using the MRAs, new isolates showing that promote *A. brasilense* growth were extracted and identified by 16S sequencing as *Serratia mercescens*, *Serratia nematodiphila*, *Serratia ureilytica*, *Pantoea agglomerans*, *Enterobacter tabaci*, and *Acinetobacter bereziniae*, and the interactions were validated off-chip in 96 well plate reader. Also, the growth enhancement and the improvement of the survival and colonization of *A. brasilense* in *Zea mays* roots were validated in plant growth chamber experiments, demonstrating the potential to apply the interactions found *in vitro* towards *in vivo* systems of agricultural relevance.

In the final chapter of the thesis, the screening capabilities using MRAs were further extended towards screening non-pathogenic *Agrobacterium* isolates for the growth inhibition of pathogenic *A. tumefaciens*, which is a key plant biotechnology tool and also the causative agent of Crown Gall disease. MRAs were used to combine fluorescently labeled *A. tumefaciens* sp.15955 with non-pathogenic *Agrobacterium* isolates collected from native plant roots at the Konza Prairie Biological Station (Manhattan, KS) to uncover several candidates for inhibiting *A.tumefaciens* sp. 15955 growth. The discovery of such growth-inhibiting isolates will help improve plant productivity by using them as reliable biocontrol agents that prevent Crown Gall disease, and further demonstrates the unique capability of the MRA platform to screen natural isolate collections to discover bacteria capable of inhibiting pathogens.

Table of Contents

List of Figures

List of Tables

Acknowledgements

It would be impossible for me to pursue the arduous journey of a doctoral degree while being 8000 miles from my home without the continuous support from my family and my advisor Dr. Ryan Hansen. I will always be indebted to Dr. Hansen for his insightful feedback and his enormous contribution to my professional development. I want to express my highest gratitude to him for his invaluable supervision, support, and tutelage from the formative stages of this dissertation to formulating the final draft.

I would like to appreciate the valuable guidance I received from my co-major advisor Dr. Thomas Platt for all the opportunities I was given to further my research. My gratitude extends to Dr. Christopher Culbertson, Dr. Won Min Park, and Dr. Jianfa Bai for agreeing to serve on my dissertation committee. I would also like to thank Dr. Andre Van der Vlies for helping me formulate important research questions and methodology for successfully completing my dissertation.

I would also like to thank the former and current members of Hansen Biointerface Lab and Platt lab, Dr. Mohammadali Masigol, Niloufar Fattahi, Esther Radaha, Moises Gutierrez, Kyle Stern, Priscila Guzman, Ashlee Herken, and the staffs at the Tim Taylor Department of Chemical Engineering at KState. I also want to thank the amazing people of the Bangladeshi student community at KState who made my journey at KState forever memorable.

Most importantly, I want to express my special gratitude to my parents, whose life-long sacrifices have made me the person I am today. And finally, words are not enough to thank my loving wife, Suvadra Barua, who constantly encouraged me and supported me throughout this difficult journey. Above all, I am eternally grateful to Lord Buddha for blessing me with this opportunity and giving me the strength to complete my research successfully.

Dedication

This Thesis is dedicated to my beloved wife

Suvadra Barua

To my Dad and Mom

Bihari Lal Barua and Shipra Barua

To Lord Buddha

Thank you for inspiring me to dream big

Chapter 1 : Introduction

1.1 Importance for screening microbe-microbe interactions

The dynamic and diverse microbial communities play a critical role in therapeutic drug development [1, 2], crop production [3, 4], high-value product development [5], bioenergy production [6, 7], bioremediation of environmental contamination [8, 9], soil clean-up [8], digestion of municipal solids [9], and enhancement water quality [10]. The inter-species and intra-species interactions among the microbial population in a natural environment are often shaped by factors such as microbe-microbe interactions, species abundance, structural organization and environmental cues. Such interactions facilitate the development and success of functionally important engineered microbial communities [3, 11]. Despite leveraging from the development of genomic and metagenomic approaches to determine community structure and species abundance [12, 13], understanding and harnessing the function of these communities remain difficult [14–16]. Gaining a fundamental understanding of these factors is important, as this knowledge can be used to aid efforts to engineer microbiomes to achieve desired outcomes or produce specific products [17, 18]. Despite this knowledge gap, uncovering important interactions is critical for understanding natural community structure and function, response to environmental perturbations, and for design of constructed communities for engineered outcomes. However, the limited understanding of microbial interactions limits the rational design of synthetic communities in the majority of applications.

Uncovering the interactions among highly diverse microbial communities requires the development of high-throughput technologies capable of combining cellular and phenotypic observations with the characterization of the interactions and addressing the qualitative, low throughput limitations of traditional microbiology methods. Traditional microbiological methods

relied on hand-spotting different microbes together and could only do qualitative analysis of bulk populations, making this technology low-throughput [19]. These methods for probing interactions are dependent on the bulk co-cultures of interacting cell populations in nutrient media [15, 16, 20]. With the development of micro- and nanoscale fabrication techniques, major improvements has been made for the advancements in high-throughput measurement, observation of single-cell behavior, and precise design and manipulation of the microenvironment. Although, the conventional high throughput technologies have aided in understanding microbial mutualism [21], community response to environmental pressures [22–24], and physico-chemical aspects of the microenvironments contributing to driving community phenotypes [25–28], they are widely limited to low-throughput detection without integrating downstream sample processing steps after screening.

This research aims to develop a high throughput, operationally simple, yet powerful platform capable of simultaneously screening thousands of unique microbial interactions in a single experiment using a simple microscope setup across thousands of pairs or collections of root-associated bacterial isolates and microbes. This platform would address the qualitative, low throughput limitations of traditional microbiology methods to screen thousands of interactions instead of a few in high throughput resolution. As bacterial communities can be effectively influenced by the modification of local environment [1], the platform will also be designed to tune the chemical and physical microenviornments and study their influence on biochemical mechanisms interaction. This platform will dramatically expedite the rate at which unknown microbial interactions are discovered and characterized and will uncover context-dependent interaction mechanisms. With the analysis of bacterial cell-to-cell communication and virulence mechanisms, this platform will also be developed as a general microbiology tool for screening

bacterial interactions in any microbiome. This can surely help solve longstanding and emerging questions, such as how microbiomes can protect against pathogenic bacteria. To complete these goals, bacteria cells were cultured on the platform and then removed using photodegradable membranes to analyze cell-to-cell interactions between them.

1.2 Emerging Technologies to Analyze Microbe-Microbe Interaction

1.2.1 Traditional co-culture methods

The classical approach for screening microbe-microbe interaction solely relied on hand-spotting different microbes together and monitoring their growth, followed by microscopic and biochemical identification [29]. The first example of culture-based isolation was demonstrated by Alexander Fleming, when he accidentally discovered the presence of a colony of *Penicillium notatum* in his culture dish containing colonies of *Staphylococcus*, paving the way for the era of antibiotics. But with these traditional methods, only 10's of interactions can be monitored. Also, only qualitative measurements can be made from the observation of bulk colonies.

However, these methods require several days for completion and are rather time-consuming [30]. Also, culture-based methods sometime lack specificity in selecting or identifying unknown organisms [31] because most microbes have sophisticated and poorly understood growth conditions and cannot be readily cultured *in vitro* [32]. As this approach relies mainly on measuring a bulk population [33], quantitative cell-to-cell interaction data cannot be obtained [34]. Such drawbacks make this technology low throughput. Self-alteration of Gram staining (distinguishing between Gram-positive and Gram-negative groups), colony formation, and antigenicity (the capacity of an antigen to bind specifically with a group of certain products that have adaptive immunity) of many pathogens often make conventional detection methods

inefficient, and new effective control measures and improved diagnostic tools are required [35, 36].

1.2.2 Flow Cytometry

Flow cytometry (FC) is a powerful technology for investigating many aspects of cell biology and isolating cells of interest. Developed in the late 1960s, FC utilizes highly focused, extremely bright beams of light (usually lasers) to directly reveal aspects of cells by the way light is scattered or indirectly by attaching fluorescent probes to cellular receptors or other cellular components. Originating from microscopy, blood cell counting instruments, and inkjet printing technology [19], FC can be utilized to analyze interactions among bacteria colonies based on their size and fluorescence properties [37]. High-throughput cell sorting, combined with fluorescent labeling, allows semi-quantitative determination; for example, various protein levels in a population of cells made FC a successful technology for single-cell analysis [38, 39]. The power of flow cytometry derives from the fact that it quantitatively analyzes individual cells, thus permitting the identification of sub-populations within a sample [37].

FC is a “state-of-the-art” technique for characterizing distributions of individual cell behavior in a high throughput (up to 10000 cells/s) manner. It is also possible to measure multiple parameters simultaneously on each cell in a time-dependent manner, where cells are sampled at different time points [37]. Conventional FC requires many cells for analysis (at least 100,000 cells), and cells must be mixed again before the second round of analysis. Hence FC gives information on the distribution of a group of cells. Likewise, tracking cell divisions using FC is performed in bulk [40]. But, FC was neither designed for handling, manipulating and dynamic analysis of single cells nor observing spatial localization of fluorescence within a cell. Using FC alone, it is not possible to quantify individual cell behavior. Also, FC was not designed to culture bacteria while

analyzing the interactions. Currently, the limitations of flow cytometry is being addressed by fluorescence-activated single cell sorting (FACS) to measure and characterize multiple cell generations by using highly specific antibodies tagged with fluorescent dyes.

1. 2.3 Microfluidic devices

Several microfluidic approaches have been developed for studying bacterial growth, interactions, and behavior in precisely controlled physicochemical environments [23, 41, 42]. Such devices make it possible for modification of microbiomes at the single-cell level and analysis of microbial synergy and mutualism [22], study quorum-mediated behaviors, i.e., production and secretion of certain signaling molecules called *autoinducers* [43] and the role of spatial habitat structure in driving new community phenotypes [44, 45]. The key reasons for the emerging popularity of microfluidic devices in microbial engineering are the laminar flow of fluids, the requirement of small volumes of reagents, and short diffusion lengths [46]. These attributes promote ease in creating and accurately controlling the fluid flow in specific microenvironments with automation [26, 47, 48]. This enables high sensitivity, high-throughput, and a high level of control for the study of cell-to-cell interactions, specifically when studying multi-species microbial communities as opposed to study of single species in isolation [10]. Microfluidic platforms enable researchers to perform controlled ecological experiments in well-defined ecosystems and facilitate the characterization of naturally occurring communities [49]. Drescher *et al.* demonstrated that flow through soil-like porous materials, industrial filters, and medical stents dramatically modifies the morphology of *Pseudomonas aeruginosa* biofilms to form 3D streamers, which, over time, bridge the spaces between obstacles and corners in non-uniform environments. They discovered that the accumulation of surface-attached biofilm has little effect on flow through such environments, whereas biofilm streamers cause sudden and rapid clogging [50].

Microfluidic techniques can be effective in isolating and analyzing individual bacteria from environmental samples. The ability to confine individual cells can eliminate the need for pre-analysis culturing and provide the opportunity for single-cell genomics on cells obtained from natural communities [51, 52]. This approach has proven useful for characterizing environmental communities by allowing researchers to link specific species to specific community functions or identify new host-phage interactions [12, 23, 52]. Liu *et al.* demonstrated screening of antibiotic-resistant *E. coli* by initially encapsulating *E. coli* and generating picodroplets containing proliferating cells from those with non-proliferating cells [53]. This method can be further improved with quantitative analysis of the bacterial number and scattering signal and sorting techniques.

1.2.4 3D printed bacterial communities

Mimicking ecological microenvironments can play a vital role in understanding interactions within bacterial communities. For example, varying the geometry of the microenvironment the microbiomes reside in can prove effective in modifying parameters that influence cell-cell interaction between two species. Synthetic ecosystems can use bacterial communities inhabiting engineered landscapes as model systems for socio-microbiology studies [1]. The ability to track large numbers of individual cells competing in complex landscapes makes synthetic ecosystems ideally suited to test ecological predictions for a microbiome. The opportunity to probe the same community in diverse ecological scenarios is valuable for elucidating bacterial social behaviors. Hol *et al.* showed that in a spatially structured habitat, two strains of bacteria only compete with their local neighbors and self-organize into a structured community in which they coexist [54]. Connell *et al.* developed a micro-3D printing strategy for creating “designer” ecosystems tailored to investigate the interaction and integration of multiple bacterial populations within essentially

any 3D arrangement [55]. In his approach, bacteria were mixed with gelatin and a photosensitizing molecule and cooled to ambient temperatures to suspend bacteria at various 3D positions throughout the thermally set gel to maintain cell viability [56, 57]. Then two-photon-polymerization was used to crosslink gelatin into a hydrogel and achieve polymer–protein hybrid structures for cell encapsulation.

Enclosures of specified geometry are fabricated around one or more bacteria providing the ability to print populations of bacteria with submicrometer 3D resolution. Moreover, printed structures' mechanical and chemical properties can be tuned by adding desired proteins, such as BSA, to the fabrication gel. Bacteria embedded in a thermally set gelatin precursor are dispersed in three dimensions, allowing multiple populations of cells to be printed in complex configurations that can have definable chemical and physical inter-connectivity. Two such enclosures containing *S. aureus* and *Pseudomonas aeruginosa* were prepared by nesting *Staphylococcus. aureus* microcolony surrounded by *P. aeruginosa* on all sides [55]. Each suspension containing a single species was nested in a 3D printed enclosure and surrounded by a suspension of another species. While separated by a highly porous material like gelatin, they showed that a picoliter-volume aggregate of *S. aureus* could display substantial resistance to β-lactam antibiotics by enclosure within a shell composed of *P. aeruginosa*. It can be seen from their results that the presence of *P. aeruginosa* in the outer shell improved the survival percentage of *S. aureus* in the core enclosure, showing better antibiotic resistance. This is surely a novel approach to study diffusional interactions between two species. Nonetheless, being able to study the interactions between a pair of species makes it low-throughput, and not well positioned to explore an entire microbiome where potentially thousands of unique species are present. For a high-throughput study of interactions within diverse microbiomes alternative approaches are neccesary.

1.2.5 Cell microarrays

A cell microarray is a microscope slide printed with thousands of microscale spots in defined positions, with each spot containing living cells [58]. Scientists have previously used cell microarrays for probing and screening of extracellular matrices and phenotypic functions of specific genes of bacteria [59]. In most cases, cell microarrays use some surface functionality (lectin, antibody surface functionalization) to isolate and profile cell populations in a high-throughput fashion. Lectin microarrays are printed on a solid support for profiling of glycome within a cell or tissue [60, 61]. There have been applications of microarrays containing cells and extracellular or genetic materials to investigate the interactions between individual cell growth [62, 63], physiological differentiation [64], secreted proteins [65], polymers [66] and small molecules [67], microenvironmental heterogeneity [68], and resistance to liquid wetting and gas penetration [69, 70].

Cell microarrays are inherently high-throughput and typically require low reagent consumption [71–73]. But the agglomeration of cells [74], leading to neighboring effects due to the homogeneity of culture media [72] limits cell microarrays' capabilities for high-throughput screening. This phenomenon paves the way to cross-contamination and makes high throughput non-adherent cellular studies difficult [75]. As a result, the association of medium and cells with surfaces [76, 77] and the separation of cell agglomerates are mandatory.

1.3 Microwell Recovery Arrays to Screen Symbiotic and Antagonistic Interactions

Microwell recovery arrays (MRA) consist of high-density, compositionally unique, independent array of wells to partition bacteria into small culture sites. The growth of a fluorescently labeled bacteria in an array of microwells can be tracked using time lapse fluorescent microscopy. In MRAs surface-associated bacteria construct biofilms and pattern spontaneously on periodic

nanostructure arrays [78]. The variety of micro and nanoscale topology of a surface can highly influence attachment such communities [79]. An array of microwells with different pitches can modify various microenvironment parameters easier while confining multiple species to study inter and intra-species interactions. Microwell arrays can isolate species or cells within the microstructures by varying the microenvironment properties while maintaining cell viability and functionality for a relatively long period and individually controlling microenvironments in each culture unit. In order to maintain physical separation of culture units, arrays must be sealed with heavily weighted covers [80] or mineral oil [81, 82] . Microfluidic perfusion-culture systems have also demonstrated the capability of long-term cell culture [83, 84].

Microwell arrays have been coupled with fluorescence time-lapse microscopy to track parallel growth of bacterium from replicate microscale bacterial populations in controlled microenvironments, as demonstrated by Hansen *et al.*, where *P. aeruginosa* growth was monitored in 20 μm diameter microwell arrays in a highly parallel fashion to investigate growth under spatial confinent [85]. It is also feasible to accommodate two different species of bacteria expressing different fluorescent markers in a microwell format to track individual species for study of cell-to-cell interactions. . Alteration of the structure and depth of the microwells can enhance the trapping of species [86]. Thus, investigating multispecies interactions via microwell arrays can be a viable option, leading to future studies with monoculture and multi-culture studies, genome sequencing, quorum sensing, and other characterization experiments. Modifications of these microwell arrays can be possible when the communities or populations of bacteria are instead trapped within a single hydrogel [87].

1.4 Thesis Approach and Central Objective

The main objective and focus of this dissertation are to outline high throughput microwell recovery

arrays (MRA) combined with advanced bioinformatics techniques for the simultaneous detection and screening of microbial interactions across thousands of compositionally unique communities to discover bacteria collections that antagonize or promote the survival and growth of bacteria with an important function. The workflow of MRAs include stochastic seeding of a fluorescently labeled focal species with a known beneficial function (i.e., plant growth promotion) or detrimental function (i.e., pathogenesis) with an environmental isolate mixture from a plant/soil microbiome of interest into an array of microwells [85] to confine interacting cells together in small microwells (diameter =10 μm). Confinement of the cells in such small length scales mimic the formation of multispecies biofilms [88] in natural environment and facilitates inter-cellular interactions [89]. Cells are then trapped within the wells using a photodegradable polyethylene glycol (PEG)-based membrane (developed in Chapter #2) [90] to co-culture and track the growth of the fluorescently labeled focal strain with time-lapse fluorescent microscopy (TLFM). Then a Polygon 400 patterned light source is used to extract cellular communities showing highly enhanced or diminished focal species growth in any individual well by spatiotemporally degrading the membrane above the target well and recover the interacting cells by releasing them into a solution. The proof-of-concept of MRAs demonstrated here enables sequential screening and isolation of a microbial community from any well of interest indicating the desired phenotype, identify the interacting strains using advanced sequencing techniques, and validate the interactions in follow-up bioassays.

This report will detail the development and application of the MRA, beginning with development of the hydrogel membrane (Project #1), use of the MRA to explore interspecies interactions between a model interaction pair (Project #2), and application of the MRA to discover critical microbe-microbe interactions in *Populus* rhizosphere, in effort to promote the production of woody

biomass for use as a biofuel feedstock (Project #3), application of MRA for enhancing the survival and colonization of commercial nitrogen-fixing, plant growth-promoting bacteria, *Azospirillum brasilense*, into maize roots to improve crop yield (Project #4), use of MRA for screening non-pathogenic *Agrobacterium* isolates for the growth inhibition of pathogenic *A.tumefaciens* (Project #5).

1.4.1 Project #1 Development of photodegradable hydrogel membrane for selective extraction of microbes

The need for extending the high-throughput screening capabilities of microwell recovery arrays from microscopic observations of fluorescently labeled bacteria to subsequent genetic and phenotypic characterizations necessitates the development of a cell retrieval approach for off chip validation of the interactions observed on chip. The utility of such cell retrieval approach can successfully get extended towards combining microwell array measurements, selective extraction and subsequent enrichment of cells from wells with "omic" technologies (e.g., 16S rRNA sequencing, whole-genome sequencing, RNA-seq, etc.). In project #1, in collaboration with Dr. Andre van der Vlies, a new cell retrieval approach was outlined using a semipermeable, photodegradable membrane that permits the exchange of nutrients and waste products and seals motile bacteria within microwells [90]. For the development of the workflow, a novel, light-responsive, step-polymerized poly(ethylene glycol) hydrogel membrane was used to trap *Agrobacterium tumefaciens* seeded in silicon microarrays. *Agrobacterium tumefaciens* is an economically important plant pathogen which causes crown gall disease in plants [91, 92]. The endpoint observations of mCherry-expressing *A. tumefaciens* cell growth in microwells were tracked using TLFM and the photodegradability of the membrane was utilized to release and retrieve viable cells from the individual wells of interest by exposing to patterned UV light in a

spatiotemporal manner. This material-based approach was later used to perform bacteria retrieval with a high degree of spatial control and adapted to screening interactions in model and non-model interaction systems.

1.4.2 Project #2 Exploiting stochastic cellular processes of a model system to generate outlier communities with rare phenotypes in microwell arrays

The microwell array platform was developed as a general microbiology tool for screening interactions in any microbiome. The goal of this work was to investigate the inter-bacterial interactions in MRA format between two ubiquitous and well-defined microbes *Agrobacterium tumefaciens* and *Pseudomonas aeruginosa*. Since, *A. tumefaciens* is an important model and the causative agent of Crown Gall disease in plants [93], extensive studies have been conducted to study it's impact on host-microbe signaling [94], bacterial cell-to-cell communication [95] and virulence mechanisms [96, 97]. Here, the MRA proof-of-concept was developed by combining *A. tumefaciens* with *P. aeruginosa*, a human pathogen previously demonstrated to suppress *A. tumefaciens* growth in biofilms [98], in MRAs to study the model interactions between the two microbes. The study of the competitive factors between these two model bacteria produced novel insights for the development of the MRA workflow for non-model systems.

1.4.3 Project #3 Application of microwell arrays for the screening of positive and negative interactions in non-model systems

The goal of this work was to extend the MRA screening capabilities to a non-model focal species. For this, we chose *Pantoea* sp. YR343. YR343 is a Gram-negative, plant growth-promoting bacteria (PGPB) isolated from the rhizosphere of an eastern cottonwood *Populus deltoides* tree [99, 100]. As *P. deltoides* is a promising biofuel feedstock [101], uncovering interactions that influence the function of beneficial organisms in its rhizosphere has received intensive interest in

recent years [102–104]. YR343 can also colonize *Triticum aestivum* roots to stimulate food production [100, 103, 104] and has garnered interest in antibiotic production [102, 103], bioremediation and waste recycling [105, 106], and cancer treatment [107, 108]. On the other hand, other *Pantoea* sp. are pathogenic in plants, animals, and human systems. Thus, uncovering unique sets of organisms that can either promote or inhibit *Pantoea* growth, as demonstrated here, has use in several contexts [109].

1.4.4 Project #4 Screening and discovery of plant growth-promoting bacteria to enhance plant growth using microwell recovery arrays

To address the negative impacts of commercial chemical fertilizers and pesticides on the environment and human health, more emphasis is given to biofertilizers, i.e., plant growth-promoting bacteria (PGPB) inoculants capable of enhancing plant growth by beneficially interacting with the plant root microbiome [110–113]. This project aims to develop microwell recovery arrays (MRAs) to screen symbiotic interactions between maize (*Zea mays* L.) rhizosphere microbiome and *Azospirillum brasilense* , a commercially available diazotroph PGPB, to improve its survival and colonization into maize roots and enhance crop yield. *A. brasilense* is the most widely adopted diazotroph. It displays versatile C- and N-metabolism [114]. It also promotes plant growth through additional mechanisms, including phytohormone production [115], development of stress tolerance [114], biocontrol of phytopathogens [116], solubilization of phosphates [117] and production of siderophores [118]. Since maize (*Zea mays*) is a non-leguminous crop of great significance in food production, consistent efforts have been extended towards understanding the association and colonization of diazotrophs with maize [119–121]. However, the broad adoption of N-fixing PGPB for the growth promotion of maize is impaired by the lack of knowledge on different symbiotic plant-bacteria interactions [112, 113]. Successful establishment of a PGPB

inoculant in the root of non-leguminous plants is widely dependent on symbiotic interactions between the PGPB and the species present in the plant rhizosphere and endosphere microbiome [122–124]. Therefore, identifying symbiotic bacteria that improve the growth and survival of *A.brasilense* in *Zea mays* roots is critical for biofertilizer development.

1.4.5 Project #5 Screening of biocontrol agents for disease prevention in plants

This project aimed to screen pathogenic *A. tumefaciens* SP.15955 against hundreds of non-pathogenic *Agrobacterium* isolates collected from Kansas native plant roots to discover new *Agrobacterium* strains capable of suppressing the establishment of this pathogen. The MRA is adapted to a pathogen "challenge model" that is designed to select and isolate the non-pathogenic *Agrobacterium* isolates that are the most potent inhibitors of pathogenic *A. tumefaciens* 15955. Here, a small number of *A. tumefaciens* sp. 15955 expressing GFP were combined with *Agrobacterium* isolates extracted from the roots of *Helianthus annuus* plants and seeded into arrays of 10 μm diameter microwells in different cell ratios. To effectively "challenge" candidate isolates against *Agrobacterium* 15955 (Agro 15955-GFP hereafter), the number of *Agrobacterium* isolates in each well is sequentially reduced. Wells that show greatest inhibition of Agro 15955-GFP at the lowest ratio are identified as the most potent inhibitors**.** With the extraction and recovery capabilities of the MRAs, the collection of *Agrobacterium* isolates most capable of diminishing Agro 15955-GFP are sampled for follow-up phenotypic characterization with whole-genome sequencing techniques.

Chapter 2 : Development of photodegradable hydrogel membrane for selective extraction of microbes

2.1 Overview

Microwell arrays are important tools for studying single cell behavior and cell-cell interactions, both in microbial and mammalian systems. However, retrieval of cells from microwell arrays with high spatial precision remains a major technical hurdle that prevents follow-up genetic and phenotypic characterization of cells within observed microwells. This work describes a new, material-based approach to grow and retrieve live bacterial cells from small (≥20 μm diameter) microwells in an array using the plant pathogen *Agrobacterium tumefaciens* as a model bacterium. Our approach uses a light-responsive, steppolymerized poly(ethylene glycol) hydrogel interface as a membrane that confines motile cells within microwells while allowing nutrient exchange and cell growth. The key design feature is the photodegradability of the membrane, as it enables individual wells of interest to be opened using patterned UV light for selective release and retrieval of cells. Extraction can occur in parallel from any number and combination of wells defined by the user. These advancements represent a new use for light-responsive hydrogels and the ability to retrieve cells from microwells with high spatial precision enables several applications that require the isolation and characterization of cells with rare phenotypes from heterogeneous populations.

---

* Manuscript appearing in: André J. van der Vlies, Niloy Barua, Priscila A. Nieves-Otero, Thomas G. Platt, and Hansen R.R. On Demand Release and Retrieval of Bacteria from Microwell Arrays Using Photodegradable Hydrogel Membranes. *ACS Applied Bio Materials*, 2, 266−276 (2019). doi: 10.1021/acsabm.8b00592

2.2 Introduction

Microwell arrays allow for high-throughput manipulation and study of cells. These platforms have several key features including their small size, high well density, and ease with which they allow for cell confinement [12, 125–128]. In recent years, microwell arrays have been used to probe single cells to understand cellular heterogeneity [129] and rare cell function [130], among other applications [131, 132]. While the majority of microwell applications focus on mammalian systems, microwells are also useful in the study of microbial systems. These platforms have been used to examine mutant libraries [82] and to characterize the growth dynamics of single bacterial cells [133]. If microwells are large enough to confine multiple cells or designed to promote exchange of materials between wells, they become excellent tools for studying cell-cell interactions [12, 25]. In this context, microwell formats have been used to examine the ecological dynamics of microbial communities under selective environmental pressures [4, 44], the consequences of contact-mediated interactions [134], and quorum sensing [133, 135]. Despite the plethora of current applications, a critical limitation often exists: cells remain in wells during the entire analysis [10]. As a result, characterizations are typically limited to on-chip fluorescence-based measurements. The utility of microwell arrays, particularly in screening applications, could be significantly expanded if cells of interest could be removed from individual wells for subsequent genetic and phenotypic characterizations. In particular, coupling of "omic" technologies (e.g., 16S rRNA sequencing, whole genome sequencing, RNA-seq, etc.) with microwell array measurements could be enabled if selective extraction of cells from wells and in some cases subsequent enrichment through culture is achieved. For example, microwells could be used to examine a large number of mutant genotypes for a target phenotype during a mutant library

screen but would require subsequent isolation of selected mutants from individual wells for mutation mapping [10, 136].

Hansen and co-workers recently reported a microwell screening platform designed to probe microbe−microbe interactions [85, 134, 137–139]. Although this platform had the benefit of high-throughput measurement, it had limited characterization capabilities due to the lack of cell retrieval. Kim and co-workers recently addressed this problem using a manual capillary driven bacteria retrieval strategy from 100 μm diameter wells [82]. This approach allows for cell retrieval; however, it requires relatively large microwell sizes. Additionally, their strategy makes individual microwells closed systems with limited nutrient flux due to the use of fluorinated oil to compartmentalize the wells. These constraints motivate the development of new materials and interfaces that enable efficient nutrient exchange as well as selective extraction of live cells from microwells at improved spatial resolutions.

In this paper, we outline a new cell retrieval approach using a semipermeable, photodegradable membrane that permits exchange of nutrients and waste products and seals motile bacteria within microwells. The photodegradability of the membrane enables individual wells of interest to be opened using patterned UV light for selective release and retrieval. The proof of concept studies use a light-responsive poly(ethylene glycol) (PEG) hydrogel as a photodegradable membrane and silicon microarrays seeded with the bacterium *Agrobacterium tumefaciens*, the causative agent of crown gall disease in a wide range of plants including apples, walnuts, and sunflowers [91]. As is common among bacteria, the success of this plant pathogen is heavily influenced by interactions with other bacteria, many of which are unknown [92]. The platform allows tracking or endpoint observation of cell growth based on fluorescence intensity measurement of mCherry-expressing *A. tumefaciens i*nside of microwells. Using a light patterning tool, selected microwells can be

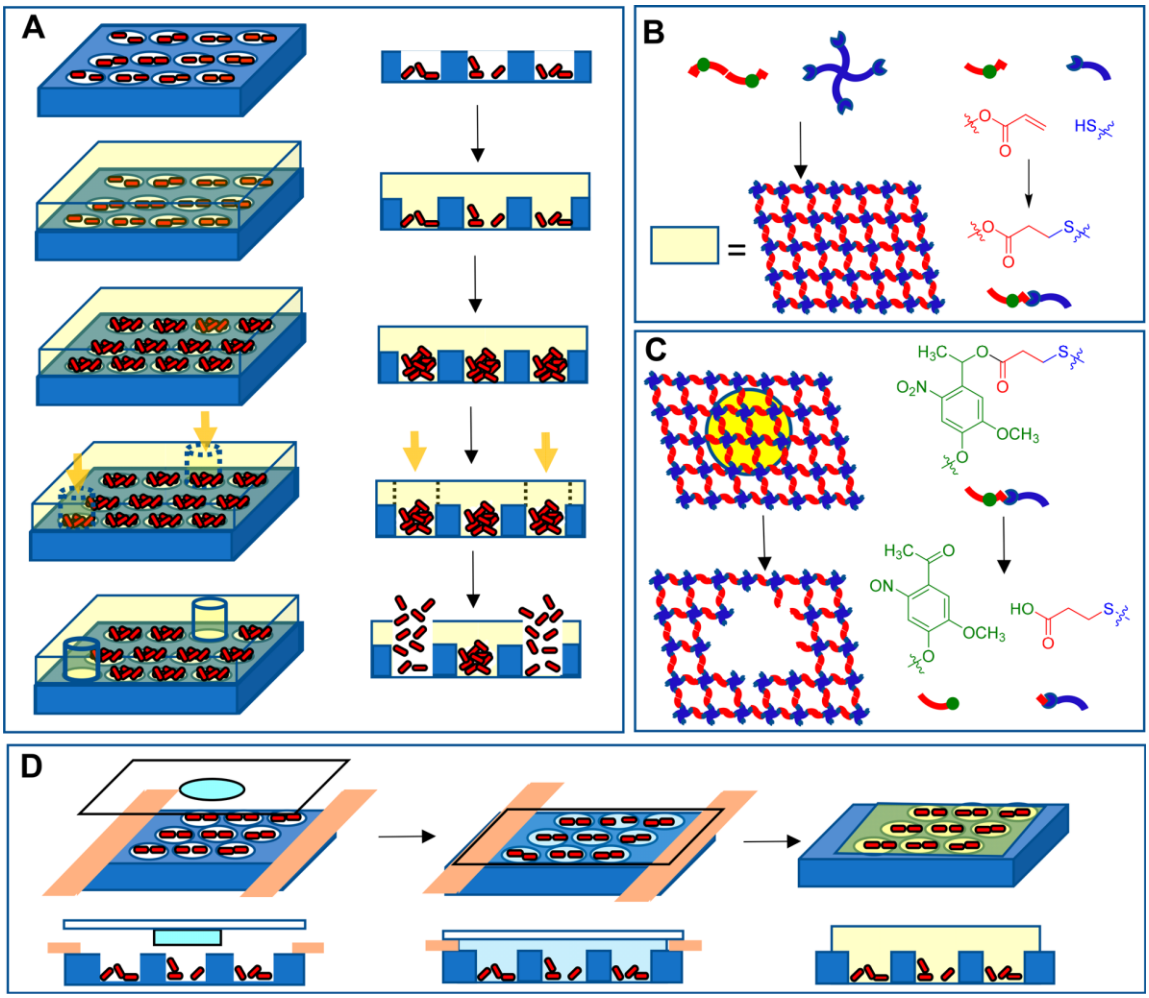

Figure 2.1: Concept of on demand release and retrieval of bacteria from microwell arrays using a photodegradable membrane. (A) Microwell array (blue) is seeded with fluorescent cells (red) that are confined to the wells by attaching a membrane (yellow) that supports cell growth. Irradiation with light (yellow arrows) degrades the membrane and opens selected microwells after which cells can be retrieved. (B) Photodegradable membrane is made by reacting a four arm PEG-thiol (blue) with a photodegradable PEG diacrylate (red with green dot) by a Michael-type addition reaction. (C) Polymer network of the membrane is degraded when the photodegradable nitrobenzyl group (green) present in the crosslinks is cleaved by light (yellow circle) and the polymeric reaction products dissolve in the aqueous medium. (D) To seal seeded cells (red) into microwells with the photodegradable hydrogel, we placed a glass slide with a mixture of the four arm PEG-thiol and PEG-diacrylate (cyan) on top of the seeded microwell with spacers (peach) in between. The membrane precursor solution mixes with the medium (white) inside the wells and cross-links to form the membrane (light blue). After the glass slide is removed, the membrane swells (yellow) when placed in the culture medium.

opened individually or in parallel, thereby allowing subsequent retrieval of viable cells. This material-based approach affords a high degree spatial control over bacteria retrieval and can be adapted to other high-throughput screening formats. For these reasons, we expect that this

approach will be a powerful tool for microbiome engineering efforts, as well as other applications where screening or studying cell−cell interactions is important.

2.3. Results and Discussion

2.3.1. Concept and Material Selection.

A key feature of our strategy for on-demand release of bacteria from microwell arrays is the attachment of a photodegradable membrane (yellow) on a silicon microarray (blue) that confines motile, live cells (red) in the wells (**Figure 2.1A**). The membrane forms a physical barrier that prevents bacteria from escaping the microwells but allows diffusion of nutrients, oxygen, and metabolic waste products. The membrane can also be locally degraded by bacteria to generate space for growth within the wells. Light irradiation of selected microwells opens the wells, allowing for retrieval and characterization of the present cells (**Figure 2.1A**).

Hydrogels are cross-linked networks of hydrophilic polymers that have a high water content and tend to swell. Hydrogels are widely used for sustained drug delivery systems, tissue engineering applications, nonfouling coatings, and material adsorption [140]. Because of their high water content, biocompatible hydrogels are well-suited for use as the membrane-enclosing bacteria within microwells required for our on demand cell retrieval scheme. Anseth and co-workers [141] reported the development of photodegradable hydrogels using the thiol-acrylate Michael-type addition reaction between functionalized multiarm PEG polymers pioneered by Hubbell et al. [142].The photodegradability of these hydrogels stems from the incorporation of a light-cleavable nitrobenzyl group within their network structure, which allows for a controlled decrease in cross-linking density throughout the network upon light exposure to the point of reverse-gelation. These materials allow for high spatiotemporal control over degradation [143] and are nontoxic to cells [143, 144], and their aqueous nature permits transport of nutrients and waste products [145] to

support bacterial cell growth within microwells. For these reasons, we identified photodegradable PEG hydrogels as a good material for use as responsive membranes over microwells. To generate membranes, a step-growth polymerization mechanism that uses a tetra-functional PEG-thiol crosslinker and a photodegradable PEG-diacrylate was used **(Figure 2.1B).** A key advantage of this polymerization approach is that it generates hydrogel networks with uniform cross-linking density and microstructure, allowing for uniform diffusion across the array [141].

2.3.2. Membrane Attachment to the Microwell Array.

It was reasoned that the swelling properties of PEG hydrogels, i.e., the increase in volume by adsorption of water, could be used as a means of attaching the membrane to the microwell array. PEG hydrogels are prepared by mixing PEG diacrylate with multiarm PEG thiol at basic pH to

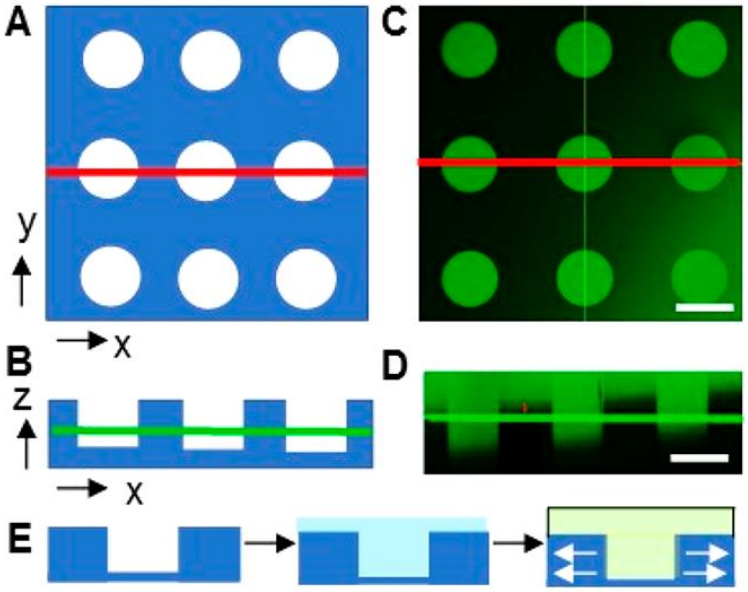

Figure 2.2: Confocal images of the membrane attached to a microwell array. Schematic representations of the microwell viewed in the (A) xy and (B) xz planes to aid interpreting the data in C and D. (C) Fluorescence signal, indicating fluorescein labeling of the PEG hydrogel membrane, coming from the xy plane along the green line in the xz plot shown in D. (D) Fluorescence signal coming from the xz plane along the red line shown in the xy plot in C. (E) Proposed locking mechanism for membrane attachment. The membrane precursor solution mixes with culture medium (white) and crosslinks to form the hydrogel (light blue). When placed in culture medium the membrane swells (yellow) creating forces on the walls of the microwells preventing detachment. Microwell size: 100 μm, scale bar: 100 μm, (n = 2).

form the cross-linked network [142]. This precursor solution can form a thick film on the microwell array and move into the microwells before complete cross-linking and gelation occurs. Upon immersing the microwell array in culture medium, swelling of the crosslinked polymer network can then lock the membrane into place and seal the microwells, preventing motile bacteria from moving out (**Figure 2.2E**). Physical attachment of the membrane to the microwell array may be facilitated by the scalloped sidewalls of the microwells resulting from the Bosch etching process [85]. In this way, attachment of the membrane could be achieved without the need for a reactive surface.

To test the attachment strategy, we first filled microwells with LB medium and prepared them as shown in **Figure 2.1D**. Upon removing the glass slide, the membrane remained firmly attached to the microwells and no membrane movement was observed after incubating the array in LB medium for 2 days (n= 2). The number of microwells per unit surface area appeared to be critical for stable membrane attachment. Microwell arrays with large blank areas, i.e., areas without microwells showed membrane detachment within several hours when placed in LB medium. To verify that membrane attachment occurred through an anchoring mechanism, we used confocal laser scanning microscopy to obtain three-dimensional reconstructions of fluorescently labeled membranes on the microwell arrays (**Figure 2C, D**). Because of its nonfluorescence, the silicon microwell array appears black whereas the membrane appears green after labeling the membrane with fluorescein (for details see section 4.8 in the Experimental Section). The membrane is present throughout microwells with observed diameters (100 μm) and depths (20 μm) that correspond to well dimensions (**Figure 2.2**). Similar results were obtained for microwells with 4, 20, 40, 50, and 60 μm diameters (data not shown). Swelling of the membrane was confirmed by measuring membrane thickness after arrays were placed in LB medium. Hydrogels were observed to be

approximately 150 μm thick despite having been polymerized on microwell arrays using 38 μm spacers, suggesting that swelling had occurred.

2.3.3. Bacteria Can Grow When Encapsulated in the Hydrogel Membrane Material.

A potential limitation to attaching the membrane to the microwells via the anchoring mechanism described in the previous section is that the membrane may occupy well space required for bacterial growth. However, these photodegradable PEG hydrogels have ester groups in the cross-links that in theory could be degraded via hydrolysis, as has been reported for ester-containing

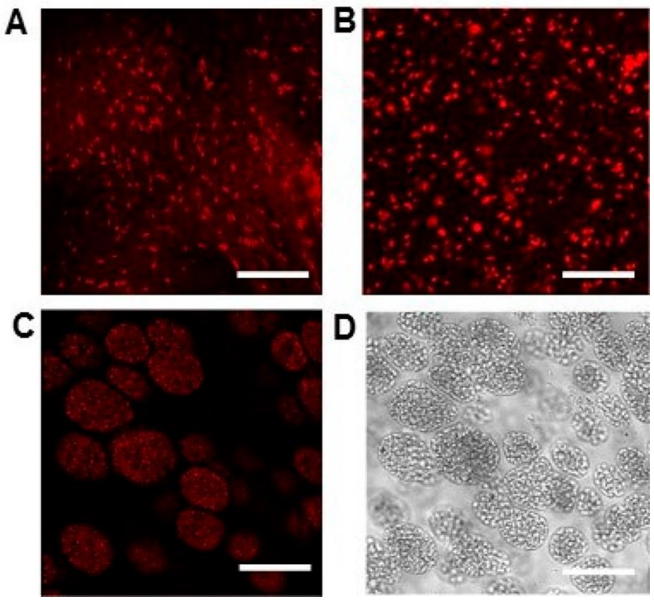

Figure 2.3: Confocal images of *A. tumefaciens* after encapsulation inside the membranes at different time points. Bacteria in the hydrogel were fixed after (A) 0, (B) 10, and (C) 24 h before acquiring fluorescence confocal images. (D) Bacterial clusters are present in the hydrogel 24 h after encapsulation (differential interference contrast (DIC) image). Thiol concentration: 35 mM, acrylate concentration: 35 mM. Scale bar: 50 μm, (n = 3).

PEG hydrogels [146]. We reasoned that the presence of the ester structure throughout the hydrogel network should allow for bacteria-dependent network degradation. Consequently, bacteria embedded within the hydrogel membrane should be able to grow within spaces that they create by locally degrading the membrane. To test this, we encapsulated A. tumefaciens cells expressing the fluorescent protein mCherry by adding the cells to the membrane precursor solution (**Figure S1**).

After gelation, individual bacteria cells encapsulated within the membrane could be observed by microscopy (data not shown). After 24 h, the membrane itself appeared opaque (**Figure S2A, B**) indicating that bacteria had grown within the membrane (n = 4). This was confirmed by microscopy which showed the presence of large (20-40 μm) clusters of cells (**Figure S2C**). These clusters also formed inside membranes prepared at higher thiol/acrylate concentrations (35 mM instead of 22 mM) (**Figure 2.3, Figure S3A, B**). Membranes were fixed at different time points to see how the initial single bacteria grow into larger clusters over the course of 1 day. To confirm that the bacteria inside these clusters were alive after 24 h, we placed unfixed membranes in LB containing triphenyltetrazolium chloride (TTC) [147]. This compound is colorless but is reduced by metabolically active bacteria resulting in the formation of pink, water-insoluble crystals. When TTC was added the membrane turned pink and microscopic observation showed the presence of crystals indicating that the bacteria in the clusters were alive (**Figure S3C**) (n = 3). The mesh size of PEG hydrogels is typically in the nanometer range [146]. For this reason, it is unlikely that the space occupied by the observed clusters of bacterial cells (**Figure 2.3**) was initially present in the membrane. The presence of the large clusters also suggests that the mesh size of the membrane allows for sufficient mass transfer of nutrients to support bacteria growth. To further investigate mass transfer from the wells, we loaded GFP protein (MW = 27 kDa) into the wells, attached the membrane, and monitored well fluorescence (**Figure 2.4**). Although protein aggregation and adsorption to the well walls may impede GFP diffusion, the decrease in well fluorescence intensity over 10 h indicates that the system allows for diffusion of nutrients and large biomolecules. PEG hydrogels formed with higher polymer concentrations and a smaller mesh size [148–150] also supported the formation of large clusters of viable bacteria (data not shown). Finally, to quantify the effect of the hydrogel on cell growth and metabolic activity, we encapsulated A. tumefaciens

in the hydrogel and compared its growth to the same number of cells grown in suspension using the TTC assay. Bacteria encapsulated within the hydrogel showed 40% reduction in metabolic activity compared to those grown in suspension (**Figure S4**). Because TTC measures metabolic activity, this reduction could be explained by lower cell numbers and/or less metabolically active bacteria in the hydrogel compared to those grown in suspension.

2.3.4. Culture of Cells in Microwell Arrays with Attached Hydrogel Membranes.

Our platform requires that the photodegradable membrane both prevents cells from leaving microwells and does not interfere with cell growth. Three hours after seeding cells into 20 μm diameter wells, fluorescein-labeling of the hydrogel shows that the membrane is present

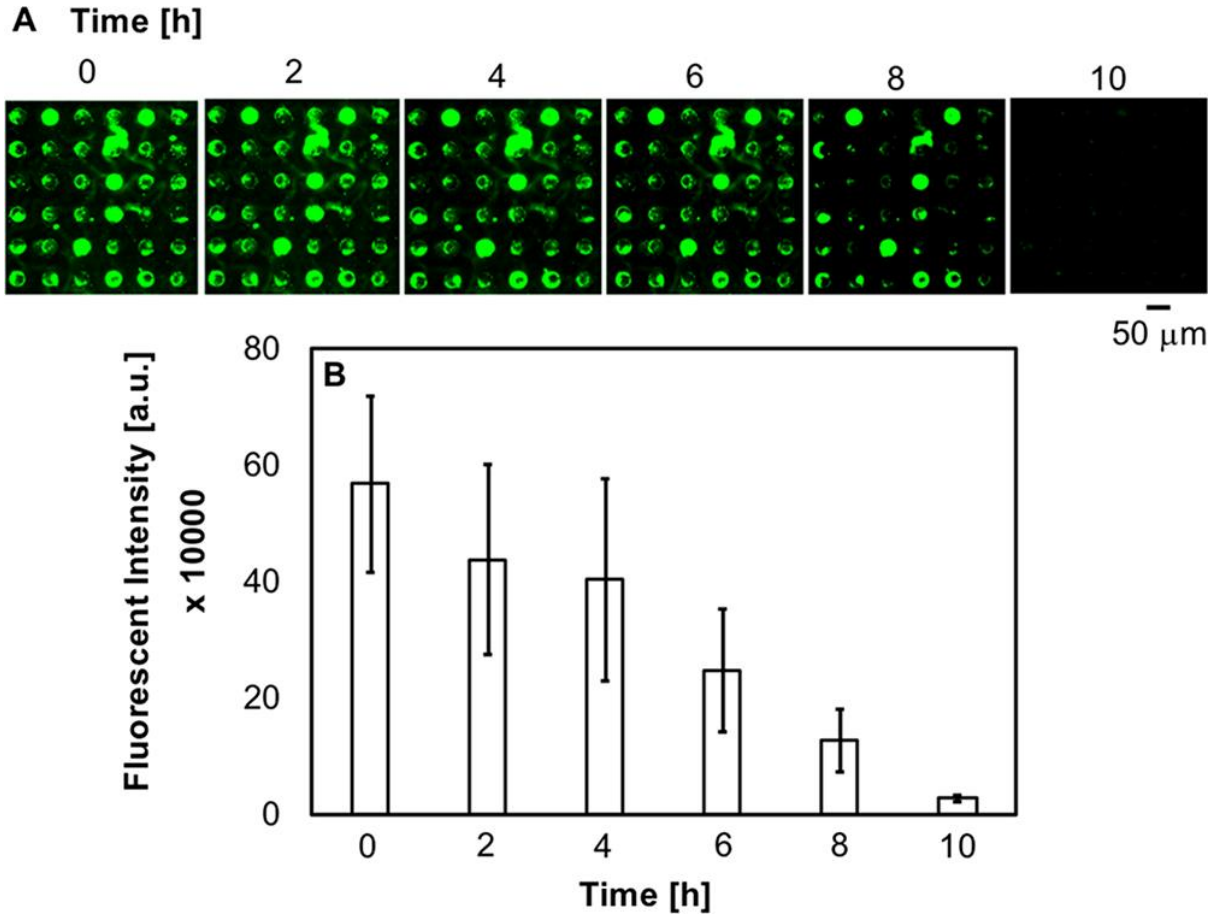

Figure 2.4: GFP diffusion from the wells. (A) Time-lapse fluorescent images of wells after loading them with GFP, membrane attachment, and soaking in 1X PBS media. (B) Average fluorescence intensity from the wells at each time point..

throughout these microwells with localized spots of higher fluorescence intensity (**Figure 2.5A**, left panel). These spots spatially correspond to the location of the seeded bacteria (**Figure 2.5A**, middle and right panels). We propose that reaction of fluorescein maleimide with thiol groups present on the bacteria result in cells having fluorescent signal in both the green and red channels. To show that the bacteria can grow with the membrane attached to the array, we seeded *A. tumefaciens* at the same optical density but kept the microwell immersed in medium for 24 h. Consistent with bacterial growth, there is an increase in the red fluorescence signal following this

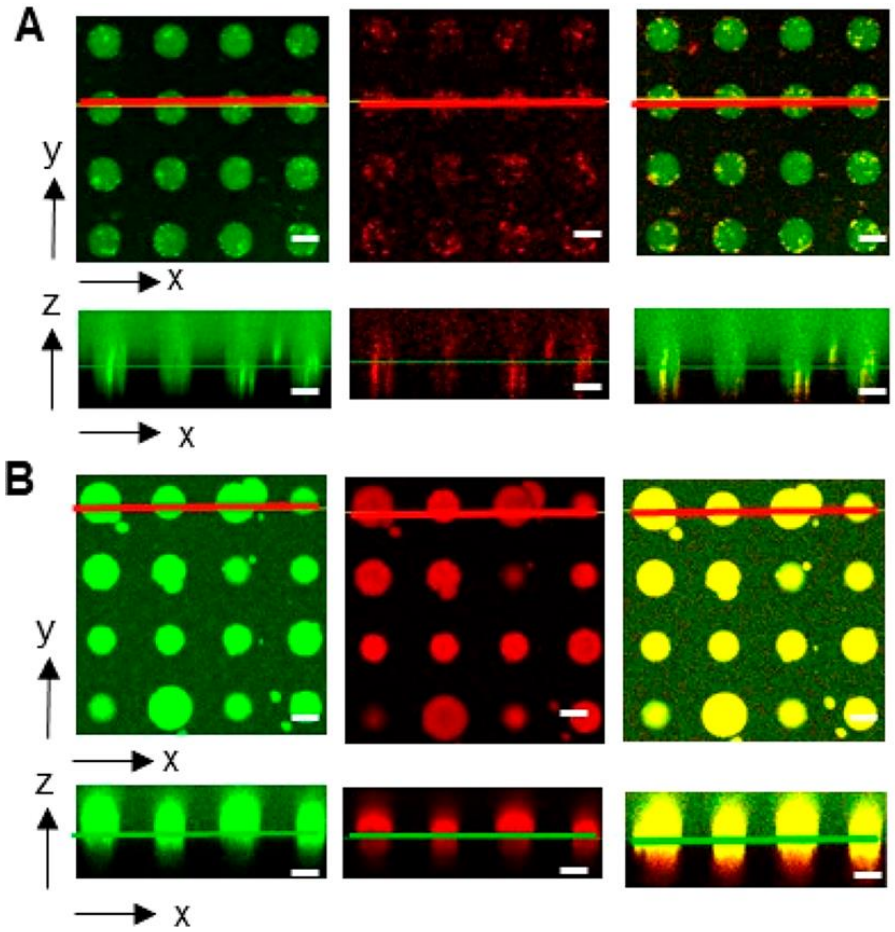

Figure 2.5: Confocal images of A. tumefaciens-seeded microwell array with an attached hydrogel membrane. (A) Fluorescence intensities 3 h after cell seeding coming from the xy plane along the green line and the xz plane along the red line. Left panel green fluorescence fluorescein-labeled membrane; middle panel red fluorescence of the bacteria; right panel overlay of both. (B) Same as A but after culturing for 24 h. Samples were fixed prior to measurements. Well diameter, 20μm; seeding OD = 0.2; scale bar = 20 μm, n = 5.

incubation (**Figure 2.5B**, middle panel). Further, bacteria are present above the silicon/membrane interface (**Figure 2.5B**, middle and right panels). Although 38 μm spacers were used during hydrogel preparation, the thickness of the membrane is much greater due to swelling of the membrane in the culture medium (approximately 150 μm thick). Bacteria are present approximately 40 μm above this interface, indicating that bacteria invade the membrane. However, membrane degradation appears to occur mainly in the z-direction, with relatively little degradation occurring in the x and y-directions **(Figure S5)**. For this reason, we observe no mixing between neighboring wells over the 24 h time period required for growth **(Figure 2.5B)**. Although we did not observe mixing of cells from neighboring wells in our experiments, this might not be the case for other bacterial strains or experimental conditions. For this reason, use of this platform may

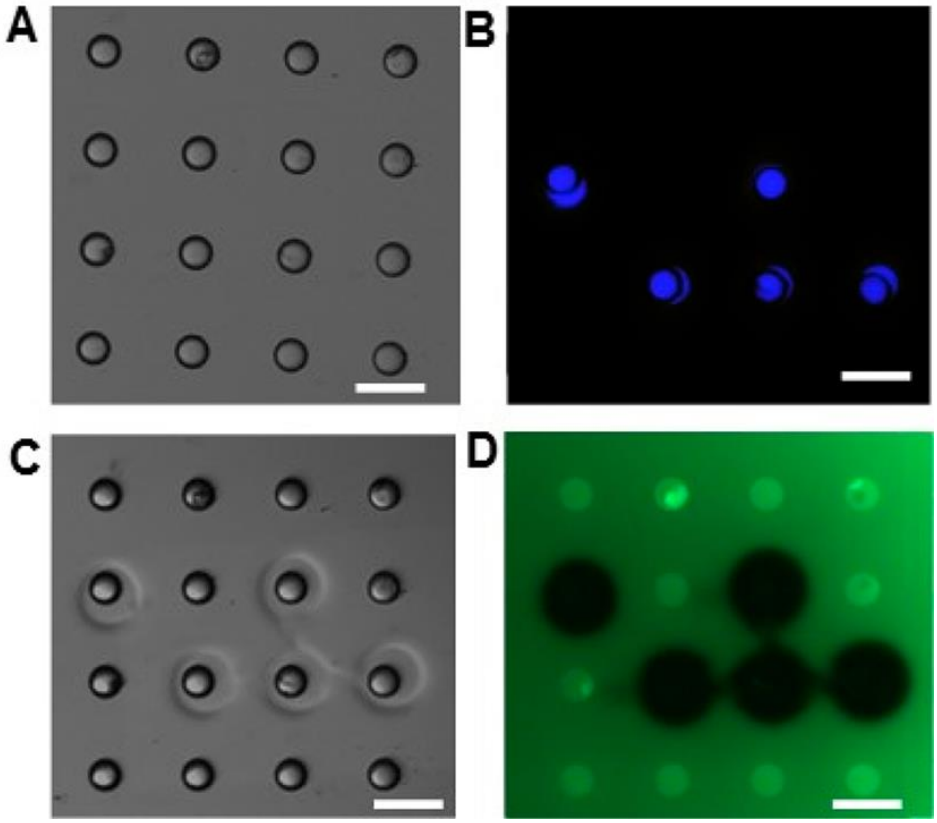

Figure 2.6: Microwells can be opened by degrading the membrane with light. (A) 45 μm wells after membrane attachment, (B) patterned light during irradiation (blue), (C) after irradiation (D) and after labeling with fluorescein maleimide. Exposed area, 50 μm diameter circle; irradiation time, 5 min; light output, 1.4 mW/mm2; scale bar = 100 μm; n = 3.

require optimization of experimental conditions such as bacteria seeding density or further optimization of microwell design.

In summary, these observations indicate that the membrane polymerized over a seeded microwell array serves as an effective barrier that compartmentalizes the microwells while allowing bacteria to proliferate inside of the microwells-a critical requirement when screening for growth or growth inhibition. The process of attaching the membrane and observing growth is robust and has been carried out many times (n = 22). Although we have not experimentally determined an upper limit of assay time, based on the degree of membrane degradation observed after 24 h (≈ 40 μm) and the membrane thickness (≈ 150 μm) it is estimated that the membrane should be operational for at least 3 days in its current configuration.

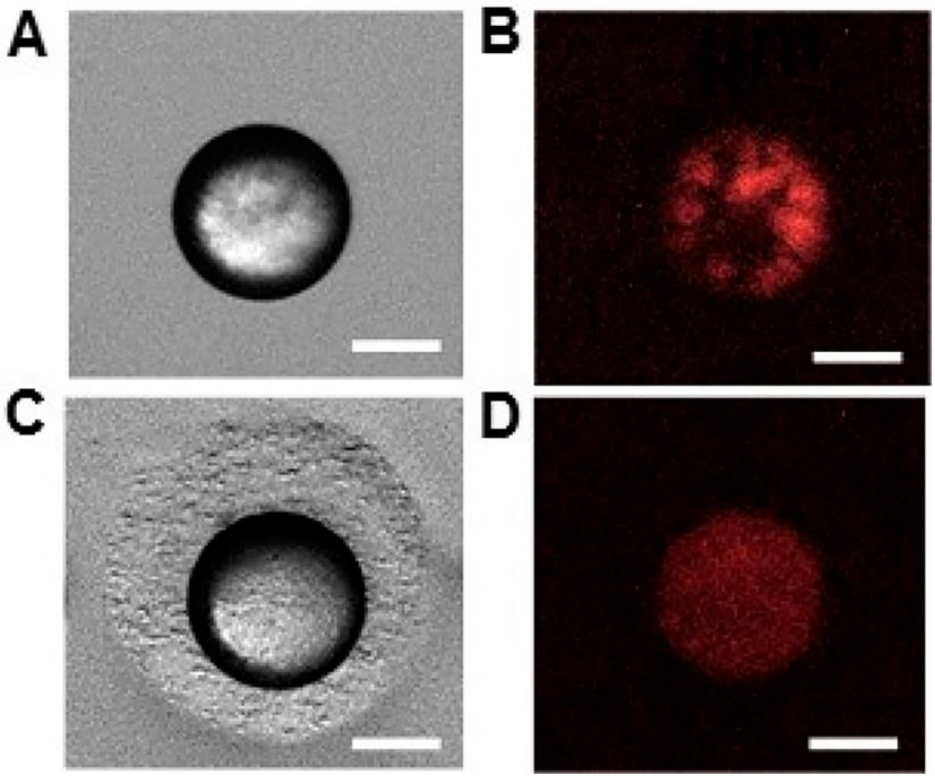

Figure 2.7: Membrane degradation of bacteria-seeded microwells leads to bacteria release. Bright-field and fluorescence images (A, B) before and (C, D) after irradiating a 60 μm microwell with the Polygon400. A. tumefaciens was seeded at OD = 0.2 and cultured for 2 days. Exposed area, 120 μm circle; irradiation time, 5 min; light output, 2 mW/mm^2; scale bar = 30 μm.

2.3.5. Membrane Photodegradation and Cell Release.

The ability to selectively open microwells is critical for our application. To demonstrate this, we used patterned illumination with the Polygon400 to degrade the membrane over, and thereby open, targeted 45 μm diameter microwells **(Figure 2.6)**. To confirm membrane degradation has occurred only in irradiated areas, we labeled the membrane with the thiol-reactive fluorescein maleimide dye and observed by fluorescence microscopy. As expected, irradiated areas are devoid of fluorescent signal indicating that polymer network degradation is localized to directly irradiated areas.

To demonstrate the ability to release bacteria from microwells, we seeded A. tumefaciens in 60 μm wells, allowed them to grow for 2 days, and then irradiated the membrane with light **(Figure 2.7)**. As expected, the polymer network degrades, opens the microwells, and releases cells. A few

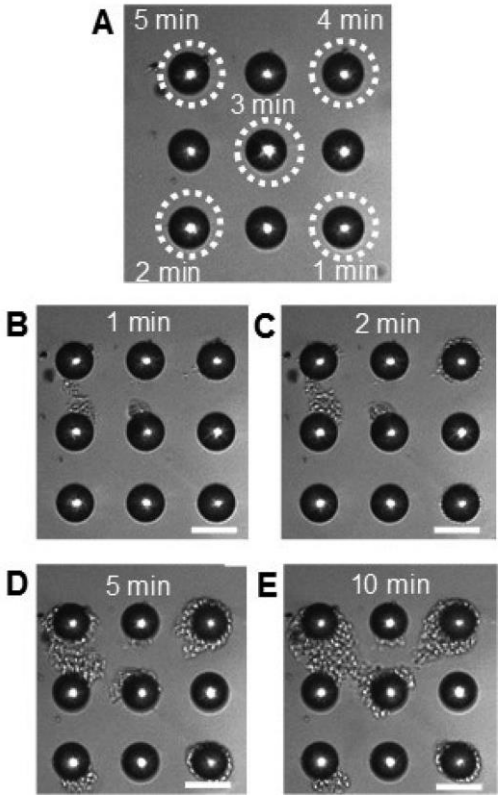

Figure 2.8: Effect of irradiation time on bacteria release from 20 μm diameter wells. (A) Wells were irradiated as indicated for either 1, 2, 3, 4, or 5 min and afterward (B−E) observed over the course of 10 min. Light output 0.7 mW/mm2. Scale bar = 25 μm, n = 2.

minutes after light exposure, bacteria move to the irradiated area next to the microwell **(Figure 2.7C)**, whereas other cells stay in the microwell **(Figure 2.7D)** (n = 6). Notably, localized clusters of cell fluorescence present within microwells prior to irradiation **(Figure 2.7B)** are no longer visible after irradiation. Instead the fluorescence signal observed within irradiated microwells appears diffuse, suggesting that cells remaining in wells are no longer structured into clusters by the hydrogel **(Figure 2.7D)**. Thus, under these experimental conditions *A. tumefaciens* cell clusters appear to be readily removed upon light exposure, corresponding to the release of bacteria. This may not be true for all experimental conditions or bacteria, and so additional sample processing may be necessary in cases where bacteria remain as stable cell clusters or biofilms after irradiation.

The Polygon400 allows spatiotemporal control over membrane degradation. To examine how irradiation time at a fixed light intensity impacts bacteria release from 20 μm diameter microwells, we irradiated adjacent microwells for 1, 2, 3, 4, or 5 min **(Figure 2.8A)**. Cells were observed moving out of all of these wells by 5 min after irradiation **(Figure 2.8D)**, however cells were observed exiting microwells that were irradiated for longer periods of time only 1 or 2 min after irradiation **(Figure 2.8B, C)**.

A benefit of this method is that any number and combination of wells can be simultaneously opened, enabling parallel extraction of cell populations, if desired. To demonstrate this, ten nearby 50 μm diameter microwells were simultaneously irradiated using the Polygon400 **(Figure 2.9A, B)**, resulting in cell release **(Figure 2.9C, E)** and membrane degradation **(Figure 2.9D, F)** from each targeted well. The cell-dependent fluorescence signal drops to background levels after washing the microwells with LB medium showing that the bacteria can be removed **(Figure 2.9E)**. The release of bacteria can be semi-quantified by measuring the fluorescence intensity from the individual wells before and after opening. The fluorescence intensity of opened wells decreases by

about 60% **(Figure S6)**, consistent with our observations of cells are leaving the microwells after irradiation. After the wells are washed, the fluorescence intensity of opened wells drops by another 30%, suggesting that most cells can be removed.

2.3.6. Retrieval of Bacterial.

To verify that bacteria from selected wells can be harvested from wells and cultured for follow-up analysis, opened wells were washed with an extraction medium. Washing after well opening is an easy and straightforward approach to retrieve cells. Additionally, this approach allows easy verification that bacteria have been extracted by using a microscope to inspect washed microwell

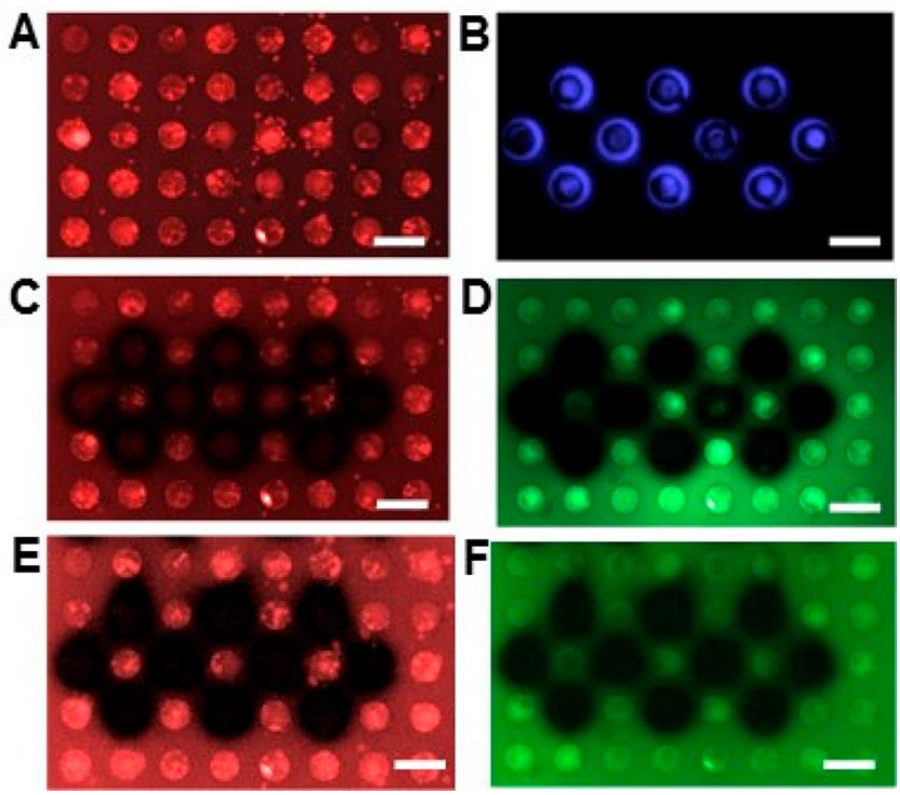

Figure 2.9: Several wells can be opened simultaneously using the Polygon400. (A) *A. tumefaciens* expressing fluorescent mCherry was seeded at OD = 0.2 and cultured for 1 day. (B) Simultaneous irradiation of ten 50 μm microwells with a 60 μm circle pattern for 5 min at 0.7 mW/mm2. (C) Microwells that were irradiated show diffuse red fluorescence due to the moving bacteria. (D) Fluorescein maleimide labeling confirms membrane degradation. (E, F) Same as C and D but after washing with LB medium. Scale bar = 100 μm. Simultaneous opening of multiple wells has been done numerous times (>20).

arrays (e.g., **Figure 2.9E**). To show that we can retrieve bacteria from selected microwells, 72 microwells (40-50 μm in diameter) were opened in four different runs **(Figure S7).** The arrays were then washed with extraction medium (LB with 0.05% Tween20) to remove the bacteria from the microwells. To show that the bacteria were viable and could be enriched, the washings were cultured overnight in a polystyrene well plate. As a control to show that the isolated bacteria originate from the opened microwells, the microwell array was also washed with the same volume of extraction medium prior to the well opening. The washings taken from opened wells showed

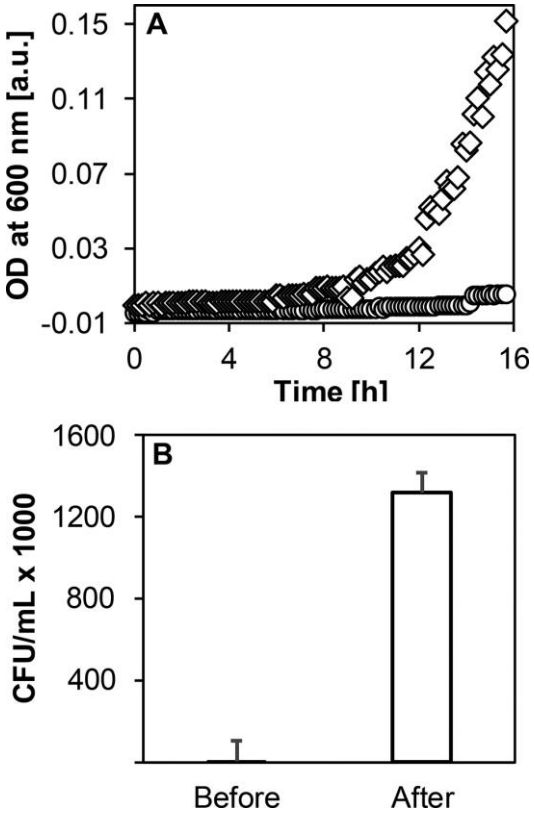

Figure 2.10: *A. tumefaciens* isolated from microwells are viable and can be cultured. (A) Total of 72 microwells (40−50 μm in diameter) were opened with light. After careful washing of the membrane with LB with 0.05% Tween20, the solution was placed inside a plate reader and the OD tracked over time. Washings after opening the microwells (rhombus) show an increase in OD over the course of 16 h whereas washings before opening the microwells (circles) do not show bacterial growth (n = 3). (B) Quantification of bacteria colony forming units (CFU/mL) present in the washing solutions before and after opening of ten 50 μm diameter wells (n = 3).

bacteria growth, as measured by the increase in OD at 600 nm. In contrast, the control washings

taken from wells prior to opening did not increase in OD over time **(Figure 2.10A).** This suggests that the bacteria cultured from washings after well opening originated from the opened microwells. Because the observed OD increase is only qualitative, we repeated the experiment and plated the washing solutions on agar to quantify cell density **(Figure 2.10B).** Colony forming units per mL (CFU/mL) were approximately 1000-fold higher in the extract after opening ten wells. This suggests that >99.9% of the cells present in the extract originated from the wells. These results demonstrate that under these experimental conditions A. tumefaciens cells can be retrieved from the microwells and remain sufficiently viable to be cultured for follow-up analysis. However,

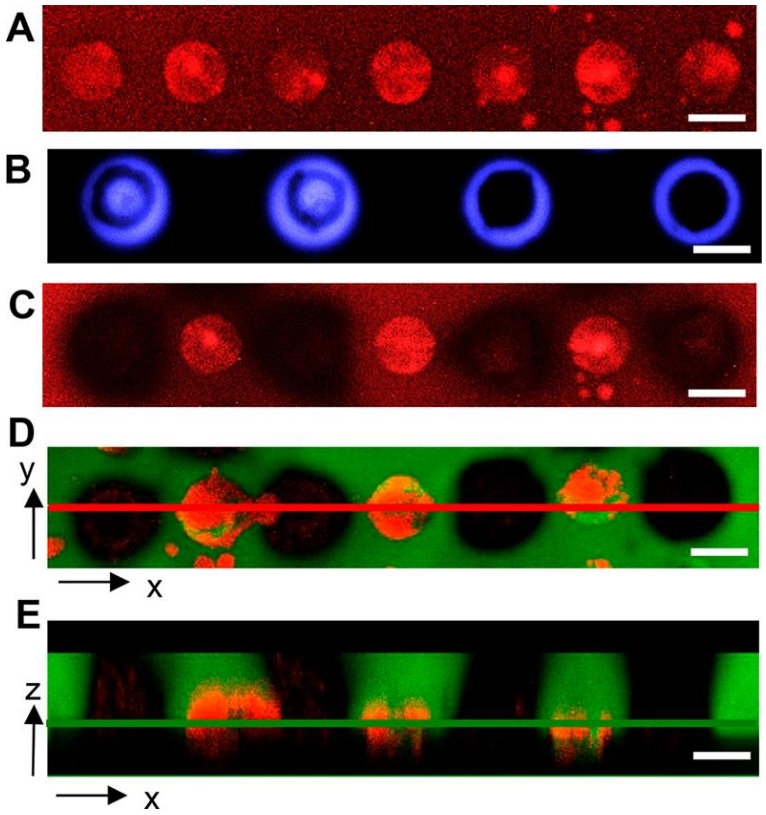

Figure 2.11: Effect of light pattern on bacteria removal from microwells after culture for 1 day (OD = 0.2 seeding density). (A) 40 μm microwells containing bacteria were (B) irradiated either with 60 μm light circle or 60/40 μm light ring patterns (blue) for 5 min at 0.7 mW/mm2. (C) Cells are released as shown by the diffuse red fluorescence. After washing, the membrane is fixed and imaged by confocal microscopy. (D) Fluorescence signal (green indicating fluorescein-labeled membrane, red indicating cells expressing mCherry) coming from the xy plane along the green line in E. (E) Fluorescence signal coming from the xz plane along the red line in D. Scale bar = 40 μm. Effect of ring versus circle irradiation on cell release was done in triplicate

irradiation may problematically reduce cell viability when experiments use other bacterial strains or experimental conditions. Accordingly, use of this platform under other conditions may require the optimization of irradiation time, membrane thickness, or other design features to maintain cell viability through the extraction and retrieval procedure.

2.3.7. Avoiding Direct Exposure of Bacteria to UV Light.

A well-recognized problem in applications using light for manipulation of cells is its effects on cell viability and behavior [151]. The use of a two-photon process for cleavage of the nitrobenzyl group has been reported and can be used to avoid this problem [152]. However, we found that projecting light in ring patterns with an inner diameter corresponding to the diameter of the well can also release bacteria from the wells while avoiding direct UV exposure **(Figure 2.11A-C).** Here, the membrane surrounding the perimeter of the well is removed, and the remaining membrane island likely diffuses into solution. This has the advantage that the bacteria inside the wells are not directly exposed to UV light, thereby reducing its effect. We found that irradiation of 40 μm diameter microwells with either full light circles or light ring patterns resulted in loss of the membrane above the wells **(Figure 2.11D).** In both cases, cells in targeted wells were released as observed by the diffuse mCherry fluorescence patterns **(Figure 2.11C).** Confocal microscopy after washing the wells **(Figure 2.11D, E)** confirmed that the bacteria were released for both light patterns. The ability to illuminate only the well perimeter is a critical feature of this approach, allowing the user to illuminate the surface with higher intensities and longer exposure times if necessary.

2.4. Experimental Section

2.4.1. Instrumentation.

2.4.1.1. Bright-Field and Fluorescence Microscopy.

All images were taken with an upright (BX51, Olympus Japan) microscope equipped with a 3S camera (Luminara, Ottawa, ON, Canada) controlled by the Infinity Capture Software unless otherwise stated. For experiments involving the Polygon400 (Mightex Systems), the camera was controlled by the Mightex Polyscan2 software. Greyscale images were processed and colored using ImageJ software [153] for visualization: blue for Polygon400 light patterns, red for mCherry, and green for fluorescein.

2.4.1.2. Confocal Laser Scanning Fluorescence Microscopy (CLSFM).

Fluorescent images were acquired on an Olympus FluoView FV1000-D confocal laser scanning fluorescence microscope equipped with 473 and 559 nm lasers and controlled by Fluoview software.

2.4.1.3. Polygon400 Light Patterning Instrument.

Light patterns were projected onto the membrane using the Polygon400 instrument attached to the BX51 upright microscope via an adapter containing a dichroic/filter cube. The 365 nm high-power LED source (50 W) was controlled by a BioLED light source control module and delivered to the Polygon400 with a liquid light guide **(Figure S8).** A BioLED analog and digital I/O control module provided computer control and TTL trigger when used with the LED controller. Size and shape of the pattern, light intensity as well as irradiation time were controlled with the Mightex PolyScan2 software. Approximate light intensities for the 10×/0.3NA and 20×/0.5NA objectives according to the manufacturer are 7 and 20 mW/mm2, respectively, with the LED source at

maximum intensity (100%). Prior to each experiment, the Polygon400 was calibrated with a mirror and the calibration software.

2.4.1.4. Measurements of Optical Densities and Growth Curves.

Optical densities (OD) of bacteria cultures (100 μL) at 600 nm were measured in 96 well plates on an Epoch2 microplate reader (Biotek). Time course experiments were done by measuring the OD at 600 nm using 100 μL of bacteria suspension in 96 well plates with a cover at 28 °C and with continuous orbital shaking at 237 cpm (cycles per minute).

2.4.1.5. ^{1}H NMR Spectroscopy.

^{1}H NMR spectra were recorded on a Varian Mercury 400 MHz or Varian System 500 MHz spectrometer in deuterated chloroform ($CDCl_3$) or dimethyl sulfoxide (d_6-DMSO). The number of scans was 32-64 and the D1 was 1 s for small compounds and 10 s for polymers.

2.4.1.6. Plasma Cleaner.

The plasma cleaner was a PDC-001-HGP instrument (Harrick Plasma).

2.4.1.7. pH Meter.

The pH of solutions was measured with an Oakton pH 700 instrument.

2.4.2. Materials.

2.4.2.1. Chemical Reagents.

N-hydroxy succinimide (NHS), dicyclohexyl carbodiimide (DCC) and poly(ethylene glycol) (PEG)-diamine (MW 3400), deuterated chloroform ($CDCl_3$), dimethyl sulfoxide (d_6-DMSO), phosphorpentoxide (P_4O_{10}), sodium phosphate dibasic (NaH_2PO_4), Alconox detergent, 4A molecular sieves, sodium hydroxide (NaOH), triethylamine (Et_3N), trichloro- (1H,1H,2H,2H-perfluorooctyl)silane, 1 M HCl (aq), and anhydrous toluene were purchased from Sigma-Aldrich. Four arm PEG-thiol (MW 10000) was purchased from NOF America Corporation.

Dimethylformamide (DMF), ethanol (EtOH), dichloromethane (CH_2Cl_2), ethyl acetate (EtOAc), diethyl ether (Et_2O), sodium hydrogen sulfate ($NaHSO_4$), anhydrous magnesium sulfate ($MgSO_4$), and isopropanol were purchased from Fisher. Fluorescein maleimide was purchased from Cayman. All chemicals were used as received unless stated otherwise. CH_2Cl_2 and Et_3N were dried over 4A molecular sieves. NB-COOH (for chemical structure see Scheme S1) was prepared in five steps starting from acetovanillone following reported procedures [143, 154, 155]. The ^1H NMR chemical shifts in $CDCl_3$ or d_6-DMSO for all intermediates were consistent with reported ^1H NMR chemical shifts.

2.4.2.2. Bacteria Culture.

Tryptone soy agar, yeast extract, kanamycin, isopropylthiogalactoside (IPTG), triphenyltetrazolium chloride (TTC), Tween20, and sodium chloride (NaCl) were purchased from Sigma-Aldrich. A. tumefaciens C58 pSRKKm-mCherry was prepared using established electroporation methods [156]. This plasmid carries the gene encoding the fluorescent protein mCherry under control of the lac promoter allowing for IPTG induction of mCherry expression [157].

2.4.3. Synthesis of the Photodegradable Poly(ethylene glycol) PEG Diacrylate.

The synthesis of this polymer has been reported [143] and was prepared in a different way by reacting PEG-diamine with the N-hydroxysuccinimide ester of the nitrobenzyl carboxylic acid as outlined in **Scheme S1**.

NB-NHS. NB-COOH (251.6 mg, 0.71 mmol) and 82.0 mg of (0.71 mmol) of NHS were dissolved in a mixture of 2 mL of DMF and 4 mL of CH_2Cl_2. The solution was cooled at 0 °C for 25 min before a solution of 146.9 mg (0.71 mmol) of DCC in 2 mL of CH_2Cl_2 was added. The mixture was stirred for 19 h. The suspension was concentrated in a flow of nitrogen and filtered through a

plug of glass wool inside a glass Pasteur pipet. The residue was washed with 2 mL of EtOAc and the filtrate diluted to 25 mL with the same solvent. The yellow solution was washed with water (3 × 25 mL), dried over $MgSO_4$, and concentrated in a flow of nitrogen. The solid was dried under reduced pressure to yield NB-NHS as a yellow solid in quantitative yield. ^{1}H NMR ($CDCl_3$) δ = 7.60 (s, 1H, CH_{aromat}), 7.01 (s, 1H, CH_{aromat}), 6.54 (m, 1H, CH), 6.43 (d, 1H, CH = CH_{trans}), 6.17 (dd, 1H, CH=CH_2), 5.87 (d, 1H, CH = CH_{cis}), 4.16 (t, 2H, CH_2O), 3.91 (s, 3H, OCH_3), 2.88 (t, 2H, CH_2CO), 2.84 (s, 4H, $COCH_2CH_2CO$), 2.29 (m, 2H, $CH_2CH_2CH_2$), 1.66 (d, 3H, CH_3CH).

2.4.3.1 Photodegradable PEG Diacrylate.

NB-NHS and PEG-diamine were dried under reduced pressure in the presence of P_4O_{10} at 40 °C to constant weight; 317.8 mg (0.71 mol, 4.2 equiv (eq) relative to amine) of NB-NHS was dissolved in 2 mL of CH_2Cl_2 and to the slightly hazy solution was added over the course of 5 min a solution of 290 mg (0.085 mmol, 0.17 mmol amine groups) of PEG-diamine and 29.7 μL (0.21 mmol) of Et_3N in 5 mL of CH_2Cl_2. The mixture became clear and was stirred in the dark at room temperature. After 23 h, the solution was concentrated in a flow of nitrogen and the residue suspended in 2 mL of CH_2Cl_2. The mixture was filtered and the residue washed with CH_2Cl_2 (2 × 2 mL). The filtrate was diluted with 100 mL of Et_2O to precipitate the polymer that was recovered by filtration through a glass filter. The residue was dissolved in 25 mL of 1 M $NaHSO_4$ (aq) and filtered (0.22 μm). The clear solution was extracted with CH_2Cl_2 (3 × 25 mL), dried over $MgSO_4$, and concentrated in a flow to a volume of 6 mL. This solution was diluted with 100 mL of Et_2O to precipitate the polymer. The polymer was recovered by filtration, dissolved in 8 mL CH_2Cl_2 and diluted with 100 mL of Et_2O. The precipitate was filtered, dried under reduced pressure to yield 267.1 mg of a faint yellow solid. 1H NMR ($CDCl_3$) δ = 7.58 (s, CH_{aromat}), 6.99 (s, 1H, CH_{aromat}), 6.51 (m, CH + NH), 6.42 (d, CH = CH_{trans}), 6.15 (dd, CH=CH_2), 5.86 (d, CH = CH_{cis}), 4.10 (t,

CH_2O), 3.92 (s, OCH_3), 4.18-3.26 (CH_2CH_2O), 2.38 (t, CH_2NH), 2.16 (m, $CH_2CH_2CH_2$), 1.64 (d, CH_3CH). The degree of functionalization for a MW = 3400 was 80% by comparing the integral ratios of the aromatic and CH_2CH_2 PEG protons. This degree of functionalization was considered when preparing the aqueous stock solutions.

2.4.4. Microwell Fabrication.

Microwell arrays were fabricated to contain a parylene liftoff mask to allocate cells in microwells while eliminating background cells, according to the procedures outlined in Hansen et al. [85]. Arrays were designed to contain wells with diameters ranging from 8 to 200 μm at different pitches.

2.4.5. Bacteria Culture.

LB medium was supplemented with 150 μg/mL kanamycin and 0.5 mM IPTG and prepared fresh for each experiment from frozen stocks stored at -20 °C. Under laminar flow a frozen 25% glycerol stock of A. tumefaciens was inoculated in 2 mL LB medium in round-bottom borosilicate glass tubes (13 mm × 100 mm, 10 mL, Globe Scientific). The culture tubes were closed with Bacti-caps (Clark Scientific) having openings to provide oxygen at atmospheric conditions inside the tube. Cultures were grown at 28 °C for 22 h by shaking at 200 rpm. After spinning down at 2000 g for 10 min the bacteria pellet was suspended in medium and diluted 1:250 in fresh medium (culture volume 2 mL). After 11 h at 28 °C and 200 rpm, the bacteria reached mid log phase and the culture had a typical OD of 0.2 (100 μL). The bacteria were spun down at 2000 g for 10 min and resuspended in 100 μL of fresh LB medium at the desired OD.

2.4.6. Membrane Fabrication.

2.4.6.1. Cross-Linking Buffers.

Phosphate buffered saline LB pH8 was prepared by adding NaH_2PO_4 to LB and adjusting the pH of the solution with 5 M NaOH (aq). The final phosphate concentration was 100 mM. This solution was sterile filtered (0.22 μm), lyophilized, and dissolved in half the volume of ultrapure water to make the 2× LB phosphate buffer solution used for membrane fabrication.

2.4.6.2. Membrane Precursor Solutions.

Solutions of four arm-PEG thiol and photodegradable PEG diacrylate in ultrapure water were sterile filtered (0.22 μm), aliquoted, lyophilized and stored at -20 °C for long-term use. Working solutions were prepared by dissolving aliquots in water to give four arm PEG thiol and photodegradable PEG diacrylate solutions with concentrations of 20 and 49 mM [141], respectively, and stored at -20 °C until use. Because of the high PEG concentration, the amount of water added to make the solutions was corrected by subtracting the volume of PEG calculated from the amount dissolved assuming a PEG density of 1 g/mL.

2.4.6.3. Perfluoroalkylated Glass Slides.

Five glass slides 25 × 75 × 1 mm (Fisher Scientific) were washed with 20 mL of a 2% w/v Alconox solution for 20 min with sonication inside a polypropylene slide mailer. Slides were then washed with ultrapure water (3 × 20 mL) and finally sonicated in water (20 mL) for 20 min. Slides were blown dry with nitrogen and both sides plasma treated for 2 min in air at 800 mTorr with the RF power set to high output (45 W). The slides were placed inside a slide mailer and 20 mL of 0.5% v/v of trichloro(1H,1H,2H,2H-perfluorooctyl)silane in toluene was added. After 3 h at room temperature, the slides were washed with toluene (3 × 20 mL) and EtOH (3 × 20 mL) and dried by blowing nitrogen. Slides prepared in this way were easier to separate after membrane

preparation compared to slides prepared by chemical vapor deposition under reduced pressure inside a vacuum desiccator. For long-term storage, the slides were kept in 70% isopropanol.

2.4.6.4. Spacers to Control Membrane Thickness.

Initial thickness of the membrane was controlled in the range 38 to 102 μm using steel thickness feeler gage poc-kit assortment blades (Precision Brand).

2.4.6.5. Encapsulation of A. tumefaciens Inside the Membrane.

Bacteria in the mid log phase were diluted to an OD of 0.2 (100 μL). The cell suspensions were spun down in a 500 μL Eppendorf tube and resuspended in the same volume of 2× LB phosphate buffer after supernatant removal. To 12.5 μL of bacteria suspension was added 5.6 μL of the photodegradable PEG diacrylate and the suspension was carefully mixed with the pipet, before 6.9 μL of the four-arm PEG thiol solution was added [141]. After careful mixing the mixture was pipetted (e.g., 4 × 6 μL) onto a glass slide having 102 μm spacers on opposite sides **(Figure S1).** A second glass slide was placed on top and left for 25 min at room temperature for thiol-acrylate cross-linking and subsequent hydrogel formation. After carefully separating the slides, membranes were washed with LB (5 × 1 mL) to remove nonencapsulated bacteria. The membranes were then placed inside a 24-well plate in 2 mL of LB and cultured in the incubator at 28 °C without shaking.

2.4.6.6. Cell Viability Assay.

TTC was dissolved in LB medium at 5 mg/mL and diluted 10-fold into LB medium containing the hydrogel.

2.4.6.7. Membrane Fabrication on Microwells Directly.

The microwell array was layered with 600 μL of medium and placed inside a desiccator. A vacuum was applied for 30 min to replace air trapped inside the wells with LB medium **(Figure S9).** For experiments without bacteria the surface was blotted at the sides with Kimwipes tissue paper and

the parylene carefully removed using Scotch tape [85]. For experiments with *A. tumefaciens*, the wells were inoculated with 600 μL of a bacteria suspension (OD = 0.2). After 1 h the bacteria suspension was removed with a pipet and the array carefully blotted with a Kimwipe before removing the parylene with Scotch tape. For microarrays without parylene coating, bacteria could also be removed with a PDMS slab after seeding [82]. Immediately after cell seeding, 12.5 μL of 2× LB phosphate buffer was mixed with 5.6 μL of the photodegradable PEG diacrylate and 6.9 μL of the four-arm PEG thiol, then 15 μL of the mixture pipetted onto a glass slide. The glass slide was inverted and placed on top of the microwell array having two 38 μm spacers on opposite sides **(Figure 2.1D)** and incubated at room temperature for 25 min for hydrogel formation. After careful separation of the glass slide from the microwell array, the membrane-covered microwell array was placed inside a rectangular well made of polydimethylsiloxane on a glass slide containing 1-2 mL of LB medium **(Figure S10)** and kept inside the incubator at 28 °C without shaking. This setup prevented drying up of the membrane and enabled easy handling of the microwell array on the microscope stage.

2.4.7. Membrane Degradation with the Polygon400.

The microarray with membrane was kept in LB medium during the experiments in order to prevent membrane dehydration and to dissipate local heating due to the LED light. In addition, immersion in the medium allowed PEG products cleaved from the membrane to solubilize and diffuse away from the wells during irradiation. The Polygon400 tool allows for exposure of a user-defined pattern light in any shape within the working area of the objective, as well as control of light intensity and irradiation time [158, 159]. Light patterning experiments were done using 10× and 20× objectives, corresponding to (maximum) rectangular working areas of 330 μm × 590 and 165 μm × 295 μm, respectively.

2.4.8. Fluorescent Labeling of the Membrane.

After light exposure, membranes were visualized by fluorescence microscopy by coupling pendant thiol groups with fluorescein maleimide [160]. 20 μL of a 10 mM stock solution of fluorescein maleimide in DMF was added to the microwell array in 1 mL of LB. This reaction occurs in the pH range 6.5-7.4 and was therefore done directly in LB (pH 6.7). Labeling was typically done for 2 h or overnight. Before image collection, the membrane was washed with LB (3 × 1 mL) to remove unreacted fluorophore.

2.4.9. Fixing Bacteria Inside the Membrane and Microwells.

The bacteria were fixed in 2.5% glutaraldehyde and 2.5% formaldehyde overnight in LB and washed with LB (3 × 1 mL) before the confocal microscope measurements.

2.4.10. Retrieval of Live Bacteria from Membrane-Covered Microwell Arrays.

A. tumefaciens was seeded at OD = 0.2 (100 μL), washed with LB medium (2 × 5 mL), placed inside a polystyrene Petri dish, and cultured for 24 h in 5 mL LB medium at 28 °C without shaking. The array was washed (2 × 5 mL) with extraction medium (0.05% Tween20 in LB) to remove any bacteria that could be present outside the membrane, and placed inside the sample holder. The array was again washed in the sample holder with extraction medium (4 × 2 mL) using a pipet. The washings were spun down at 2000 g for 10 min and the supernatant carefully removed leaving 1 mL inside the culture tube. This sample served as the negative control. The microarray was immersed in 1 mL extraction medium and a total of 72 wells were opened in four different runs. After the experiment, another 1 mL of extraction medium was added and the wells washed by pipet. After transferring the washing to a culture tube the microwell array was washed with additional extraction medium (3 × 2 mL). The washings were combined and spun down at 2000 g for 10 min and the supernatant carefully removed leaving 1 mL inside the culture tube. After

suspending with the pipet, a volume of 100 μL of retrieved bacteria and 100 μL of the negative control were placed inside the well plate and the OD at 600 nm was measured as a function of time inside a plate reader. The remaining (0.9 mL) solutions were placed inside an incubator at 28 °C and shaken at 200 rpm.

2.5. Conclusions

The retrieval capabilities demonstrated here connect the high-throughput screening benefits inherent to microwell array formats with the ability to extract, isolate, and enrich cells from any well of interest to determine molecular or phenotypic information about that cell population. The approach has potential to be used for follow-up characterizations on cell populations that show a desired and/or rare function. Follow-up assays could include but are not limited to whole genome sequencing, a variety of cellular functional assays, discovery of new strains or genotypes, and identification of genetic determinants of key phenotypes.

The proof-of-principle studies demonstrated here show that the photoresponsive membrane attaches to microwell substrates, confines bacteria while allowing for nutrient exchange and cell growth, and is degradable with patterned light for cell release and retrieval from any well of interest at high (20 μm) spatial precision. Key design features are the presence of the photoreactive nitrobenzyl group, allowing for polymer network degradation, thereby opening the wells in a spatially controlled manner using the Polygon400 pattern illumination instrument, and the ability to avoid direct exposure of cells to UV using patterned ring illumination. In our laboratory, these methodological advancements will be used for screening, 16S rRNA sequencing, and identification of environmental microbes with antagonistic or synergistic impacts on bacteria of key functional importance, such as A. tumefaciens and other pathogens. Although our focus is on

bacteria, the platform and method should be amendable for applications involving mammalian cells as well.

Chapter 3 : Exploiting stochastic cellular processes of a model system to generate outlier communities with rare phenotypes in microwell arrays

3.1 Background and Motivation

The goal of this work was to develop the platform for co-culture, using a dual-species interaction between two well-defined microbes, *A. tumefaciens* and *Pseudomonas aeruginosa*. This pair has high abundance and similarity in culture parameters [161] and a well-studied, competitive interaction in bulk and biofilm co-cultures, characterized by *P.aeruginosa* propagating over *A. tumefaciens* with quorum-regulated growth-rate and motility advantages [162]. *A. tumefaciens* is an important model bacterium whose study has yielded key insights into host-microbe signaling [95], bacterial cell-to-cell communication [96] and virulence mechanisms [93, 97]. Further, *A. tumefaciens* is a key plant biotechnology tool with strong agricultural relevance and an economically important pathogen of several crops [163]. Although, *A. tumefaciens*' pathogenesis and intraspecific interactions have been studied extensively [162], little is known about *A. tumefaciens* interactions with other members of plant microbiomes. Also, most of the functions of *A. tumefaciens* in plant soil are unknown. Identifying interactions that suppress *A. tumefaciens*' function will inform biocontrol strategies that use other microbes to attain antibiotic resistance against *A. tumefaciens*. The study of the competitive factors between these two bacteria can also produce novel insights on the development, nutrition, host finding and reproduction in co-culture systems [55, 164].

---

* This chapter consists of excerpts taken from the manuscript appearing in: Niloy Barua, Ashlee M Herken, Kyle R Stern, Sean Reese, Roger L Powers, Jennifer L Morrell-Falvey, Thomas G Platt, Ryan R Hansen. Simultaneous Discovery of Positive and Negative Interactions Among Rhizosphere Bacteria Using Microwell Recovery Arrays. *Frontiers in Microbiology*, 11: 601788 (2020). doi: 10.3389/fmicb.2020.601788
Reproduced with the permission from the Frontiers Media Limited.

3.2 Materials and Methods

3.2.1 Preparation of bacteria strains

Bacteria strains and plasmids used are listed (**Supplementary Table 1**). We introduced pSRKKm-sfGFP into *A. tumefaciens* C58 and pSRKKm-mcherry into *P. aeruginosa* PAO1 via mating with *Escherichia coli* S17-1 λpir carrying the respective plasmids using previously described methods [165]. These plasmids were transformed into competent S17-1 λpir *E. coli* strains using calcium chloride heat-shock transformation.

3.2.2 Bacteria Seeding and Trapping on Microwell Arrays

C58-GFP and PAO1-mCherry were grown in LB and YR343-GFP was grown in R2A media to mid-log phase and then resuspended in their respective growth media to an OD_{600} of 0.2. To inoculate microwell substrates, 700μL of this cell suspension was then incubated over an individual MRA substrate (**Supplementary Figure 2**) at room temperature for 1h. The substrates were dried and the parylene was peeled off of the microwell surface along with the cells attached to the background regions of the array by applying Scotch tape and forceps [85]. For studies involving C58-GFP and PAO1-mCherry co-culture, the seeding solution contained C58-GFP and PAO1-mCherry cells in a 1:1 or 1:100 ratio at a total OD_{600} of 0.1.

3.2.3 MRA design and fabrication

MRAs were designed to contain 10 μm diameter microwells etched to 20 μm well depths, spaced at a 30 μm pitch. The array consisted of a 7×7 grid of sub-arrays, each sub-array contained a 15×15 array of microwells, totalling 11,025 microwells available for analysis. Each well in the 15×15 sub-array was assigned with its own unique on-chip address for identification using brightfield microscopy (**Supplementary Figure 2**). Microwell arrays were fabricated on 3-inch diameter N-type silicon wafers (University Wafers) after coating with a 1μm thick layer of Parylene N (PDS

2010 Labcoater, Specialty Coating Systems. Arrays were then fabricated in a cleanroom environment using photolithography (**Supplementary Figure 3**) following previous protocols [85, 166, 167].

3.2.4 Time lapse fluorescence microscopy (TLFM)

A Nikon Eclipse Ti-E inverted microscope with NIS Elements software, a motorized XYZ stage, a humidified live-cell incubation chamber (Tokai Hit), and a DS-QiMc monochromatic digital camera was used for TLFM measurements. Seeded microwell arrays (with or without the photodegradable membrane) were attached to an LB-agar PDMS coverslip (**Supplementary Figure 4**). PDMS was required to enable sufficient oxygen diffusion into the wells during, prior experiments using glass coverslips resulted in poor culture for aerobic bacteria due to limited oxygen diffusion [85]. The substrate was then placed in a custom 3D printed scaffold designed to accommodate the microwell array while submerged under liquid media. The scaffold aided in image acquisition by maintaining a constant distance (100 μm) between the array and the glass slide, enabling the microwell substrate to stay within the focal plane during the culture period (**Supplementary Figure 5**). More information on microwell attachment to these materials and on the design of the scaffold can be found in the Supplementary information. The scaffold along with the inverted microwell substrate were then placed inside a humidified live-cell incubation chamber at 28ºC for imaging. A FITC filter was used to image C58-GFP strains (20×, 200 ms, 17.1× gain) and a TRITC filter was used to image PAO1-mCherry strains (20×, 300 ms, 17.1× gain). For YR343-GFP, images were taken with a FITC filter (20×, 300 ms, 36× gain) with a neutral density filter with 25% standard light intensity to minimize photobleaching. With these imaging conditions, individual cells within the wells could be resolved. Brightfield images were also taken at each section of the array after fluorescent imaging. Images of the microwell arrays were taken

every 60 minutes during culture. Green and red fluorescent images from the C58-GFP and PAO1-mCherry co-culture system were analyzed using Protein Array Analyzer tool in ImageJ to generate growth profiles for each organism. YR343-GFP in monoculture or mixed culture was evaluated using an image analysis routine in MATLAB to identify wells with highest and lowest growth levels for extraction.

3.2.5 Image Analysis

Time-lapse fluorescent microscopy and fluorescence-based image analysis can be routinely used to generate and access bacteria growth trajectories in this microwell format, as recently described by Timm *et al*. [137]. ImageJ was used to quantify growth trends of the C58-GFP and PAO1-mCherry. MATLAB was used to identify wells with highest and lowest levels of growth for YR343-GFP monoculture and co-culture studies. Here, simultaneous brightfield and fluorescence images of each array subsection consisting of 15×15 microwells were taken every hour for a 15 hr culture period. Brightfield and fluorescence images were imported and sorted based on subarray location, then the location of the wells was recorded and fluorescence intensities were averaged across each individual well and subtracted from background levels for each time point. Average growth rates and end point well intensities were then quantified across the entire microwell population. Outlier wells with highest levels of deviation in end-point fluorescence (t=12 h) were identified as target wells using the Grubb's outlier test [168] and their addresses were recorded. From these outlier wells, the top 5 growth promoting wells with highest average growth rates and top 4 antagonist wells with the lowest average growth rates were picked for extraction. In addition, 4 wells with nominal average growth rates were picked for extraction.

3.3 Results and discussions

3.3.1 Microwell Recovery Arrays enable parallel monitoring of microscale co-culture sites and generation of outlier wells with unique growth phenotypes

Our prior results demonstrated that microwell arrays could be used for parallel tracking of the growth of *P. aeruginosa* PAO1 communities during mono-culture in microwells, where small (5

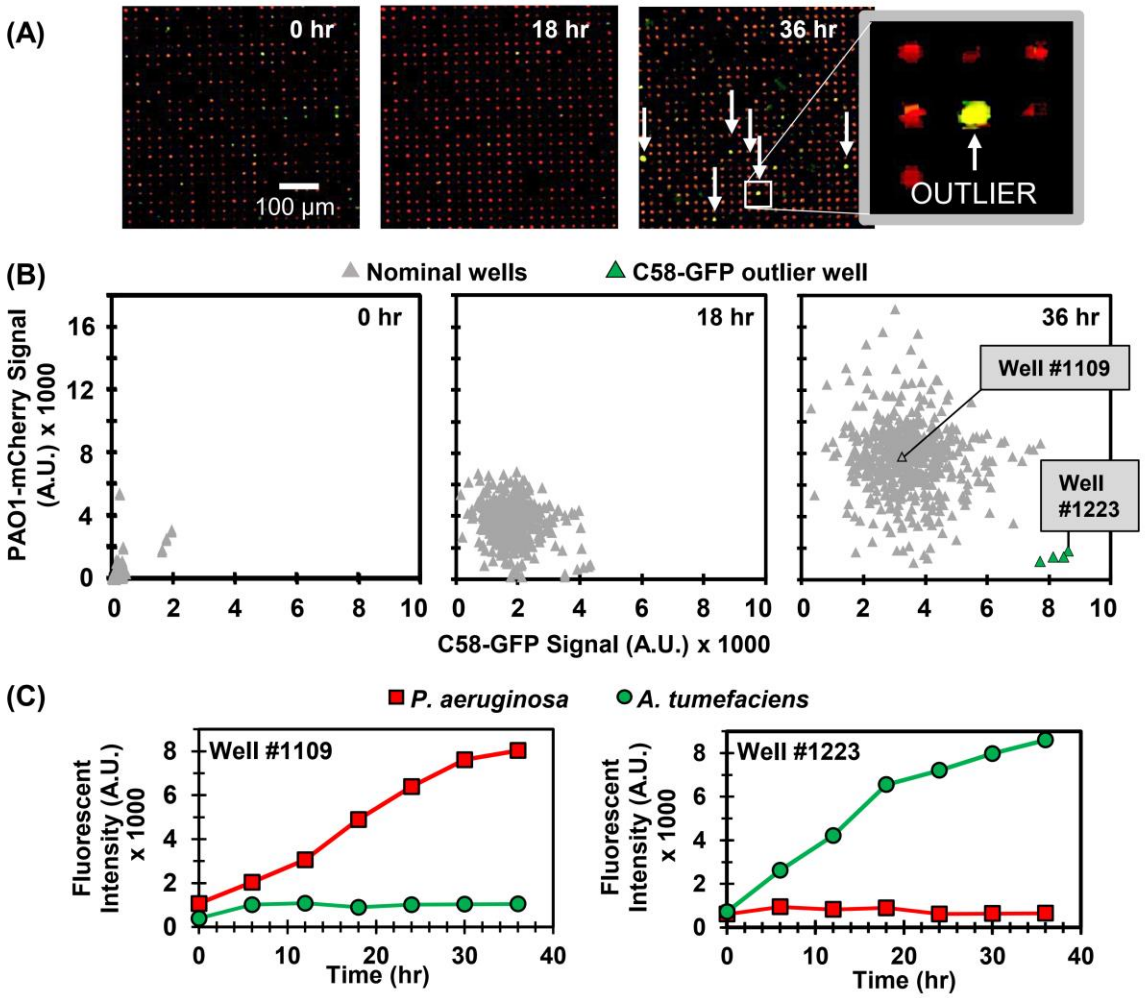

Figure 3.1: (A) Model C58-GFP (green) – PAO1-mCherry (red) co-culture in the MRA. Arrows indicate rare outlier wells where C58-GFP outgrew PAO1-mCherry. (B) Scatter plot of green (C58-GFP) versus red (PAO1-mCherry) well signals from a sample 549 well array at various time points. Outlier wells where C58 outgrew PAO1 are identified after the culture period (green). (C) Individual growth trajectories from a sample nominal well (well #1109), where PAO1 growth rate was significantly higher than that of C58 and an outlier well (Well #1223), where C58 outgrew PAO1.

and 10 μm diameter) wells were used to generate high variations in inoculum densities across the array during the seeding step, and growth outcomes were dependent on inoculum density and the level of spatial confinement present [85]. To develop the platform for multi-species co-culture, here we added *Agrobacterium tumefaciens* C58 to this system. Strains PAO1 and C58 have a well-characterized, competitive interaction *in vitro*, where PAO1 tends to outcompete C58 due to quorum sensing-regulated growth rate and motility advantages [98, 169]. A mixture of C58 cells expressing green fluorescent protein (GFP; hereafter C58-GFP) to PAO1 cells expressing mCherry protein (hereafter PAO1-mCherry) was inoculated into 10 μm diameter wells at a seeding concentration of OD_{600}=0.1). Based on our previous characterizations [85], we estimate that this results in ~20 cells per well. Under these conditions, PAO1-mCherry and C58-GFP cells are paired together at a high-dispersity due to the stochastic, Poisson seeding process [85]. C58-GFP:PAO1-mCherry seeding ratios of 1:1 and 1:100 were both investigated.

We observed similar qualitative outcomes at both seeding ratios. In each case, the MRA platform enabled parallel tracking of species growth according to the respective fluorescence emission signals from each addressable well during co-culture and end-point growth levels as well as signature growth profiles could be attained from each well with image analysis (**Figure 3.1**, **Supplementary Figure 7**). For the 1:100 seeding ratio, which was the seeding ratio used in the following studies, a comparison of end-point fluorescence signals after a 36 h co-culture period identified that the majority of the wells (96%) generated outcomes where PAO1-mCherry outgrew C58-GFP **(Figure 3.1B,C).** This was likely because of a favorable PAO1 seeding ratio, PAO1 growth advantages, or a combination of both factors. However, in the MRA format, outlier testing identified a minority (4%) of wells with communities dominated instead by C58-GFP cells after co-culture (**Figure 3.1B,D**). This finding reveals that high-dispersity microbe pairing between

competing species produces wells with rare growth outcomes after co-culture. Here, despite C58 cells being present at lower concentrations in the seeding solution, the stochastic seeding process generated a minority of wells with conditions allowing C58-GFP to grow well. This finding was leveraged towards more complex co-culture systems, where the stochastic seeding and parallel growth tracking features of the MRA are applied to screening interactions in environmental microbiomes.

3.4 Summary and Conclusion

In this project we successfully demonstrated the proof of concept of microwell arrays to detect rare phenotypes / rare growth outcomes in a well-characterized PAO1-C58 interaction system. We seeded bulk co-culture of the two fluorescently labeled species in microwell arrays to achieve stochastic assembly. With the aid of TLFM we could track the growth of both species in co-culture. It was demonstrated that in the majority of the wells, PAO1 suppressed the growth of C58, consistent with the claim that PAO1 can act as an antagonist against C58 in bulk co-culture. We could also identify rare outliers where C58 showed more enhanced growth than PAO1 when we had an inoculum ratio favorable for C58 growth. It is expected that by assembling a low number of cells in small wells we can identify rare outcomes driven by stochastic cellular processes. This technique will be used to screen and discover symbiotic and antagonistic interactions in the *Populus* root microbiome in Chapter 4.

Chapter 4 : Simultaneous Discovery of Positive and Negative Interactions Among Rhizosphere Bacteria Using Microwell Recovery Arrays

4.1 Overview

Understanding microbe-microbe interactions is critical to predict microbiome function and to construct communities for desired outcomes. Investigation of these interactions poses a significant challenge due to the lack of suitable experimental tools available. Here we present the Microwell Recovery Array, a new technology platform that screens interactions across a microbiome to uncover higher-order strain combinations that inhibit or promote the function of a focal species. One experimental trial generates 10^4 microbial communities that contain the focal species and a distinct random sample of uncharacterized cells from plant rhizosphere. Cells are sequentially recovered from individual wells that display highest or lowest levels of focal species growth using a high-resolution photopolymer extraction system. Interacting species are then identified and putative interactions are validated. Using this approach, we screen the poplar rhizosphere for strains affecting the growth of *Pantoea* sp. YR343, a plant growth promoting bacteria isolated from *Populus deltoides* rhizosphere. In one screen, we montiored 3600 microwells within the array to uncover multiple antagonistic *Stenotrophomonas* strains and a set of *Enterobacter* strains that promoted YR343 growth. The later demonstrates the unique ability of the platform to discover multi-membered consortia that generate emergent outcomes, thereby expanding the range of phenotypes that can be characterized from microbiomes. This knowledge will aid in the development of consortia for *Populus* production, while the platform offers a new approach for screening and discovery of microbial interactions, applicable to any microbiome.

---

* This chapter consists of excerpts taken from the manuscript appearing in: Niloy Barua, Ashlee M Herken, Kyle R Stern, Sean Reese, Roger L Powers, Jennifer L Morrell-Falvey, Thomas G Platt, Ryan R Hansen. Simultaneous Discovery of Positive and Negative Interactions Among Rhizosphere Bacteria Using Microwell Recovery Arrays. *Frontiers in Microbiology*, 11: 601788 (2020). doi: 10.3389/fmicb.2020.601788
Reproduced with the permission from the Frontiers Media Limited.

4.2 Introduction

Microbial communities are often highly diverse and have widespread impacts on human health [170, 171], agricultural productivity [17, 172], energy production [18, 173], and water quality [174, 175]. Interactions among the species and strains that co-occur within microbiomes often influence their function and the establishment and success of functionally important taxa [3]. While genomic and metagenomic approaches have transformed our ability to determine community composition and species co-occurrence patterns [176, 177], understanding how interactions amongst strains impact community structure and function remains difficult [14–16]. Despite this knowledge gap, there is a considerable need for understanding how natural community structure influences function, how communities respond to environmental pressures, and how communities can be constructed for engineered outcomes [13]. Engineered communities have provided ground-breaking approaches in a few applications such soil clean-up [8] and digestion of municipal solids [9], however the limited understanding of microbial interactions has impeded the use of synthetic communities in the majority of applications. For example, commercial development of plant growth promoting bacteria (PGPB) formulations for plant production has been limited by the fact that many useful bacterial species are incompatible with each other [20]. These limitations require the development of new experimental tools to holistically study and understand microbe-microbe interactions [10, 178].

The high species diversity of many microbiomes necessitates new screening tools that are designed to explore the vast number of potentially important microbe-microbe interactions. These tools must connect an observed cellular or community phenotype with genetic information from the interacting species as well as information on the interaction itself. Classical microbiological techniques for probing interactions rely on manually pairing isolates together [29],

inherently low-throughput approaches that in practice are often based on qualitative observations of bulk populations. Micro- and nanoscale devices offer vast improvements by providing high-throughput measurement, observation of single cell behavior, and precise design and manipulation of the microenvironment. These approaches have advanced our understanding of microbial mutualism [179], metabolite exchange [180], community adaptation to environmental pressures [42, 181], and the role of spatial structure in driving community phenotypes [27, 44, 182], among other findings. Recently, Kehe *et al.* [28] introduced the k-Chip, an innovative microscale platform designed to screen multi-membered communities consisting of various combinations of known isolates for emergent phenotypes. While these tools are expected to provide important advancements in our understanding of microbiomes, they are widely limited to on-chip measurements. Consequently, cells must be identified and manipulated during or prior to the screening observations, which greatly constrains both the number of strains that can be considered and undermines the ability to discover interactions involving unknown strains present in a microbiome.

Here, we present the microwell recovery array (MRA), a discovery-driven, lab-on-a-chip device designed to first screen interactions within mixtures of unknown environmental isolates taken from plant root microbiomes, then uncover pair-wise or multi-species communities that best antagonize or promote the function (e.g. growth) of a non-model focal species (**Figure 4.1**). The strategy uses microwells to randomly combine the focal species — typically one with a known beneficial function (e.g. plant growth promotion) or deleterious function (e.g. pathogenesis) — with a unique sample of cells from a microbiome into an array of microwells. Our previous studies demonstrated that seeding bacteria into small (2 to 10 μm diameter) wells enables only small numbers of cells to be seeded into wells, where the number of seeded cells shows high dispersity

across the array and follows a randomized, Poisson distribution - a process we refer to as stochastic seeding. Thus, even when a small number of unique species are present in the seeding solution, thousands of distinct, separated combinations of cells can be generated across the array for parallel observation [85].

Here, a 10 μm well diameter was chosen to confine a small number of interacting cells together at length scales similar to those found in multi-species biofilms [88], confinement at these length scales often facilitates inter-cellular interactions [89]. Cells are then trapped within the wells using a previously developed photodegradable polyethylene glycol (PEG)-based membrane [90], co-cultured, and then focal strain growth in each well is tracked with time lapse fluorescent microscopy (TLFM). Cellular communities showing a desired phenotype (e.g. highly enhanced or diminished focal species growth) can be extracted from any individual well using a patterned light source to spatially ablate the membrane, releasing cells into solution for recovery. The extraction and recovery capabilities are the key enabling features of the platform, allowing for sampling of a microbial community from any number of individual microwells that indicate a desired outcome, in a sequential fashion. Ultimately, this allows one to identify the interacting strains after the screening step. Relying on the stochastic seeding to generate randomized combinations between multiple species, thousands of distinct combinations of cells can be observed in a single screen. Extraction also enables follow-up phenotypic characterization with standardized assays to confirm the interaction.

To develop the approach, we first investigate co-culture in the MRA format using a well-characterized interaction between *Pseudomonas aeruginosa* and *Agrobacterium tumefaciens* [98, 169], followed by a microbiome screen using *Pantoea* sp. YR343 as the non-model focal species. Strain YR343 is a Gram-negative, plant growth promoting bacterium (PGPB) isolated from the

rhizosphere of an eastern cottonwood *Populus deltoides* tree [100, 183]. As *Populus* trees are promising biofuel feedstocks [101], uncovering interactions that influence the function of beneficial organisms in its rhizosphere has received intensive interest in recent years [102, 104, 184, 185]. However, due to the fact that the *Populus* root microbiome is highly complex and diverse, many microbe-microbe interactions are unknown [186]. *Pantoea* sp. YR343 can also colonize *Triticum aestivum* and stimulate lateral root formation [100, 183]. Likewise, related *Pantoea* strains have garnered interest for antibiotic production [105], bioremediation and waste recycling [109], and cancer treatment [187]. On the other hand, other *Pantoea* sp. can be pathogenic in plant, animal and human systems [188]. Thus, uncovering

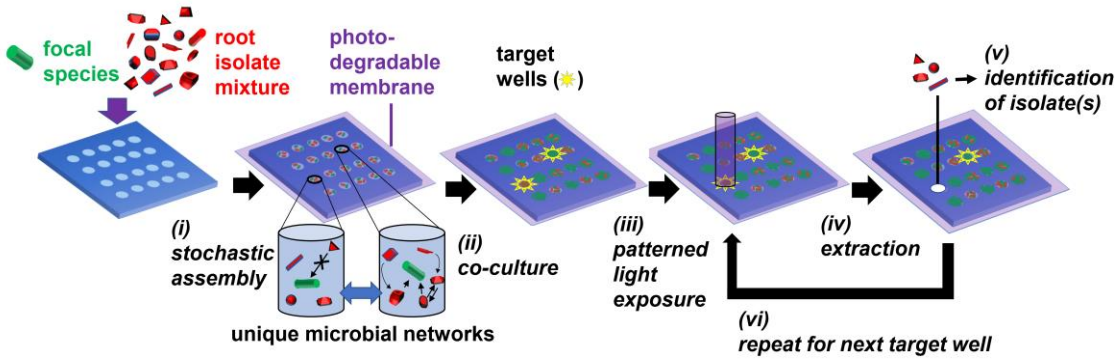

Figure 4.1: Microwell recovery arrays for screening microbe-microbe interactions. (i) GFP-expressing focal species are combined with a random combination of bacteria cells from an environmental microbiome in a stochastic seeding process. Different shapes represent unique microorganisms. (ii) Cells are trapped within their wells using a photodegradable PEG hydrogel membrane and monitored in parallel during co-culture using TLFM. (iii) The membrane is ablated over a target well showing highest or lowest levels of focal species growth using patterned light exposure, then (iv) isolates are extracted and recovered from an opened well. (v) Isolates are identified using 16S amplicon sequencing. (vi) Steps (iii-v) are repeated in iterative fashion to remove each community of interest.

unique sets of organisms that both promote or inhibit *Pantoea* growth, as demonstrated here, has use in several contexts.

4.3 Materials and methods

4.3.1 Preparation of bacteria strains and *P. trichocarpa* samples.

Bacteria strains and plasmids used are listed (**Supplementary Table 1**). *Pantoea* sp. YR343-GFP constitutively expresses EGFP from a chromosomal insertion as previously described by Bible *et al.* [183]. All strains and isolates used were stored in 25% glycerol at -80 ºC. Further information on *A. tumefaciens* C58, *P.aeruginosa* PAO1, and *Pantoea* sp. YR343 culture is included in Supplementary Information. For extraction of microbes from *Poplar* root, a sample of Nisqually-1 *Populus trichocarpa* root was first obtained from the greenhouse facilities at Oak Ridge National Laboratory. Roots were removed from soil and the aerial parts of the plant were separated from the root system. Large soil aggregates were removed by manually shaking by hand. The remaining portions of the roots were removed with sterile blades. Root pieces were then washed extensively with 1.5 L of sterile ice-cold PBS-tween20 solution (7 mM Na_2HPO_4, 3 mM NaH_2PO_4, pH 7.0 and 0.05% tween20). The washed solution was filtered through 0.45µm sterile syringe filters (Whatman) to remove larger particles in the suspension. The filtered solution was centrifuged for 15 min at 4400 rpm to obtain the pellet containing rhizosphere-enriched isolates (de Souza et al., 2016). Glycerol stocks were prepared for *P. trichocarpa* root isolates and stored frozen at -80°C. Bacterial cells were later revived by scrapping off a small amount of frozen cells using a sterile inoculation loop and mixing in 2 mL R2A broth media (pH: 7.2 ± 0.2, Teknova) in sterile test tubes and cultured for 24 hrs (28°C, 215 rpm). The community composition of both the rhizosphere-enriched isolate sample and the R2A media culture used to seed the microarray were analyzed using 16S rRNA community analysis (**Supplementary Figure 1**).

4.3.2 MRA design and fabrication.

MRAs were designed to contain 10 μm diameter microwells etched to 20 μm well depths, spaced at a 30 μm pitch. The array consisted of a 7×7 grid of sub-arrays, each sub-array contained a 15×15 array of microwells, totalling 11,025 microwells available for analysis. Each well in the 15×15 sub-array was assigned with its own unique on-chip address for identification using brightfield microscopy (**Supplementary Figure 2**). Microwell arrays were fabricated on 3-inch diameter N-type silicon wafers (University Wafers) after coating with a 1μm thick layer of Parylene N (PDS 2010 Labcoater, Specialty Coating Systems). Arrays were then fabricated in a cleanroom environment using photolithography (**Supplementary Figure 3**) following previous protocols [85, 166, 167].

4.3.3 Bacteria seeding and trapping on microwell arrays.

For studies involving YR343-GFP and *P. trichocarpa* rhizobiome co-culture, washed YR343-GFP cells and *P. trichocarpa* rhizobiome cells were mixed to achieve a YR343-GFP:isolate ratio of approximately 1:100 in the seeding solution at an OD_{600} of 0.2. To keep the cell concentrations of C58-GFP in co-culture experiments constant, PAO1-mcherry at OD_{600}=10 was added to C58-GFP at OD_{600}=0.1 to reach a C58-PAO1 ratio of 1:100. The inoculum was then diluted to OD_{600}=0.1 and 700μL of this inoculum was then seeded into microwell array substrates as described above. Similarly, OD_{600}=0.2 cultures of *P. trichocarpa* rhizobiome was mixed with OD_{600}=20 of YR343-GFP to reach a YR343-*P. trichocarpa* ratio of 1:100. This seeding suspension was diluted to OD_{600}=0.2 and seeded on top of microwell arrays for co-culture studies. For YR343-*P. trichocarpa* studies, the photodegradable membrane was then attached to the seeded array [90]. A schematic describing the seeding and trapping steps is provided (**Supplementary Figure 4**).

4.3.4 Time lapse fluorescence microscopy (TLFM)

A Nikon Eclipse Ti-E inverted microscope with NIS Elements software, a motorized XYZ stage, a humidified live-cell incubation chamber (Tokai Hit), and a DS-QiMc monochromatic digital camera was used for TLFM measurements. Seeded microwell arrays (with or without the photodegradable membrane) were attached to an LB-agar PDMS coverslip (**Supplementary Figure 4**). PDMS was required to enable sufficient oxygen diffusion into the wells during, prior experiments using glass coverslips resulted in poor culture for aerobic bacteria due to limited oxygen diffusion [85]. The substrate was then placed in a custom 3D printed scaffold designed to accommodate the microwell array while submerged under liquid media. The scaffold aided in image acquisition by maintaining a constant distance (100 μm) between the array and the glass slide, enabling the microwell substrate to stay within the focal plane during the culture period (**Supplementary Figure 5**). More information on microwell attachment to these materials and on the design of the scaffold can be found in the Supplementary information. The scaffold along with the inverted microwell substrate were then placed inside a humidified live-cell incubation chamber at 28ºC for imaging. A FITC filter was used to image C58-GFP strains (20×, 200 ms, 17.1× gain) and a TRITC filter was used to image PAO1-mCherry strains (20×, 300 ms, 17.1× gain). For YR343-GFP, images were taken with a FITC filter (20×, 300 ms, 36× gain) with a neutral density filter with 25% standard light intensity to minimize photobleaching. With these imaging conditions, individual cells within the wells could be resolved. Brightfield images were also taken at each section of the array after fluorescent imaging. Images of the microwell arrays were taken every 60 minutes during culture. Green and red fluorescent images from the C58-GFP and PAO1-mCherry co-culture system were analyzed using Protein Array Analyzer tool in ImageJ to generate growth profiles for each organism. YR343-GFP in monoculture or mixed culture was evaluated

using an image analysis routine in MATLAB to identify wells with highest and lowest growth levels for extraction.

4.3.5 Image Analysis

Time-lapse fluorescent microscopy and fluorescence-based image analysis can be routinely used to generate and access bacteria growth trajectories in this microwell format, as recently described by Timm *et al*. [137]. ImageJ was used to quantify growth trends of the C58-GFP and PAO1-mCherry. MATLAB was used to identify wells with highest and lowest levels of growth for YR343-GFP monoculture and co-culture studies. Here, simultaneous brightfield and fluorescence images of each array subsection consisting of 15×15 microwells were taken every hour for a 15 hr culture period. Brightfield and fluorescence images were imported and sorted based on subarray location, then the location of the wells was recorded and fluorescence intensities were averaged across each individual well and subtracted from background levels for each time point. Average growth rates and end point well intensities were then quantified across the entire microwell population. Outlier wells with highest levels of deviation in end-point fluorescence (t=12 h) were identified as target wells using the Grubb's outlier test [168] and their addresses were recorded. From these outlier wells, the top 5 growth promoting wells with highest average growth rates and top 4 antagonist wells with the lowest average growth rates were picked for extraction. In addition, 4 wells with nominal average growth rates were picked for extraction.

4.3.6 Recovery of isolates from wells and isolate naming convention.

The extraction procedure was slightly modified from van der Vlies *et al.* which was previously developed for highly efficient removal of cells from individual wells with minimal cross-talks, thus offering well-specific extraction [90] and is described in Supplementary Information. Extraction occurred from the microwell array in a sequential fashion, first from five different target

wells in which YR343-GFP exhibited promoted growth (P1, P2, P3, P4, P5), then four different target wells in which YR343-GFP exhibited antagonized growth (A1, A2, A3, A4) and finally four different target wells in which YR343-GFP exhibited intermediate growth (N1, N2, N3, N4). Extracts from each well were plated onto solid R2A media (28°C, overnight) for recovery. After culture, five distinct isolates (A, B, C, D, and E) were picked based on unique colony morphology and streak purified. Isolates in **Supplementary Figure 6** are thus labelled according to the microwell they were isolated from, then the order at which it was extracted from the array, then the order at which it was picked from the plate after recovery. For example, isolate A4A, the isolate that most strongly antagonizes YR343 growth, was extracted from the fourth antagonistic well and was the first colony picked from the R2A plate. Following extraction, extract containing the suspension of cells from an individual microwell was plated onto R2A media. Colonies were again cultured in liquid media overnight (28ºC, 215 rpm) and stored in glycerol stocks at -80°C.

4.3.7 Identification with 16S rRNA sequencing.

Individual colonies were cultured in R2A media and genomic DNA of each isolate was extracted using the Promega (Madison, WI) Wizard® DNA Purification kit, diluted to 20 ng/µL in 20µL aliquots and sent to Genewiz (South Plainfield, NJ, USA) for 16S ribosomal RNA (rRNA) Sanger sequencing of the V1 to V9 regions, enabling identification with approximately genus-level specificity. The sequences were aligned using MUSCLE [189] and generated a maximum likelihood phylogenetic tree based on partial 16S rRNA sequences (1007 bp) using PhyML 3.3.20190909 [190] with 1000 bootstrap replicates and using the Smart Model Selection [191] tool based on Akaike Information Criterion, a starting tree estimated using BIONJ, and the NNI method for tree topology improvement.

4.3.8 Validation using 96 well plate cultures

To obtain cell free culture fluid (CFCF) from individual isolates, each isolate was cultured (28ºC, 3000 rpm) in 2mL of R2A broth media overnight, and then cells were removed from the media by centrifugation (2000g, 10 min). To obtain CFCF from combinatorial mixtures, isolate panels were inoculated individually in R2A media and cultured overnight, followed by cell removal by centrifugation. CFCF from each isolate was then mixed together at equal volumes to obtain combinatorial CFCF. To obtain conditioned media, isolate or combinatorial CFCF was mixed with YR343-GFP in fresh R2A media at a 1:1 volumetric ratio to reach an initial OD_{600} value of 0.1 (final volume = 100 µL), at which point growth was quantified with a Biotek Epoch 2 Multi-Mode Microplate Reader (28 ºC, 300rpm). Unconditioned media was obtained following the same procedure except 1X PBS was added to fresh R2A media instead of isolate CFCF. To verify the OD_{600} measurement was due to YR343-GFP growth, CFCF from selected isolates without inoculation of YR343 was also measured. A total of n=6 independent replicates were measured for each culture condition. Growth rates and carrying capacities of each condition were quantified using Growthcurver [192] and compared using the Wilcoxon two-sample test.

4.4 Results and discussion

4.4.1 Co-culture of Pantoea sp. YR343 with stochastically assembled communities from the P. trichocarpa rhizosphere simultaneously generates positive and negative YR343 growth outcomes.

To extend the microwell platform capabilities to screening non-model test species against unknown isolates, we screened rhizobiome samples from the *P. trichocarpa* root microbiome for

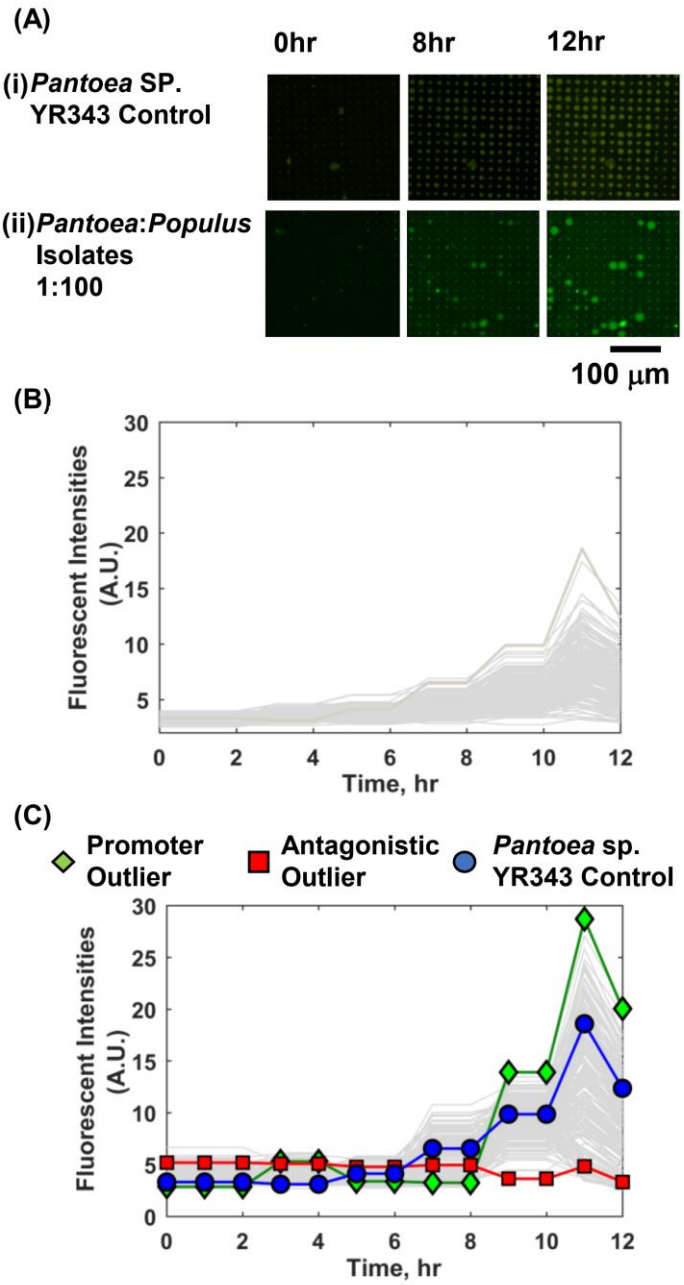

Figure 4.2: YR343-GFP growth in mono-culture and co-culture within 10 µm microwells. **(A)** TLFM images of a sample 15×15 array of microwells after (i) seeding only YR343-GFP or (ii) seeding YR343-GFP with isolates from a *P. trichocarpa* rhizobiome. **(B)** Growth curves generated from a sample 900 microwell array during YR343-GFP mono-culture, or **(C)** YR343-GFP co-culture with rhizosphere isolates. Outlier wells representing growth promoting and antagonistic communities, respectively were identified from the growth curves.

effects on the growth of focal species *Pantoea* sp. YR343 expressing GFP (hereafter denoted YR343-GFP). Here, we used stochastic seeding, attachment of the photodegradable PEG

membrane [90], and focal species growth monitoring to identify rare combinations of cells generating unique YR343-GFP growth profiles (**Figure 4.1**, steps i and ii). To characterize the composition of the seeding solution, 16S community analysis was used (**Supplementary Figure 1**) and we observed 120 OTUs from the root washing and 85 OTUs after culturing the root washing in R2A media to prepare the isolate mixture used to seed the wells. Thus, it was expected that the YR-343 focal species is combined with random samplings of cells belonging to 85 different OTUs in wells throughout the array.

Cell mixtures were seeded into 10 μm diameter microwells at high density (OD_{600} = 0.2) and at a 1:100 YR343:isolate ratio, cultured, and growth kinetics in each well were tracked over the course of 12 h using TLFM. Based on prior results [85], we estimate this seeding condition generates ~35 cells/well. The 1:100 seeding ratio follows the from the previous system and ensures that the focal species will be combined with several unknown isolates in each well during the co-culture. For comparison, monoculture arrays consisting of only YR343-GFP focal species was used as a control. In each case, YR343-GFP growth was evaluated in 225 co-culture microwells from a 15×15 well grid (**Supplementary Figure 2**) across 16 selected arrays on a single substrate (n=3600 microwells total). Here, R2A media was chosen as a generalist culture media. This media has been used to recover more than 300 phylogenetically diverse isolates from *P. trichocarpa* rhizosphere and endosphere samples, and so should permit co-culture of a large number of combinatorial strain mixtures within the microwell environment [184]. While the YR343-GFP monoculture generated growth profiles across the array with relatively low variance (σ^2=3.55) according to final end-point fluorescence levels, mixed cultures generated a wider range of growth profiles, with final growth levels of higher variance (σ^2=17.55), indicating an impact due to the addition of the environmental isolates (**Figure 4.2A-C**).

In co-culture, 14% of the wells contained microcolonies that appeared to grow out of the wells and into the membrane space, causing the microcolony diameter to expand beyond the well diameter (>10 µm) (**Figure 4.2Aii**), indicating a positive interaction. While the locations on the array where this effect occurred appeared random, we checked for the possibility of crosstalk between

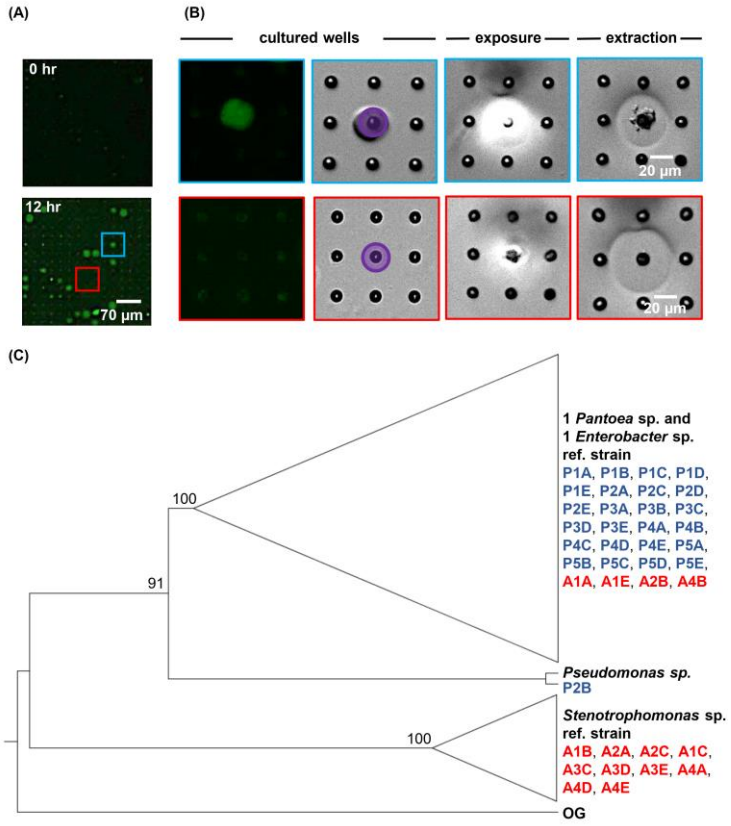

Figure 4.3: Sequential removal of growth-promoting and antagonistic communities from an array sub-section after co-culture. (A) Microwell array before and after co-culture. This 15×15 microwell array contained both a YR343 growth promoting community (blue) and YR343 antagonistic (red) community that were targeted for extraction. (B) Targeted removal of the microwell community in which YR343 grows to its highest observed end-point fluorescence (top row, blue outline), followed by targeted removal of a microwell community in which YR343-GFP grew poorly (bottom row, red outline). Purple area denotes UV exposure area used for membrane degradation. (C) Maximum likelihood phylogenetic tree based on partial 16S rRNA sequences (1007 sites) of select reference strains and isolates extracted from promoted (P) and antagonized (A) wells. We collapsed the branches of the monophyletic group composed of Enterobacter sp. and Pantoea sp. strains and the clade of Stenotrophomonas sp. strains. *A. tumefaciens* C58 was used as the outgroup (OG) organism and the following reference strains were included: *Pantoea* sp. YR343, *Enterobacter cloacae* E3442, *Pseudomonas putida* S13.1.2, *Stenotrophomonas maltophilia* NCTC10259. We labelled nodes with corresponding bootstrap percentages.

neighboring wells, where a developing microcolony may influence growth in another well due to diffusion of metabolites or other biomolecular products. Of wells with this enhanced growth phenotype, 2% of neighboring wells also showed this phenotype, suggesting that well-to-well crosstalk can occur. The possiblity of falsely identifying an interaction due to well-to-well crosstalk is accounted for with follow-up, off-chip validation experiments that verify the interaction after it is found in the inital screen (described in Section 3.4). On the other end, wells showing decreases in well fluorescence signal were also identified, these decreases were caused by lysis of the focal species and GFP diffusion from the wells, as previously observed when using PAO1 as the focal species [85]. This effect was noted in 34% of co-culture microwells. Wells that initially contained a fluorescent signal above background levels, followed by highest decreases in fluorescence signal were identified as containing candidate cells antagonistic to YR343-GFP. This ensured that these wells initially contained the focal species, and that its growth was inhibited during co-culture. The rest of the wells did not show evident increases or decreases in YR343-GFP growth.

4.4.2 Sequential extraction, recovery and identification of isolates from microwell communities.

Following on-chip analysis in mixed culture arrays, the patterned illumination tool was used to extract communities from the five wells with highest fluorescence signal after 12 hours of culture (**Figure 4.3A, B**). This was followed by extraction of communities from four wells with the lowest levels of YR343-GFP growth, and four wells where YR343-GFP grew to intermediate levels. Extraction required exposure of a patterned 365 nm light (20 mW/cm^2, 10 min) to remove the membrane over the well. While 365nm light has the potential to damage bacteria, these exposure conditions were previously found suitable for retrieving viable bacteria from wells [90]. Membrane

removal was confirmed by brightfield microscopy, at which point cellular material was observed moving out of the wells and into solution (**Figure 4.3B**). After exposure, arrays were washed with extraction buffer (R2A media + 0.05% Tween20 solution) to retrieve cells from an opened well. Extraction buffer was then plated onto R2A-agar for growth and recovery of individual colonies. During our previous characterizations of this procedure, we noted that >99.9% of bacteria originated from opened wells as opposed to outside contamination [90], which provided high confidence that the recovered product here originated from the target well. We also previously observed that bacteria could be completely removed from wells after washing [90], thus we expected minimal cross-contamination when opening additional wells for further sampling. After recovery, phylogenetic analysis based on 16S rRNA sequences of all strains isolated from each targeted microwell was performed (**Supplementary Figure 6**). The analysis revealed that all extracted microwells identified as growth promoting for YR343-GFP (5 of 5) harbored *Enterobacter* sp. / *Pantoea* sp. strains, and one of these wells contained at least one *Pseudomonas* sp. strain. In stark contrast, all wells identified as antagonistic to YR343-GFP contained at least one *Stenotrophomonas* sp. strain. Several of these wells (3 of 4) also contained at least one *Enterobacter* sp. or *Pantoea* sp. strain (**Figure 4.3C**). All isolates obtained from the wells with nominal effects on YR343-GFP are phylogenetically related to *Enterobacter* sp. and *Pantoea* sp. strains. Given that the extraction method was efficient and specific for recovering cells from the targeted wells [90], the recovered isolates were expected to be responsible for the promoting or antagonistic effects on YR343, but required validation with an independent, off-chip test.

4.4.3 Interactions can be recapitulated in 96-well plate format for validation.

The extraction of cellular communities from the MRA allows for off-chip validation and characterization of the microbial interactions observed during the screen. This capability is critical

for validation, as the high density of microwells (625 wells/mm^2) has potential to cause false positives, perhaps due well-to-well cross-talk due to diffusion of molecules. This necessitates that

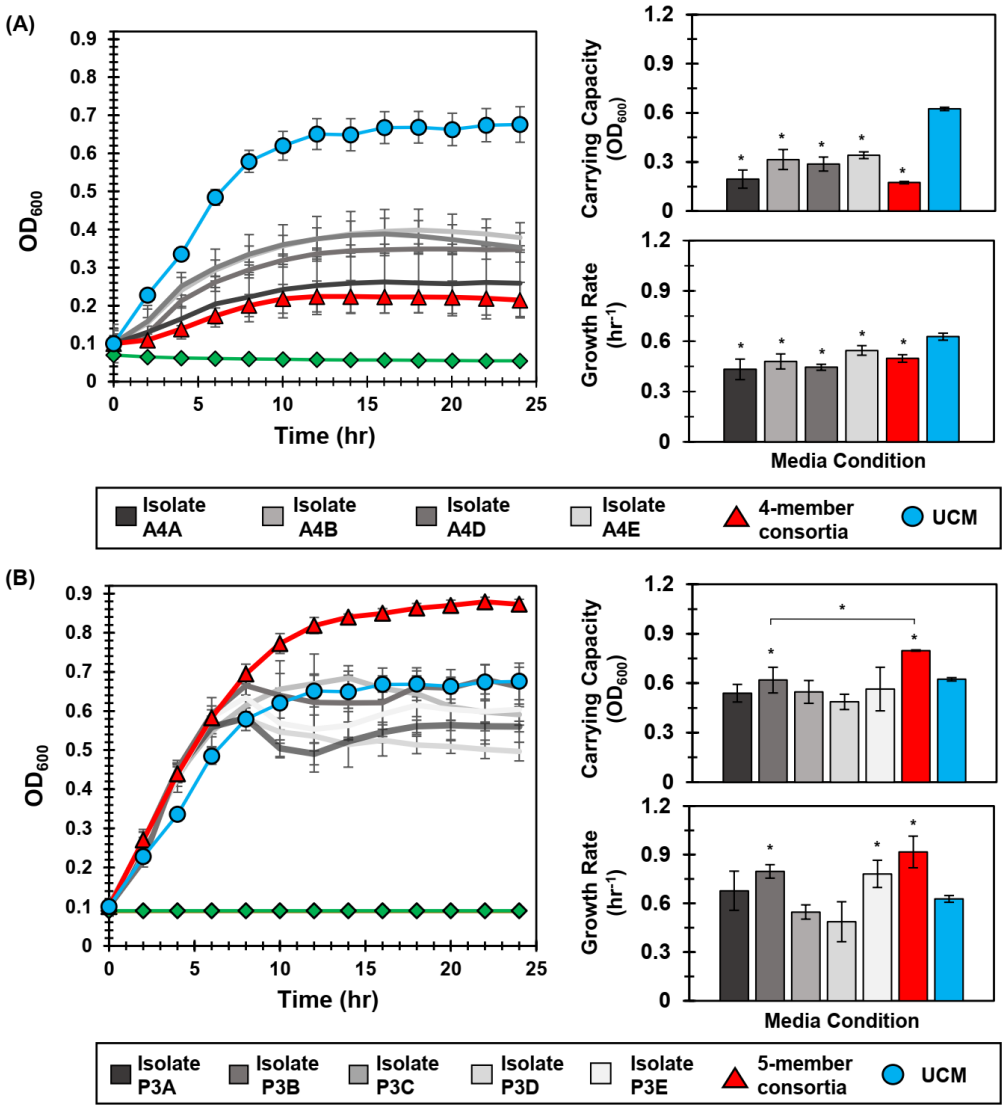

Figure 4.4: Interactions identified in the MRA can be validated in 96-well plate format. (A) Left: YR343 growth curves after inoculation into conditioned media from the antagonistic isolate, the isolate consortia, or unconditioned media (UCM). The control (green line) is conditioned media that was not inoculated with YR343 to verify that there was no growth carry over or contaminating microbes present. Right: Corresponding carrying capacity and growth rates for each growth curve. (B) Left: Analogous YR343 growth curves after inoculation into conditioned media from a promoter isolate or the promoter isolate combination. Right: Corresponding carrying capacity and growth rates. All growth experiments occurred at 28°C, 215 RPM. Statistical differences were identified by comparison of growth metrics between YR343 culture in conditioned media from each isolate or isolate mixture and YR343 growth in UCM (Wilcoxon two-sample test, *=P<0.01, n=6 independent experiments).

the interactions observed in the screen are also observed in an independent validation assay. To address this, we used a 96-well plate format to measure how strains isolated from MRA influenced the growth of YR343-GFP. This represented a scaled-up environment (from 1.6 pL microwell volumes to 100 µL solution volumes) that precludes diffusive crosstalk from neighboring wells.

For these evaluations, we hypothesized that both growth promotion and inhibition measured in MRA format resulted from diffusive interactions between the focal species and the collection of isolates present within a well. To test this hypothesis, YR343-GFP was cultured in 96-well plate format in media conditioned by four selected isolates recovered from a selected antagonist well (Well A4, **Supplementary Figure 6**). Conditioned media was obtained by first culturing isolates in R2A media to stationary phase, then removing the cells to obtain cell free culture fluid (CFCF). Fresh R2A media was then added to the CFCF in a 1:1 volumetric ratio to supply growth nutrients, and YR343-GFP was inoculated for growth monitoring. Conditioned media obtained using CFCF from a combined co-culture of all 4 antagonistic strains was also evaluated. These growth curves were compared to a control curve with YR343-GFP growth in unconditioned media, which consisted of R2A media instead supplemented with blank 1X PBS buffer at the same volumetric ratio. A second control curve consisting of conditioned media without YR343 inoculum was also included to verify that measured growth was not due to contaminating microbes. Growthcurver R was then used to estimate bacterial carrying capacity and growth rate [192] in each experiment (**Supplementary Figure 8**). Congruent with microwell observations, we observed that conditioned media from 4 isolates significantly reduced the carrying capacity and growth rate of YR343-GFP compared to its culture in unconditioned media (**Figure 4.4A**). Conditioned media from the combined 4-member antagonist combination also showed significantly lower carrying capacity and growth rate compared to the unconditioned

control media (**Supplementary Tables 2, 3**). CFCF from *Stenotrophomonas* isolate A4A had statistically equivalent growth metrics as that from the CFCF consortia, suggesting that this strain is the most potent inhibitor of YR343.

To investigate the effect of the strains identified as YR343 growth promoters, YR343-GFP growth was again monitored in media conditioned with CFCF from clonal cultures, here using 5 isolates selected from a selected promoter well (Well P3, **Supplementary Figure 6**). To test for an emergent effect, additional control curves from conditioned media containing CFCF produced from a co-culture of the combined 5 isolates was also evaluated. When YR343 growth in conditioned media from the CFCF of individual isolates was measured, only two were able to increase growth rate and one was able to increase carrying capacity (**Figure 4.4B, Supplementary Figure 9**). Strikingly however, the CFCF from the 5-member consortia was able to provide highest increases in both YR343 growth rate and carrying capacity. The 5-member consortia also provided a statistically significant increase in carrying capacity compared to isolate P3B, the individual isolate that generated the highest increase in YR343 carrying capacity after conditioning media on its own (**Supplementary Tables 4**, **5**). To further verify that antagonistic or promoting behavior was unique to the strains isolated from the promoting and inhibitory microwells, the same 96-well plate analysis was performed using nominal isolates taken from a microwell that showed intermediate growth of YR343-GFP during on-chip co-culture. This served as a final control to verify the 96-well plate assay accurately recapitulates growth behavior observed on the MRA. Here, a well with final endpoint growth level comparable to YR343 monoculture was identified and 4 isolates were extracted from the well. YR343-GFP growth was then monitored in media conditioned with CFCF from clonal cultures and the combined 4 member consortia cultures. YR343 growth in conditioned media from the CFCF of individual isolates and the CFCF from the

4-member consortia did not provide significant increases or decreases in YR343 growth rate or carrying capacity (**Supplementary Figures 10, 11; Supplementary Tables 6, 7**).

Taken together, these findings indicate that the observed enhancement of YR343's population growth corresponds with the behavior observed in the microwell environment, and that in some cases it can depend on the presence of multiple strains, not simply the consequence of a pairwise interaction. As such, the enhanced YR343 growth is an emergent property of the community of species recovered using the MRA, demonstrating the unique power of this approach to identify functions dependent on higher-order interactions among bacterial species.

4.5 Conclusions

The MRA examines thousands of combinatorial unique, multi-species communities to discover both antagonistic and growth promoting interactions on a focal species. Using this new approach, we simultaneously identified individual strains that antagonize focal species growth, as well as multi-strain consortia that uniquely promotes focal species growth only when co-cultured in combination. The platform is the first of its kind, unique because it (i) screens organisms that are unknown during the screening step, dramatically expanding the number of interactions and cellular combinations that can be accommodated, and (ii) screens in combinatorial fashion to uncover higher-order microbial networks that generate emergent phenotypes, which cannot be measured with other platforms or devices. The platform allows for the user to perform the co-culture in a defined culture medium, which must be carefully selected based on the question or goal of the screen. The key innovation underlying this capability is the ability to recover cells from specific microwells of interest, thereby allowing for subsequent off-chip genetic characterization for species identification then phenotypic characterization for validation of the interaction. This enables one to input any number of bacteria strains into the device for analysis. Extraction then

enables one to steamline the screen with established techniques, such as -omic based analysis of samples and follow-up validation of the uncovered interactions using standardized methods, as demonstrated in this work. In our laboratory, MRA fabrication and materials cost ~$20 per screen, which compares favorably to other comparable techniques such as flourescence-activated cell sorting (FACS), which often has a higher associated cost ($100-$200/hr) and is not directly amenable to a co-culture format. The improved throughput at which different interactions can be tested also provides a significant saving in both time and effort.

For the first generation of the MRA, we have developed its use towards screening interactions that influence growth phenotypes. A drawback of the current platform is that it screens interactions based on growth in an environment that is both chemically and physically different than the rhizosphere, thus interactions that are identified in the MRA must still be evaluated in the relevant natural enviornment (e.g. *in vivo*). Also, the MRA requires that the interacting isolates are also culturable in the media added, limiting the number of interactions that can be accounted for. Finally, the user should excersize caution when extracting cells using the 365 nm light source, as this wavelength can have a bactericidal effect. If direct UV exposure is a concern, the pattern of light can be varied to expose only the edges or sides of the wells, which is also effective in releasing cells from wells and the hydrogel membrane while minimizing light exposure [90]. Despite these current limitations, the MRA approach has potential to be expanded towards screening microbiomes for organisms that have positive or negative effects on other focal species functions, provided that the function can be coupled to a fluorescence reporter (e.g. a GFP promoter-reporter). This may include microbial interactions that affect quorum sensing activation [193], virulence factor expression [194], and plasmid conjugation [195], to name a few. While demonstrated here for the *P. trichocarpa* root microbiome, the platform is directly amenable to screening interactions

across any microbiome where high species diversity is present, which may include the gut, soil, freshwater and marine ecosystems, and other rhizosphere environments.

Chapter 5 : Microwell Recovery Array Screening of the Maize Rhizosphere to Improve *Azospirillum brasilense* Colonization and Plant Growth Outcomes

5.1 Overview

Plant growth-promoting bacteria (PGPB) are key for sustainable food production and may alleviate negative impacts of chemical fertilizers on human health and environment. Successful application requires PGPB survival and colonization into the root microbiome, which is influenced by interactions with other microbes present. This paper develops the microwell recovery array (MRA), a microfabricated high-throughput screening device, as a novel bioprospecting tool to rapidly isolate and discover bacteria that improve *Azospirillum brasilense* colonization in corn root. The device simultaneously tests 10^4 interactions between *A. brasilense* and members of the *Zea mays* rhizobiome. In a single test, the MRA isolated *Serratia marcescens*, *Serratia nematodiphila*, *Serratia ureilytica*, *Pantoea agglomerans*, *Enterobacter tabaci*, and *Acinetobacter bereziniae*, which were confirmed as symbiotes to *A. brasilense* using off-chip validation assays. Isolates were then co-inoculated with *A. brasilense* on axenic maize seedlings inside a plant growth chamber and accelerated plant growth after 15 days, only when co-inoculated with *A. brasilense*. Follow-up root colonization assays identified that isolates also increased *A. brasilense* levels. These findings uncover new interactions useful for developing improved PGPB consortia and demonstrate that the MRA tool can rapidly explore complex environmental microbiomes for new isolates useful for generating positive phenotypic outcomes on a host.

Manuscript: Barua N., Clouse M.K., Wagner M., Diaz D.R., Platt T.G., Hansen. R., Microwell Recovery Array Screening of the Maize Rhizosphere to Improve *Azospirillum brasilense* Colonization and Plant Growth Outcomes., *In preparation*.

5.2. Introduction

Increasing crop production and enhancing plant health in a sustainable manner is critical in the face of climate change [196], increasing population [197], reduction of cultivable lands [198], and pest or pathogen mediated diseases in crops [110, 199]. While chemical fertilizers and pesticides have significantly contributed to enhancing food production [110], their indiscriminate use has proven unsustainable and negatively impacts human and environmental health [111]. Much effort has been given to exploiting plant growth-promoting bacteria (PGPB) as bioinoculants, i.e., biofertilizers, to enhance plant growth [112, 113] and address the limitations of chemical approaches. Biofertilizers offer a low energy, environmentally friendly, and sustainable approach to promoting plant growth and increasing biomass production by nitrogen fixation [196, 200], phytohormone synthesis [201], stimulating root development [202], pathogen defense [203], and alleviating environmental [204] and human-induced stresses [13, 196].

Currently, the biofertilizer market is dominated by diazotroph PGPB, such as *Rhizobium spp., Bradyrhizobium spp., Actinorhizobium spp., Azotobacter spp., and Azospirillum spp.* [114, 205]. *A. brasilense* is the most widely adopted diazotroph, and it displays versatile C- and N-metabolism. It also promotes plant growth through additional mechanisms, including phytohormone production [115], development of stress tolerance [114], inhibition of phytopathogens [116], solubilization of phosphates [117] and production of siderophores [118]. With this array of benefits, much effort has been given to understanding the microbial interactions that influence the association and colonization of *A. brasilense* and other diazotroph bacteria with non-leguminous maize (*Zea mays*) crops [119–121, 206]. Prior studies have also shown that co-inoculation of *A. brasilense* with complimentary organisms such as *Bradyrhizobium* [207, 208] and cyanobacteria isolates [209–

212] improves maize yield, suggesting that PGPB applied as symbiotic, multi-species consortia may be key for biofertilizer improvement.

Despite its importance in food production, most interactions that influence PGPB in the root environment remain poorly understood [112, 113] and as a result, PGPB are often unreliable and pose a high economic risk amongst agricultural producers, limiting broad adoption of N-fixing PGPB [20, 110]. Uncovering favorable PGPB interactions is a daunting task due high species diversity and abundance in the native root microbiome, which also varies widely due to differences in soil type/conditioning, irrigation, and climate at different producer sites [213]. Such a task necessitates development of new high-throughput screening technologies that can rapidly explore interactions in a microbiome and accelerate the pace of discovery. Here, microwell recovery arrays (MRAs) [85, 90, 214] were used to rapidly search the maize (*Zea mays L.*) rhizosphere microbiome for bacteria that improve *A. brasilense* colonization on corn roots for accelerated plant growth.

To develop this approach, rhizosphere isolates from *Zea mays L.* were first collected from agricultural soils at a producer site in central Kansas and the composition of the microbial communities was analyzed with 16S community analysis to identify the culture medium that recovers the highest diversity of isolates. Then, *A. brasilense* species Sp7 expressing GFP [215] (herein referred to as Sp7) and small numbers of maize rhizosphere isolates are inoculated into individual microwells. Due to the randomized cell seeding process characterized previously [85, 139], only a few isolates are partitioned into each well with Sp7, thus wells are compositionally unique from each other. Cells in the MRA are then co-cultured and Sp7 growth is monitored in parallel using time-lapse fluorescent microscopy (TLFM). Image analysis reveals the location of individual wells containing bacteria symbiotic to *A. brasilense* by increasing its growth rate and final growth level. Equipped with a photoresponsive hydrogel membrane extraction system and a

patterned light source [90], the MRA system can then selectively remove isolates from any individual well where a favorable effect on *A. brasilense* growth is found. Isolates are identified with 16S sequencing, interactions are validated in 96-well plate co-cultures, and symbiotic isolates are then applied in seedling co-inoculations to study their effect on *A. brasilense* root colonization

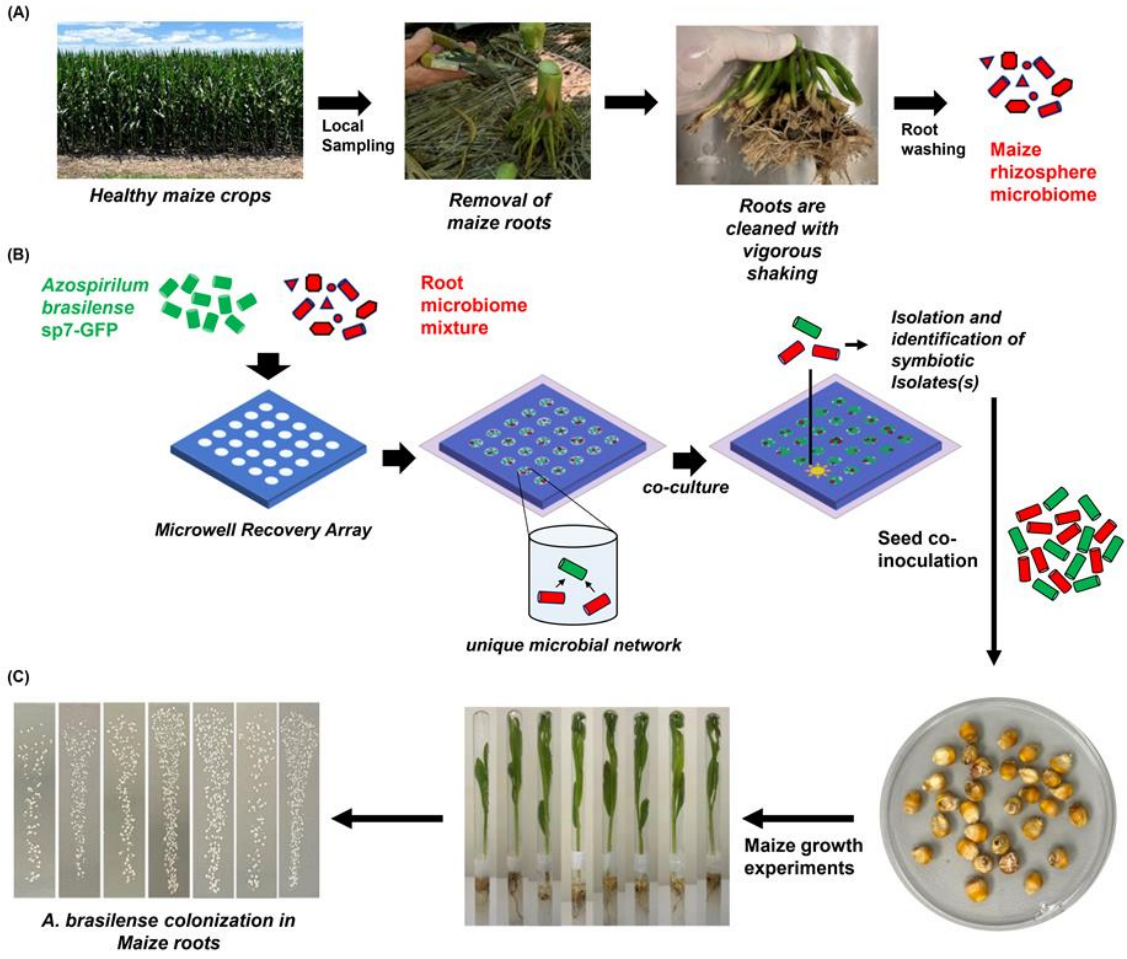

Figure 5.1: MRAs for discovery of isolates that improve the colonization of *A. brasilense* in maize roots. (A) Healthy maize crops are picked in the flowering season for extraction of the rhizosphere microbiome. Stems are cut from the roots, soil is removed, and roots are washed to collect the rhizosphere microbiome. Different shapes represent unique microorganisms. (B) GFP-expressing *A. brasilense* strain Sp7 is combined with random isolates from the maize rhizosphere microbiome in 10 mm diameter microwells and trapped a photodegradable PEG hydrogel membrane. The growth of Sp7 was monitored in parallel during co-culture using TLFM, and the wells showing the highest level of Sp7 growth were extracted by selective ablation of the photodegradable membrane using patterned light exposure. The isolates extracted and recovered from the opened wells were then identified using 16S amplicon sequencing. (C) Isolates were co-inoculated with *A. brasilense* on healthy maize seeds (genotype B73), and plant growth studies were conducted to measure Sp7 colonization in maize roots and resulting plant growth.

and plant development (**Figure 5.1**). Here, we demonstrate that with one screen, the successful discovery of a panel of new isolates, each of which enhanced *A. brasilense*-mediated plant development, can be uncovered. This demonstrates the unique ability of the MRA as a bioprospecting tool that can rapidly access an environmental microbiome and uncover new strains with potential application as biofertilizers. Similar MRA methodology can be followed for screening for root and soil microbiomes for biocontrol agents or for discovery of bacteria producing new antimicrobial compounds.

5.3. Experimental Methods

5.3.1 Extraction and culture of *Zea mays* root isolates

Soil and root samples were collected from four sampling sites at Budke field (co-ordinate: 39.3533616 and -98.362541, 1147 m above sea level) and four sampling sites at Boyde field (co-ordinate: 39.3950754 and -98.3470027, 968 m above sea level) at Glen Eder, Kansas during the flower blooming season. The soil samples were sent to K-State Soil Testing Lab for a complete analysis of carbon, nitrogen, phosphorous content, and soil pH. The comprehensive analysis of the soil samples from the two fields is listed in **Supplementary Table 1**. A total of 8 sets of rhizosphere soil and root samples were collected from maize plants grown in both fields (**Figure 5.1A**). The rhizosphere soil and root samples were immediately kept on ice, transferred to the laboratory, and stored at 4 ºC. The suspensions were extracted by washing 200 g of each rhizosphere soil and root samples with 200mL of sterile, ice-cold 1X phosphate buffer saline (PBS buffer: 8 g/L NaCl, 0.2 g/L KCL, 0.2 g/L KH_2PO_4,1.15 g/L Na_2HPO_4, pH 7) for 20 minutes [216]. The resulting suspensions were sterile filtered using 0.8 µm sterile filters and suspended at 4400

rpm for 20 minutes to collect pellets containing rhizosphere isolates. Pellets containing *Zea mays* rhizosphere isolates were stored at -80ºC in 25% glycerol [214].

5.3.2 Media selection

Bacterial colonies of *Zea mays* rhizosphere samples were picked up from glycerol stocks using a sterile inoculation loop and incubated in TY Media (10g/L Bacto-tryptone, 10g/L NaCl, 5g/L Yeast Extract, pH: 7 ± 0.2), R2A media (0.50 g/L Yeast extract, 0.50 g/L Proteose Peptone, 0.50g/L Casamino acids, 0.50 g/L Glucose, 0.50 g/L Soluble starch, 0.30 g/L Na-pyruvate, 0.30 g/L K_2HPO_4, 0.05 g/L $MgSO_4.7H_2O$, pH: 7 ± 0.2), LB media (10g/L Tryptone, 10g/L NaCl, 5g/L Yeast Extract, pH: 7 ± 0.2), in sterile test tubes for 24 hrs (28°C, 215 rpm). After incubation, rhizosphere-enriched pellets from each culture media were stored at -80ºC in 25% glycerol before the selection, classification, and 16S community analysis to detect the media that recovered the highest diversity of *Zea mays* rhizosphere isolates.

5.3.3 16S community analysis of *Zea mays* root isolates

Purified gDNA samples of the *Zea mays* rhizosphere and their cultures in TY, R2A, and LB media were extracted using E.Z.N.A soil DNA kit (Omega Bio-Tek, Norcross, GA) and DNeasy Blood & Tissue Kit (Qiagen, Germantown, MD), diluted to 20 ng/µL in 100 µL aliquots and sent to Integrated Genomics Facility (Department of Plant Pathology, Kansas State University, Manhattan, KS) for 16S Illumina sequencing of the hypervariable V3 and V4 region using Nextera XT index Kit v2 (Illumina, Inc., San Diego, CA). 16S rRNA community analysis was performed with Qiime2-2020.8 (Bolyen et al., 2019). The multiplexed raw sequence data with the barcodes were demultiplexed using q2-demux plugin, quality filtered, and denoised with q2-dada2 (Callahan et al., 2016) plugin aligned with mafft (Katoh et al., 2002). The q2-diversity plugin was used to determine alpha-diversity metrics (observed OTUs [217] and Shannon's diversity index

[218] after the rarefaction of the samples to 900 sequences per sample. Taxonomy was assigned to amplicon sequence variants using the silva-138-99-515-806 [219] classify-sklearn naïve Bayes taxonomy classifier against the Silva 138 99% O.T.U.s reference sequences [220]. The q2-taxa plugin was used to explore and visualize the taxonomic composition of the classified sequences by creating taxa bar plots [221] for the *Zea maize* rhizobiome.

5.3.4 MRA design and fabrication

MRAs were fabricated by following the protocols described by Barua *et al.* [214]. Each array was divided into a 7×7 grid of sub-arrays, consisting of a 15×15 microwell arrays of 10 µm diameter, 20 µm depth, and 30 µm pitch. A total of 11,025 microwells were etched on a single 3-inch diameter N-type silicon wafer (University Wafers), coated with 1 µm thick layer of Parylene N (PDS 2010 Labcoater, Specialty Coating Systems), using standard photolithography techniques described in previous publications [166, 167].

5.3.5 Bacteria seeding and trapping in microwell arrays

A. brasilense SP7-GFP and *Zea mays* rhizosphere isolates were cultured in LB, R2A and TY media to mid-log phase and resuspended in their respective growth media to an OD_{600} of 0.1. Bacteria cells were inoculated in microwell arrays using protocols described previously (**Figure 5.1B**) [90, 139, 214]. For co-culture studies, cultures of SP7 (OD_{600}=0.1) and *Zea mays* rhizosphere isolates were mixed at a ratio of 1:1 to reach a final OD_{600} of 0.1. 700 µL of each cell suspension was seeded on top of microwell arrays for 1 hr at room temperature for co-culture studies. Then, the substrates were dried, followed by the parylene lift-off process to remove cells attached to the array's background regions [85, 90, 214].

5.3.6 Photodegradable membrane attachment

A novel poly-ethylene glycol (PEG) photodegradable membrane was attached on top of the MRA seeded with cells by following previously described methods [90]. The protocol for the attachment of the photodegradable membrane is described in detail in supplementary information.

5.3.7 Time-lapse fluorescent microscopy and image analysis

Wells were monitored with TLFM and outlier wells showing improved *A. brasilense* growth in the MRA were identified using image analysis in ImageJ. TLFM and image analysis methods have been described previously [214] and are also included in supplementary information.

5.3.8 Recovery and storage of Isolates from microwell arrays

Isolates were extracted from microwell arrays following previously described procedures [90, 214]. The top two individual wells (A, B) with enhanced growth of Sp7 were opened by exposing them to a UV lighted in a ring pattern area with a 10 μm inner diameter and a 20 μm outer diameter to minimize cellular damage. The individual isolate cell suspensions were then plated onto agar growth media after extraction, and three colonies were sampled from each extracted microwell based on differences in colony morphology and color. Then individual colonies were cultured in respective media and stored in glycerol stocks to remove each isolate's genomic DNA. A total of 8 individual promoter isolates were recovered in this process and labeled as isolate A1, A2, A3, A4, B1, B2, B3, B4 for validation.

5.3.9 Validation using 96-well plates

It was previously demonstrated that the interactions observed in the promoter wells in MRA can be recapitulated in a 96-well plate validation assay [214]. Same methodology was applied to

validate the growth enhancement of *A. brasilense* in co-culture with the eight individual promoter isolates. The methods for the validation assays are included in the supplementary information.

5.3.9 Identification of promoter isolates, culture and storage

Eight individual isolates were identified with 16S rRNA sequencing described in the supplementary information. Six bacteria species capable of enhancing *A. brasilense* growth were identified as *Acinetobacter bereziniae*, *Pantoea agglomerans*, *Serratia ureilytica*, *Serratia marcescens*, *Serratia nematodiphila*, and *Enterobacter tabaci.* Bacterial strains were streaked in R2A agar plates and incubated at 28°C for 24 hrs. A single colony of each strain was inoculated in 2 mL of R2A broth at 28 °C and 215 rpm overnight and stored in glycerol at -80°C.

5.3.10 Plant growth studies to validate survival and colonization of *A.brasilense SP7-GFP*

Plant growth studies were conducted to validate the enhancement of *Zea mays* growth and SP7 survival and colonization in maize roots in the presence of SP7 combined with each of the six bacterial strains using the protocol described by Niu and Kolter [222]. First, a small colony from the frozen stocks of the six bacterial strains and SP7 were inoculated in 2 mL of R2A broth at 28°C and 215 rpm overnight. 50 µL of overnight culture of each strain was transferred to 2 mL of fresh R2A broth and cultured for another 8 hr at 28°C. Cells were suspended at 4400 rpm for 10 min and resuspended in 1X PBS. Cell suspensions were diluted to ~10^8 cells per milliliter for each strain. Each cell suspension was mixed with SP7 in 50 mL falcon tubes in equal volume to prepare the dual-species bacterial suspensions [222]. 80 surface-sterilized and germinated maize seedlings were soaked in the six co-culture cell suspensions, SP7 monoculture cell suspension, mono-culture control cell suspensions of six individual isolates, and a sterile 1X PBS control, without shaking at room temperature for 1 hr. The maize seedlings adhered to bacteria, and the sterile seedlings

were transferred onto 20 ml ½ Murashige and Skoog (MS) agar (0.8%) in 16 x 150 mm glass tubes with sterile forceps**.** Sterile empty glass tubes of the same size were attached to the tubes containing seeds in a mouth-to-mouth way using porous air porous tape [222]. Sealed glass tubes were then placed in test tube racks and were transferred in a growth chamber under the conditions mentioned above, and the growth of the maize seedlings was observed for 15 days to measure root lengths and SP7 colonization in the maize roots in combination with one of the six bacterial strains (**Figure 5.1C**).

5.3.11 Quantification of *A.brasilense SP7-GFP* colonization on maize roots

Three maize seedlings inoculated with SP7 monoculture and co-culture with one of the six bacteria strains were sampled on day 15 after inoculation. Roots from each maize seedling were cut and washed with sterile 1x PBS to remove agar adhered to the root surface. A 1-cm long primary root fragent below the maize kernel was then cut and transferred into 1.5 mL centrifuge tubes containing six glass beads (diameter: 3 mm, Propper) and 1 mL sterile 1x PBS buffer. The bacterial cells colonized on the root surfaces were dislodged by sonicating (amplitude: 30%; pulse: on 01 sec, off 01 sec; time: 30 sec) for 1 min, then vortexing for another 1 min. This step was repeated twice, and the tube was put on ice for 1 min. The bacteria cell suspensions were collected and sequentially diluted by a dilution factor of 10^8. 10 µL of the diluted bacterial suspensions were spotted on R2A agar plates supplemented with 200 µg/mL of ampicillin and 10 µg/mL of tetracycline**.** The plates were tilted to spread the cells on agar surfaces and air-dried before incubating the plates at 28 °C in the dark for 16 to 60 hrs. The numbers of the colony-forming units (CFUs) were counted and recorded to calculate SP7 abundance in the roots colonized with SP7 monoculture and co-culture with the six bacterial strains using the following formula [222]:

$$\textit{A. brasilense}\ \text{SP7-GFP abundance} = \frac{\text{CFU number} \times 100 \times \text{Dilution times}}{\text{Weight of root fragent (mg)}} \quad (1)$$

5.4. Results and Discussions

5.4.1 Development of the Microwell Recovery Arrays for Screening the *Zea mays L.* Rhizobiome for Isolates Symbiotic to *A. brasilense*.

To screen interactions between *Zea mays* rhizosphere isolates and Sp7, it was first necessary to identify nutrient media that recovered the highest taxonomic diversity. This ensured that a maximum number of interactions would be observed during co-culture. Here, LB, TY, and R2A media were used to culture the rhizosphere microbiome of *Zea mays* L., cultures were then characterized using 16S community analysis. Sequencing unveiled 368 OTUs from the root washing, 233 OTUs after culturing the root washing in LB media, 330 OTUs after culturing the root washing in TY media, and 351 OTUs after culturing the root washing in R2A (**Supplementary Figure 1A**). Shannon's diversity indexes for the isolates after root washing and after culture in LB, TY, and R2A media were 11.51, 9.334, 10.829, and 11.436, respectively (**Supplementary Figure 1B**). Taxonomic bar plots for the rhizosphere microbiome showed members of four bacterial phyla (Proteobacteria, Firmicutes, Bacteroidetes, and Actinobacteria), with *Pseudomonas*, *Serratia*, *Salmonella*, and *Bacillus* genus making up the majority of the communities (**Figure 5.2A**). Based on the highest number of OTUs and the highest Shannon's diversity index, R2A media was selected as the culture media for the MRA screen.

After media selection, the MRA was used to screen for unknown interactions between the *Zea mays L* rhizobiome samples and *A. brasilense* strain Sp7-GFP. Prior MRA screens used 10 μm diameter wells to confine bacteria together and facilitate interaction, and bacteria were seeded at a concentration of OD_{600} = 0.2. Such conditions generated inoculum densities of ~35 cells/well, where each well was inoculated with a unique multispecies combination of bacteria [85, 214]. These conditions were again used here, cells were then trapped inside wells by attaching a

photodegradable PEG membrane [90] and growth of Sp7 in each well was tracked during culture over 24 hrs using TLFM (**Supplementary Figure 2,3, and 4**). Growth kinetics were compared to those of Sp7 monoculture control arrays to identify wells showing Sp7 growth promotion. Both monoculture and co-cultures were evaluated across 3600 microwells.

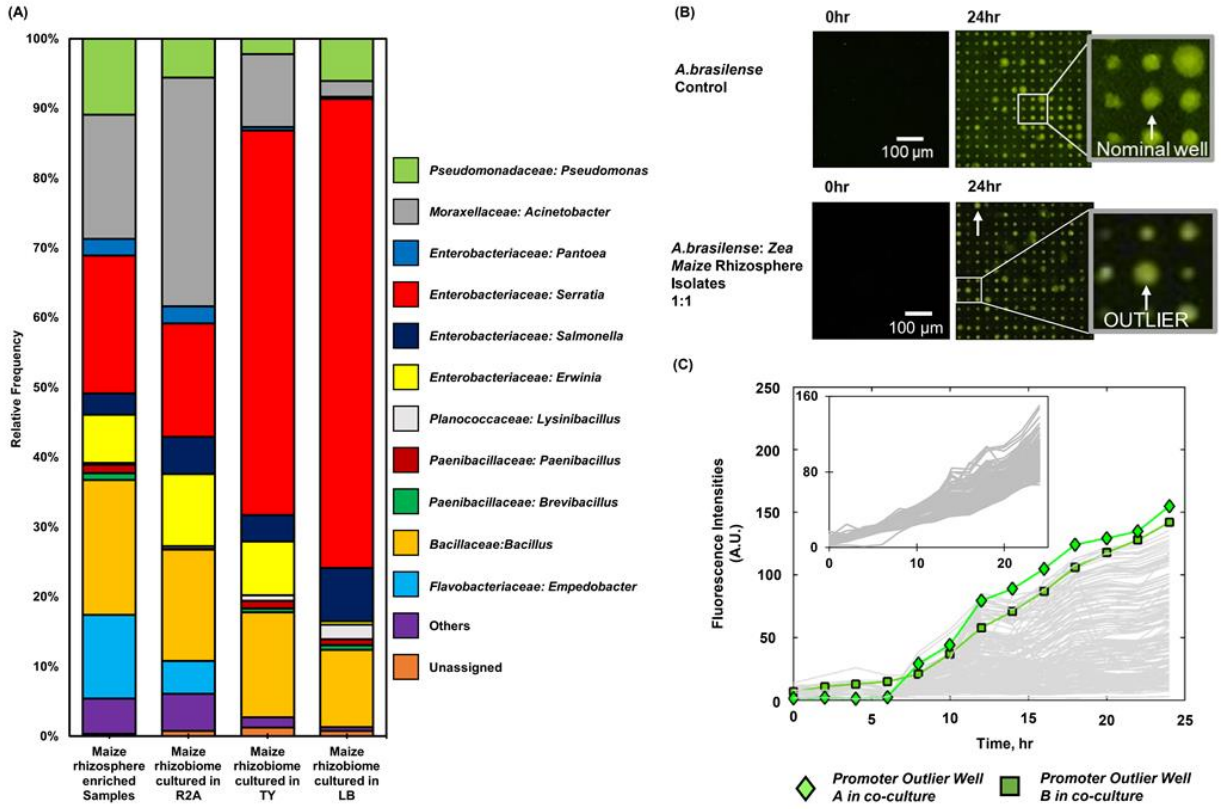

Figure 5.2: (A) Taxanomic bar plots of *Zea mays* rhizosphere enriched samples from roots and after culture in R2A, TY, and LB media. (B) TLFM images of a sample 15×15 array of microwells during monoculture of *A. brasilense* Sp7-GFP or during co-culture of *A. brasilense* Sp7-GFP with *Zea mays L.* rhizosphere isolates seeded into wells at a Sp7:isolate ratio of 1:1. The promoter outlier well A (indicated by the white square) and the promoter outlier well B (indicated by the white arrow) demonstrated the highest end-point fluorescent signal and growth rate of Sp7. (C) Sp7 growth curves generated from a sample 900 microwell array during Sp7 monoculture (inset) and co-culture.

Compared to the monoculture control, significant changes in Sp7 growth metrics were observed on co-culture. Averaged endpoint fluorescence levels of Sp7 monoculture across the measured wells (n=3600 wells) showed relatively low variance (σ^2=67) compared to co-culture (σ^2=553), indicating an impact due to the addition of the rhizosphere microbiome (**Figure 5.2B**). Individual

wells with increases in growth rates and final growth levels (**Figure 5.2C**) were also frequently observed. Wells containing Sp7 symbiotic interactions were detected by comparing both endpoint fluorescent signals and growth rates of Sp7 to monoculture wells using Grubb's outlier testing [168]. The top two outlier wells (well A and B) with highest growth rates and end-point fluorescence signals of Sp7 (**Figure 5.2B**) were picked using Grubb's outlier testing as the promoter wells containing the most potent symbionts of Sp7. A noticeable lag time was observed for Sp7 growth in promoter outlier wells compared to the monoculture wells. But the promoter

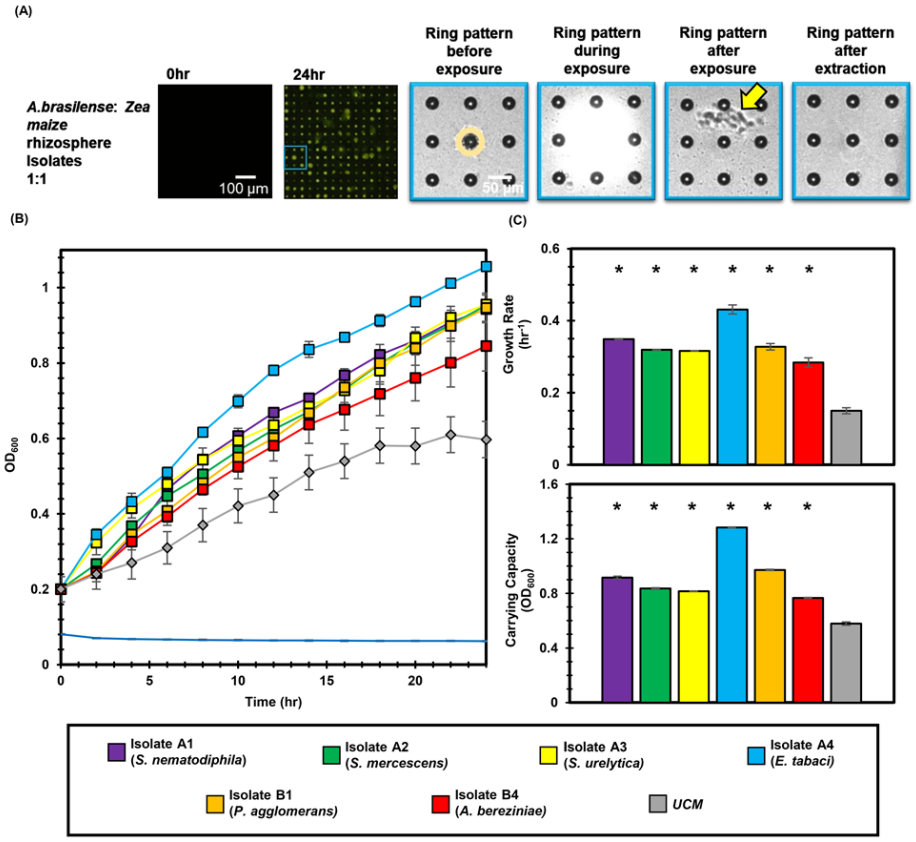

Figure 5.3 Isolate extraction and validation of interactions. **(A)** Sequential removal of symbiotic communities from Sp7 co-culture with maize root isolates. Target wells were exposed to UV light in a ring pattern with a 10 µm inner diameter and a 20 µm outer diameter to remove the photodegradable membrane above the well. After degradation, cells were washed out of the opened wells using R2A media. Yellow arrow denotes bacteria cells during removal from a well. **(B)** Sp7 growth curves after inoculation into conditioned media from each of the six symbiotic isolates or unconditioned media (UCM). **(C)** Corresponding carrying capacity and growth rates. All growth experiments occurred at 28°C, 215 RPM. Statistical differences were identified by comparing Sp7 growth metrics in conditioned media from each isolate with Sp7 growth in UCM (Wilcoxon two-sample test, *=P<0.01, n=3 independent experiments).

isolates present in the promoter wells significantly enhanced the end-point fluorescent signals and growth rates of Sp7, indicating symbiotic interactions. With this criteria, 16.5% of the wells in the co-culture array exhibited symbiotic interactions. The top two outliers with the highest Sp7 endpoint fluorescence signals and growth rates after 24 hours of culture were identified for selective recovery of the symbiotic isolates.

5.4.2 Symbiotic Isolate Extraction, Identification, and Validation

The Polygon400 patterned illumination tool was used to extract Sp7 symbiotic communities from the two highest outlier wells in the co-culture MRA for species identification and off-chip validation. Target wells were exposed to ring patterned (20 μm outer diameter,10 μm internal diameter) 365 nm light (20 mW/cm^2, 10 min [90, 214]) to degrade the membrane over the well and retrieve viable bacteria. Membrane degradation and extraction was confirmed by brightfield microscopy (**Figure 5.3A**). Cells from an opened well were then retrieved by washing the arrays with corresponding nutrient media (R2A media). Media used in the extraction was then streak isolated on corresponding agar plates (R2A agar) to recover individual isolate colonies. During previous development of this extraction protocol, it was demonstrated that >99.9% of bacteria extracted originated from an opened well with minimal cross-contamination from other wells or from the outside environment [90], which ensured that the isolates recovered here originated from one of the two target wells.

After extraction, phylogenetic analysis using 16S rRNA amplicon sequencing of all recovered isolates was performed (**Supplementary Figure 5**). Eight symbiotic isolates were identified as *Serratia marcescens* (2 of 8), *Serratia nematodiphila* (1 of 8), *Serratia ureilytica* (1 of 8), *Enterobacter tabaci* (2 of 8), *Acinetobacter bereziniae* (1 of 8), and *Pantoea agglomerans* (1 of 8). At this point, the MRA reduced the initial root microbiome isolate sample to a panel of six

isolates for further investigation (**Figure 5.1C**). Details on the symbiotic isolates and their specific plant growth-promoting capabilities are listed in **Table 1**. It was notable that five out of the six different isolates were previously characterized as plant growth-promoting rhizobacteria [183, 223–227], however, to our knowledge, none have been reported to have a symbiotic effect on *A. brasilense*.

To verify the on-chip observations, interactions between each isolate and Sp7 were recapitulated in an independent off-chip co-culture. Following our previous validation assay procedure [214], cell free culture fluid (CFCF) from each isolate was added with R2A growth media at a ratio of 1:1 to create conditioned media. Sp7 was then inoculated into conditioned media at an initial OD_{600} of 0.2 and cultured in a 96-well plate format to quantify its growth metrics (**Figure 5.3B**). Culture in CFCF accounts for diffusive interactions between the focal species and the isolate and thus the interactions observed in a 1.6 pL volume of an individual microwell are scaled up to 100 mL solution volumes in individual wells of a 96-well plate [214]. A monoculture of Sp7 (OD_{600}=0.2) in unconditioned media (UCM), which was R2A culture media instead supplemented with a blank solution (1X PBS) at a 1:1 ratio, was also performed and used for comparison. As a negative control, conditioned media was inoculated without Sp7 to verify that the measured growth was solely due to the isolates, not contaminating microbes. Growthcurver R [192] was then used to estimate the carrying capacities and growth rates of Sp7 in each experiment (**Supplementary Figure 6**). The quantified growth metrics revealed that, congruent with microwell observations, all six isolates significantly increased the growth rate and carrying capacity of Sp7 compared to the UCM monoculture control (**Figure 5.3C)**, validating the interactions uncovered in the MRA screen and motivating further investigation of the interacting pair in the context of a root host.

Isolate	Isolate ID	Effect on growth promotion	References
Serratia nematodiphila	A1	N-fixing PGPR	[223]
Serratia marcescens	A2	Indole-3 acetic acid (IAA) and siderophore production	[224, 225]
	B3		
Serratia ureilytica	A3	N-fixing PGPR	[223]
Enterobacter tabaci	A4	Indole-3 acetic acid (IAA) and siderophore production; solubilization of phosphate and potassium; nitrogen metabolism	[226]
	B2		
Pantoea agglomerans	B1	IAA production	[228, 229]
Acinetobacter bereziniae	B4	No known application in plant growth promotion	[230]

Table 5.1: Identification of Sp-7 mutualist isolates extracted from the *Zea mays* L. rhizosphere microbiome using the MRA and their previously described impact on plant growth promotion.

5.4.3 Effect of *A. brasilense* - isolate co-inoculation on *Zea Mays* growth

With a panel of validated isolates, the effect of co-inoculation with Sp7 and each individual isolate on the growth of axenic maize seedlings was studied in a growth chamber environment. After inoculating the surface-sterilized and germinated seeds with a cell suspension containing both Sp7 and an isolate at a cellular ratio of 1:1, the axenic seedlings were transferred to a glass tube growth chamber and allowed to grow in ½ MS agar for 15 days (**Figure 5.4A and B**). Two control treatments, one with no inoculation and one with Sp7 inoculation only were used for comparison. Because several isolates also had known plant growth promoting properties (**Table 1**) surface-sterilized and germinated seedlings inoculated only with individual isolates was added as a final set of controls (**Supplementary Figure 7**). All glass tube growth chambers were then placed

under diurnal light in a plant growth chamber, and height of the plants were measured every five days.

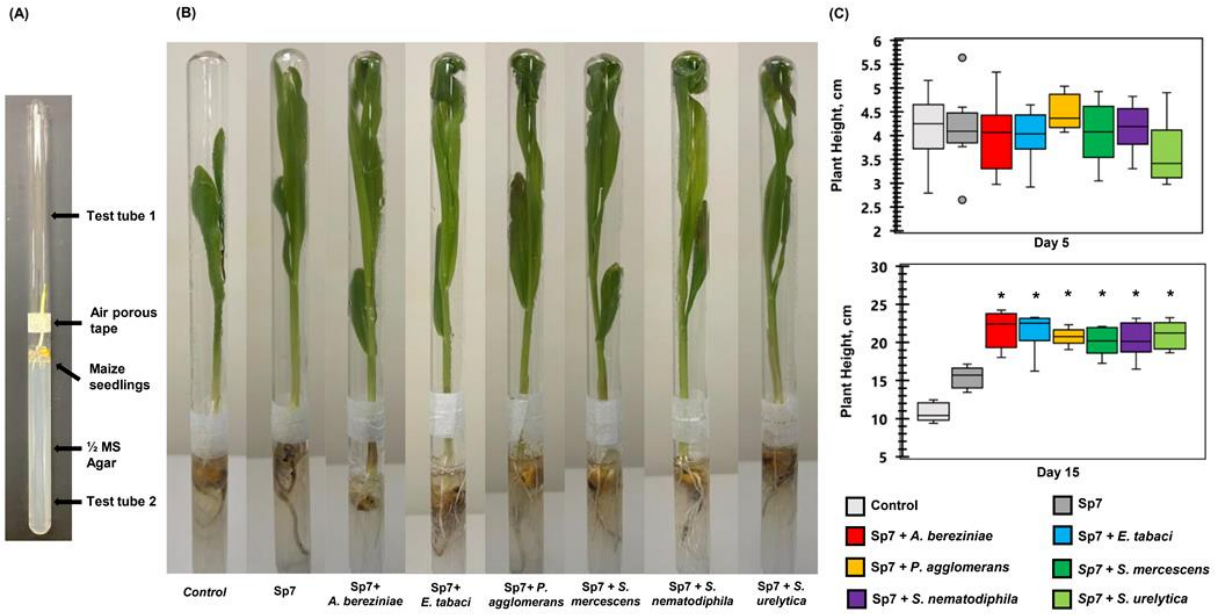

Figure 5.4: Growth of axenic maize seedlings in growth chamber environment. (A) The double-tube growth chanber for accomodating surface-sterilized and germinated maize seedlings inoculated with ultrapure water (control), Sp7 monoculture, and Sp7 with a promoter isolates. Two test tubes were attached in a mouth-to-mouth fashion with air-porous tape. (B) Growth of the axenic maize seedlings in the double-tube growth chamber at Day 15. (C) Comparison of plant heights for each treatment at Day 5 and Day 15 (*, Wilcoxon Rank test: p-value < 0.01).

In all the treatments, leaf emergence from the maize seedlings was observed on Day 2, it was therefore concluded that the isolate co-inoculation with Sp7 did not have an observed impact on leaf emergence. Co-inoculations also did not significantly impact plant height at Day 5. However, significant differences were observed at Day 15 (**Figure 5.4B and C**). At this time, seedlings grown after inoculating with Sp7 monoculture showed significantly higher plant height compared to the axenic maize seedlings grown in no-inoculum conditions, demonstrating the positive impact of *A. brasilense* alone. Additionally, axenic seeds soaked with Sp7 and each individual isolate showed significantly higher plant height at Day 15 compared to both control treatments of Sp7 only and no inoculum. Finally, plant height for the seedlings inoculated only with individual isolates showed diminished growth compared to seedlings inoculated with Sp7 only

(**Supplementary Figure 7**). This control rules out growth enhancement only from individual isolates, and demonstrates that improvements in plant growth are achieved when co-inoculating *A. brasilense* together with promoter isolates.

5.4.4 Survival and Colonization of *A. brasilense* on Maize roots

Given the *A. brasilense* growth promotion observed in MRA and 96-well plate co-cultures combined with improved maize growth outcomes with co-inoculation, we hypothesized that the promoter isolates enhanced *A. brasilense* colonization levels over the root host during plant growth studies. To test this hypothesis, standard plating methodology was used to measure Sp7 colonization levels in maize roots from the plant growth studies [222]. Cell suspensions were collected by washing 20 mg of the roots after Day 15 using 1X PBS, then sequentially diluted by a factor of 10^8. Suspensions were then plated in 3 parallel columns to quantify *A. brasilense* levels in CFU/mL. Plating was done on antibiotics-supplemented R2A agar plates (100 µg/mL ampicillin, 100 µg/mL tetracycline) to selectively recover Sp7. To verify that only Sp7 would be recovered, individual cultures of six individual isolates were also plated on R2A agar plates supplemented with these antibiotics and cultured for 72 hr, and no cell colonies were observed (**Supplementary Figure 8**).

After plating the cell suspensions, it was observed that seedling co-inoculation with *S. ureilytica, S. marcescens, P. agglomerans, E. tabaci,* and *A. bereziniae* generated significantly higher levels of Sp7 compared to inoculations with only Sp7 (p-value<0.01), with *S. nematodiphila* showing less of and increase (p-value<0.05) . Among the six-cell suspensions, *S. ureilytica* generated the highest levels of Sp7. The CFU/mL value was normalized to the root mass to compute the relative abundance of Sp7. While all isolates generated elevated levels of Sp7 relative abundance values compared to the control ($p<0.05$), *S. ureilytica, S. marcescens, P. agglomerans,* and *A. bereziniae*

generated the most significant increases (p-value<0.01). Similar to the CFU/mL data, co-inoculations with *S. ureilytica* generated the highest levels of relative abundance (**Figure 5.5A and B**). This verifies that the isolates increased the survival and colonization of Sp7 in maize roots and strongly suggests this as the reason for the improvements in plant growth on co-inoculation, as observed in **Figure 5.4**.

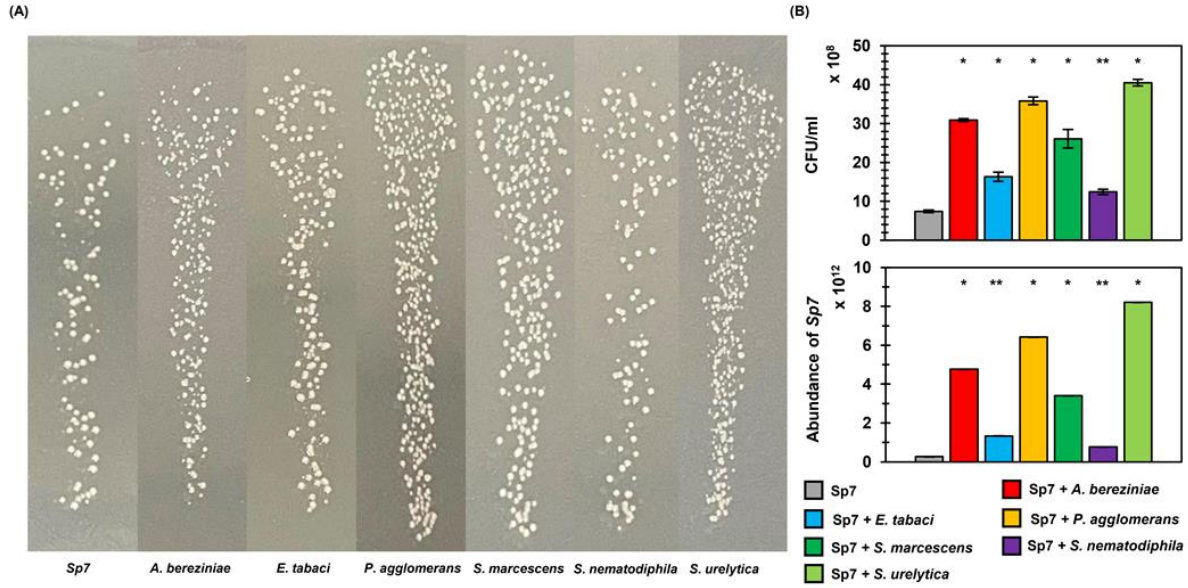

Figure 5.5: *Sp7-GFP* colonization in *Zea mays* roots. (A) Plated colonies after 10^8 fold diluted cell suspensions from *Zea mays* roots in R2A agar plates supplemented with 100 µg/ml ampicillin and tetracycline. (B) CFU/ml and relative abundance of Sp7-GFP from each co-inoculation in *Zea mays* roots.

5.6 Conclusions

Unraveling microbe-microbe interactions that exist between PGPB and indigenous bacteria in the rhizosphere of crops is critical for efficient and reliable use of PGPB in sustainable food and agriculture production [231]. Poor survival and colonization of inoculated PGPB in the rhizosphere is commonly cited as a limiting factor in reliable PGPB field application [232], highlighting the need to expedite the pace at which important interactions are discovered. Building off of previous progress [90, 139, 214], here we applied the MRA tool towards identification of symbiotic interactions between a well-known diazotrophic PGPB and maize rhizobiome samples taken from

the field. In one screen, the MRA device uncovered six complementary bacteria from a maize rhizosphere community that were complementary to *A. brasilense*. Compared to traditional, low-throughput methods of observing interactions that require sequencing candidate isolates before the interaction is observed, the MRA first provides high-throughput observation of thousands of interactions between PGPB and unknown microbiome members. Only isolates that elicit the highest impact on PGPB growth metrics are removed for sequencing, identification and further investigation. Combined with the high-density of microscale co-culture cites, a single MRA device can accommodate interactions from diverse and complex microbiomes consisting of thousands of unique bacteria species or strains.

Here we also demonstrate, for the first time, that interactions initially observed in the MRA screen can also be observed in the context of a root host, and that pairing of symbiotic isolates found in the MRA with the PGPB can elicit a positive phenotypic impact on plant development. The finding supports a growing body of literature suggesting that application of PGPB as complementary, multispecies consortia instead of as single-strain inoculations can improve plant health and development [233, 234]. Moreover, the workflow developed here - consisting of field sampling, media selection, MRA screening, cross validation, and application - lays the ground work for future bioprospecting endeavors that search for environmental isolates with symbiotic or antagonistic interactions to bacteria with known functional importance. The rapid pace at which interactions can be discovered and new isolates can be obtained can lead to savings in cost and time, advantageous from both academic and commercial standpoints. Beyond the search for microbes useful for PGPB consortia, the approach holds promise for discovery of pathogen

inhibitors, both for biocontrol applications and for discovery of new bacteriocins that can combat antimicrobial resistance.

Chapter 6 : Microwell Recovery Array for Rapid Screening of Large Isolate Collections for Identification of Pathogen-Suppressing Bacteria

6.1 Overview

Screening soil and root microbiomes to discover microorganisms that can inhibit the survival and growth of pathogenetic bacteria is important for developing improved probiotic and biocontrol agents. Microwell recovery arrays (MRA), a novel high throughput screening tool, is designed to generate random combinations between a fluorescently labeled bacterial pathogen and a controlled number of microbiome isolates. Isolates that display the highest levels of pathogen antagonism can be extracted, validated with off-chip assays, then characterized with whole sequencing. With the aid of the MRAs, libraries containing 576 unique *Agrobacterium* isolates are rapidly screened for pathogen suppression. MRAs were designed to operate in a pathogen challenge mode that screens for the most potent inhibitors of *Agrobacterium tumefaciens*, the causative agent of Crown Gall disease in plants. While *A. tumefaciens* pathogenesis and intraspecific interactions have been studied extensively, far less is known about *A. tumefaciens* interactions with other members of plant microbiomes. Therefore, a high number of fluorescently labeled *A. tumefaciens* sp.15955 was combined with a low number of non-pathogenic *Agrobacterium* isolates collected from *Helianthus annuus* roots to isolate the *Agrobacterium* isolates most capable of suppressing *A. tumefaciens* sp.15955. First, an inoculum of *A. tumefaciens* sp. 15955 expressing GFP and *Agrobacterium* isolates was seeded in microwells at various cellular ratios. After culture, selective recovery of cells from individual wells displaying the highest levels of Agro 15955-GFP inhibition was achieved using a high-resolution, light-based extraction system. The interactions are then validated in 96-well plate assays, and the phenotypic characterization of the candidate isolates is performed. Here, several *Agrobacterium* isolates were uncovered for inhibiting *A. tumefaciens* sp.

15955 growth. A total of nine non-pathogenic *Agrobacterium* isolates were discovered as potent inhibitors of Agro 15955-GFP, and a bacteriocin bioassay was conducted to validate the inhibitory effects of isolates. The discovery of such growth-inhibiting isolates will help improve plant productivity by using them as reliable biocontrol agents that prevent Crown Gall disease. Further, the MRA pathogen challenge model developed here is broadly applicable to screening microbiomes or isolate collections for pathogen-inhibiting bacteria and their associated gene clusters, relevant to discovery of probiotic strains and discovery of new antibiotics in response to the emergence of antimicrobial resistant pathogens.

6.2 Introduction

Pathogenic microorganisms are often causative agents of plant disease [235, 236], blood contamination [237, 238], lung infection [239, 240], and food poisoning [238, 241] in humans and animals. Probiotic bacteria that are antagonistic towards these pathogens represent a potential alternative in preventing and controlling pathogenic microorganisms. Application of microbes that are antagonistic towards these pathogens has recently emerged as a promising alternative approach to traditional biocontrol methods, which are limited by time sensitivity, low host specificity, unpredictability, and high capital cost. With this approach, screening and isolation of beneficial bacteria from their natural environment, followed by genomic characterization, is essential for their discovery and application [242]. However, despite recent advances in genomic and metagenomic approaches to determine community structure and species abundance [12], identification of those organisms with the highest potential for pathogen inhibition from a complex microbiome remains difficult, primarily due to the wide range of functional diversity found in natural isolates and the missing link between genomic information and function in most organisms.

Based on their observed interactions with pathogens, screening microorganisms is a promising alternative for selecting potential biocontrol agents [11, 243]. Observing microbe-microbe interactions can provide insight into the antagonizing organisms' ecological fitness and its effectiveness against the competing pathogen [244]. Such an approach has proven to provide the discovery of landmark biocontrol agents. For example, *Agrobacterium tumefaciens*, a ubiquitous α-proteobacterium of the Rhizobiaceae family and the causative agent of crown gall disease in plants [245, 246], infects more than 90 families of dicotyledonous plants, resulting in significant agronomic losses [247–250]. [251, 252]. *Rhizobium rhizogenes* K84 and its plasmid-transfer-deficient derivative K1026 have been widely used as crown gall biocontrol agents because

of their innate capabilities to produce the antibiotic agrocin 84 [253]. This was the first natural bacterial isolate used as a commercial biocontrol agent and was initially isolated from the soil around a plant gall [254]. While traditional techniques for environmental control include reducing plant wounds [251], abandoning pathogen infested soils [255], soil fumigation [245], and *Agrobacterium*-induced programmed cell death [256] have also been explored, use of avirulent *Agrobacterium* strains such as K84 have proven to be the most effective for inhibiting *A. tumefaciens* [257]. Despite its commercial success, K84 has been impeded by limited host specificity, necessitating the need for a more diverse and robust panel of biocontrol agents against *A. tumefaciens*. For example, Kawaguchi *et al.* conducted in vitro antibiosis assay for biological control of crown gall by combining non-pathogenic *Agrobacterium vitis* strain VAR03-1 from a nursery stock of grapevine (*Vitis vinifera* L.) with *A. tumefaciens* strains in yeast-mannitol agar plates [258]. Non-pathogenic *Agrobacterium vitis* strain VAR03-1 produced a bacteriocin and successfully inhibited tumor formation on the stems of tomato and grapevine seedlings caused by *Agrobacterium tumefaciens* [258]. Recently, Li *et al.* screened *Agrobacterium* vitis sp. E26 can produce the antibacterial compound Ar26, with proven inhibition against crown gall tumors [259]. While both applications successfully screened non-pathogenic *Agrobacterium* strains to inhibit pathogenic *A. tumefaciens* strains, they were widely reliant on qualitative, low throughput observation of manually paired, dual-species bulk populations in agar plates.

Micro- and nanoscale devices are useful alternatives for addressing the limitations of classical methods for studying bacteria interaction because they facilitate high-throughput measurement and can track single-cell behavior while providing a well-controlled microenvironment. These approaches have advanced our understanding of microbial mutualism [179], metabolite exchange [180], community adaptation to environmental pressures [25, 181],

and the role of spatial structure in driving community phenotypes [44, 182], among other findings. Here, microwell recovery array (MRA), a high-throughput, lab-on-a-chip device was demonstrated to screen pair-wise or multi-species interaction networks among environmental bacterial isolates and a fluorescently-labeled focal species in the pathogen challenge mode. The platform offers the benefit of combining then screening up to 10^4 unique microbial combinations, then recovery of any sample from any well for genetic characterization, dramatically increasing the pace at which significant interactions can be uncovered. Our previous studies [214] provided an initial demonstration of this approach by screening interactions between a beneficial plant growth-promoting bacteria (PGPB) and the *Populus* rhizobiome to uncover higher-order networks of bacteria that promoted PGPB growth. Building on this approach, the MRA screen was adapted to a "pathogen challenge mode" where the focal species is instead a fluorescently labeled pathogen used to challenge isolates that are potential candidates for biocontrol. By controlling the pathogen-to-isolate seeding ratios [85], isolates are countered against increasingly higher numbers of pathogens to identify the most potent inhibitors. Using this methodology, a small number of *A. tumefaciens* sp. 15955-the plant pathogenetic focal species expressing GFP was combined with *Agrobacterium* isolates extracted from the roots of *Helianthus annuus* plants and seeded into arrays of 10μm diameter wells in different cell ratios. While seeding interacting cells together in such very small confinement, multi-species biofilms are successfully mimicked [88] and inter-cellular interactions are facilitated. The seeded cells are then trapped inside the microwells with a previously developed photodegradable polyethylene glycol (PEG)-based membrane [90], co-cultured, and then focal strain growth in each well is tracked with time-lapse fluorescent microscopy (TLFM). Microwells with diminished Agro 15955-GFP are extracted from any individual well using a patterned light source by spatially eroding the membrane, releasing cells

into a solution for recovery and downstream genome characterization (**Figure 6.1**). With the extraction and recovery capabilities of the MRAs, a collection of *Agrobacterium* isolates capable of diminishing Agro 15955-GFP were sampled for follow-up phenotypic characterization and whole genome sequencing. A total of nine *Agrobacterium* isolates capable of inhibiting the growth of Agro 15955-GFP were extracted in the pathogen challenge mode and were validated off-chip using 96-well plate validation assays and bacteriocin bioassays. Currently, the whole genome sequences of the Agro 15955-GFP are undergoing bioinformatics analysis to identify bacteriocin gene clusters responsible for pathogen inhibition.

6.3 Experimental Methods

6.3.1 Preparation and culture of *A.tumefaciens* sp. 15955 Strains

Bacteria strains and the plasmids used in this research are listed in the **Table S1**. *A.tumefaciens* sp. 15955 expressing sfGFP from a T-DNA insertion, as described by Platt et al. [260]. Plasmid pSRKKm-sfGFP was introduced into *A. tumefaciens* sp. 15955 via mating with *Escherichia coli* S17-1 λpir carrying the plasmids using previously described methods [165]. These plasmids were transformed into competent S17-1 λpir E. coli strains using calcium chloride heat-shock transformation. *A. tumefaciens* sp. 15955 were stored in 50% glycerol at -80 ºC. Sterile inoculation loops were used to pick up cells from the frozen stocks and culture in ATGN media (0.079 M KH_2PO_4, 0.015 M $(NH_4)_2SO_4$, 0.6 mM $MgSO_4.7H_2O$, 0.06 mM $CaCl_2.2H_2O$, 0.0071mM $MnSO_4.H_2O$, 0.125 M $FeSO_4.7H_2O$, 28 mM Glucose, pH: 7 ± 0.2) in sterile test tubes supplemented with Kanamycin (150 μg/mL) for 24 hrs (28°C, 215 rpm).

6.3.2 Extraction and culture of Agrobacterium root isolates

Sunflowers were identified as *Helianthus annuus* before blooming based on leaf and stem morphology. Sunflowers were extracted by gently removing soil from around the base of the plant

using a spade. Roots were exposed by gently shaking the root to remove excess soil. Samples were then placed in a Ziploc bag and placed on ice until at the lab. Once at the lab, the samples were weighed and soaked in 1X phosphate buffer saline added to the Ziploc bag. The bags were agitated every 10 minutes for 1 hour. 100 mL were then removed from the soil-water slurry and diluted. The dilutions were plated on media 1A and placed at 28°C for 3 to 5 days. Colonies that were round, black, and shiny were then struck onto yeast lactose media and ATGN. These samples were placed at 28°C overnight. The next day the yeast lactose plates were flooded with Benedict's reagent, and colonies that formed a yellow precipitate were selected from the corresponding ATGN plate and struck for isolation on ATGN and incubated overnight at 28°C. A colony was selected from that primary isolation streak and was struck again for isolation on ATGN, which was then incubated overnight at 28°C. A colony from the secondary streak was then selected and grown in liquid ATGN to freeze at -80°Celsius. From the freezer stock, the isolate was grown in liquid ATGN overnight until an OD_{600} of between 0.4 and 1.0 was reached, which should correspond to cells in the mid-log growth phase.

6.3.3 Initial Sequencing of *Agrobacterium* root isolates

The Qiagen blood and tissue kit were used to extract the DNA. DNA concentrations were measured with a pico green assay kit. The DNA was then sent to Integrated Genomics Facility (IGF) at Kansas State University, and we received the raw files back once they have sequenced them.

6.3.4 MRA design and fabrication

MRAs containing 10μm diameter microwells, 20μm depth, and spaced at a 30μm pitch were etched on silicon wafers (University Wafers). The array was divided into a 7×7 grid of sub-arrays; each sub-array consisted of 15×15 arrays of microwells and contained 11,025 microwells available for analysis [214]. Wells were assigned with unique on-chip addresses for identification during

brightfield microscopy. 3-inch diameter N-type silicon wafers (University Wafers) were coated with a 1μm thick layer of Parylene N (PDS 2010 Labcoater, Specialty Coating Systems), and standard photolithography techniques following previous protocols were applied to fabricate MRAs [90, 214].

6.3.5 Bacteria seeding and trapping in microwell arrays

A.tumefaciens sp. 15955-GFP and *Agrobacterium* root isolates were grown in ATGN minimal media to mid-log phase and resuspended in their respective growth media to an OD_{600} of 0.1. Cells were inoculated in microwell arrays using the protocols described in previous papers [90, 214]. 700μL cell suspensions were incubated over the substrates at room temperature for 1hr. Then, the substrates were dried, followed by the parylene lift-off process to remove cells attached to the background regions of the array [85, 214]. For co-culture studies of screening *Agrobacterium* root isolates, the seeding solution contained SP 15955-GFP, and *Agrobacterium* root isolates were mixed at ratios of 1:1, 10:1, and 100:1. For 1:1 ratio, OD_{600}=0.1 cultures of SP 15955-GFP and *Agrobacterium* root isolates were mixed at equal volumes to reach a final OD_{600}=0.1. Again, for the 10:1 ratio, OD_{600}=1 cultures of SP 15955-GFP and OD_{600}=0.1 cultures of *Agrobacterium* root isolates were mixed and diluted to reach OD_{600}=0.1. Similarly, for the 100:1 ratio, OD_{600}=10 cultures of SP 15955-GFP and OD_{600}=0.1 cultures of *Agrobacterium* root isolates were mixed and

diluted to reach OD_{600}=0.1. 700µL of each of these suspensions were seeded on top of microwell arrays for 1hr at room temperature for co-culture studies.

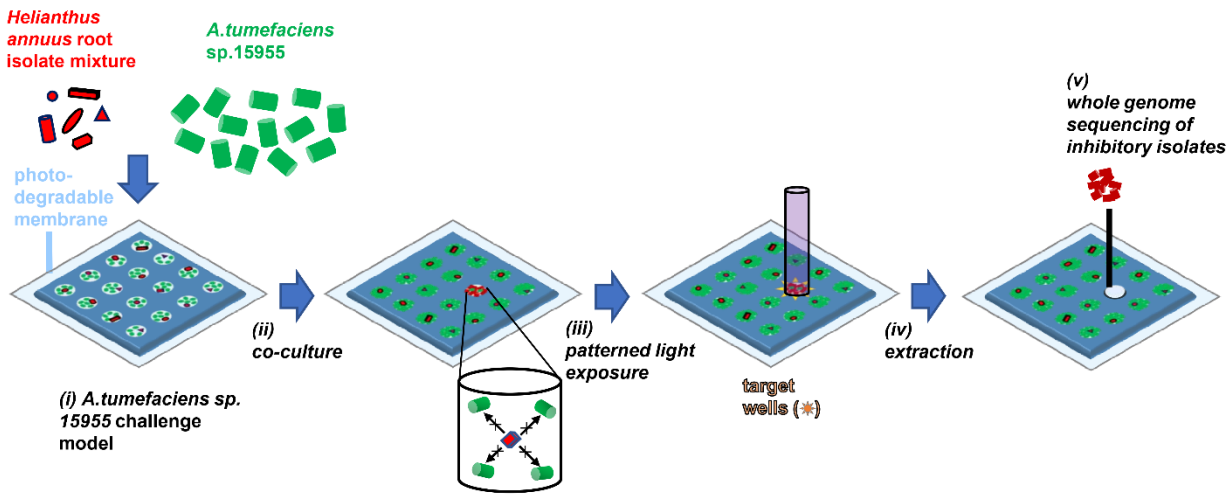

Figure 6.1: Microwell recovery arrays for screening in the pathogen challenge mode. (i) GFP-expressing *Agrobacterium tumefaciens* sp. 15955 are combined with *Agrobacterium* isolates from *Helianthus annus* rhizosphere at a cellular ratio favorable for *A.tumefaciens* sp. 15955 growth. Here, a limited number of *Agrobacterium* isolates were challenged against *A.tumefaciens* sp. 15955 to discover the most potent inhibitors of *A. tumefaciens* sp. 15955. Here, different shapes represent unique *Agrobacterium* isolates. Cells are stochastically seeded and trapped within microwells using a photodegradable PEG hydrogel membrane to get unique combinations of interaction networks and monitored in parallel during co-culture using TLFM. (ii) Wells with lowest levels of focal species growth were identified as anatagonistic outliers. (iii) The membrane over the target antagonistic well is eroded using patterned light exposure, then (iv) isolates inhibiting the growth of *A.tumefaciens* sp. 15955 were extracted and recovered from an opened well and characterized using whole genome sequencing.

6.3.6 Photodegradable membrane attachment

A previously described protocol for attaching the photodegradable hydrogel membranes to microwell arrays was used here [90, 214]. At first, perfluoroalkylated glass slides were prepared by incubating 25×25 mm clean glass slides (Fisher Scientific) in 20 mL of 0.5% v/v trichloro(1H,1H,2H,2H-perfluorooctyl) silane in toluene for 3 hrs [90, 214]. Then, NaH_2PO_4 was added with ATGN liquid media to obtain phosphate buffer saline (PBS) with 100mM final phosphate concentration, and the pH of the solution was adjusted eight by adding 5M NaOH (aq.).

12.5 µL of this PBS-ATGN solution was then mixed with 5.6 µL of photodegradable PEG diacrylate monomer (MW 3400) and 6.9 µL of a four-arm PEG thiol solution monomer to obtain membrane precursor solution [141] (MW 10000, NOF America Corporation, DE-100SH) with equal concentrations of both PEG diacrylate monomer (22mM) and four-arm PEG thiol solution monomer (22mM). The membrane precursor solution was then transferred on top of the microwell substrates by pipetting 15µL of the liquid precursor solution on top of the perfluoroalkylated glass slides and placing the solution over the seeded microwell substrate. A constant 38µm gap between the glass slide and the microwell for the precursor solution was provided with the aid of metal spacers were used. The membrane was then formed through monomer crosslinking and gelation by incubating for 25min at room temperature [90, 214]. After careful separation of the glass slide from the membrane-functionalized microwell array, the microwell array was placed inside a custom 3D printed scaffold, previously designed for imaging microwell arrays with time-lapse fluorescence microscopy [214].

6.3.7 Time-lapse fluorescent microscopy

Time-lapse fluorescent microscopy images were acquired with a Nikon Eclipse Ti-U inverted microscope equipped with a 20× objective, a motorized XYZ stage, a humidified live-cell incubation chamber (Tokai Hit) a DS-QiMc monochromatic digital camera, and NIS Elements Image acquisition software. The seeded microwell arrays were sealed with the photodegradable PEG membrane, and the inverted arrays were placed in a custom 3D printed scaffold to keep them submerged under liquid media while imaging [214]. Then the scaffold was placed inside a humidified live-cell incubation chamber at 28ºC during imaging. A FITC filter was used to image 15955-GFP and YR343-GFP strains (20×, 200 ms, 17.1× gain) with a neutral density filter with 25% standard light intensity to ensure imaging without photobleaching. Brightfield images were

also taken at each section of the array after fluorescent imaging. Images of the microwell arrays were taken every 60 minutes during culture.

6.3.8 Image Analysis

GFP fluorescent images from the 15955-GFP and *Agrobacterium* root isolate co-culture system was analyzed by the protocol described by Timm *et al.* We used the Protein Array Analyzer tool in ImageJ to generate growth profiles for each organism to identify the top 3 wells with the lowest growth levels for extraction [137]. At first, the timelapse fluorescent images were imported as image sequences corrected by subtracting darkfield images from illumination field images with the image calculator plugin. Then image backgrounds were removed by selecting a 125 radius sliding paraboloid, and illumination correction was performed using calculator plus plugin. Finally, each strain's growth in the microwells was calculated using ImageJ "Micro Array" plugin [137].

6.3.9 Recovery and storage of Isolates from microwell arrays

Isolates were extracted from microwell arrays by following the procedures described previously [90, 214]. The top three individual wells (A, B, C) with diminished growth of Agro 15955-GFP were then opened by exposing them to a ring pattern UV exposure area with 10µm inner diameter and 20µm outer diameter. The individual isolate cell suspensions were plated onto ATGN agar media after extraction, and three colonies were sampled from each extracted microwell based on differences in colony morphology and color. Then individual colonies were cultured in AT minimal media and stored in glycerol stocks to extract genomic DNA of each isolate. 9 individual antagonistic isolates were recovered in this process and labeled as isolate A1, A2, A3, B1, B2, B3, C1, C2 and C3 for validation.

6.3.10 Validation using 96 well plates.

To obtain CFCF from individual isolates, each isolate was cultured (28ºC, 3000 rpm) in 2mL of ATGN liquid media overnight, and then cells were removed from the media by centrifugation (2000g, 10 min). To obtain CFCF from combinatorial mixtures, isolate panels were instead inoculated together in R2A media and cultured overnight, followed by cell removal by centrifugation. To obtain conditioned media, isolate CFCF was mixed with Agro 15955-GFP in fresh ATGN media at a 1:1 volumetric ratio to reach an initial OD_{600} value of 0.1 (final volume = 100 µL), at which point growth was quantified with a Biotek Epoch 2 Multi-Mode Microplate Reader (28ºC, 300rpm). Unconditioned media was obtained following the same procedure, except 1X PBS was added to fresh ATGN media instead of isolate CFCF. To verify, the OD_{600} measurement was due to Agro 15955-GFP growth, CFCF from selected isolates without inoculation of Agro 15955-GFP was also measured. A total of n=3 independent replicates were measured for each culture condition. The growth kinetics of Agro 15955-GFP in all co-culture and mono-culture wells were analyzed with Growthcurver, an R package to determine the growth rates and carrying capacities of bacteria cells [192]. The average growth rates of Agro 15955-GFP were calculated for each co-culture, and mono-culture wells and the average growth rates of each combination were compared with those from the mono-culture using the Wilcoxon two-sample test.

6.3.11 Bacteriocin bioassays

Strains to be tested for bacteriocin production were detected on ATGN agar plates using *A. tumefaciens* sp. 15955 as an indicator, following the protocol described by Fattahi et al. [87]. *Agro* 15955-GFP and recovered nine antagonist isolates were cultured overnight in ATGN liquid media at 28 °C and 215 rpm. All cultures were diluted to OD_{600}=0.6 in ATGN media. 35 µl of the

antagonist isolates were inoculated in tubes containing 10ml of molten ATGN agar (65 °C), vortexed vigorously for 10 s, and then poured onto sterile 60 × 15 mm Petri dishes. 7.5 µL of the Agro 15955-GFP cells were spotted in the center of the solidified agar previously overlaid with antagonist isolates and allowed to air-dry. The plates were then wrapped with parafilm to prevent

Figure 6.2: Phylogeny tree for Agrobacterium isolates extracted from *Helianthus annuus* roots the shrinking of the media and incubated at 28 °C for 72 hrs to validate the accumulation of bacteriocin [257].

6.4. Results

6.4.1 Whole-genome sequencing uncovers a diverse collection of *Agrobacterium* isolates

The whole-genome sequencing of the *Helianthus annuus* root isolate collection generated a diverse collection of *Agrobacterium* isolates. A total of 576 *Agrobacterium* isolates were identified from the whole-genome sequencing data.

6.4.2 Co-culturing a reduced number of Agrobacterium root isolate cells with A. tumefaciens sp. 15955 for the MRA screening in pathogen challenge mode

To demonstrate operation of the MRA in pathogen challenge mode, *A. tumefaciens* sp. 15955 (hereafter denoted Agro 15955-GFP) and *Agrobacterium* root isolates were stochastically seeded in microwell arrays at different cellular ratios, trapped the cells inside the microwells using photodegradable PEG membrane, and tracked. Agro 15955-GFP fluorescent signals were used to screen for isolates inhibiting the growth of Agro 15955-GFP. Control Agro 15955-GFP mono-culture arrays seeded only with Agro 15955-GFP at OD_{600}=0.1 were tracked with time-lapse fluorescence microscopy (TLFM) for comparison. In each case, Agro 15955-GFP growth was tracked across 4×4 arrays of microwells, with each array containing 225 wells (n=3600 in total). Fluorescent signals of each well were calculated every hour and over 24 hours using ImageJ [137]. The seeding of Agro 15955-GFP contributed to a consistent growth trend throughout the array in the Agro 15955-GFP in mono-culture control **(Figure 6.3A).** This resulted in a low variance of the distribution of endpoint fluorescent levels (σ^2=97) and a nominal growth rate of ~6.01 hr^{-1} in most wells. Despite having nominal growth in most wells, a fraction of wells in the mono-culture arrays were outlier wells showing endpoint fluorescent signals significantly lower than the nominal wells. This can be due to the presence of a very low number of cells initially seeded in these wells,

which can occur due to the Poisson seeding process [85]. Although the outlier wells in mono-

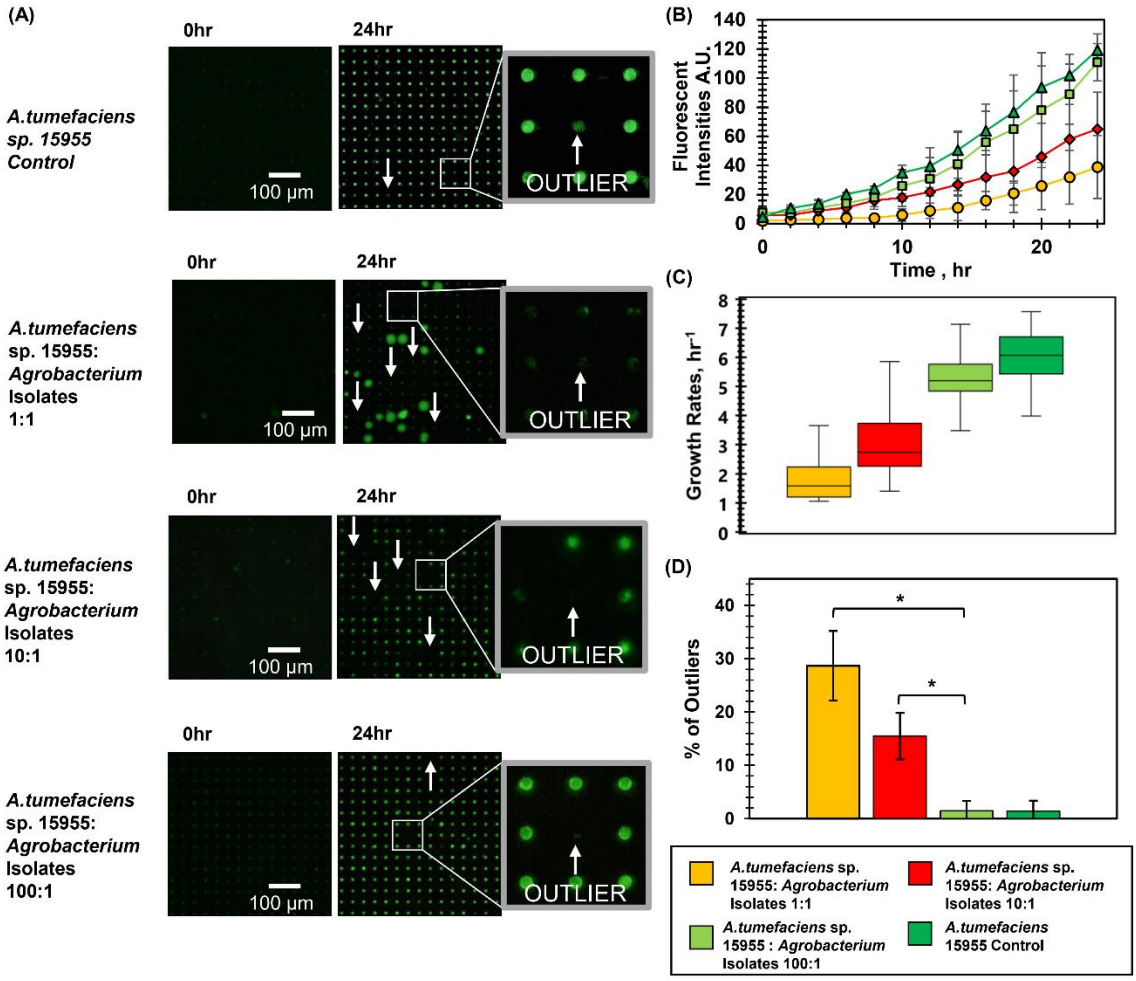

Figure 6.3: The MRA pathogen challenge mode. (A) TLFM images of a sample 15×15 array of microwells after (i) seeding only Agro 15955-GFP (monoculture control) (ii) seeding Agro 15955-GFP with *Agrobacterium* isolates at a ratio of 1:1, (iii) seeding Agro 15955-GFP with *Agrobacterium* isolates at a ratio of 1:10, (iv) seeding Agro 15955-GFP with *Agrobacterium* isolates at a ratio of 1:100. (B) Averaged growth curves generated from a sample 900 microwell array during mono-culture and co-cultures, (C) averaged growth rates from the 900 microwell array calculated for mono-culture and co-cultures, (D) % of outliers in co-culture arrays exhibiting inhibition against Agro 15955-GFP. Wilcoxon two sample tests were conducted to compare the % of outliers in co-culture with the % of outliers in Agro 15955-GFP mono-culture. The % of outliers in the case of Agro 15955-GFP and *Agrobacterium* isolates co-culture at a ratio of 1:100 showed no-significant differences with the % of outliers in Agro 15955-GFP mono-culture. The % of outliers in 1:1 and 1:10 co-culture ratios were significantly higher compared to the % outliers in 1:100 co-culture ratio and hence the Agro 15955-GFP mono-culture (*, p-value<0.01).

culture showed significantly lower endpoint fluorescence signals of Agro 15955-GFP, the growth

rates of Agro 15955-GFP were similar to the nominal growth rates. The nominal growth rate of Agro 15955-GFP in mono-culture was later used as an important growth metric for comparison with Agro 15955-GFP growth measurements in co-cultures (**Figure 6.3B, C, and D**).

For co-culture, Agro 15955-GFP and *Agrobacterium* root isolates, cultured in ATGN media, were mixed (OD_{600}=0.1) at a ratio of 1:1 and seeded in 10µm diameter microwell arrays and the growth kinetics of Agro 15955-GFP were tracked in each well for every hour over a period of 24 hours. Compared to the monoculture control (**Figure 6.3A**), the first co-culture generated a variety of growth outcomes (**Figure 6.3B**). As evident, the majority (28%) of wells showed no fluorescent signal, indicating isolates that were able to inhibit Agro 15955-GFP at a low challenge level (**Figure 6.3A, D)**. To further challenge the *Agrobacterium* isolates against Agro 15955-GFP, the number of isolates seeded in each well was decreased by one and two orders of magnitude using Agro 15955-GFP : isolate seeding ratios of 10:1 and 100:1. The different seeding ratios generated higher ratios of Agro 15955-GFP cells against *Agrobacterium* root isolates during co-culture to further select the top inhibitory isolates. In the case of the co-culture of Agro 15955-GFP and *Agrobacterium* isolates at a ratio of 1:10, the number of outliers inhibiting Agro 15955 dropped to 15.5% (**Figure 6.3D**). The number of Agro 15955-GFP inhibiting outliers dropped to only 1.5% when *Agrobacterium* isolates were further challenged by combining with Agro 15955-GFP at a ratio of 1:100 (**Figure 6.3D**). This is due to the higher Agro 15955 initially seeded, presenting a greater challenge to antagonistic isolates.

In co-cultures, outlier wells with negative interactions were observed with decreased endpoint fluorescence signals of the wells. The outlier wells were picked with Grubb's outlier test [168] by comparing the endpoint fluorescent signals, as well as the growth rates of Agro 15955-GFP in co-culture with the nominal growth rate and endpoint fluorescent signal of Agro 15955-GFP in mono-

culture to ascertain that the wells were showing positive and negative interactions between Agro 15955-GFP and *Agrobacterium* isolates in a single well. Wells with lower endpoint fluorescent signals and with a growth rate similar to the nominal wells were omitted as outliers since these wells can have only a limited number of Agro 15955-GFP cells and no *Agrobacterium* isolates to

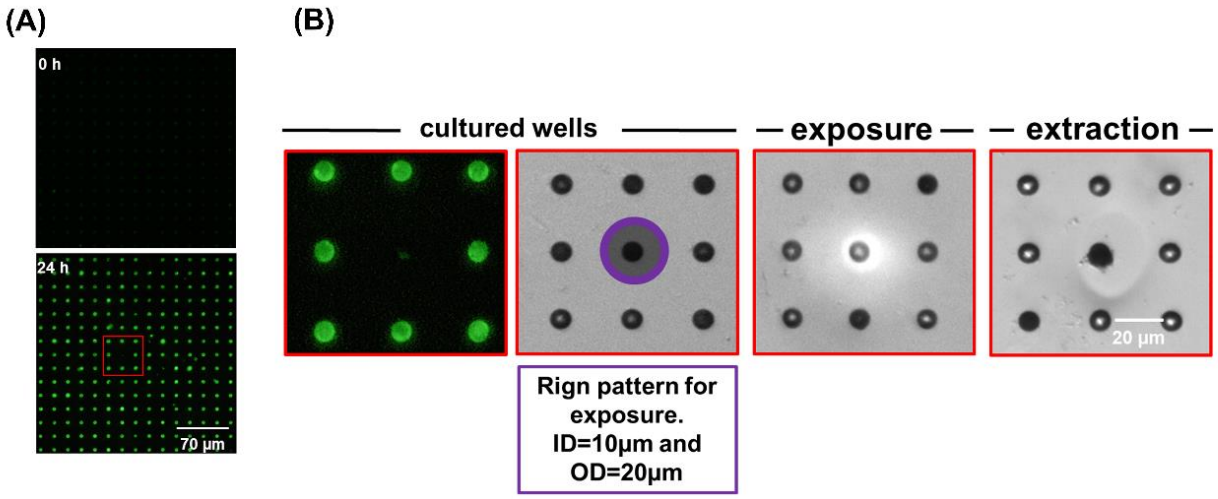

Figure 6.4: Sequential removal of antagonistic communities from an array sub-section after co-culture. (A) Microwell array before and after co-culture. This 15×15 microwell array contained Agro 15955-GFP antagonistic (red) community that were targeted for extraction. (B) Targeted removal of the microwell community in which Agro 15955-GFP grew poorly (red outline). Purple area denotes a ring pattern UV exposure area with 10µm inner diameter and 20µm outer diameter used for membrane degradation.

interact with. The distribution of the endpoint fluorescent levels of the Agro 15955-GFP showed very low variance in mono-culture (σ^2=97) compared to the co-cultures at 15955-isolate ratios of 1:1 (σ^2=619), 1:10 (σ^2=471), and 1:100 (σ^2=162), indicating an impact due to the addition of the *Agrobacterium* isolates (**Figure 6.3A**). The growth curves based on the average fluorescent signals of each array also indicated that the addition of *Agrobacterium* isolates generated variable growth scenarios (**Figure 6.3B, C).**

6.4.3 Sequential extraction, recovery, and identification of isolates from microwell communities.

A Polygon 400 patterned illumination tool was used to extract Agro 15955-GFP inhibiting communities from the three wells with the lowest Agro 15955-GFP endpoint fluorescence signal after 24 hours of culture to run off-chip identification and validation (**Figure 6.4A, B**). The target wells were exposed to a patterned 365 nm light (20 mW/cm^2, 10 min), exposure conditions previously applied for membrane degradation, to ablate the membrane over the well and retrieve viable bacteria from wells [90, 214]. The degradation of the membrane was confirmed by brightfield microscopy (**Figure 6.4B**). After exposure, cells were retrieved from an open well by washing the arrays with extraction buffer (ATGN media + 0.05% Tween20 solution). Later, individual isolate colonies were recovered by streak isolating the extraction buffer on ATGN-agar plates. It was previously observed that >99.9% of bacteria were extracted from the opened wells rather than from outside contamination [90], providing high confidence that the target well was the source of the recovered bacteria. It was further validated in the previous characterization that bacteria could be removed entirely from the target well with minimal cross-contamination when opening additional wells for further sampling [90]. Following recovery, whole-genome phylogenetic analysis was conducted for comparative genomic analysis of the extracted isolates against the Agro 15955-GFP genome. The analysis revealed that 6 out of 9 isolates extracted from the wells contained at least one unique gene (**Figure 6.4B**).

6.4.4 Validation of interactions by recapitulating in 96-well plate format.

It was previously demonstrated that positive and negative microbial interactions observed in microwell recovery arrays can be validated off-chip by recapitulating in a 96-well plate format [214]. Here a scaled-up environment was presented (from 1.6 pL microwell volumes to 100 µL

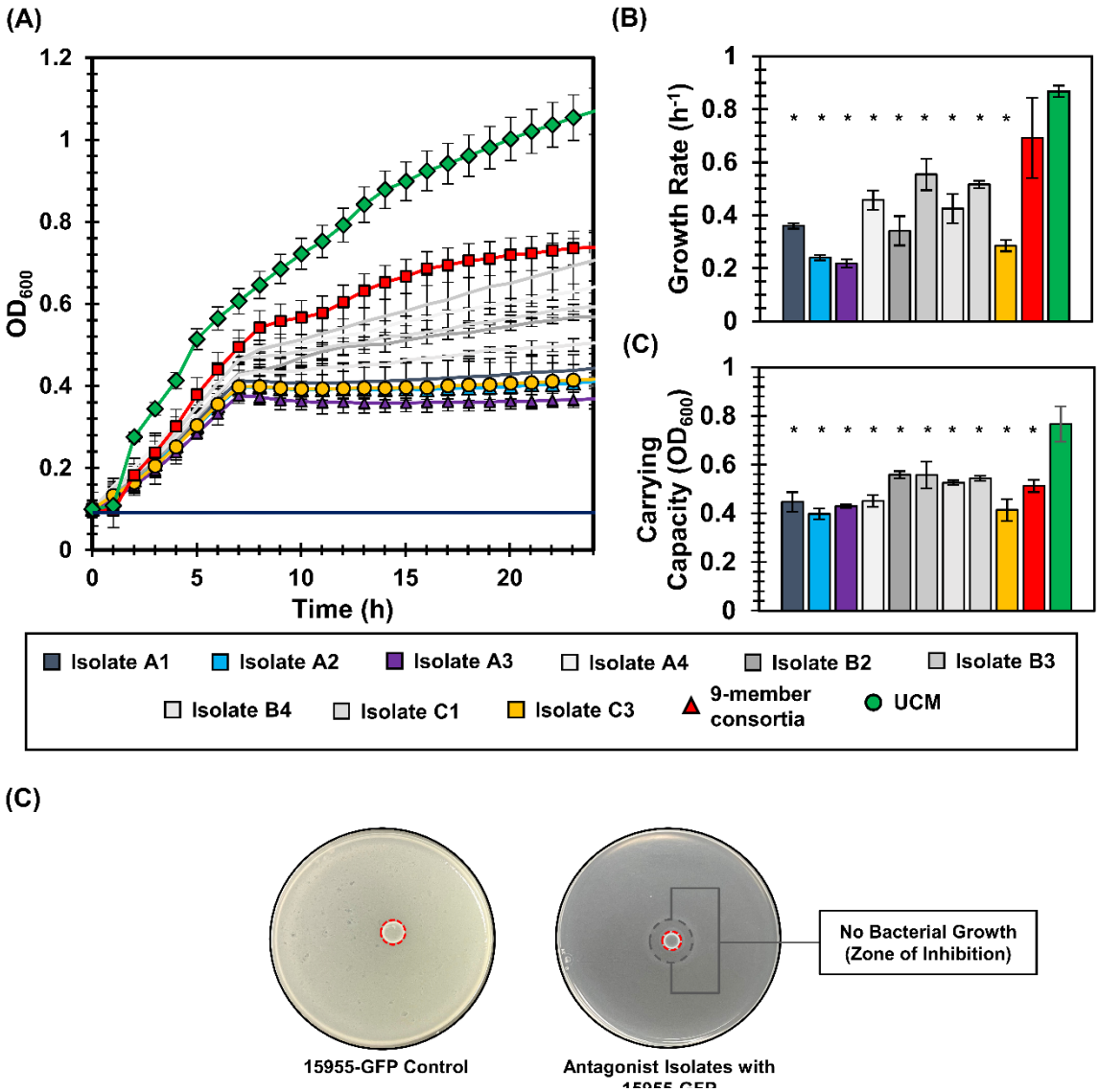

Figure 6.5: Interactions identified in the MRA can be validated in 96-well plate format. (A) Agro 15955-GFP growth curves after inoculation into conditioned media from the antagonistic isolates, the 9-member isolate consortia, or unconditioned media (UCM). The control (black line) is conditioned media that was not inoculated with Agro 15955-GFP to verify that there was no growth carry over or contaminating microbes present. (B) Corresponding carrying capacity and growth rates for each growth curve. All growth experiments occurred at 28°C, 215 RPM. Statistical differences were identified by comparison of growth metrics between Agro 15955-GFP culture in conditioned media from each isolate or isolate mixture and YR343 growth in UCM (Wilcoxon two-sample test, *=P<0.01, n=3 independent experiments). (C) Observations of the follow up bacteriocin bioassay. The control plate consisted of Agro 15955-GFP in both center and in the agar and a uniform growth was observed throughout the plate. Control Agro 15955-GFP bacterial growth is contained inside the red dashed line. The antagonist isolates in the center of the plate showed a zone of inhibition surrounded by Agro 15955-GFP. Here, bacterial growth of the antagonistic isolates is contained inside the red dashed line.

solution volumes) to measure how strains isolated from MRA influenced the growth of Agro

15955-GFP. It was hypothesized in the previous studies that the inhibition measured in MRAs was direct caused by diffusive interactions between the focal species and the collection of isolates present within a well. This hypothesis was tested in the current approach by culturing Agro 15955-GFP in 96-well plate format in media conditioned by nine selected isolates selected from the top 3 antagonist wells (Well 7008, **Figure 6.2**). To obtain conditioned media, each antagonist isolates were first cultured in ATGN media to stationary phase, and cell-free culture fluid (CFCF) was collected by removing cells. Fresh Agro 15955-GFP cultured in ATGN media was then added to the CFCF in a 1:1 volumetric ratio for growth monitoring. These growth curves were compared to a control curve with Agro 15955-GFP growth in unconditioned media, which consisted of ATGN media instead supplemented with blank 1X PBS buffer at the same volumetric ratio. A second control curve consisting of conditioned media without Agro 15955-GFP inoculum was also included to verify that measured growth was not due to contaminating microbes. Growthcurver R was then used to estimate bacterial carrying capacity and growth rate [192] in each experiment (**Figure S1**). Congruent with microwell observations, it was observed that conditioned media from 9 isolates significantly reduced the carrying capacity and growth rate of Agro 15955-GFP compared to its culture in unconditioned media (**Figure 6.5A**). Conditioned media from the combined 9-member antagonist combination showed significantly lower carrying capacity and growth rate than the unconditioned control media (**Figure 6.5B**, **Tables S2, S3**).

6.4.5 Follow-up phenotypic characterization of antagonist isolates

Following cell retrieval and recovery, the antagonistic isolates were streaked onto ATGN agar plates. The bacteriocin bioassay was performed as described in experimental methods to corroborate phenotypic observations in the microwell arrays with standard microbiological approaches [87, 257, 261]. The co-culture of the antagonistic isolates and Agro 15955-GFP

generated a zone of inhibition, i.e., a region near antagonistic isolates with no bacterial growth due to inhibition (**Figure 6.5C**). Additionally, Agro 15955-GFP cultured in the center of the ATGN plate supplemented with Agro 15955-GFP as control generated a uniform growth throughout the plate (**Figure 6.5C**). It was concluded from these observations that the inhibitory phenotype observed between the isolates and Agro 15955-GFP in the microwell screen can be validated using standard follow-up assays.

6.5 Discussions

Crown gall disease in plants, caused by tumorigenic Agrobacterium tumefaciens, has often been regarded as an economically important disease-causing extensive damage to plant health [262]. Biological control of *A.tumefaciens* with antagonistic strains of non-pathogenic Agrobacterium isolates has been successful in many applications [252, 253, 257–259]. But, classical microbiological techniques for probing interactions rely on manually pairing isolates together (Goers et al., 2014); inherently low-throughput approaches are often based on qualitative observations of bulk populations. Micro- and nanoscale devices offer vast improvements by providing high-throughput measurement, observation of single-cell behavior, and precise design and manipulation of the microenvironment.

Here, the rapid isolation of *Agrobacterium* isoloates that were top *A.tumefaciens* was performed by operating the MRA in a pathogen challenge mode. Agro 15955-GFP and Agrobacterium isolates were co-cultured and seeded in microwell recovery arrays in three co-culture ratios (1:1, 10:1, and 100:1) under conditions favorable growth conditions for Agro 15955-GFP. By challenging the isolates with increasing numbers of Agro 15955-GFP, we were able to lower numbers of antagonistic outliers generated across the array and thereby selected only the most potent who learned to survive and grow in excess of Agro 15955-GFP. It was demonstrated that

the Agro 15955-GFP and the *Agrobacterium* isolate co-culture ratio of 100:1 generated Agro 15955-GFP growth trends similar to Agro 15955-GFP mono-culture (**Figure 6.3B**). Here the average growth rate of Agro 15955-GFP among the microwells in 100:1 co-culture ratio showed no significant difference with the Agro 15955-GFP mono-culture (**Figure 6.3C**) and the number of antagonistic outliers showing inhibition of Agro 15955-GFP was significantly less compared to the other two co-culture ratios (**Figure 6.3D**). However, under these 100:1 co-culture conditions, only a limited number of antagonistic outliers were generated (1 in 67 wells), based on endpoint fluorescent signal and growth rate of Agro 15955-GFP. These wells were identified as containing the most potent inhibitory isolates .

Outlier wells were exposed to ring patterned UV light of internal diameter 10µm and outer diameter 20µm. Using the ring pattern, only the perimeter of the microwells was exposed to UV light while keeping the inside of the wells covered to preserve the functionality of the isoalte. After exposure and removal of the membrane on top of the outlier wells, the majority of the cells out of the opened wells were extracted by washing with ATGN nutrient media. The extracted cells were stored in glycerol stocks and sterile isolated using ATGN agar plates to recover nine individual agrobacterium isolates. The isolates were then cultured in ATGN media, and the genomic DNA was extracted from these isolates to perform whole-genome sequencing. The interactions observed in the microwell arrays were recapitulated in 96-well plate assays to validate the inhibition of Agro 15955-GFP. This off-chip assay demonstrated that all nine agrobacterium isolates selected from the MRA also diminished the growth rates and carrying capacities of Agro 15955-GFP in a standardized assay. Later, the nine isolates were validated for the diffusive interactions due to bacteriocin gene clusters in a standard bacteriocin assay. The bacteriocin assay generated a zone of inhibition around the *Agrobacterium* isolates, indicating further proof of the diffusive

interactions causing the inhibition of Agro 15955-GFP. Currently, bioinformatics analysis is being conducted in the Platt Lab at KSU to identify the candidate bacteriocin gene clusters from the extracted isolates using whole-genome sequencing.

6.6 Conclusions

Agrobacterium tumefaciens is the natural genetic engineer because of its widespread application in transgenic plant production [93]. In natural settings, it is the agent of Crown Gall Disease, and it is crucial to develop biocontrol agents capable of inhibiting this immensely important plant pathogen. Here MRAs were applied for screening a library of 576 non-pathogenic *Agrobacterium* isolates capable of preventing *Agrobacterium tumefaciens* growth. Combining an unknown collection of rhizosphere isolates with *A.tumefaciens* in MRA, a library of *A.tumefaciens* antagonizing isolates was rapidly screened. Although the capability of MRAs in screening the *Agrobacterium* challenge model was demonstrated, the platform is maneuverable to screening interactions across any microbiome, including the gut, the respiratory tracts, soil, aquatic systems, and other rhizosphere environments.

The pathogen challenge model demonstrated in this work will be critical in the field of therapeutic drug development. For example, new antibiotics for pathogen suppression can be developed quickly by combining important human pathogen with a collection of the gut microbiome and challenging the gut microbiome isolates to find the most potent inhibitors. Currently, addressing the challenges due to the emergence of antibiotic-resistant pathogens has become a daunting task for scientists. And using the MRA in the pathogen challenge mode will certainly play a vital role in screening new antibiotics to fight against antibiotic-resistant pathogens. Moreover, the MRA operation in the pathogen challenge mode can be critical for developing probiotic formulations for gut and soil microbiome. The highly diverse human gut microbiome alterations are associated with

serious diseases like cancer [263]. The screening of inhibitory interactions demonstrated here can be extended towards manipulating the gut microbiome to improve the activity of anti-cancer agents.

Chapter 7 : Conclusion and Future Goals

7.1 Development of photodegradable hydrogel membrane for selective extraction of microbes

In chapter 2, a polyethylene glycol (PEG) based, photoresponsive membrane with photocleavable nitrobenzyl group was developed to connect the microscopic observations in microwell recovery array platform with the ability to confine, extract, isolate, identify cells from any well of interest via off-chip validation and 'omic' type characterizations. The retrieval capabilities developed in this approach were used in most of the dissertation (**Chapters 4, 5, and 6**) to enable follow-up characterizations on cell populations that showed the desired function. The proof-of-principle studies demonstrated in Chapter 2 show that the photodegradable PEG hydrogel can be attached onto silicon microarrays seeded with the bacterium *Agrobacterium tumefaciens*, allowing cell growth and nutrient exchange, and was degraded with a user-defined pattern of 365 nm light in a spatiotemporally controlled manner using the Polygon400 pattern illumination instrument. Although as low as 20 μm diameter wells were demonstrated in this application, the approach was later applied to extract, isolate, and recover cells from any well of interest at 10 μm resolution. This approach was combined with advanced sequencing techniques to identify microbes with antagonistic or synergistic impacts on bacteria of key functional importance in later applications.

7.1.1 Future Goals

For future work, I would recommend enhancing the ability to selectively extract the cells out of microwells by overlaying the microwell substrates with microfluidic channels dedicated to transport cells out of the opened wells. This can eliminate the chances of cross-contamination while extracting multiple wells simultaneously and ensure that cells are extracted at high purity into low solution volumes, which is necessary for many single-cell applications. Also, the design

of the microwells can be altered by fabricating a nanofluidic channel between two wells and study the single-cell interaction between two connected, adjacent wells. Another layer of PEG diacrylate hydrogel can be developed on top of the PEG hydrogel with nitrobenzyl group attached to the microwells in such a setup. After degradation of the photoresponsive hydrogel layer, the interacting cells can be trapped inside the non-photoresponsive PEG diacrylate hydrogel and removed with the aid of microfluidics. In addition, the functionalization of the microwell substrate surface needs to be improved to enhance the successful attachment of the hydrogel membrane on MRA substrates.

After attaching the PEG diacrylate hydrogel membrane on top of MRAs and allowing the trapped cells to grow, it was observed that the membrane swelled due to the water absorbency properties of the hydrogel membrane. . The swelling phenomenon caused the membrane to detach from the MRA surface after just 48 hr of cell growth. The biofilm structure in the microwell arrays significantly contributes to the hydrogel membrane's degradation and needs to be thoroughly studied to achieve favorable membrane attachment to the MRA substrate. I would recommend modifying the membrane to be resistant to degradation and making a chemically and biologically stable, photodegradable membrane to improve the swelling behaviors of the hydrogel. Application of polysaccharide or polymeric adhesives such as HSA crosslinked disuccinimidyl tartarate (DST), acrylate and N-hydroxysuccinimide (NHS) bifunctional tetronic hydrogels, a dextran-based hydrogel comprised of amino dextran and oxidized dextran, or acrylate end-functionalized poloxamine adhesives can be investigated to increase adhesion strength and improve the issue of hydrogel swelling. External stimuli such as temperature, pH, light, magnetic/electric field can also be investigated to increase the attachment of the membrane for a longer period. Finally, there lies

a major scope to investigate the chemical properties of cell culture medium on the mechanical interactions between bacterial cells and hydrogels.

7.2 Application of microwell arrays for the screening of positive and negative interactions in model and non-model systems

The majority of this thesis (**Chapters 3, 4, 5, and 6**) implemented the high-throughput screening abilities of the microwell platform to identify the desired growth outcome of a fluorescently labeled focal species with an isolate collection of interest. In Chapter 3, the proof-of-concept of the MRAs was used to trap a model interaction pair, *A. tumefaciens* and *P. aeruginosa,* and detect rare phenotypes / rare growth outcomes in outlier wells. After monitoring the end-point and growth kinetics of the two species during co-culture, the majority of wells showed co-culture outcomes consistent with previous literature findings (*P. aeruginosa* favored growth). In contrast, rare phenotypes / rare growth outcomes (*A. tumefaciens* favored growth) were detected in a minority of the outlier wells indicating rare growth outcomes.

7.2.1 Future Goals

The model interaction between *A. tumefaciens* and *P. aeruginosa* needs further investigation due to the quorum sensing-regulated growth rate and motility advantages of *P. aeruginosa*. I would propose investigating the type VI secretion system of *A. tumefaciens* on *P. aeruginosa* in the presence of phenylpropanoid-type phytochemicals such as Acetosyringone in MRAs and extend this knowledge to prevent wounding and other physiologic changes in plants caused by *A. tumefaciens*. Such quorum-mediated interaction studies can be extended towards the development of biocontrol agents in other plant systems.

7.3 Application of microwell arrays for the screening of positive and negative interactions in non-model systems

In Chapter 4, the microwell platform capabilities to detect rare growth outcomes developed in Chapter 3 were demonstrated to screen a non-model test species against unknown isolates. A four-membered microbe community extracted from biofuel crop *P. deltoides* roots was screened to enhance and antagonize the growth of plant growth-promoting rhizobacteria *Pantoea* sp. YR343. The motile bacteria cells from the bulk co-cultures of YR343-GFP and *P. deltoides* root microbiome were trapped in microwell arrays using the crosslinked, photo-degradable PEG hydrogel membrane developed in Chapter 2. Therefore, a unique combination of isolates and YR343-GFP was randomly combined to study desired interactions within each microwell. Later, a MATLAB-based computational image analysis tool was used to detect the YR343-GFP growth promoter/antagonist outliers from the fluorescent images. Then the cells were extracted out of these outlier wells, and four-member growth-promoting consortia and a four-member antagonist consortia were identified by 16S rRNA sequencing. The interactions were validated by recombining the cell-free culture fluids (CFCF) from these consortia with YR343-GFP and comparing them with YR343-GFP monoculture. Thus, the *Populus* root microbe community of a few hundred thousand was scaled down to a consortium of 4 isolates inside a single MRA chip. Such capability can aid efforts to engineer plant growth-promoting rhizobacteria. Using *YR343* as a biocontrol agent, genome-level modification of the *P.deltoides* plant can be performed to improve lignocellulosic content, stress resistance, cell wall traits, and root development. In the future, this library of isolates can be associated with the rhizosphere microbiome of plants with high biofuel production potential.

The MRA workflow developed in Chapters 4 was applied in Chapter 5 to screen the *Zea mays* rhizobiome for isolates capable of enhancing the survival and colonization of the plant growth-promoting bacteria (PGPB) *A. brasilense,* and in Chapter 6, to screen non-pathogenic *Agrobacterium* isolates as biocontrol agents against *A. tumefaciens*. In Chapter 5, *Zea mays* rhizosphere isolates were combined with *A. brasilense* strain Sp7-GFP in 10 µm diameter microwells, and seven bacteria isolate responsible for Sp7-GFP growth enhancement were extracted. In addition to the 96-well plate validation assays developed in Chapter 4, the Sp7-GFP mutualist isolates were co-inoculated with healthy maize seeds in a plant growth chamber to validate the enhancement of maize growth. Thus, the *in vitro* observations from the microwell studies were extended towards *in vivo* systems where *A. brasilense*, combined with the isolates, elicited a positive phenotypic outcome (i.e., plant growth enhancement). Demonstrating the ability to connect *in vitro* MRA observations with an *in vivo* environment to generate desirable phenotypic outcomes on a host is a major step forward for this technology, as it opens the door to many practical applications.

In Chapter 6, MRA capabilities were extended towards the screening of biocontrol agents for pathogen inhibition. Pathogenic *A. tumefaciens* sp. 15955-GFP was screened against 576 non-pathogenic *Agrobacterium* isolates in a "pathogen challenge mode" to identify bacteriocin gene clusters responsible for the inhibition of Agro 15955-GFP. The MRA challenge mode was achieved by sequentially reducing *Agrobacterium* isolates in the co-culture with Agro 15955-GFP in MRAs to provide the most favorable growth condition for Agro 15955-GFP the most potent inhibitors of Agro 15955-GFP can be discovered from the isolate collection. Using the MRA in pathogen challenge mode, nine of the most potent inhibitors of Agro 15955-GFP were extracted, validated for antagonism, and are currently undergoing bioinformatics analysis on the whole

genome sequence data to identify bacteriocin gene clusters responsible for Agro 15955-GFP inhibition. Discovery of new environmental isolates that efficiently inhibit *A.tumefaciens* 15955 can help improve plant productivity by providing new biocontrol agents to protect against *A. tumefaciens* sp. 15955, the causative agent of Crown Gall disease.

7.3.1 Future Goals

In Chapter 5, the microwell capabilities were successfully extended towards validating phenotypic growth outcomes in a growth chamber environment. Since the workflow of the MRAs can be extended and modified for any microbiome of interest, there are many potential applications of MRAs for developing bio inoculants, biofertilizers,s and biocontrol agents for disease prevention, plant growth promotion, improvement of plant health under drought stress, and soil bioremediation. In the future, I would propose inoculating the Agro 15955-GFP antagonistic isolates in plant roots containing Crown Gall tumors and conduct *in vivo* assay for determining their inhibitory effect against *A. tumefaciens*. MRAs can also be extended towards ELISA-type immunoassays using antibodies against indole-3-acetic acid (IAA) to validate the claim that the *Pantoea* YR 343 growth-enhancing isolates extracted from the *P. trichocapra* rhizosphere are capable of improving the secretion of IAA from *Pantoea* YR 343. I would propose functionalizing the MRAs with an anti-IAA-C-monoclonal antibody and inoculating the surface with the cell-free culture fluid from the co-culture of *Pantoea* YR 343 with a mutualist isolate, and quantify the release of IAA with the aid of time-lapse fluorescent microscopy. This workflow can be implemented to detect other metabolites influencing plant-microbe interactions and broadly extend to screening consortia for bioproduction of secondary metabolites.

In recent years, global warming and the decrease of water sources near the cultivable lands have reduced water retention in agricultural lands. Therefore, a sustainable approach for increasing

water retention in the soil is necessary. Soil-dwelling bacteria such as *Bacillus subtilis* are known for their ability to alter soil wetting properties, enhancing plant drought tolerance. Specifically, *B. subtilis* produces a cyclic lipopeptide 'surfactin' that can enhance water retention in soil by lowering the surface tension of the surrounding fluid. In future studies, I would recommend screening fluorescently labeled *Bacillus subtilis* strain against soil microbiome in the MRAs to identify bacterial species capable of enhancing the survival and colonization of *B. subtilis* in soil for increased soil wetting and water retention. The *B. subtilis* mediated biophysical changes in the agricultural soil can be extended towards plant drought stress and validated *in vivo* with parameters such as soil water retention levels, hydraulic conductivity, and water evaporation.

To prevent greenhouse gas (GHG) emission, more emphasis is being given to biofuels' production. Switchgrass (*Panicum virgatum* L.) is considered a promising source for biofuel for its potential for carbon sequestration, inherently high-stress resistance, low water, nutrient consumption, and biomass production. Similar to *Populus* plants, most of the interactions between *Panicum virgatum* rhizosphere isolates and biofertilizers are unknown. I want to suggest screening *Panicum virgatum* rhizosphere isolates for beneficial interactions with biofertilizer *V. paradoxus* sp. JM63 to identify the isolates capable of enhancing the colonization of *V. paradoxus* and enhance *Panicum virgatum* growth. Also, I recommend combining *Panicum virgatum* root exudates with *V. paradoxus* in MRAs to couple this workflow with an advanced metabolomics approach to determine interaction pathways for *V. paradoxus* in *Panicum virgatum* roots.

And the final exciting potential application of the MRA is screening bacterial components of the gut microbiome. Recently the role of microorganisms in carcinogenesis has attracted much attention. The anti-tumor immune responses from bacteria such as *Lactobacillus* and *Bifidobacterium* are very well studied. Therefore, screening the gut microbiome to identify the

microbes responsible for tumor inhibition is essential for cancer immunotherapy. Thus, I propose combining *Streptomycetes* bacteria from the gut microbiome with a fluorescently labeled melanoma cell in MRAs and identifying and extracting the isolates capable of inhibiting the growth of melanoma cells. These screens have the potential to uncover anti-cancer bacteria candidates useful for cancer immunotherapy rapidly.

References

1. Connell JL, Whiteley M, Shear JB. Sociomicrobiology in engineered landscapes. *Nat Chem Biol* 2012; **8**: 10–13.

2. Xu J. Microbial ecology in the age of genomics and metagenomics: concepts, tools, and recent advances: MICROBIAL ECOLOGICAL GENOMICS. *Mol Ecol* 2006; **15**: 1713–1731.

3. Coyte KZ, Schluter J, Foster KR. The ecology of the microbiome: Networks, competition, and stability. *Science (80-)* 2015; **350**: 663–666.

4. Hol FJH, Galajda P, Nagy K, Woolthuis RG, Dekker C, Keymer JE. Spatial Structure Facilitates Cooperation in a Social Dilemma: Empirical Evidence from a Bacterial Community. *PLoS One* 2013; **8**: 2–11.

5. Loeschcke A, Thies S. Pseudomonas putida—a versatile host for the production of natural products. *Appl Microbiol Biotechnol* 2015; **99**: 6197–6214.

6. Verlinden RAJJ, Hill DJ, Kenward MA, Williams CD, Radecka I. Bacterial synthesis of biodegradable polyhydroxyalkanoates. *J Appl Microbiol* 2007; **102**: 1437–1449.

7. Nelkner J, Henke C, Lin TW, Patzold W, Hassa J, Jaenicke S, et al. Effect of Long-Term Farming Practices on Agricultural Soil Microbiome Members Represented by Metagenomically Assembled Genomes (MAGs) and Their Predicted Plant-Beneficial Genes. *Genes (Basel)* 2019; **10**: 424.

8. Ojuederie OB, Babalola OO. Microbial and Plant-Assisted Bioremediation of Heavy Metal Polluted Environments: A Review. *Int J Environ Res Public Health* 2017; **14**: 1504.

9. Bolzonella D, Fatone F, Pavan P, Cecchi F. Anaerobic Fermentation of Organic Municipal Solid Wastes for the Production of Soluble Organic Compounds. *Ind Eng Chem Res* 2005; **44**: 3412–3418.

10. Kou S, Cheng D, Sun F, Hsing I-MM. Microfluidics and microbial engineering. *Lab Chip* 2016; **16**: 432–446.

11. Koskella B, Hall LJ, Metcalf CJE. The microbiome beyond the horizon of ecological and evolutionary theory. *Nat Ecol Evol* 2017; **1**: 1606–1615.

12. Keymer JE, Galajda P, Muldoon C, Park S, Austin RH. Bacterial metapopulations in nanofabricated landscapes. *Proc Natl Acad Sci* 2006; **103**: 17290–17295.

13. Dodds WK, Zeglin LH, Ramos RJ, Platt TG, Pandey A, Michaels T, et al. Connections and Feedback: Aquatic, Plant, and Soil Microbiomes in Heterogeneous and Changing Environments. *Bioscience* 2020; **70**: 548–562.

14. Foster KR, Schluter J, Coyte KZ, Rakoff-Nahoum S. The evolution of the host microbiome as an ecosystem on a leash. *Nature* . 2017. Nature Publishing Group. , **548**: 43–51

15. Levine JM, Bascompte J, Adler PB, Allesina S. Beyond pairwise mechanisms of species

coexistence in complex communities. *Nature* 2017; **546**: 56–64.

16. Ratzke C, Denk J, Gore J. Ecological suicide in microbes. *Nat Ecol Evol* 2018; **2**: 867–872.

17. Singh BK, Trivedi P. Microbiome and the future for food and nutrient security. *Microb Biotechnol* 2017; **10**: 50–53.

18. Koch C, Müller S, Harms H, Harnisch F. Microbiomes in bioenergy production: From analysis to management. *Curr Opin Biotechnol* . 2014. Elsevier Ltd. , **27**: 65–72

19. Lindström S, Andersson-Svahn H. Miniaturization of biological assays — {Overview} on microwell devices for single-cell analyses. *Biochim Biophys Acta - Gen Subj* 2011; **1810**: 308–316.

20. Tabassum B, Khan A, Tariq M, Ramzan M, Iqbal Khan MS, Shahid N, et al. Bottlenecks in commercialisation and future prospects of PGPR. *Appl Soil Ecol* 2017; **121**: 102–117.

21. Hol FJH, Dekker C. Zooming in to see the bigger picture: Microfluidic and nanofabrication tools to study bacteria. *Science (80-)* 2014; **346**: 1251821.

22. Murray JL, Connell JL, Stacy A, Turner KH, Whiteley M. Mechanisms of synergy in polymicrobial infections. *J Microbiol* 2014; **52**: 188–199.

23. Boedicker JQ, Li L, Kline TR, Ismagilov RF. Detecting bacteria and determining their susceptibility to antibiotics by stochastic confinement in nanoliter droplets using plug-based microfluidics. *Lab Chip* 2008; **8**: 1265.

24. Zhang Y, Ho Y-PP, Chiu Y-LL, Chan HF, Chlebina B, Schuhmann T, et al. A programmable microenvironment for cellular studies via microfluidics-generated double emulsions. *Biomaterials* 2013; **34**: 4564–4572.

25. Austin RH, Tung CK, Lambert G, Liao D, Gong X. An introduction to micro-ecology patches. *Chem Soc Rev* 2010; **39**: 1049–1059.

26. Benedetto A, Accetta G, Fujita Y, Charras G. Spatiotemporal control of gene expression using microfluidics. *Lab Chip* 2014; **14**: 1336–1347.

27. Masigol M, Fattahi N, Barua N, Lokitz BS, Retterer ST, Platt TG, et al. Identification of Critical Surface Parameters Driving Lectin-Mediated Capture of Bacteria from Solution. *Biomacromolecules* 2019; **20**: 2852–2863.

28. Kehe J, Kulesa A, Ortiz A, Ackerman CM, Thakku SG, Sellers D, et al. Massively parallel screening of synthetic microbial communities. *Proc Natl Acad Sci* 2019; **116**: 12804–12809.

29. Goers L, Freemont P, Polizzi KM. Co-culture systems and technologies: Taking synthetic biology to the next level. *J R Soc Interface* 2014; **11**.

30. Stubbendieck RM, Vargas-Bautista C, Straight PD. Bacterial communities: Interactions to scale. *Front Microbiol* 2016; **7**: 1–19.

31. Abubakar I, Irvine L, Aldus CF, Wyatt GM, Fordham R, Schelenz S, et al. A systematic

review of the clinical, public health and cost-effectiveness of rapid diagnostic tests for the detection and identification of bacterial intestinal pathogens in faeces and food. *Health Technol Assess (Rockv)* 2007; **11**.

32. Matsune S, Kono M, Sun D, Ushikai M, Kurono Y. Hypoxia in paranasal sinuses of patients with chronic sinusitis with or without the complication of nasal allergy. *Acta Otolaryngol* 2003; **123**: 519–523.

33. Deisingh AK, Thompson M. Strategies for the detection of Escherichia coli O157:H7 in foods. *J Appl Microbiol* 2004; **96**: 419–429.

34. Ray NF, Baraniuk JN, Thamer M, Rinehart CS, Gergen PJ, Kaliner M, et al. Healthcare expenditures for sinusitis in 1996: Contributions of asthma, rhinitis, and other airway disorders. *J Allergy Clin Immunol* 1999; **103**: 408–414.

35. Law JWF, Mutalib NSA, Chan KG, Lee LH. Rapid metho ds for the detection of foodborne bacterial pathogens: Principles, applications, advantages and limitations. *Front Microbiol* 2014; **5**: 1–19.

36. Rajapaksha P, Elbourne A, Gangadoo S, Brown R, Cozzolino D, Chapman J. A review of methods for the detection of pathogenic microorganisms. *Analyst* 2019; **144**: 396–411.

37. McKinnon KM. Flow cytometry: An overview. *Curr Protoc Immunol* 2018; **2018**: 5.1.1-5.1.11.

38. Krutzik PO, Nolan GP. Fluorescent cell barcoding in flow cytometry allows high-throughput drug screening and signaling profiling. *Nat Methods* 2006; **3**: 361–368.

39. Nolan’ JP, Sklar’ LA. The etnergence of flow cytotnetry for sensitive, real-titne tneasuretnents of tnolecular interactions. 1998; **16**: 6.

40. Roostalu J, Jõers A, Luidalepp H, Kaldalu N, Tenson T. Cell division in Escherichia coli cultures monitored at single cell resolution. *BMC Microbiol* 2008; **8**: 1–14.

41. Zhang Y, Ho Y-P, Chiu Y-L, Chan HF, Chlebina B, Schuhmann T, et al. A programmable microenvironment for cellular studies via microfluidics-generated double emulsions. *Biomaterials* 2013; **34**: 4564–4572.

42. Austin RH, Tung CK, Lambert G, Liao D, Gong X. An introduction to micro-ecology patches. *Chem Soc Rev* 2010; **39**: 1049–1059.

43. Boedicker JQ, Vincent ME, Ismagilov RF. Microfluidic confinement of single cells of bacteria in small volumes initiates high-density behavior of quorum sensing and growth and reveals its variability. *Angew Chemie - Int Ed* 2009; **48**: 5908–5911.

44. Zhang Q, Lambert G, Liao D, Kim H, Robin K, Tung CK, et al. Acceleration of emergence of bacterial antibiotic resistance in connected microenvironments. *Science (80-)* 2011; **333**: 1764–1767.

45. Hyun JK, Boedicker JQ, Jang WC, Ismagilov RF. Defined spatial structure stabilizes a synthetic multispecies bacterial community. *Proc Natl Acad Sci U S A* 2008; **105**: 18188–18193.

46. P Gravesen JB and OSJ. Microfluidics-a review. *J Micromechanics Microengineering* 1993; **168**.

47. Lim JW, Shin KS, Moon J, Lee SK, Kim T. A Microfluidic Platform for High-Throughput Screening of Small Mutant Libraries. *Anal Chem* 2016; **88**: 5234–5242.

48. Sackmann EK, Fulton AL, Beebe DJ. The present and future role of microfluidics in biomedical research. *Nature* 2014; **507**: 181–189.

49. Rappé MS, Giovannoni SJ. The Uncultured Microbial Majority. *Annu Rev Microbiol* 2003; **57**: 369–394.

50. Drescher K, Shen Y, Bassler BL, Stone HA. Biofilm streamers cause catastrophic disruption of flow with consequences for environmental and medical systems. *Proc Natl Acad Sci U S A* 2013; **110**: 4345–4350.

51. Ottesen E a. Environmental Bacteria. *Science (80-)* 2006; 1464–1467.

52. Arbel D. T, Elizabeth A. O, Jared R. L, Phillips R. Probing Individual Environmental Bacteria for Viruses by Using Microfluidic Digital PCR. *Science (80-)* 2007; **333**: 58–62.

53. Liu X, Painter RE, Enesa K, Holmes D, Whyte G, Garlisi CG, et al. High-throughput screening of antibiotic-resistant bacteria in picodroplets. *Lab Chip* 2016; **16**: 1636–1643.

54. Hol FJHH, Galajda P, Nagy K, Woolthuis RG, Dekker C, Keymer JE. Spatial Structure Facilitates Cooperation in a Social Dilemma: Empirical Evidence from a Bacterial Community. *PLoS One* 2013; **8**: e77042.

55. Connell JL, Ritschdorff ET, Whiteley M, Shear JB. 3D printing of microscopic bacterial communities. *Proc Natl Acad Sci* 2013; **110**: 18380–18385.

56. Ovsianikov A, Deiwick A, Van Vlierberghe S, Dubruel P, Möller L, Drager G, et al. Laser fabrication of three-dimensional CAD scaffolds from photosensitive gelatin for applications in tissue engineering. *Biomacromolecules* 2011; **12**: 851–858.

57. Engelhardt S, Hoch E, Borchers K, Meyer W, Krüger H, Tovar GEM, et al. Fabrication of 2D protein microstructures and 3D polymer-protein hybrid microstructures by two-photon polymerization. *Biofabrication* 2011; **3**.

58. Ziauddin J, David M. S. Microarrays of cells expressing defined cDNAs. *Nature* 2001; **411**: 107.

59. Jiang CY, Dong L, Zhao JK, Hu X, Shen C, Qiao Y, et al. High-throughput single-cell cultivation on microfluidic streak plates. *Appl Environ Microbiol* 2016; **82**: 2210–2218.

60. Ribeiro JP, Mahal LK. Dot by dot: Analyzing the glycome using lectin microarrays. *Curr Opin Chem Biol* 2013; **17**: 827–831.

61. Shen H, David T. W. Lectin microarray. *Proteomics Clin Appl* 2009; **3**: 148–154.

62. Seminara A, Angelini TE, Wilking JN, Vlamakis H, Ebrahim S, Kolter R, et al. Osmotic spreading of Bacillus subtilis biofilms driven by an extracellular matrix. *Proc Natl Acad Sci U S A* 2012; **109**: 1116–1121.

63. Arnfinnsdottir NB, Ottesen V, Lale R, Sletmoen M. The design of simple bacterial microarrays: Development towards immobilizing single living bacteria on predefined micro-sized spots on patterned surfaces. *PLoS One* 2015; **10**: 1–15.

64. Jonczyk R, Kurth T, Lavrentieva A, Walter J-G, Scheper T, Stahl F. Living Cell Microarrays: An Overview of Concepts. *Microarrays* 2016; **5**: 11.

65. Asally M, Kittisopikul M, Rué P, Du Y, Hu Z, Çağatay T, et al. Localized cell death focuses mechanical forces during 3D patterning in a biofilm. *Proc Natl Acad Sci U S A* 2012; **109**: 18891–18896.

66. Wilking JN, Zaburdaev V, De Volder M, Losick R, Brenner MP, Weitz DA. Liquid transport facilitated by channels in Bacillus subtilis biofilms. *Proc Natl Acad Sci U S A* 2013; **110**: 848–852.

67. Nadell CD, Xavier JB, Foster KR. The sociobiology of biofilms. *FEMS Microbiol Rev* 2009; **33**: 206–224.

68. Oliveira NM, Martinez-Garcia E, Xavier J, Durham WM, Kolter R, Kim W, et al. Biofilm formation as a response to ecological competition. *PLoS Biol* 2015; **13**: 1–23.

69. Kolchinsky AM, Gryadunov DA, Lysov YP. Gel-Based Microchips : History and Prospects. 2004; **38**: 4–13.

70. Epstein AK, Pokroy B, Seminara A, Aizenberg J. Bacterial biofilm shows persistent resistance to liquid wetting and gas penetration. *Proc Natl Acad Sci U S A* 2011; **108**: 995–1000.

71. Zhang P, Zhang J, Bian S, Chen Z, Hu Y, Hu R, et al. High-throughput superhydrophobic microwell arrays for investigating multifactorial stem cell niches. *Lab Chip* 2016; **16**: 2996–3006.

72. Gobaa S, Hoehnel S, Roccio M, Negro A, Kobel S, Lutolf MP. Artificial niche microarrays for probing single stem cell fate in high throughput. *Nat Methods* 2011; **8**: 949–955.

73. Reticker-flynn NE, Winslow MM, John M, Xu MJ, Underhill GH, Hynes RO, et al. Extracellular Matrix Interactions That Correlate With Metastasis. 2013.

74. Flaim CJ, Teng D, Chien S, Bhatia SN. Combinatorial signaling microenvironments for studying stem cell fate. *Stem Cells Dev* 2008; **17**: 29–39.

75. Rasi Ghaemi S, Harding FJ, Delalat B, Gronthos S, Voelcker NH. Exploring the mesenchymal stem cell niche using high throughput screening. *Biomaterials* 2013; **34**: 7601–7615.

76. Brafman DA, Shah KD, Fellner T, Chien S, Willert K. Defining long-term maintenance conditions of human embryonic stem cells with arrayed cellular microenvironment technology. *Stem Cells Dev* 2009; **18**: 1141–1154.

77. Iwasaki Y, Ota T. Efficient biotinylation of methacryloyl-functionalized nonadherent cells for formation of cell microarrays. *Chem Commun* 2011; **47**: 10329–10331.

78. Hochbaum AI, Aizenberg J. Bacteria pattern spontaneously on periodic nanostructure arrays. *Nano Lett* 2010; **10**: 3717–3721.

79. Lecuyer S, Rusconi R, Shen Y, Forsyth A, Vlamakis H, Kolter R, et al. Shear stress increases the residence time of adhesion of Pseudomonas aeruginosa. *Biophys J* 2011; **100**: 341–350.

80. Kwon CH, Wheeldon I, Kachouie NN, Lee SH, Bae H, Sant S, et al. Drug-eluting microarrays for cell-based screening of chemical-induced apoptosis. *Anal Chem* 2011; **83**: 4118–4125.

81. Du GS, Pan JZ, Zhao SP, Zhu Y, Den Toonder JMJ, Fang Q. Cell-based drug combination screening with a microfluidic droplet array system. *Anal Chem* 2013; **85**: 6740–6747.

82. Lim JW, Shin KS, Moon J, Lee SK, Kim T. A Microfluidic Platform for High-Throughput Screening of Small Mutant Libraries. *Anal Chem* 2016; **88**: 5234–5242.

83. Lecault V, Vaninsberghe M, Sekulovic S, Knapp DJHF, Wohrer S, Bowden W, et al. High-throughput analysis of single hematopoietic stem cell proliferation in microfluidic cell culture arrays. *Nat Methods* 2011; **8**: 581–589.

84. Gómez-Sjöberg R, Leyrat AA, Pirone DM, Chen CS, Quake SR. Versatile, fully automated, microfluidic cell culture system. *Anal Chem* 2007; **79**: 8557–8563.

85. Hansen RH, Timm AC, Timm CM, Bible AN, Morrell-Falvey JL, Pelletier DA, et al. Stochastic Assembly of Bacteria in Microwell Arrays Reveals the Importance of Confinement in Community Development. *PLoS One* 2016; **11**: e0155080.

86. Ketpun D, Pimpin A, Tongmanee T, Bhanpattanakul S, Piyaviriyakul P, Srituravanich W, et al. A potential application of triangular microwells to entrap single cancer cells: A canine cutaneous mast cell tumor model. *Micromachines* 2019; **10**.

87. Fattahi N, Nieves-Otero PA, Masigol M, Van Der Vlies AJ, Jensen RS, Hansen RR, et al. Photodegradable Hydrogels for Rapid Screening, Isolation, and Genetic Characterization of Bacteria with Rare Phenotypes. *Biomacromolecules* 2020; **21**: 3140–3151.

88. Tolker-Nielsen T, Molin S. Spatial organization of microbial biofilm communities. *Microb Ecol* 2000; **40**: 75–84.

89. Westhoff S, Otto SB, Swinkels A, Bode B, van Wezel GP, Rozen DE. Spatial structure increases the benefits of antibiotic production in Streptomyces*. *Evolution (N Y)* 2020; **74**: 179–187.

90. Van Der Vlies AJ, Barua N, Nieves-Otero PA, Platt TG, Hansen RR. On Demand Release and Retrieval of Bacteria from Microwell Arrays Using Photodegradable Hydrogel Membranes. *ACS Appl Bio Mater* 2019; **2**: 266–276.

91. Hooykaas PJJ, Beijersbergen AGM. The virulence system of Agrobacterium tumefaciens. *Annu Rev Phytopathol* 1994; **32**: 157–179.

92. Barton IS, Fuqua C, Platt TG. Ecological and evolutionary dynamics of a model facultative pathogen: Agrobacterium and crown gall disease of plants. *Environ Microbiol*

2018; **20**: 16–29.

93. Hwang HH, Gelvin SB, Lai EM. Editorial: "Agrobacterium biology and its application to transgenic plant production." *Front Plant Sci* 2015; **6**: 1–3.

94. Venturi V, Fuqua C. Chemical Signaling Between Plants and Plant-Pathogenic Bacteria. *Annu Rev Phytopathol* 2013; **51**: 17–37.

95. Lang J, Faure D. Functions and regulation of quorum-sensing in Agrobacterium tumefaciens. *Front Plant Sci* 2014; **5**: 1–13.

96. Peter J. C, Krishnamohan A, Vidhya K, Simon J, Cascales E. Biogenesis, Architecture, and Function of Bacterial Type IV Secretion Systems. *Annu Rev Microbiol* 2005; **59**: 451–485.

97. Nester EW. Agrobacterium: Nature's Genetic Engineer. *Front Plant Sci* 2015; **5**: 1–16.

98. An D, Danhorn T, Fuqua C, Parsek MR. Quorum sensing and motility mediate interactions between Pseudomonas aeruginosa and Agrobacterium tumefaciens in biofilm cocultures. *Proc Natl Acad Sci* 2006; **103**: 3828–3833.

99. Völksch B, Thon S, Jacobsen ID, Gube M, Völksch B, Thon S, et al. Polyphasic study of plant- and clinic-associated Pantoea agglomerans strains reveals indistinguishable virulence potential. *Infect Genet Evol* 2009; **9**: 1381–1391.

100. Estenson K, Hurst GB, Standaert RF, Bible AN, Garcia D, Chourey K, et al. Characterization of Indole-3-acetic Acid Biosynthesis and the Effects of This Phytohormone on the Proteome of the Plant-Associated Microbe Pantoea sp. YR343. *J Proteome Res* 2018; **17**: 1361–1374.

101. Polle A, Janz D, Teichmann T, Lipka V. Poplar genetic engineering: promoting desirable wood characteristics and pest resistance. *Appl Microbiol Biotechnol* 2013; **97**: 5669–5679.

102. Hacquard S, Schadt CW. Towards a holistic understanding of the beneficial interactions across the Populus microbiome. *New Phytol* 2015; **205**: 1424–1430.

103. Plett JM, Yin H, Mewalal R, Hu R, Li T, Ranjan P, et al. Populus trichocarpa encodes small, effector-like secreted proteins that are highly induced during mutualistic symbiosis. *Sci Rep* 2017; **7**: 1–13.

104. Utturkar SM, Cude WN, Robeson MS, Yang ZK, Klingeman DM, Land ML, et al. Enrichment of Root Endophytic Bacteria from Populus deltoides and Single-Cell-Genomics Analysis. *Appl Environ Microbiol* 2016; **82**: 5698–5708.

105. Sammer UF, Reiher K, Spiteller D, Wensing A, Völksch B. Assessment of the relevance of the antibiotic 2-amino-3-(oxirane-2,3-dicarboxamido)-propanoyl-valine from Pantoea agglomerans biological control strains against bacterial plant pathogens. *Microbiologyopen* 2012; **1**: 438–449.

106. Soma G-I, Inagawa H, Nishizawa T, Yoshioka N, Taniguchi Y, Kohchi C. Preventative and Therapeutic Potential of Lipopolysaccharide Derived from Edible Gram-Negative Bacteria to Various Diseases. *Curr Drug ther* 2008; **3**: 26–32.

107. Simpson ML, Cummings PT. Fluctuations and Correlations in Physical and Biological Nanosystems: The Tale Is in the Tails. *ACS Nano* 2011; **5**: 2425–2432.

108. Avery S V. Microbial cell individuality and the underlying sources of heterogeneity. *Nat Rev Microbiol* 2006; **4**: 577–587.

109. Zhu D, Wang G, Qiao H, Cai J. Fermentative hydrogen production by the new marine Pantoea agglomerans isolated from the mangrove sludge. *Int J Hydrogen Energy* 2008; **33**: 6116–6123.

110. Nakkeeran S, Fernando WGD, Siddiqui ZA. Plant growth promoting rhizobacteria formulations and its scope in commercialization for the management of pests and diseases. *PGPR Biocontrol Biofertilization* 2006; 257–296.

111. Pratap D, Harikesh S, Singh B, Prabha R. DhananjayaaPratappSingh HarikeshhBahadurrSingh RatnaaPrabha Editors Microbial Inoculants in Sustainable Agricultural Productivity Vol. 1: Research Perspectives. 2016.

112. Carvalho TLG, Ballesteros HGF, Thiebaut F, Ferreira PCG, Hemerly AS. Nice to meet you: genetic, epigenetic and metabolic controls of plant perception of beneficial associative and endophytic diazotrophic bacteria in non-leguminous plants. *Plant Mol Biol* 2016; **90**: 561–574.

113. Zhou D, Huang XF, Chaparro JM, Badri D V., Manter DK, Vivanco JM, et al. Root and bacterial secretions regulate the interaction between plants and PGPR leading to distinct plant growth promotion effects. *Plant Soil* 2016; **401**: 259–272.

114. Pedrosa FO, Oliveira ALM, Guimarães VF, Etto RM, Souza EM, Furmam FG, et al. The ammonium excreting Azospirillum brasilense strain HM053: a new alternative inoculant for maize. *Plant Soil* 2020; **451**: 45–56.

115. Cassán F, Vanderleyden J, Spaepen S. Physiological and Agronomical Aspects of Phytohormone Production by Model Plant-Growth-Promoting Rhizobacteria (PGPR) Belonging to the Genus Azospirillum. *J Plant Growth Regul* 2014; **33**: 440–459.

116. Bashan Y, de-Bashan LE. How the plant growth-promoting bacterium azospirillum promotes plant growth-a critical assessment, 1st ed. *Advances in Agronomy* . 2010. Elsevier Inc.

117. Puente ME, Li CY, Bashan Y. Microbial populations and activities in the rhizoplane of rock-weathering desert plants. II. Growth promotion of cactus seedlings. *Plant Biol* 2004; **6**: 643–650.

118. Cassán F, Diaz-Zorita M. Azospirillum sp. in current agriculture: From the laboratory to the field. *Soil Biol Biochem* 2016; **103**: 117–130.

119. Dent D, Cocking E. Establishing symbiotic nitrogen fixation in cereals and other non-legume crops: The Greener Nitrogen Revolution. *Agric Food Secur* 2017; **6**: 1–9.

120. Oliveira IJ, Fontes JRA, Pereira BFF, Muniz AW. Inoculation with Azospirillum brasiliense increases maize yield. *Chem Biol Technol Agric* 2018; **5**: 13–15.

121. Van Deynze A, Zamora P, Delaux PM, Heitmann C, Jayaraman D, Rajasekar S, et al. Nitrogen fixation in a landrace of maize is supported by a mucilage-associated diazotrophic microbiota. *PLoS Biol* 2018; **16**: 1–21.

122. Bulgarelli D, Schlaeppi K, Spaepen S, van Themaat EVL, Schulze-Lefert P. Structure and Functions of the Bacterial Microbiota of Plants. *Annu Rev Plant Biol* 2013; **64**: 807–838.

123. Santi C, Bogusz D, Franche C. Biological nitrogen fixation in non-legume plants. *Ann Bot* 2013; **111**: 743–767.

124. Rosenblueth M, Ormeño-Orrillo E, López-López A, Rogel MA, Reyes-Hernández BJ, Martínez-Romero JC, et al. Nitrogen fixation in cereals. *Front Microbiol* 2018; **9**: 1–13.

125. Forslund E, Guldevall K, Olofsson PE, Frisk T, Christakou AE, Wiklund M, et al. Novel microchip-based tools facilitating live cell imaging and assessment of functional heterogeneity within NK cell populations. *Front Immunol* 2012; **3**: 1–7.

126. Ostuni E, Chen CS, Ingber DE, Whitesides GM. Selective deposition of proteins and cells in arrays of microwells. *Langmuir* 2001; **17**: 2828–2834.

127. Rettig JR, Folch A. Large-scale single-cell trapping and imaging using microwell arrays. *Anal Chem* 2005; **77**: 5628–5634.

128. Li X, Chen W, Li Z, Li L, Gu H, Fu J. Emerging microengineered tools for functional analysis and phenotyping of blood cells. *Trends Biotechnol* 2014; **32**: 586–594.

129. Gong Y, Ogunniyi AO, Love JC. Massively parallel detection of gene expression in single cells using subnanolitre wells. *Lab Chip* 2010; **10**: 2334–2337.

130. Chen Y, Li P, Huang PH, Xie Y, Mai JD, Wang L, et al. Rare cell isolation and analysis in microfluidics. *Lab Chip* 2014; **14**: 626–645.

131. Moeller HC, Mian MK, Shrivastava S, Chung BG, Khademhosseini A. A microwell array system for stem cell culture. *Biomaterials* 2008; **29**: 752–763.

132. Lee JM, Park DY, Yang L, Kim EJ, Ahrberg CD, Lee KB, et al. Generation of uniform-sized multicellular tumor spheroids using hydrogel microwells for advanced drug screening. *Sci Rep* 2018; **8**: 1–10.

133. Ge Z, Girguis PR, Buie CR. Nanoporous microscale microbial incubators. *Lab Chip* 2016; **16**: 480–488.

134. Wilmoth JL, Doak PW, Timm A, Halsted M, Anderson JD, Ginovart M, et al. A microfluidics and agent-based modeling framework for investigating spatial organization in bacterial colonies: The case of Pseudomonas aeruginosa and H1-Type VI secretion interactions. *Front Microbiol* 2018; **9**: 1–11.

135. Li P, Dou X, Feng C, Müller M, Chang MW, Frettlöh M, et al. Isolated Reporter Bacteria in Supramolecular Hydrogel Microwell Arrays. *Langmuir* 2017; **33**: 7799–7809.

136. Levin I, Aharoni A. Evolution in microfluidic droplet. *Chem Biol* 2012; **19**: 929–931.

137. Timm AC, Halsted MC, Wilmoth JL, Retterer ST. Assembly and tracking of microbial

community development within a microwell array platform. *J Vis Exp* 2017; 6:e55701.

138. Halsted M, Wilmoth JL, Briggs PA, Hansen RR, Briggs DP, Timm AC, et al. Development of transparent microwell arrays for optical monitoring and dissection of microbial communities. *J Vac Sci Technol B, Nanotechnol Microelectron Mater Process Meas Phenom* 2016; **34**: 06KI03.

139. Hansen RR, Anderson AC, Barua N, Mcginely LM. Using ongoing laboratory problems as active learning research projects in transport phenomena. *Chem Eng Educ* 2021; **55**: 51–60.

140. Peppas NA, Hilt JZ, Khademhosseini A, Langer R. Hydrogels in biology and medicine: From molecular principles to bionanotechnology. *Adv Mater* 2006; **18**: 1345–1360.

141. Tibbitt MW, Kloxin AM, Sawicki LA, Anseth KS. Mechanical properties and degradation of chain and step-polymerized photodegradable hydrogels. *Macromolecules* 2013; **46**: 2785–2792.

142. Lutolf MP, Lauer-Fields JL, Schmoekel HG, Metters AT, Weber FE, Fields GB, et al. Synthetic matrix metalloproteinase-sensitive hydrogels for the conduction of tissue regeneration: Engineering cell-invasion characteristics. *Proc Natl Acad Sci U S A* 2003; **100**: 5413–5418.

143. Kloxin AM, Kasko AM, Salinas CN, Anseth KS. Photodegradable hydrogels for dynamic tuning of physical and chemical properties. *Science (80-)* 2009; **324**: 59–63.

144. Kloxin AM, Tibbitt MW, Kasko AM, Fairbairn JA, Anseth KS. Tunable hydrogels for external manipulation of cellular microenvironments through controlled photodegradation. *Adv Mater* 2010; **22**: 61–66.

145. Zhu J. Bioactive modification of poly(ethylene glycol) hydrogels for tissue engineering. *Biomaterials* 2010; **31**: 4639–4656.

146. Zustiak SP, Leach JB. Hydrolytically degradable poly(ethylene glycol) hydrogel scaffolds with tunable degradation and mechanical properties. *Biomacromolecules* 2010; **11**: 1348–1357.

147. Tsukatani T, Suenaga H, Higuchi T, Akao T, Ishiyama M, Ezoe K, et al. Colorimetric cell proliferation assay for microorganisms in microtiter plate using water-soluble tetrazolium salts. *J Microbiol Methods* 2008; **75**: 109–116.

148. Zustiak SP, Leach JB. Characterization of Protein Release from Hydrolytically Degradable Poly(ethylene glycol) Hydrogels. *Biotechnol Bioeng* 2011; **108**: 197–206.

149. Metters A, Hubbell J. Network formation and degradation behavior of hydrogels formed by Michael-type addition reactions. *Biomacromolecules* 2005; **6**: 290–301.

150. Tong X, Lee S, Bararpour L, Yang F, Author MB. Long-term Controlled Protein Release from Poly(ethylene glycol) Hydrogels by Modulating Mesh Size and Degradation Graphical abstract HHS Public Access Author manuscript. *Macromol Biosci* 2015; **15**: 1679–1686.

151. Wong DY, Ranganath T, Kasko AM. Low-dose, long-wave UV light does not affect gene expression of human mesenchymal stem cells. *PLoS One* 2015; **10**: 1–21.

152. Tibbitt MW, Kloxin AM, Dyamenahalli KU, Anseth KS. Controlled two-photon photodegradation of PEG hydrogels to study and manipulate subcellular interactions on soft materials. *Soft Matter* 2010; **6**: 5100–5108.

153. Schneider CA, Rasband WS, Eliceiri KW. NIH Image to ImageJ: 25 years of image analysis. *Nat Methods* 2012; **9**: 671–675.

154. Holmes CP. Model Studies for New o-Nitrobenzyl Photolabile Linkers: Substituent Effects on the Rates of Photochemical Cleavage. *J Org Chem* 1997; **62**: 2370–2380.

155. Qvortrup K, Nielsen TE. A photolabile linker for the solid-phase synthesis of 4-substituted NH-1,2,3-triazoles. *Chem Commun* 2011; **47**: 3278–3280.

156. Morton ER, Fuqua C. Genetic manipulation of Agrobacterium. *Curr Protoc Microbiol* 2012; Ch. 3, pp. 1–16, Unit3D.2.

157. Khan SR, Gaines J, Roop RM, Farrand SK. Broad-host-range expression vectors with tightly regulated promoters and their use to examine the influence of TraR and TraM expression on Ti plasmid quorum sensing. *Appl Environ Microbiol* 2008; **74**: 5053–5062.

158. Fiedler CI, Aisenbrey EA, Wahlquist JA, Heveran CM, Ferguson VL, Bryant SJ, et al. Enhanced mechanical properties of photo-clickable thiol-ene PEG hydrogels through repeated photopolymerization of in-swollen macromer. *Soft Matter* 2016; **12**: 9095–9104.

159. Adrian M, Nijenhuis W, Hoogstraaten RI, Willems J, Kapitein LC. A Phytochrome-Derived Photoswitch for Intracellular Transport. *ACS Synth Biol* 2017; **6**: 1248–1256.

160. Curtis SK, Cowden RR. Demonstration of sulfhydryl and disulfide groups by a fluorescent maleimide procedure. *Histochemistry* 1980; **68**: 23–28.

161. O'Connor TK, Humphrey PT, Lapoint RT, Whiteman NK, O'Grady PM. Microbial interactions and the ecology and evolution of Hawaiian Drosophilidae. *Front Microbiol* 2014; **5**: 1–8.

162. Danhorn T, Hentzer M, Givskov M, Parsek MR, Fuqua C. Phosphorus Limitation Enhances Bio lm Formation of the Plant Pathogen. *Society* 2004; **186**: 4492–4501.

163. Platt TG, Morton ER, Barton IS, Bever JD, Fuqua C. Ecological dynamics and complex interactions of Agrobacterium megaplasmids. *Front Plant Sci* 2014; **5**: 1–15.

164. Timm CM, Carter KR, Carrell AA, Jun S-R, Jawdy SS, Vélez JM, et al. Abiotic Stresses Shift Belowground Populus-Associated Bacteria Toward a Core Stress Microbiome. *mSystems* 2018; **3**: e00070-17.

165. Morton ER, Fuqua C. Phenotypic analyses of Agrobacterium. *Curr Protoc Microbiol* 2012; 1–15.

166. Masigol M, Barua N, Retterer ST, Lokitz BS, Hansen RR. Chemical copatterning strategies using azlactone-based block copolymers. *J Vac Sci Technol B, Nanotechnol Microelectron Mater Process Meas Phenom* 2017; **35**: 06GJ01.

167. Masigol M, Barua N, Lokitz BS, Hansen RR. Fabricating Reactive Surfaces with Brush-like and Crosslinked Films of Azlactone-Functionalized Block Co-Polymers. *J Vis Exp* 2018; **2018**: 1–10.

168. Grubbs FE. Sample Criteria for Testing Outlying Observations. *Ann Math Stat* 1950; **21**: 27–58.

169. Ma LS, Hachani A, Lin JS, Filloux A, Lai EM. Agrobacterium tumefaciens deploys a superfamily of type VI secretion DNase effectors as weapons for interbacterial competition in planta. *Cell Host Microbe* 2014; **16**: 94–104.

170. Clemente JC, Ursell LK, Parfrey LW, Knight R. The impact of the gut microbiota on human health: An integrative view. *Cell* . 2012. , **148**: 1258–1270

171. Pflughoeft KJ, Versalovic J. Human microbiome in health and disease. *Annu Rev Pathol Mech Dis* . 2012. , **7**: 99–122

172. Yadav AN, Kumar R, Kumar S, Kumar V, Sugitha TCK, Singh B, et al. Beneficial microbiomes: Biodiversity and potential biotechnological applications for sustainable agriculture and human health. *J Appl Biol Biotechnol* 2017; **5**: 45–57.

173. Doty SL. Functional importance of the plant endophytic microbiome: Implications for agriculture, forestry, and bioenergy. *Functional Importance of the Plant Microbiome: Implications for Agriculture, Forestry and Bioenergy*. 2017. Springer International Publishing, pp 1–5.

174. Ling F, Whitaker R, LeChevallier MW, Liu W-T. Drinking water microbiome assembly induced by water stagnation. *ISME J* 2018; **12**: 1520–1531.

175. Xia Y, Wen X, Zhang B, Yang Y. Diversity and assembly patterns of activated sludge microbial communities: A review. *Biotechnol Adv* . 2018. Elsevier Inc. , **36**: 1038–1047

176. Barberán A, Bates ST, Casamayor EO, Fierer N. Using network analysis to explore co-occurrence patterns in soil microbial communities. *ISME J* 2012; **6**: 343–351.

177. Malla MA, Dubey A, Kumar A, Yadav S, Hashem A, Allah EFA. Exploring the human microbiome: The potential future role of next-generation sequencing in disease diagnosis and treatment. *Front Immunol* . 2019. Frontiers Media S.A. , **10**

178. McCarty NS, Ledesma-Amaro R. Synthetic Biology Tools to Engineer Microbial Communities for Biotechnology. *Trends Biotechnol* . 2019. Elsevier Ltd. , **37**: 181–197

179. Uehling JK, Entler MR, Meredith HR, Millet LJ, Timm CM, Aufrecht JA, et al. Microfluidics and Metabolomics Reveal Symbiotic Bacterial–Fungal Interactions Between Mortierella elongata and Burkholderia Include Metabolite Exchange. *Front Microbiol* 2019; **10**.

180. Burmeister A, Hilgers F, Langner A, Westerwalbesloh C, Kerkhoff Y, Tenhaef N, et al. A microfluidic co-cultivation platform to investigate microbial interactions at defined microenvironments. *Lab Chip* 2019; **19**: 98–110.

181. White AR, Jalali M, Sheng J. A new ecology-on-a-chip microfluidic platform to study

interactions of microbes with a rising oil droplet. *Sci Rep* 2019; **9**.

182. Nagy K, Ábrahám Á, Keymer JE, Galajda P. Application of microfluidics in experimental ecology: The importance of being spatial. *Front Microbiol* . 2018. Frontiers Media S.A. , **9**

183. Bible AN, Fletcher SJ, Pelletier DA, Schadt CW, Jawdy SS, Weston DJ, et al. A Carotenoid-Deficient Mutant in Pantoea sp. YR343, a Bacteria Isolated from the Rhizosphere of Populus deltoides, Is Defective in Root Colonization. *Front Microbiol* 2016; **7**: 491.

184. Blair PM, Land ML, Piatek MJ, Jacobson DA, Lu T-YS, Doktycz MJ, et al. Exploration of the Biosynthetic Potential of the Populus Microbiome. *mSystems* 2018; **3**: e00045-18.

185. Veach AM, Morris R, Yip DZ, Yang ZK, Engle NL, Cregger MA, et al. Rhizosphere microbiomes diverge among Populus trichocarpa plant-host genotypes and chemotypes, but it depends on soil origin. *Microbiome* 2019; **7**: 76.

186. Beckers B, De Beeck MO, Weyens N, Boerjan W, Vangronsveld J. Structural variability and niche differentiation in the rhizosphere and endosphere bacterial microbiome of field-grown poplar trees. *Microbiome* 2017; **5**: 25.

187. Dutkiewicz J, Mackiewicz B, Lemieszek MK, Golec M, Milanowski J. Pantoea agglomerans: A mysterious bacterium of evil and good. Part IV. Beneficial effects. *Ann Agric Environ Med* 2016; **23**: 206–222.

188. Dutkiewicz J, Mackiewicz B, Lemieszek MK, Golec M, Milanowski J. Pantoea agglomerans: A mysterious bacterium of evil and good. Part III. Deleterious effects: Infections of humans, animals and plants. *Ann Agric Environ Med* 2016; **23**: 197–205.

189. Edgar RC. MUSCLE: Multiple sequence alignment with high accuracy and high throughput. *Nucleic Acids Res* 2004; **32**: 1792–1797.

190. Guindon S, Dufayard JF, Lefort V, Anisimova M, Hordijk W, Gascuel O. New algorithms and methods to estimate maximum-likelihood phylogenies: Assessing the performance of PhyML 3.0. *Syst Biol* 2010; **59**: 307–321.

191. Lefort V, Longueville JE, Gascuel O. SMS: Smart Model Selection in PhyML. *Mol Biol Evol* 2017; **34**: 2422–2424.

192. Sprouffske K, Wagner A. Growthcurver: An R package for obtaining interpretable metrics from microbial growth curves. *BMC Bioinformatics* 2016; **17**: 17–20.

193. Abisado RG, Benomar S, Klaus JR, Dandekar AA, Chandler JR. Bacterial Quorum Sensing and Microbial Community Interactions. *MBio* 2018; **9**: e01749-18.

194. Rutherford ST, Bassler BL. Bacterial Quorum Sensing: Its Role in Virulence and Possibilities for Its Control. *Cold Spring Harb Perspect Med* 2012; **2**: a012427–a012427.

195. Tecon R, Ebrahimi A, Kleyer H, Erev Levi S, Or D, Levi SE, et al. Cell-to-cell bacterial interactions promoted by drier conditions on soil surfaces. *Proc Natl Acad Sci* 2018; **115**: 9791–9796.

196. Ngumbi E, Kloepper J. Bacterial-mediated drought tolerance: Current and future prospects. *Appl Soil Ecol* 2016; **105**: 109–125.

197. Komarek AM, Msangi S. Effect of changes in population density and crop productivity on farm households in Malawi. *Agric Econ (United Kingdom)* 2019; **50**: 615–628.

198. Maranguit D, Guillaume T, Kuzyakov Y. Land-use change affects phosphorus fractions in highly weathered tropical soils. *Catena* 2017; **149**: 385–393.

199. Bever JD, Mangan SA, Alexander HM. Maintenance of Plant Species Diversity by Pathogens. *Annu Rev Ecol Evol Syst* 2015; **46**: 305–325.

200. Bender SF, Wagg C, van der Heijden MGA. An Underground Revolution: Biodiversity and Soil Ecological Engineering for Agricultural Sustainability. *Trends Ecol Evol* 2016; **31**: 440–452.

201. Egamberdieva D, Wirth SJ, Alqarawi AA, Abd-Allah EF, Hashem A. Phytohormones and beneficial microbes: Essential components for plants to balance stress and fitness. *Front Microbiol* 2017; **8**: 1–14.

202. Zafar M, Abbasi MK, Khan MA, Khaliq A, Sultan T, Aslam M. Effect of Plant Growth-Promoting Rhizobacteria on Growth, Nodulation and Nutrient Accumulation of Lentil Under Controlled Conditions. *Pedosphere* 2012; **22**: 848–859.

203. Compant S, Saikkonen K, Mitter B, Campisano A, Mercado-Blanco J. Editorial special issue: soil, plants and endophytes. *Plant Soil* 2016; **405**: 1–11.

204. Ma Y, Vosátka M, Freitas H. Editorial: Beneficial microbes alleviate climatic stresses in plants. *Front Plant Sci* 2019; **10**: 1–2.

205. Stamenković S, Beškoski V, Karabegović I, Lazić M, Nikolić N. Microbial fertilizers: A comprehensive review of current findings and future perspectives. *Spanish J Agric Res* 2018; **16**: 1–18.

206. Mus F, Crook MB, Garcia K, Costas AG, Geddes BA, Kouri ED, et al. Symbiotic nitrogen fixation and the challenges to its extension to nonlegumes. *Appl Environ Microbiol* 2016; **82**: 3698–3710.

207. Wang J, Li Q, Xu S, Zhao W, Lei Y, Song C, et al. Traits-based integration of multi-species inoculants facilitates shifts of indigenous soil bacterial community. *Front Microbiol* 2018; **9**: 1–13.

208. dos Santos Lima Fagotti D, Abrantes JLF, Cerezini P, Fukami J, Nogueira MA, del Cerro P, et al. Quorum sensing communication: Bradyrhizobium-Azospirillum interaction via N-acyl-homoserine lactones in the promotion of soybean symbiosis. *J Basic Microbiol* 2019; **59**: 38–53.

209. Bashan Y, de-Bashan LE, Prabhu SR, Hernandez JP. Advances in plant growth-promoting bacterial inoculant technology: Formulations and practical perspectives (1998-2013). *Plant Soil* 2014; **378**: 1–33.

210. Verma R, Chourasia SK, Jha MN. Population dynamics and identification of efficient

strains of Azospirillum in maize ecosystems of Bihar (India). *3 Biotech* 2011; **1**: 247–253.

211. Ferreira AS, Pires RR, Rabelo PG, Oliveira RC, Luz JMQ, Brito CH. Implications of Azospirillum brasilense inoculation and nutrient addition on maize in soils of the Brazilian Cerrado under greenhouse and field conditions. *Appl Soil Ecol* 2013; **72**: 103–108.

212. Hungria M, Campo RJ, Souza EM, Pedrosa FO. Inoculation with selected strains of Azospirillum brasilense and A. lipoferum improves yields of maize and wheat in Brazil. *Plant Soil* 2010; **331**: 413–425.

213. Bardgett RD, Van Der Putten WH. Belowground biodiversity and ecosystem functioning. *Nature* 2014; **515**: 505–511.

214. Barua N, Herken AM, Stern KR, Reese S, Powers RL, Morrell-Falvey JL, et al. Simultaneous discovery of positive and negative interactions among root microbiome bacteria using microwell recovery arrays. *Front Microbiol* 2021; **11**: 3361.

215. Ramos HJO, Roncato-Maccari LDB, Souza EM, Soares-Ramos JRL, Hungria M, Pedrosa FO. Monitoring Azospirillum-wheat interactions using the gfp and gusA genes constitutively expressed from a new broad-host range vector. *J Biotechnol* 2002; **97**: 243–252.

216. Machado GP, Perez Machado G, Colli Mull JG, Aguero Chapin G, Riva de la Riva GA de la, Vargas Samano CD. Plant Growth Promoting Bacteria Isolated From a Mexican Natural Ecosystem Induce Water Stress Resistance in Maize and Sorghum Plants. *J Microb Biochem Technol* 2017; **9**: 209–219.

217. DeSantis TZ, Hugenholtz P, Larsen N, Rojas M, Brodie EL, Keller K, et al. Greengenes, a chimera-checked 16S rRNA gene database and workbench compatible with ARB. *Appl Environ Microbiol* 2006; **72**: 5069–5072.

218. Shannon CE. A Mathematical Theory of Communication. *Bell Syst Tech J* 1948; **27**: 623–656.

219. Quast C, Pruesse E, Yilmaz P, Gerken J, Schweer T, Yarza P, et al. The SILVA ribosomal RNA gene database project: Improved data processing and web-based tools. *Nucleic Acids Res* 2013; **41**: 590–596.

220. Yilmaz P, Parfrey LW, Yarza P, Gerken J, Pruesse E, Quast C, et al. The SILVA and "all-species Living Tree Project (LTP)" taxonomic frameworks. *Nucleic Acids Res* 2014; **42**: 643–648.

221. Bokulich NA, Kaehler BD, Rideout JR, Dillon M, Bolyen E, Knight R, et al. Optimizing taxonomic classification of marker-gene amplicon sequences with QIIME 2's q2-feature-classifier plugin. *Microbiome* 2018; **6**: 1–17.

222. Niu B, Kolter R. Quantification of the Composition Dynamics of a Maize Root-associated Simplified Bacterial Community and Evaluation of Its Biological Control Effect. *Bio-Protocol* 2018; **8**: 1–17.

223. Tang A, Haruna AO, Majid NMA, Jalloh MB. Effects of selected functional bacteria on maize growth and nutrient use efficiency. *Microorganisms* 2020; **8**: 1–25.

224. Khan AR, Park GS, Asaf S, Hong SJ, Jung BK, Shin JH. Complete genome analysis of Serratia marcescens RSC-14: A plant growth-promoting bacterium that alleviates cadmium stress in host plants. *PLoS One* 2017; **12**: 1–17.

225. Matteoli FP, Passarelli-Araujo H, Reis RJA, Da Rocha LO, De Souza EM, Aravind L, et al. Genome sequencing and assessment of plant growth-promoting properties of a Serratia marcescens strain isolated from vermicompost. *BMC Genomics* 2018; **19**: 1–19.

226. Roux B, Rodde N, Jardinaud MF, Timmers T, Sauviac L, Cottret L, et al. An integrated analysis of plant and bacterial gene expression in symbiotic root nodules using laser-capture microdissection coupled to RNA sequencing. *Plant J* 2014; **77**: 817–837.

227. Ruppel S, Merbach W. Effect of ammonium and nitrate on 15N2-fixation of Azospirillum spp. and Pantoea agglomerans in association with wheat plants. *Microbiol Res* 1997; **152**: 377–383.

228. Verma SC, Ladha JK, Tripathi AK. Evaluation of plant growth promoting and colonization ability of endophytic diazotrophs from deep water rice. *J Biotechnol* 2001; **91**: 127–141.

229. Feng Y, Shen D, Song W. Rice endophyte Pantoea agglomerans YS19 promotes host plant growth and affects allocations of host photosynthates. *J Appl Microbiol* 2006; **100**: 938–945.

230. Atrouni A Al, Joly-Guillou ML, Hamze M, Kempf M. Reservoirs of non-baumannii Acinetobacter species. *Front Microbiol* 2016; **7**: 1–12.

231. Ahkami AH, Allen White R, Handakumbura PP, Jansson C. Rhizosphere engineering: Enhancing sustainable plant ecosystem productivity. *Rhizosphere* 2017; **3**: 233–243.

232. Haskett TL, Tkacz A, Poole PS. Engineering rhizobacteria for sustainable agriculture. *ISME J* 2021; **15**: 949–964.

233. Trivedi P, Leach JE, Tringe SG, Sa T, Singh BK. Plant–microbiome interactions: from community assembly to plant health. *Nat Rev Microbiol* 2020; **18**: 607–621.

234. Backer R, Rokem JS, Ilangumaran G, Lamont J, Praslickova D, Ricci E, et al. Plant growth-promoting rhizobacteria: Context, mechanisms of action, and roadmap to commercialization of biostimulants for sustainable agriculture. *Front Plant Sci* 2018; **871**: 1–17.

235. Ferre R, Badosa E, Feliu L, Planas M, Montesinos E, Bardají E. Inhibition of plant-pathogenic bacteria by short synthetic cecropin A-melittin hybrid peptides. *Appl Environ Microbiol* 2006; **72**: 3302–3308.

236. Kirzinger MWB, Nadarasah G, Stavrinides J. Insights into cross-kingdom plant pathogenic bacteria. *Genes (Basel)* 2011; **2**: 980–997.

237. Nikitin IK. Bacterial contamination of blood components. *Gematol i Transfusiologiya* 2010; **55**: 10–13.

238. Kim JS, Yoon SJ, Park YJ, Kim SY, Ryu CM. Crossing the kingdom border: Human

diseases caused by plant pathogens. *Environ Microbiol* 2020; **22**: 2485–2495.

239. Dumas A, Bernard L, Poquet Y, Lugo-Villarino G, Neyrolles O. The role of the lung microbiota and the gut–lung axis in respiratory infectious diseases. *Cell Microbiol* 2018; **20**: 1–9.

240. Marsland BJ, Gollwitzer ES. Host-microorganism interactions in lung diseases. *Nat Rev Immunol* 2014; **14**: 827–835.

241. Martins PMM, Merfa M V., Takita MA, De Souza AA. Persistence in phytopathogenic bacteria: Do we know enough? *Front Microbiol* 2018; **9**: 1–14.

242. Cawoy H, Debois D, Franzil L, De Pauw E, Thonart P, Ongena M. Lipopeptides as main ingredients for inhibition of fungal phytopathogens by Bacillus subtilis/amyloliquefaciens. *Microb Biotechnol* 2015; **8**: 281–295.

243. Coyte KZ, Schluter J, Foster KR. The ecology of the microbiome: Networks, competition, and stability. *Science (80-)* 2015; **350**: 663–666.

244. Deketelaere S, Tyvaert L, França SC, Hofte M. Desirable traits of a good biocontrol agent against Verticillium wilt. *Front Microbiol* 2017; **8**: 1–23.

245. Escobar MA, Dandekar AM. Agrobacterium tumefaciens as an agent of disease. *Trends Plant Sci* 2003; **8**: 380–386.

246. Gohlke J, Deeken R. Plant responses to Agrobacterium tumefaciens and crown gall development. *Front Plant Sci* 2014; **5**: 1–11.

247. Hwang H-H, Yu M, Lai E-M. Agrobacterium -Mediated Plant Transformation: Biology and Applications . *Arab B* 2017; **15**: e0186.

248. Pitzschke A. Agrobacterium infection and plant defense-transformation success hangs by a thread. *Front Plant Sci* 2013; **4**: 1–12.

249. Faist H, Keller A, Hentschel U, Deeken R. Grapevine (Vitis vinifera) crown galls host distinct microbiota. *Appl Environ Microbiol* 2016; **82**: 5542–5552.

250. Pulawska J. Crown gall of stone fruits and nuts, economic significance and diversity of its causal agents: Tumorigenic Agrobacterium spp. *J Plant Pathol* 2010; **92**.

251. Burr TJ, Bazzi C, Süle S, Otten L. Crown gall of grape: Biology of Agrobacterium vitis and the development of disease control strategies. *Plant Dis* 1998; **82**: 1288–1297.

252. Kerr A, Bullard G. Biocontrol of Crown Gall by Rhizobium rhizogenes: Challenges in Biopesticide Commercialisation. *Agronomy* 2020; **10**: 1126.

253. Kerr A. Biological control of Crown Gall. *Australas Plant Pathol* 2016; **45**: 15–18.

254. Jones DA, Ryder MH, Clare BG, Farrand SK, Kerr A. Construction of a Tra- deletion mutant of pAgK84 to safeguard the biological control of crown gall. *MGG Mol Gen Genet* 1988; **212**: 207–214.

255. De Cleene M, De Ley J. The host range of crown gall. *Bot Rev* 1976; **42**: 389–466.

256. Hansen G. Evidence for Agrobacterium-induced apoptosis in maize cells. *Mol Plant-Microbe Interact* 2000; **13**: 649–657.

257. Kim JG, Park BK, Kim SU, Choi D, Nahm BH, Moon JS, et al. Bases of biocontrol: Sequence predicts synthesis and mode of action of agrocin 84, the Trojan Horse antibiotic that controls crown gall. *Proc Natl Acad Sci U S A* 2006; **103**: 8846–8851.

258. Kawaguchi A, Inoue K, Nasu H. Inhibition of crown gall formation by Agrobacterium radiobacter biovar 3 strains isolated from grapevine. *J Gen Plant Pathol* 2005; **71**: 422–430.

259. Li JY, Wang JH, Wang HM. Mode of action of the antibacterial compound Ar26 produced by Agrobacterium vitis strain E26 with activity against A. tumefaciens, A. rhizogenes and A. vitis. *J Phytopathol* 2009; **157**: 159–165.

260. Platt TG, Bever JD, Fuqua C. A cooperative virulence plasmid imposes a high fitness cost under conditions that induce pathogenesis. *Proc R Soc B Biol Sci* 2012; **279**: 1691–1699.

261. Hayman GT, Farrand SK. Characterization and mapping of the agrocinopine-agrocin 84 locus on the nopaline Ti plasmid pTiC58. *J Bacteriol* 1988; **170**: 1759–1767.

262. Kado CI. The Tumor-Inducing Substance of Agrobacterium Tumefaciens. *Annu Rev Phytopathol* 1976; **14**: 265–308.

263. Zitvogel L, Galluzzi L, Viaud S, Vétizou M, Daillère R, Merad M, et al. Cancer and the gut microbiota: An unexpected link. *Sci Transl Med* 2015; **7**: 1–10.

264. Promoter P. Benchmark s pBBR1-GFP: A Broad- Host-Range Vector for Prokaryotic Promoter Studies. *Biotechniques* 1999; **26**: 620–622.

265. Quandt J, Hynes MF. Versatile suicide vectors which allow direct selection for gene replacement in Gram-negative bacteria. *Gene* 1993; **127**: 15–21.

266. Dennis JJ, Zylstra GJ. Plasposons: Modular self-cloning minitransposon derivatives for rapid genetic analysis of gram-negative bacterial genomes. *Appl Environ Microbiol* 1998; **64**: 2710–2715.

267. Tavaré S. Some probabilistic and statistical problems in the analysis of DNA sequences. *Am Math Soc Lect Math Life Sci* . 1986. , **17**: 57–86

268. Figueroa-Cuilan W, Daniel JJ, Howell M, Sulaiman A, Brown PJB. Mini-Tn7 insertion in an artificial attTn7 site enables depletion of the essential master regulator ctrA in the phytopathogen agrobacterium tumefaciens. *Appl Environ Microbiol* 2016; **82**: 5015–5025.

269. Simon R, Priefer U, Pühler A. A Broad Host Range Mobilization System for In Vivo Genetic Engineering: Transposon Mutagenesis in Gram Negative Bacteria. *Bio/Technology* 1983; **1**: 784–791.

Appendix A: Supporting information from Chapter 2

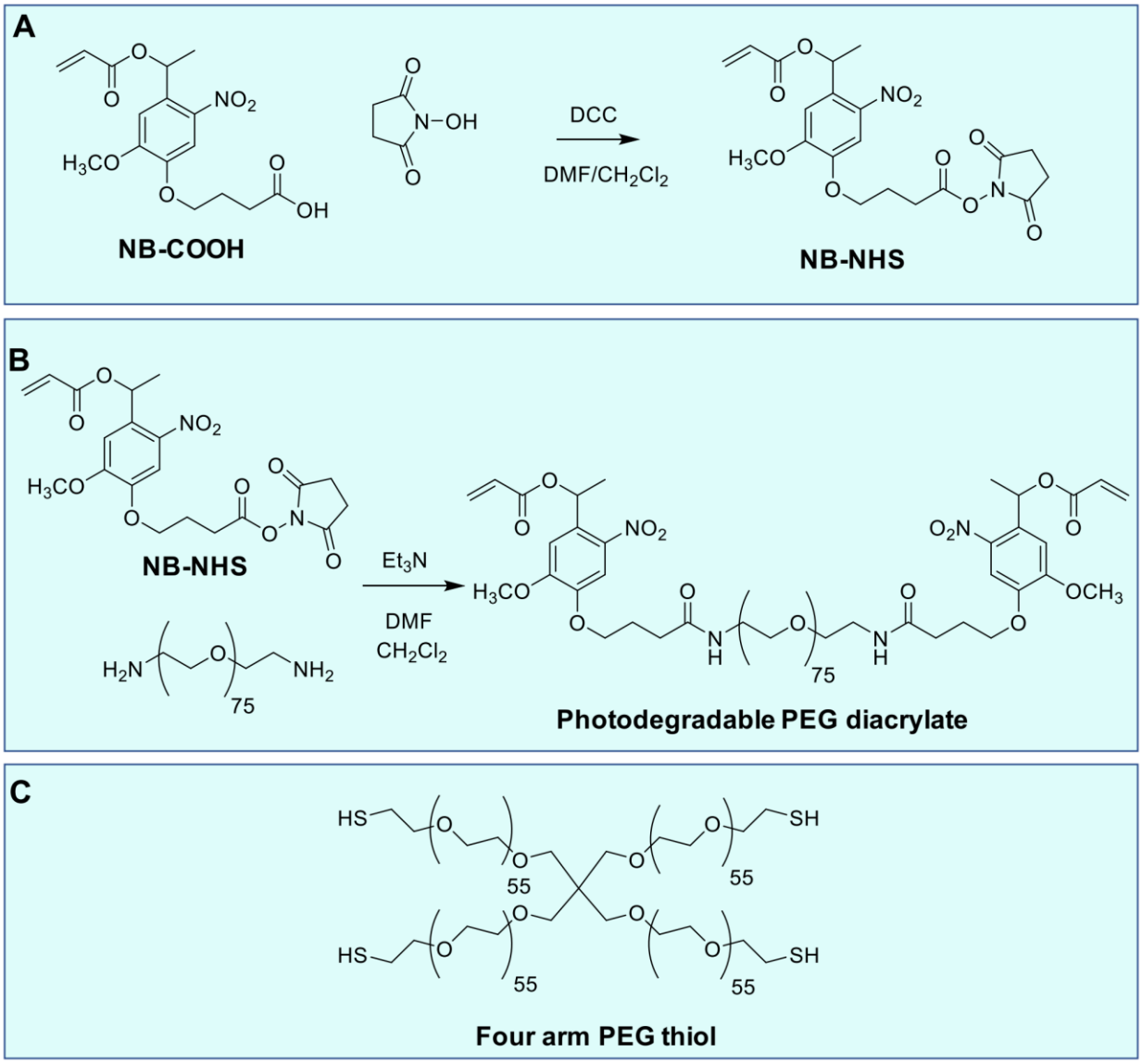

Scheme S1. (**A**) Reaction scheme to prepare NB-NHS and (**B**) photodegradable PEG diacrylate and (**C**) chemical structure of the four-arm PEG thiol.

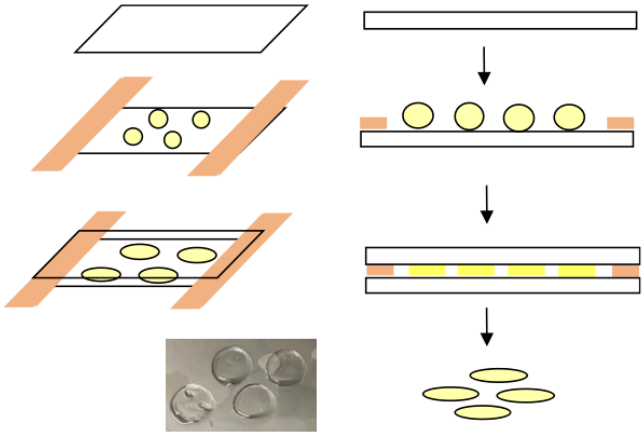

Figure S1. Setup for the fabrication of *A. tumefaciens*-encapsulated membranes. A suspension of bacteria in 2X LB are mixed with solutions of the photodegradable PEG diacrylate and the four arm PEG thiol (pH 8, acrylate/thiol concentration 22 or 35 mM). The mixture is then pipetted onto a glass slide (yellow spheres) having spacers opposite of each other (beige). Immediately, a second glass slide is placed on top and the crosslinking reaction is carried out at room temperature for 25 minutes. After carefully separating the glass slides, the bacteria-encapsulated membranes are washed and kept on agar or in liquid culture medium at 28ºC.

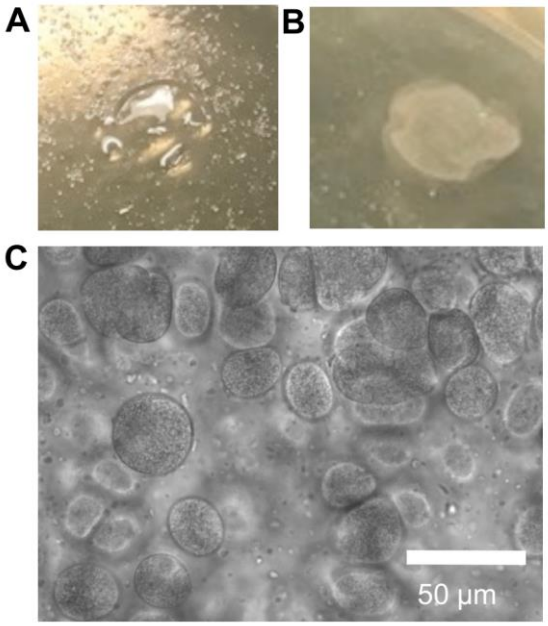

Figure S2. *A. tumefaciens* can grow inside the membrane. (**A**) Photograph of a membrane with encapsulated *A. tumefaciens* on an agar plate immediately after washing. (**B**) The same membrane after 24 hours at 28oC showing that the initial clear membrane has an opaque appearance due to growing bacteria. (**C**) Microscope image of the same membrane showing the presence of *A. tumefaciens* clusters 20 - 40 µm in size.

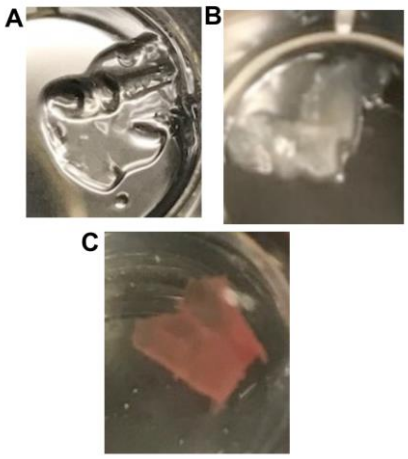

Figure S3. Cell viability test using triphenyltetrazolium chloride (TTC) shows that the bacteria inside the membrane are alive. (**A**) *A. tumefaciens*-encapsulated membrane after crosslinking and swelling in liquid LB medium. (**B**) The same membrane but 24 hours later. (**C**) The same membrane after another 24 hours cultured in the presence of TTC. TTC is reduced by metabolically active bacteria resulting in formation of water-insoluble pink crystals.

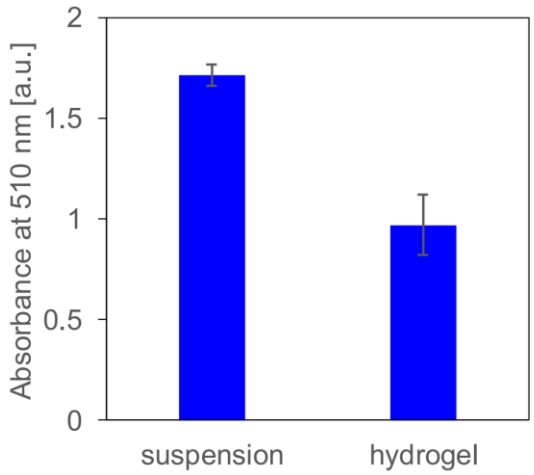

Figure S4. TTC assay results quantifying the effect of hydrogel encapsulation on *A. tumefaciens* viability. *A. tumefaciens* was grown to mid-log phase and resuspended in 2X phosphate buffered LB. 12.5 µL of bacteria suspension was mixed with 5.6 µL of crosslinker and 6.9 µL of the four-arm thiol and pipetted onto the bottom of a culture tube (n=3). After crosslinking for 25 min at room temperature, 1.5 mL LB was added. At the same time 12.5 µL of the bacteria suspension in 2X phosphate buffer was added to 1.5 mL LB directly (n=3). The tubes were placed in the shaker and incubated for 24 h at 28oC at 200 rpm. 150 µL of 5 mg/mL TTC in LB medium was then added to the culture and the tubes were shaken for 2 h at 28oC. The samples were spun down at 3000 g for 10 min and the supernatant careful decanted. The pellet was then suspended in 400 µL DMSO and the formed crystals dissolved by sonicating, vortexing and heating. The samples were spun down at 3000 g for 10 min and 100 µL of the supernatant transferred to a polystyrene 96 well plate to measure the absorbance at 510 nm.

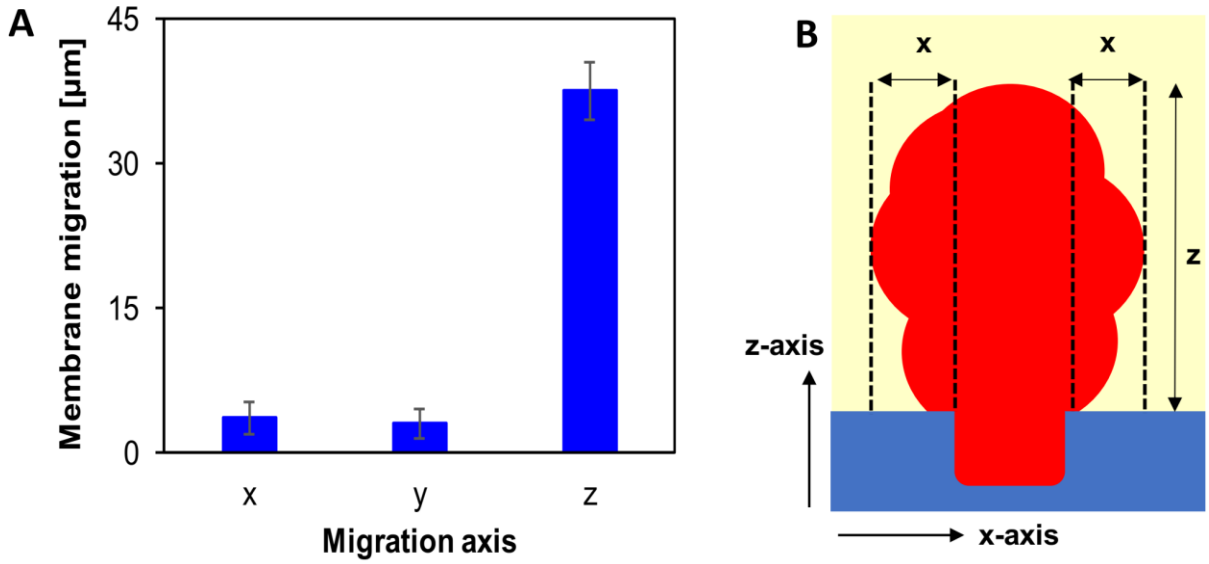

Figure S5. (A) Migration distance of bacteria through the membrane for the 4 wells in Figure 5B of the manuscript. **(B)** Migration distance of bacteria (red) through the membrane (yellow) in the x and y directions was quantified by measuring the maximum distance migrated from the edge of the wells in the x-z and y-z projections. Migration distance in z was measured as the distance migrated in the z-axis from the top of the silicon microarray in the x-z projection, as shown in the schematic. This data clearly shows that bacteria migration is favored along the z-axis

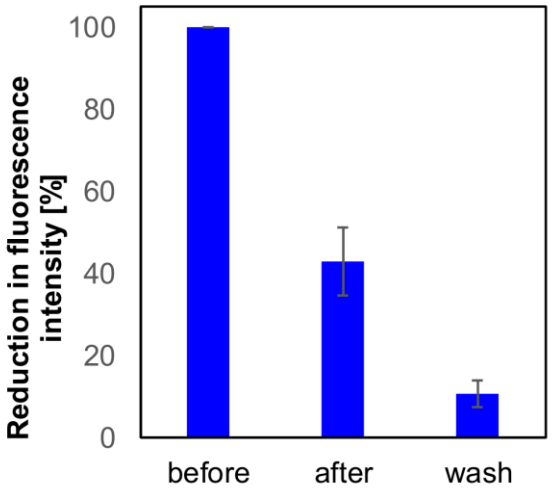

Figure S6. Fluorescence intensity after irradiation and washing the microwells in Figure 9, expressed as the percentage of the same microwells before irradiation. Intensity of "wells before" was corrected for absorbance of the membrane by measuring five different spots on the microarray.

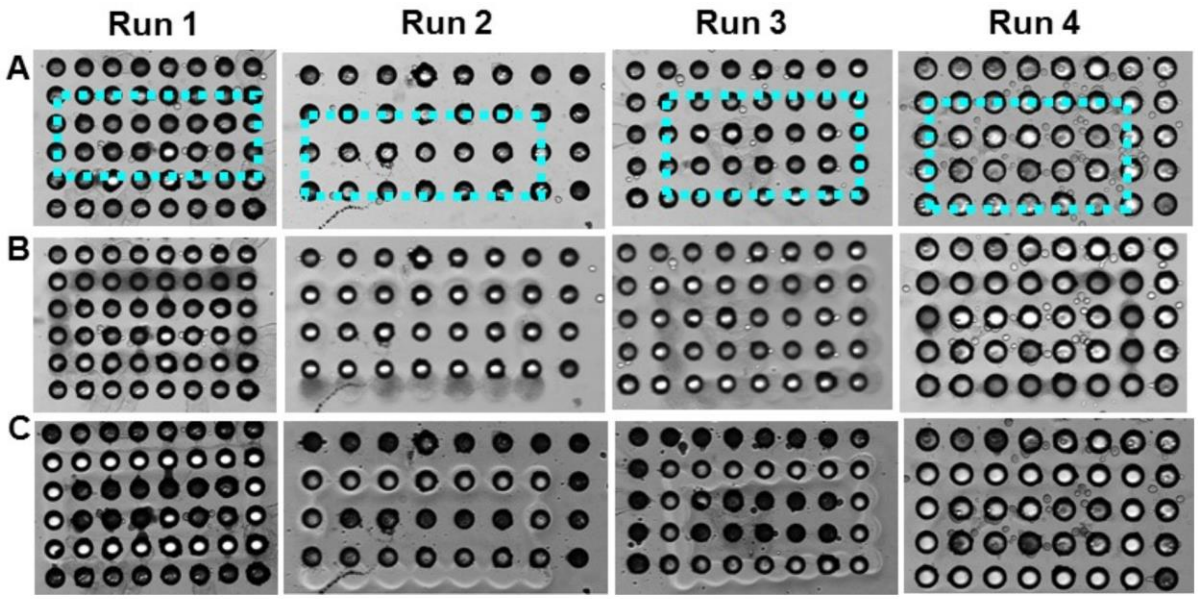

Figure S7. Images showing a total of 72 microwells that have been opened with patterned light. (**A**) Microwells before irradiation. (**B**) The same microwells immediately after irradiation and (**C**) the same microwells after washing with Tween20/LB. *A. tumefaciens* was seeded at OD = 0.2 and cultured for 1 day at 28oC. 40 µm diameter (runs 1-3) and 50 µm diameter (run 4) microwells were irradiated with 60 µm circle patterns for 5 minutes at 0.7 mW/mm^2.

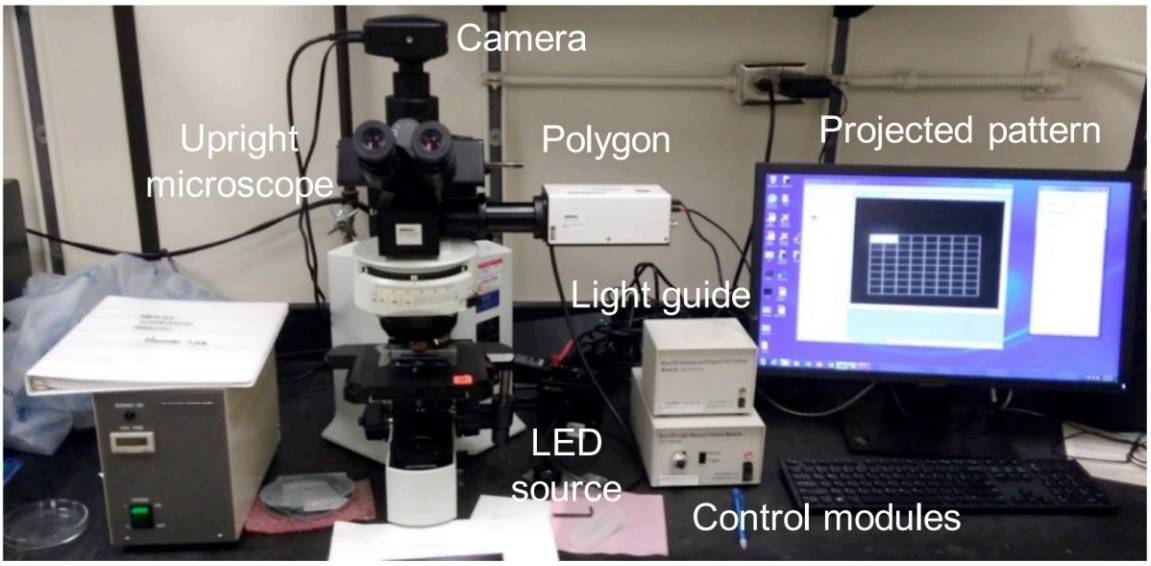

Figure S8. Setup used for the irradiation experiments. The Polygon is attached to the upright microscope via an adapter. Light (365 nm) is delivered from the LED light source by a liquid light guide. The control modules to operate the Polygon are controlled by Polyscan2 software.

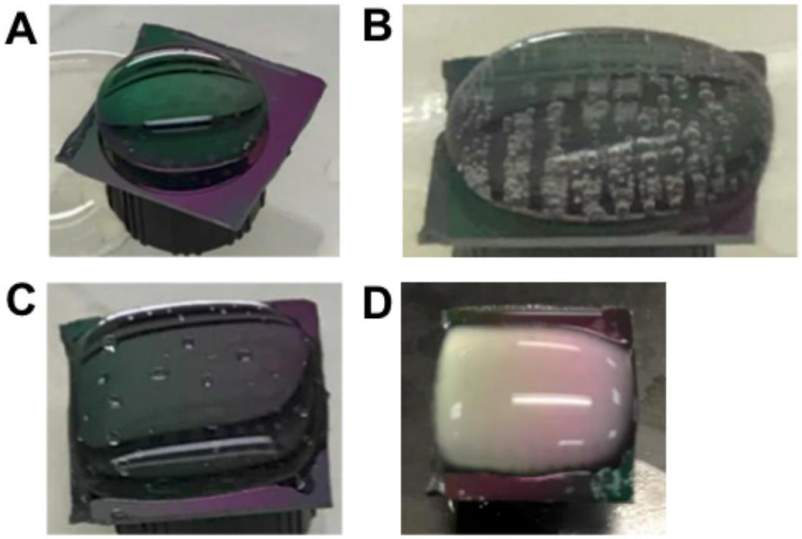

Figure S9. Seeding bacteria into the microwells. (**A**) Prior to cell seeding the hydrophobic parylene-coated microwell is layered with LB medium and (**B**) put under reduced pressure to remove air from the microwells. (**C**) Filling the microwells with LB increases the wettability of the parylene surface. (**D**) After removing the LB medium the bacteria suspension is added to seed the microwells.

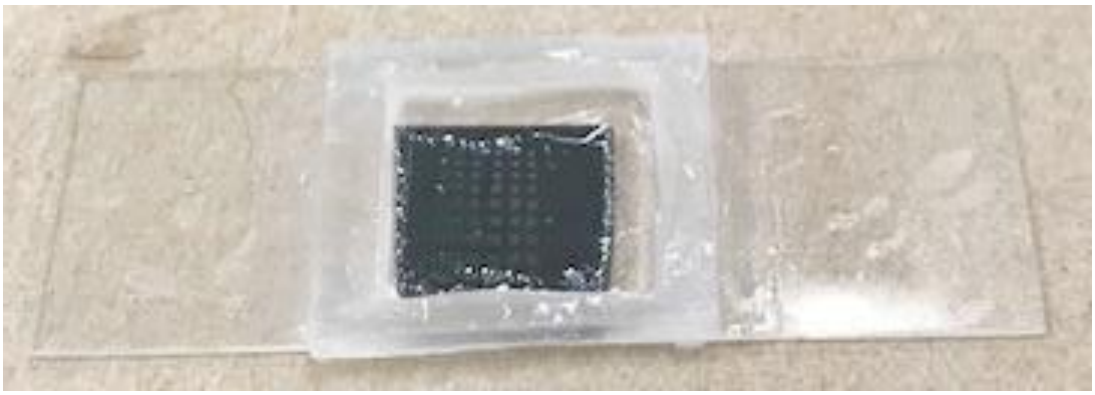

Figure S10. Sample holder used for culturing and photodegradation experiments. A rectangular area made from PDMS is glued onto a glass slide. By adjusting the height of the border, the culture volume can be controlled (1-2 mL).

Appendix B: Supporting information from Chapter 3 and 4

P. aeruginosa and *A. tumefaciens* culture

A model system comprised of *Agrobacterium tumefaciens* C58 expressing GFP (C58-GFP) and *Pseudomonas aeruginosa* PAO1 expressing mCherry (PAO1-mCherry) was used to characterize seeding behavior and interaction in microwell recovery arrays (MRAs). Glycerol stocks were prepared for both strains and stored at -80°C. C58-GFP and PAO1-mCherry were cultured on LB-agar for 24 hrs at 28 and 37°C respectively. For liquid culture of C58-GFP and PAO1-mCherry, a single colony was picked using a sterile inoculation loop, inoculated in 2 mL LB media (10g BactoTryptone, 5g Yeast, 10g NaCl and 15g agar per 1000mL) in sterile test tubes and cultured in a shaker (28 and 37°C respectively, 215 rpm) for 24 hrs. 150 µg Kanamycin and 0.5 µg IPTG (Sigma) were added to each ml of the liquid culture for both C58-GFP and PAO1-mCherry cultures. The tubes were then centrifuged (Eppendorf Centrifuge 5702 Series Ea) and the media was changed every 24 hrs for up to 1 week to keep cells viable.

Growth studies of *Pantoea* sp. YR343 monoculture

For solid phase cultures, Pantoea sp. YR343 expressing GFP (YR343-GFP) was cultured in R2A-agar media (pH: 7.2 ± 0.2, Thermo Fisher) at 28°C for 24 hr. For liquid culture studies, single colonies were picked using sterile inoculation loops and mixed in 2 mL R2A broth media (pH: 7.2 ± 0.2, Teknova) supplemented with Kanamycin (150 µg/mL) in sterile test tubes and cultured for 24 hrs (28°C, 215 rpm). To measure growth parameters of YR343-GFP, liquid cultures were diluted to OD_{600} = 0.1 and 100µL was added to a 96 well plate (28°C, 600 rpm) and absorbance (OD_{600}) readings were taken every 10 min. For YR343 monoculture, a lag phase of 2.5 hr and growth rate of 0.673 hr^{-1} were measured, the culture reached stationary phase at 8 hr.

16S rRNA community analysis of *Populus trichocarpa* rhizosphere and input samples

The purified gDNAs of the *Populus rhizosphere* sample and the R2A media culture used to seed the microwell array were extracted using E.Z.N.A soil DNA kit (Omega Bio-tek, Norcross, GA), diluted to 20 ng/µl in 100 µl aliquots and sent to Integrated Genomics Facility (Department of Plant Pathology, Kansas State University, Manhattan, KS) for the 16S Illumina sequencing of the hypervariable V3 and V4 region using Nextera XT index Kit v2 (Illumina, Inc., San Diego, CA). 16S rRNA community analysis was performed with Qiime2-2020.8 (Bolyen et al., 2019). The multiplexed raw sequence data with the barcodes were demultiplexed using q2-demux plugin, quality filtered and denoised with q2-dada2 (Callahan et al., 2016) plugin and aligned with mafft (Katoh et al., 2002). The q2-diversity plugin was used to determine alpha-diversity metrics (observed OTUs [217] (**Supplementary Figure 11A**) and Shannon's diversity index [218] (**Supplementary Figure 11B**) after rarefaction of the samples to 900 sequences per sample. Taxonomy was assigned to amplicon sequence variants using the silva-138-99-515-806 [219] classify-sklearn naïve Bayes taxonomy classifier against the Silva 138 99% OTUs reference sequences [220]. This analysis found the Populus rhizosphere sample and the microarray input cultured in R2A media to contain 120 and 85 observed OTUs and to have Shannon's diversity indices of 4.165 and 3.57, respectively. The q2-taxa plugin was used to explore and visualize the taxonomic composition of the classified sequences by creating taxa bar plots [221] (**Supplementary Figure 11C**). Raw 16S Illumina sequences were uploaded to NCBI sequence read archive (Accession Number: PRJNA678376).

Fabrication of LB-Agar coated PDMS coverslips

To prepare LB-agar coated PDMS coverslips, a modified procedure from Hansen et al. was followed [85, 139]. 21 g PDMS monomer and 3 g of curing agent were mixed for 3 min, degassed for 30 min, then placed in a 6 in. diameter polystyrene petri dish, degassed again for 30 min and baked at 80°C for 2 hr. PDMS coverslips were ~2000 µm thick. Sterile 25×75mm PDMS coverslips were then cut from the dish, placed in a second polystyrene dish and coated with LB agar by evenly pouring 3 mL of boiling LB agar over the coverslips and the dish. The dish was cooled at 4°C for 30 min to allow the media to solidify over the coverslips and to ensure minimum dehydration. The thickness of the agar layer was ~100 µm. After seeding the microwell substrate with bacteria, microwells were immediately sealed with the coverslips and placed in the humidified, live cell incubator chamber to conduct growth experiments (**Supplementary Figure 8**).

Photodegradable membrane attachment

The procedure for attaching the photodegradable hydrogel membranes to microwell arrays is described in van der Vlies et al. (Van Der Vlies et al., 2019) was used here. 25×25 mm clean glass slides (Fisher Scientific) were first functionalized with a non-reactive silane layer by incubating in 20 mL of 0.5% v/v trichloro(1H,1H,2H,2H-perfluorooctyl) silane in toluene for 180 min (Van Der Vlies et al., 2019). Phosphate buffer saline (PBS) with LB solution was then prepared by adding NaH_2PO_4 to LB liquid media to reach 100mM final phosphate concentration and adjusting to pH 8 by adding 5M NaOH (aq.). The membrane precursor solution was then obtained by mixing 12.5 µL of PBS-LB solution with 5.6 µL of photodegradable PEG diacrylate monomer (MW 3400) and 6.9 µL of a four-arm PEG thiol solution monomer (Tibbitt et al., 2013) (MW 10000, NOF America Corporation, DE-100SH). The concentrations of both PEG diacrylate monomer and four-arm PEG

thiol solution monomer were 22mM in the precursor solution. 15µL of the liquid pre-cursor solution was then quickly pipetted on top of the perfluoroalkylated glass slides, and the solution was placed over a seeded microwell substrate. Metal spacers were used to provide a constant 38 µm gap between the glass slide and the microwell for the precursor solution. The substrate was then incubated for 25 min at room temperature to allow for membrane formation though monomer crosslinking and gelation (Van Der Vlies et al., 2019). The glass slide was then carefully separated from the membrane-functionalized microwell array and the microwell array was placed on top of a PDMS coverslip and added to the 3D printed scaffold for culture and imaging.

Fabrication of 3D printed scaffolds

A custom 3D printed scaffold was designed for imaging microwells with time lapse fluorescence microscopy (TLFM). The 3D printed nylon scaffold was designed using Blender software (Coakley et al., 2014). A seeded and membrane-functionalized microwell was placed in the scaffold, the scaffold was then placed over a standard glass microscope slide. The scaffold holds the sealed microwell substrate approximately 100 µm above the slide surface, as shown in **Supplementary Figure 9**. This allows for bacteria within the wells to receive nutrients and allows the microwell substrate to remain fixed within the focal plane of the 20× objective, eliminating drift in the x,y, and z-directions during the culture period.

Membrane degradation and well extraction

Extraction of cell aggregates from microwells followed the protocol recently described in van der Vlies et al.(Van Der Vlies et al., 2019). An Olympus BX51 upright microscope equipped with an Infinity 3-1 microscopy camera (Lumenera) and Infinity Analyze software was used to identify the location of target wells according to the on-chip well address. Greyscale images of targeted microwells were taken during extraction with a 20×/0.5NA objective. The Polygon400 photo-

patterning instrument (Mightex) containing a 365 nm high-power LED source (50 W) was used to project UV light patterns onto the target well locations. The instrument was attached to the BX51 microscope though an adapter containing dichoic filter cube. A BioLED light source control module equipped with a BioLED analog and digital I/O control module was used to control the light source and a liquid light guide was used to deliver light to the Polygon400. Prior to extraction, the Polygon400 was calibrated using PolyScan2 software and a calibration mirror. For extraction, a cultured microwell array substrate with the attached membrane was first submerged in 1mL R2A broth media to prevent membrane dehydration, then placed under the microscope. PolyScan 2 software was then used to define the irradiation pattern, light intensity and irradiation time. Here, a 165×295μm rectangular working area was defined to accommodate an array of microwells. After a targeted microwell was located, it was exposed a 20 μm diameter circular pattern (20 mW/mm^2, 10 min) to erode the polymer matrix over the well. The opened microwell array was then washed with R2A broth media + 0.05% Tween20 (5×2mL) to extract cells from the opened microwell. The 10 mL wash solution was centrifuged at 2000g for 10 min and the supernatant was carefully removed leaving approximately 2 mL of solution inside the culture tube.

96-well plate validation

Separate CFCF from all 5 isolates were mixed together at equal volumes then added to Pantoea cell culture in R2A media at a volumetric ratio of 1:1 to reach an OD_{600} value of 0.1. 100μL of each treatment with 6 independent replicates were cultured overnight in 96 well plates to determine the influence of outlier isolates on the OD_{600} of Pantoea sp. YR343 growth. Wilcoxon Two-sample tests (Nahm, 2016) were conducted to test whether there is a significant difference between median values of isolate-Pantoea combinations and Pantoea monoculture.

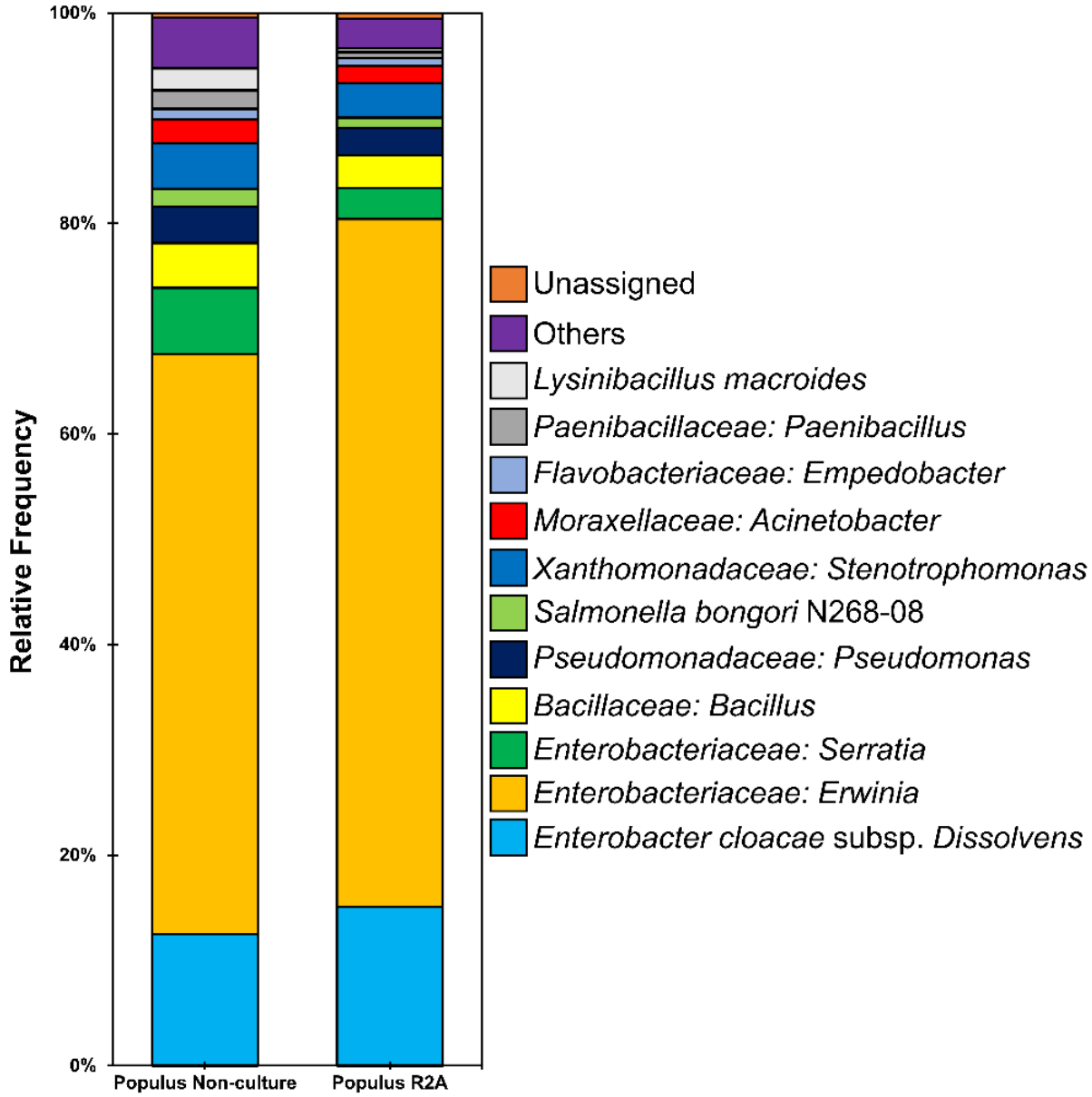

Supplementary Figure 1. Qiime2 outputs for 16S community analysis of P. trichocarpa isolates in rhizosphere (NCBI Accession no. SAMN16795465) and R2A media (NCBI Accession no. SAMN16795466). Taxa bar chart was produced to visualize relative abundance of bacteria taxas in both conditions. Sequences in 99% OTUs were classified and grouped at the genus level. Taxa representing <1% of the total sequences were grouped as Others.

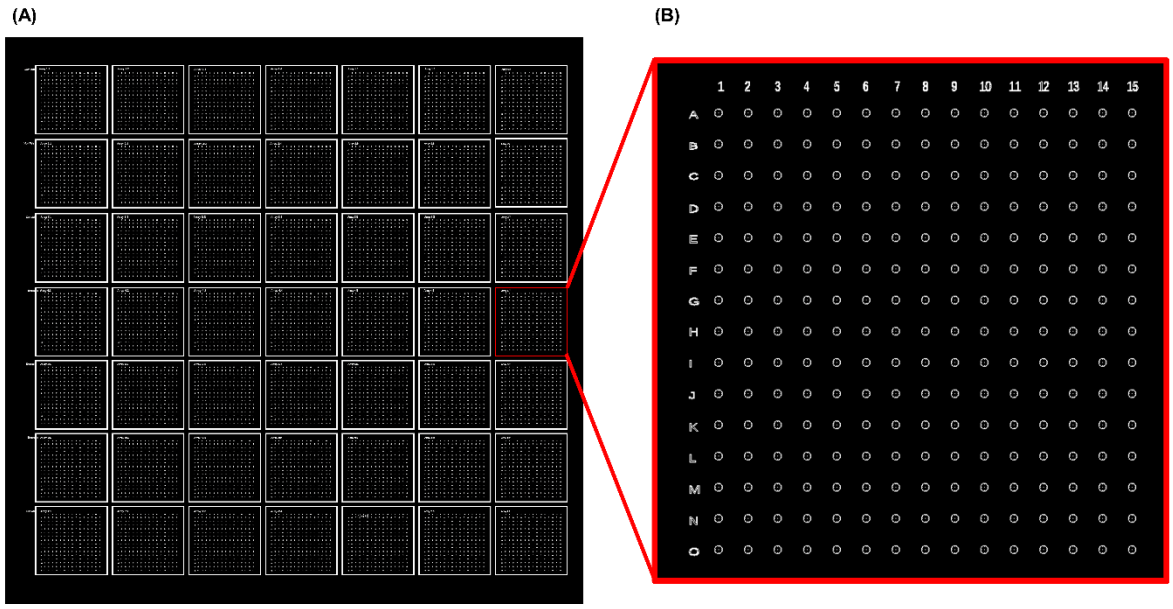

Supplementary Figure 2. MRA layout. (A) The 10μm diameter wells contained 7×7 sub-arrays, each sub-array contained 15×15 arrays of microwells. (B) All wells within the 15×15 sub-array were numbered according to their specific position in the array. Microwells were 10 μm in diameter with a 40 μm pitch.

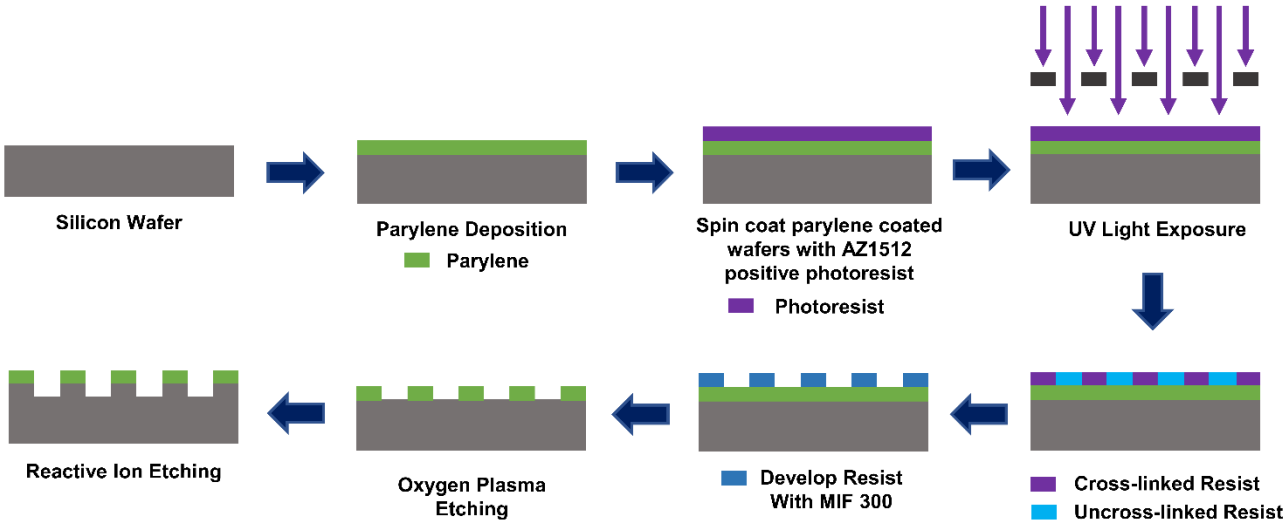

Supplementary Figure 3. Steps for microwell recovery array fabrication. Parylene N was deposited on top of silicon wafers. Then the parylene coated wafers were spin coated with positive photoresist AZ1512 and exposed with UV light though a photomask. The uncrosslinked photoresist was then washed by developing in MIF 300. Then Bosch etching was performed to get MRAs.

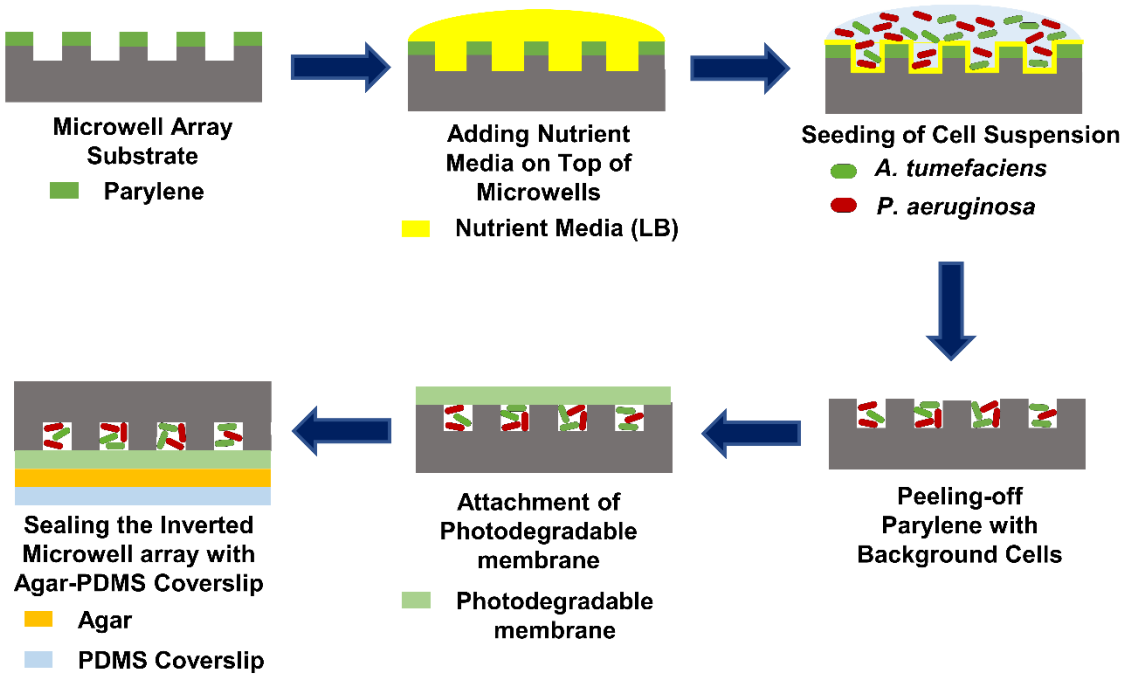

Supplementary Figure 4. Seeding and trapping of bacteria in microwell arrays with the aid of a PDMS coverslip.

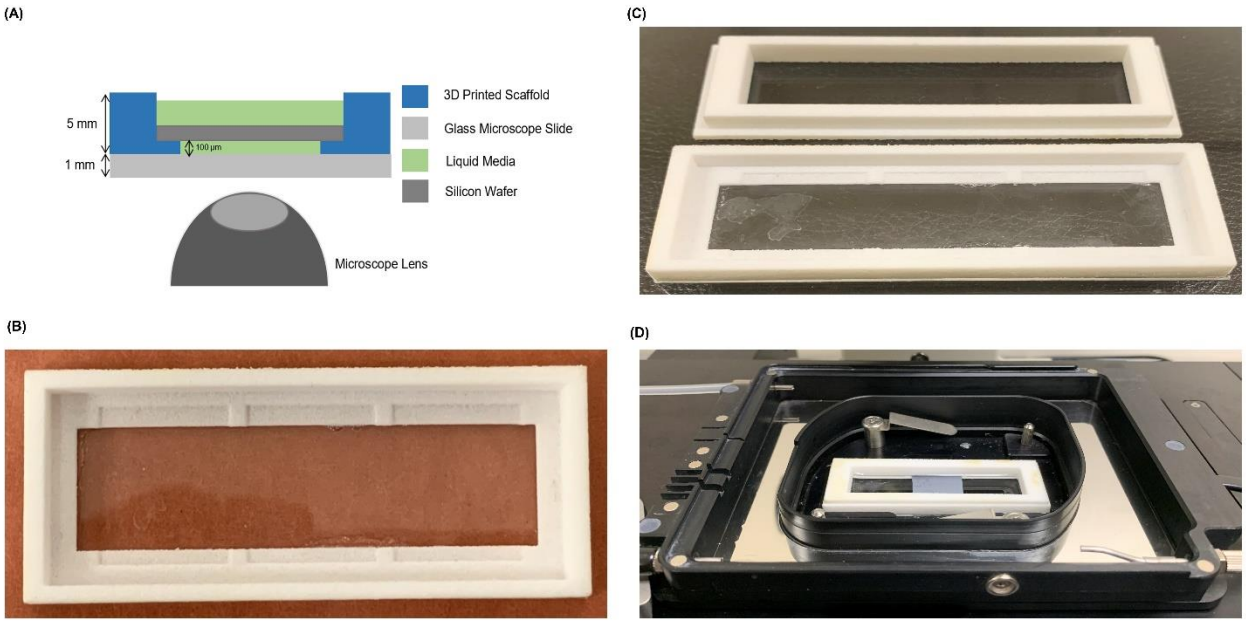

Supplementary Figure 5. (A) Cross section of the 3D printed scaffold on a glass microscope slide. (B) 3D printed Nylon scaffolds. The scaffold had 1.5×1.5cm grooves to hold up to thee microwell arrays. (C) The scaffold was glued to a 75×25mm glass slide then the scaffold lid was attached on top to firmly hold the microwell in place. Liquid nutrient media was then added to fill the space between microwell array and the glass slide, keeping the microwell array fully submerged during culture. (D) The scaffold setup was placed inside a humidified live cell imaging chamber for TLFM.

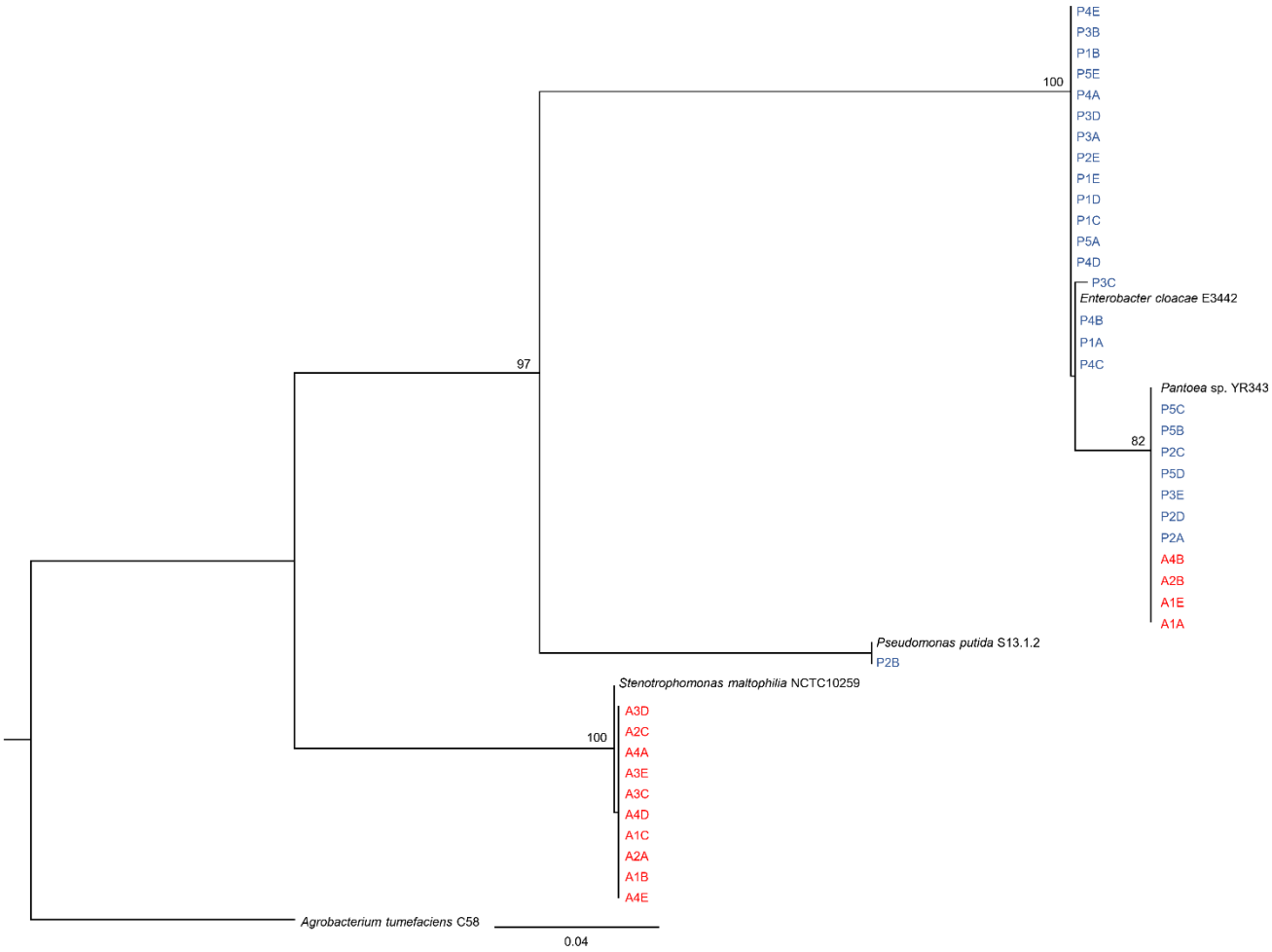

Supplementary Figure 6. Maximum likelihood phylogenetic tree based on partial sequence of the 16S rRNA (1007 bp) from isolates obtained from microwells in which YR343 growth was promoted or antagonized as well as a few reference strains. The tree was constructed using the general time reversible substitution model (Tavaré, 1986) with a gamma distribution (GTR + G) in PhyML 3.3.20190909 (Guindon et al., 2010). We used Smart Model Selection (Lefort et al., 2017) to select this substitution model. Bootstrap values (expressed as a percentage of 1000 replications) higher than 70% are shown at nodes. A. tumefaciens C58 was included as an outgroup organism. The partial 16S sequences of the isolates are accessible in GenBank with unique accession numbers (P1E: MW251950, P3C: MW251951, P4B: MW251952, P1D: MW251953, P4A: MW251954, P2E: MW251955, P1B: MW251956, P3A: MW251957, P1C: MW251958, P5E: MW251959, P4C: MW251960, P4D: MW251961, P4E: MW251962, P3B: MW251963, P5A: MW251964, P1A: MW251965, P3D: MW251966, P5C: MW251967, A1A: MW251968, P2D: MW251969, A1E: MW251970, P5B: MW251971, P5D: MW251972, P2A: MW251973, A4B: MW251974, P3E: MW251975, A2B: MW251976, P2C: MW251977, P2B: MW251978, A4E: MW251979, A1B: MW251980, A2C: MW251981, A3D: MW251982, A4A: MW251983, A3E: MW251984, A3C: MW251985, A4D: MW251986, A1C: MW251987, A2A: MW251988).

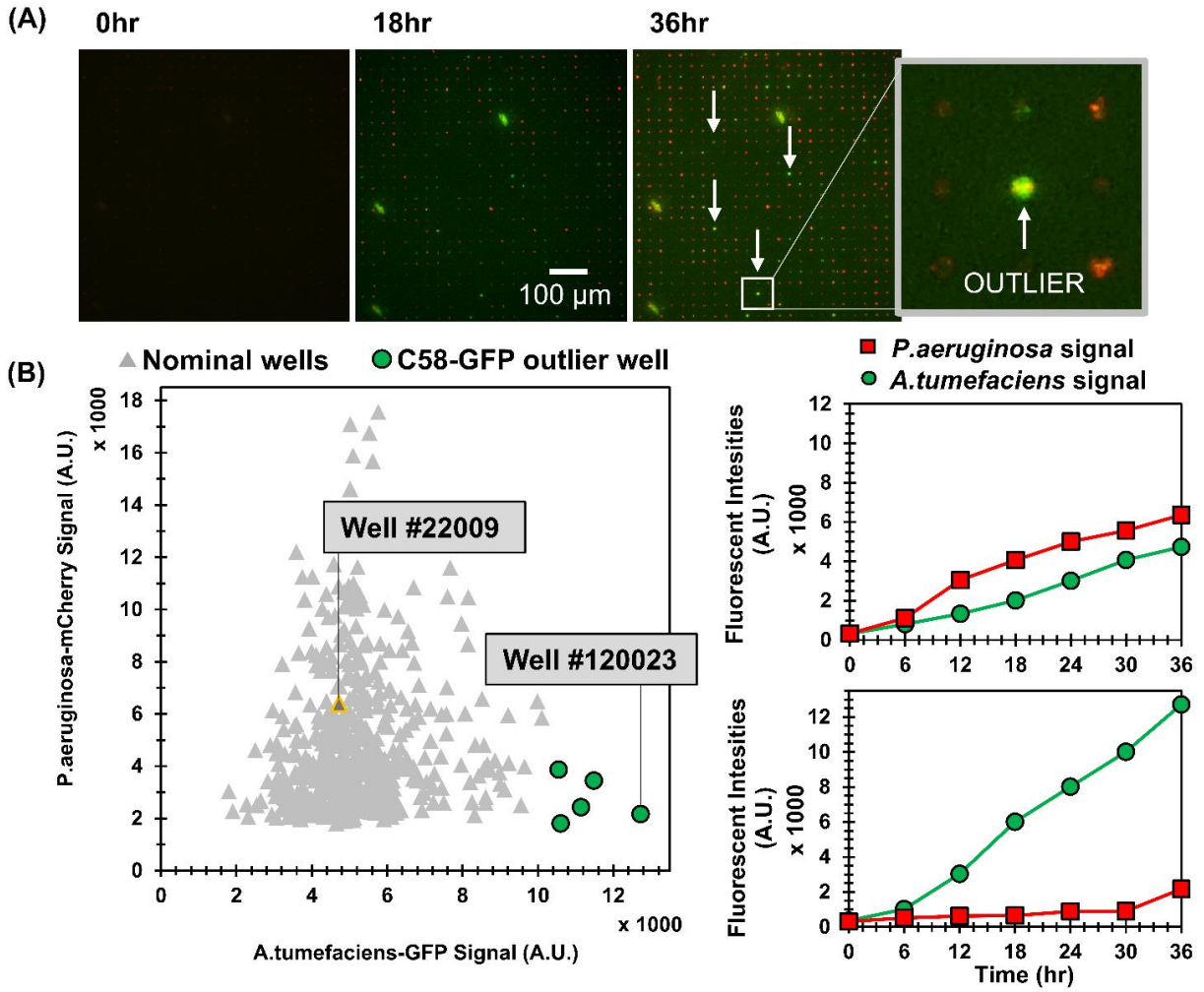

Supplementary Figure 7. C58-GFP - PAO1-mCherry co-culture after seeding at a 1:1 C58:PAO1 cellular ratio. (A) Green-red fluorescence images of co-culture at various time points. (B) Scatter plot of end-point green (C58-GFP) and red (PAO1-mCherry) fluorescent signals (t= 36 hr), C58 outlier wells are identified in green. (C) Individual well growth profile of a nominal well (well #22009 in B) and (D) individual well growth profile of an outlier well (well #120023 in B).

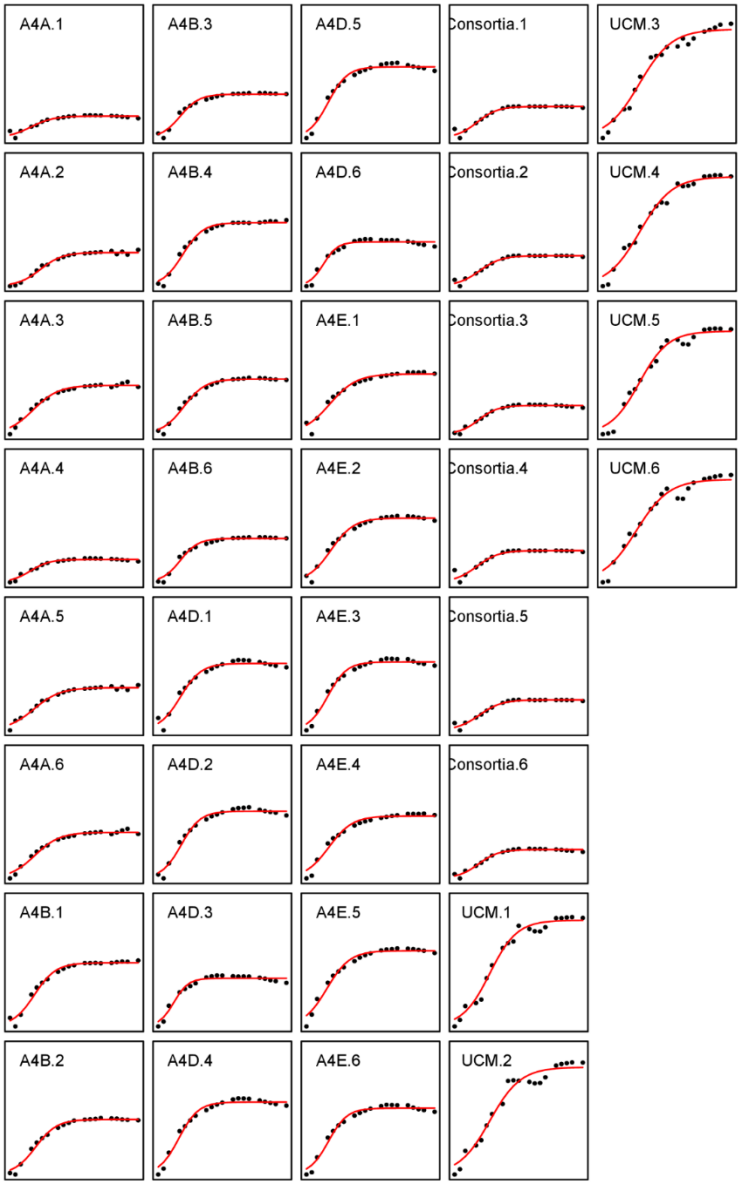

Supplementary Figure 8. Growthcurver output for analysis of growth curves generated from 96 well-plate validation assays using isolates from microwells within which YR343-GFP growth was antagonized. For each condition, YR343-GFP culture was measured for a total of n=6 independent replicates. Carrying capacity, k (OD_{600}) and growth rate, r (h^{-1}) for each isolate, isolate combination and control and were quantified [192].

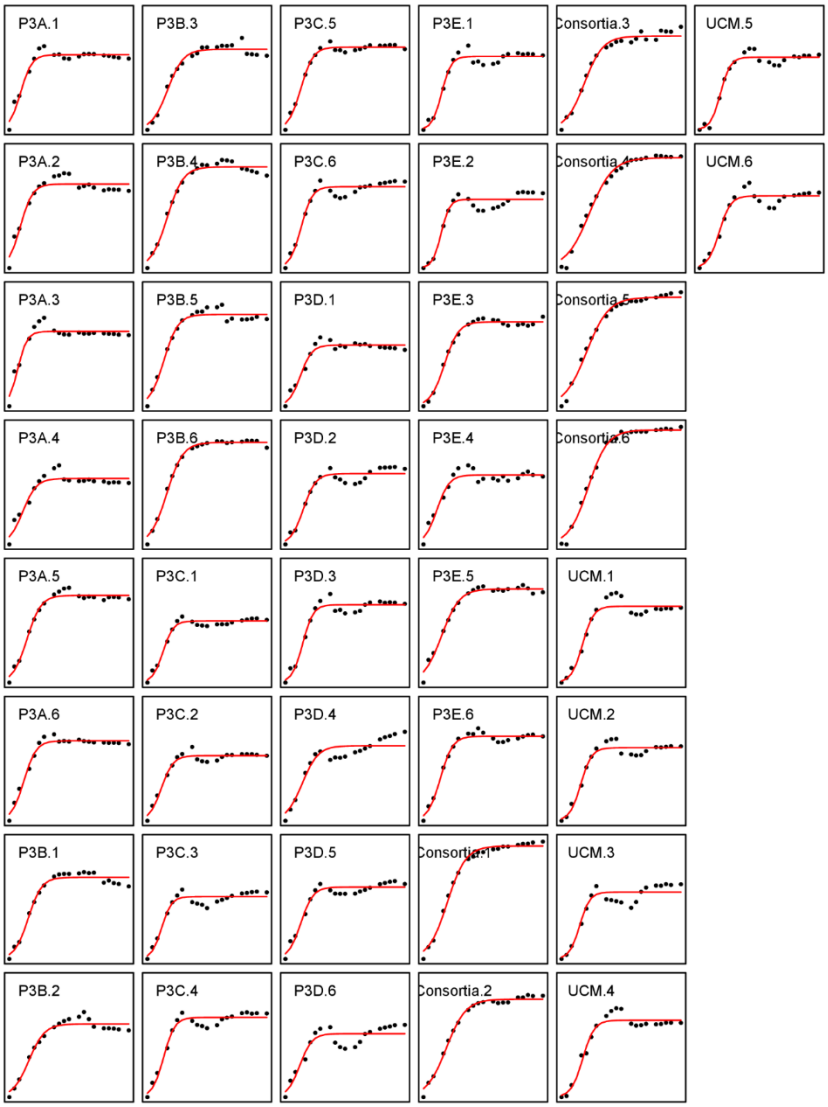

Supplementary Figure 9. Growthcurver output for analysis of growth curves generated from 96 well-plate validation assays using isolates from microwells within which YR343-GFP exhibited promoted population growth. For each condition, YR343-GFP culture was measured for a total of n=6 independent replicates. Carrying capacity, k (OD_{600}) and growth rate, r (h^{-1}) for each isolate, isolate combination and control and were quantified [192].

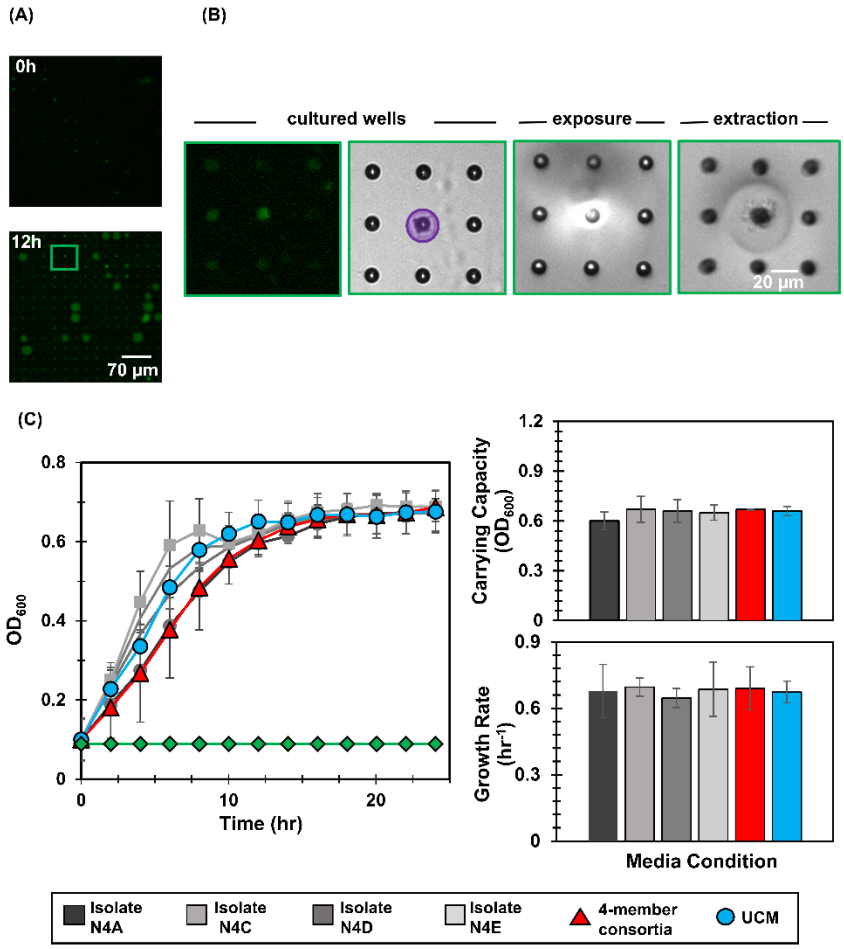

Supplementary Figure 10. Sequential removal of microwells with nominal growth from an array sub-section after co-culture. (A) Microwell array before and after co-culture. This 15×15 microwell array contained wells with no evident increases or decreases in YR343 growth (green). (B) Targeted removal of the microwell community in which YR343 did not see evident increases or decreases in end-point fluorescence (top row, green outline). Purple area denotes UV exposure area used for membrane degradation. (C) Left: YR343 growth curves after inoculation into conditioned media from the nominal isolate, isolate consortia, or unconditioned media (UCM). The control (green line) is conditioned media that was not inoculated with YR343 to verify that there was no growth carry over or contaminating microbes present. Right: Corresponding carrying capacity and growth rates for each growth curve. Statistical differences were identified by comparison of growth metrics between YR343 culture in conditioned media from each isolate or isolate mixture and YR343 growth in UCM (Wilcoxon two-sample test, n=6 independent experiments). None of the isolate mixtures showed significant differences in carrying capacities and growth rates compared to YR343 growth in UCM. These isolates were of Enterobacter genus, identified by 16S amplicon (data not shown).

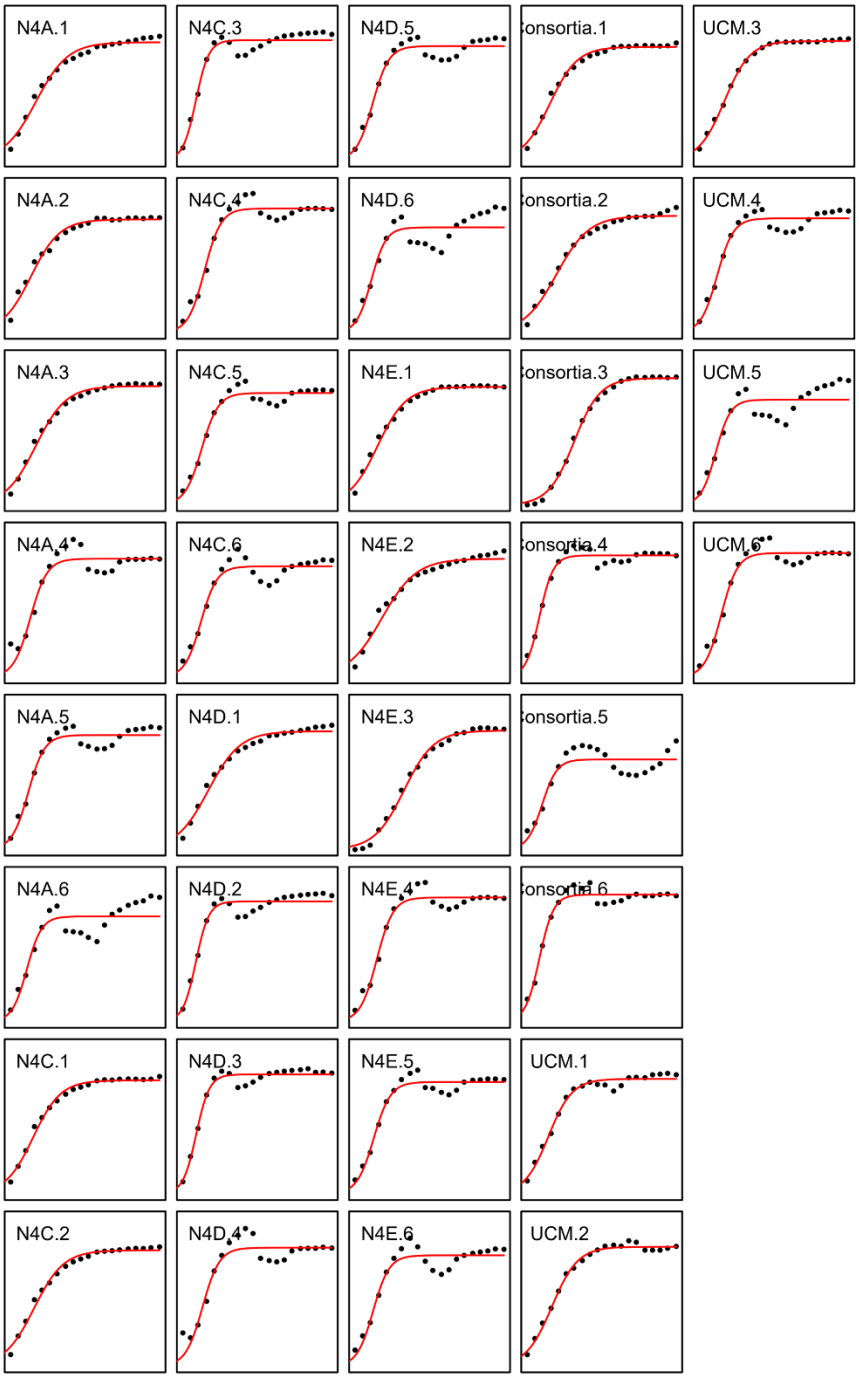

Supplementary Figure 11. Growthcurver output for analysis of growth curves generated from 96 well-plate validation assays using isolates from microwells within which YR343-GFP growth was nominal. For each condition, YR343-GFP culture was measured for a total of n=6 independent replicates. Carrying capacity, k (OD_{600}) and growth rate, r (h^{-1}) for each isolate, isolate combination and control and were quantified [192].

Supplementary Table 1. Bacterial strains used in this study.

Strain or Plasmid	Characteristics	Source or reference
Strains		
Agrobacterium tumefaciens C58	Wild-type strain	C. Fuqua
A. tumefaciens C58 pSRKKm-sfGFP	Wild-type strain carrying pSRKKm-sfGFP	This study
Pseudomonas aeruginosa PAO1	Wild-type strain	ATCC
P. aeruginosa PAO1 pSRKKm-mCherry	Wild-type strain carrying pSRKKm-mCherry	This study
Pantoea sp. YR343	Wild-type strain with a constitutively expressed chomosomal insertion of EGFP	(Bible et al., 2016)
Escherichia coli S17-1 λpir	λpir, Tra+, cloning strain	(Simon et al., 1983)
E. coli S17-1 λpir pSRKKm-sfGFP	Donor strain carrying pSRKKm-sfGFP	This study
E. coli S17-1 λpir pSRKKm-mCherry	Donor strain carrying pSRKKm-mCherry	This study
P1A	Isolate from microwell P1 within which YR343 exhibited promoted growth	This study
P1B	Isolate from microwell P1	This study
P1C	Isolate from microwell P1	This study

P1D	Isolate from microwell P1	This study
P1E	Isolate from microwell P1	This study
P2A	Isolate from microwell P2 within which YR343 exhibited promoted growth	This study
P2B	Isolate from microwell P2	This study
P2C	Isolate from microwell P2	This study
P2D	Isolate from microwell P2	This study
P2E	Isolate from microwell P2	This study
P3A	Isolate from microwell P3 within which YR343 exhibited promoted growth	This study
P3B	Isolate from microwell P3	This study
P3C	Isolate from microwell P3	This study
P3D	Isolate from microwell P3	This study
P3E	Isolate from microwell P3	This study
P4A	Isolate from microwell P4 within which YR343 exhibited promoted growth	This study
P4B	Isolate from microwell P4	This study
P4C	Isolate from microwell P4	This study
P4D	Isolate from microwell P4	This study
P4E	Isolate from microwell P4	This study
P5A	Isolate from microwell P5 within which YR343 exhibited promoted growth	This study
P5B	Isolate from microwell P5	This study

P5C	Isolate from microwell P5	This study
P5D	Isolate from microwell P5	This study
P5E	Isolate from microwell P5	This study
A1A	Isolate from microwell A1 within which YR343 exhibited antagonized growth	This study
A1B	Isolate from microwell A1	This study
A1C	Isolate from microwell A1	This study
A1D	Isolate from microwell A1	This study
A1E	Isolate from microwell A1	This study
A2A	Isolate from microwell A2 within which YR343 exhibited antagonized growth	This study
A2B	Isolate from microwell A2	This study
A2C	Isolate from microwell A2	This study
A2D	Isolate from microwell A2	This study
A2E	Isolate from microwell A2	This study
A3A	Isolate from microwell A3 within which YR343 exhibited antagonized growth	This study
A3B	Isolate from microwell A3	This study
A3C	Isolate from microwell A3	This study
A3D	Isolate from microwell A3	This study
A3E	Isolate from microwell A3	This study
A4A	Isolate from microwell A4 within which YR343 exhibited antagonized growth	This study

A4B	Isolate from microwell A4	This study
A4C	Isolate from microwell A4	This study
A4D	Isolate from microwell A4	This study
A4E	Isolate from microwell A4	This study
Plasmids		
pSRKKm	Broad-host-range P_{lac} expression vector; KmR	(Khan et al., 2008)
pSRKKm-mCherry	IPTG-inducible mCherry expression vector derived from pSRKKm; KmR	(Van Der Vlies et al., 2019)
pSRKKm-sfGFP	IPTG-inducible GFP expression vector derived from pSRKKm; KmR	(Figueroa-Cuilan et al., 2016)

Isolate ID	p-value for Wilcoxon two-sample test	Significance of difference
A4A	<0.01	Significant
A4B	<0.01	Significant
A4D	<0.01	Significant
A4E	<0.01	Significant
4-member consortia	<0.01	Significant

Supplementary Table 2. Wilcoxon two-sample tests for differences in carrying capacities between YR343-GFP culture in conditioned versus unconditioned media from individual antagonistic isolates or from the 4-membered consortia.

Isolate ID	p-value for Wilcoxon two-sample test	Significance of difference
A4A	<0.01	Significant
A4B	<0.01	Significant
A4D	<0.01	Significant
A4E	<0.01	Significant
4 member consortia	<0.01	Significant

Supplementary Table 3. Wilcoxon two-sample tests for differences in growth rates between YR343-GFP culture in conditioned versus unconditioned media from individual antagonistic isolates or from the 4-membered consortia.

Isolate ID	p-value for Wilcoxon two-sample test	Significance of difference
P3A	0.2876	Not Significant
P3B	0.0093	Significant
P3C	0.4051	Not Significant
P3D	0.0931	Not Significant
P3E	0.1149	Not Significant
5-member consortia	<0.01	Significant

Supplementary Table 4. Wilcoxon two-sample tests for differences in carrying capacities between YR343-GFP culture in conditioned versus unconditioned media from individual promoting isolates or from the 5-membered consortia.

Isolates ID	p-value for Wilcoxon two-sample test	Significance of difference
P3A	0.2876	Not Significant
P3B	<0.01	Significant
P3C	0.1490	Not Significant
P3D	0.0656	Not Significant
P3E	<0.01	Significant
5 member consortia	<0.01	Significant

Supplementary Table 5. Wilcoxon two-sample tests for differences in growth rates between YR343-GFP culture in conditioned versus unconditioned media from individual promoting isolates or from the 5-membered consortia.

Isolate ID	p-value for Wilcoxon two-sample test	Significance of difference
N4A	0.1861	Not Significant
N4C	0.4297	Not Significant
N4D	0.5249	Not Significant
N4E	0.4377	Not Significant
4-member consortia	0.3496	Not Significant

Supplementary Table 6. Wilcoxon two-sample tests for differences in carrying capacities between YR343-GFP culture in conditioned versus unconditioned media from individual nominal isolates or from the 4-membered consortia.

Isolate ID	p-value for Wilcoxon two-sample test	Significance of difference
N4A	0.2284	Not Significant
N4C	0.4870	Not Significant
N4D	0.1429	Not Significant
N4E	0.1656	Not Significant
4 member consortia	0.5314	Not Significant

Supplementary Table 7. Wilcoxon two-sample tests for differences in growth rates between YR343-GFP culture in conditioned versus unconditioned media from individual nominal isolates or from the 4-membered consortia.

Appendix C: Supporting information from Chapter 5

Plasmid Construction for *Azospirillus brasilense* strain Sp7-GFP

The plasmid pHRGFPTC (approximately 9.2 kb) [215]is a derivative of the broad host range plasmid pBBR1-GFP containing the gfpmut3 gene [264]. To construct this plasmid, a 1.3-kb BamHI/BglII fragment from pJQ200SK [265] containing the promoter (pc) and part of the gentamycin resistance gene (*aacC1*) was cloned into the BglII site of pBBR1-GFP to create pHRGFP3. A 1.3-kb fragment from p34S-Tc [266], which contains ampicillin, chloramphenicol, and tetracycline resistance genes, was cloned into the KpnI site of plasmid pHRGFP3 to create plasmid pHRGFPTC. This plasmid was transformed into *E. coli* S17-1 λpir using calcium chloride heat-shock transformation and introduced to *A. brasilense* Sp7 (ATCC 29145) by biparental mating.

Preparation and culture of *Azosprillium brasilense* SP7-GFP Strains

Bacteria strains and plasmids used in this research are listed in **Supplementary Table 2**. *A. brasilense* SP7-GFP was created in the Alexandre lab and was used as received. *A. brasilense* SP7-GFP was stored in 25% glycerol at -80 ºC. Sterile inoculation loops were used to pick up cells from the frozen stocks and culture in TY Media (5g/L Bacto-tryptone, 3g/L yeast extract, 1.2g/L $CaCl_2$, pH: 7 ± 0.2), R2A broth media (pH: 7.2 ± 0.2, Teknova), or LB media (10g/L tryptone, 5g/L NaCl, 5g/L yeast extract, pH: 7 ± 0.2), in sterile test tubes supplemented with ampicillin (100 μg/mL) and tetracycline (5 μg/mL) for 24 hrs (28°C, 215 rpm).

Photodegradable membrane attachment

A previously described protocol for attaching the photodegradable hydrogel membrane to microwell arrays was used here [90, 214]. First, perfluoroalkylated glass slides were prepared by incubating 25×25 mm clean glass slides (Fisher Scientific) in 20 mL of 0.5% v/v

trichloro(1H,1H,2H,2H-perfluorooctyl) silane in toluene for 3 hrs [90, 214]. Then, NaH_2PO_4 was added with ATGN liquid media to obtain phosphate buffer saline (PBS) with 100mM final phosphate concentration, and the pH of the solution was adjusted to 8 by adding 5M NaOH (aq.). 12.5 µL of this PBS-ATGN solution was then mixed with 5.6 µL of photodegradable PEG diacrylate monomer (MW 3400) and 6.9 µL of a four-arm PEG thiol solution monomer to obtain membrane precursor solution [141] (MW 10000, NOF America Corporation, DE-100SH) with equal concentrations of both PEG diacrylate (22mM) and four-arm PEG thiol solution monomer (22mM). The membrane precursor solution was placed on top of the microwell substrates by pipetting 15µL of the liquid precursor solution on top of the perfluoroalkylated glass slides and placing the solution over the seeded microwell substrate. Metal spacers ensured a constant 38µm gap between the glass slide and the microwell for the precursor solution. The membrane was then formed through monomer crosslinking and gelation by incubating for 25min at room temperature [90, 214]. After careful separation of the glass slide from the membrane-functionalized microwell array, the microwell array was placed inside a custom 3D printed scaffold, previously designed for imaging microwell arrays with time-lapse fluorescence microscopy [214].

Time-lapse fluorescent microscopy

Time-lapse fluorescent microscopy images were acquired with a Nikon Eclipse Ti-U inverted microscope equipped with a 20× objective, a motorized XYZ stage, a humidified live-cell incubation chamber (Tokai Hit), a DS-QiMc monochromatic digital camera, and NIS Elements Image acquisition software. The seeded microwell arrays were sealed with the photodegradable PEG membrane, and the inverted arrays were placed in a custom 3D printed scaffold to keep them submerged under liquid media while imaging [214]. Then the scaffold was placed inside a humidified live-cell incubation chamber at 28ºC during imaging. A FITC filter was used to image

SP7-GFP (20×, 200 ms, 17.1× gain) with a neutral density filter with 25% standard light intensity to ensure imaging without photobleaching. Brightfield images were also taken at each section of the array after fluorescent imaging. Images of the microwell arrays were taken every 60 minutes during culture.

Image Analysis

GFP fluorescent images from the SP7-GFP and *Zea mays* rhizosphere isolate co-culture system was analyzed by the protocol described by Timm *et al.* [137]. Protein Array Analyzer tool in ImageJ was used to generate growth profiles for each organism to identify the top 2 wells with the highest growth levels for extraction [137]. The time-lapse fluorescent images were imported as image sequences corrected by subtracting darkfield images from illumination field images with the image calculator plugin. Then image backgrounds were removed by selecting a 125 radius sliding paraboloid, and illumination correction was performed using calculator plus plugin. Finally, the growth of each strain in the microwells was calculated using the ImageJ "Micro Array" plugin [137].

Identification with 16S rRNA sequencing

Individual colonies of *A. brasilense* SP7-GFP growth-enhancing isolates were inoculated in R2A media to extract genomic DNA of each isolate using the DNeasy Blood & Tissue Kit (Qiagen, Germantown, MD). Genomic DNA samples were then diluted to 20 ng/µL in 20µL aliquots and sent to Genewiz (South Plainfield, NJ, U.S.A.) for 16S rRNA Sanger sequencing of the V1 to V9 regions, enabling identification with approximately genus-level specificity. The sequences were aligned using MUSCLE (Edgar, 2004). They generated a maximum likelihood phylogenetic tree based on partial 16S rRNA sequences (1007 bp) using PhyML 3.3.20190909 (Guindon et al.,

2010) with 1000 bootstrap replicates and using the Smart Model Selection (Lefort et al., 2017) tool based on Akaike Information Criterion, a starting tree estimated using BIONJ, and the NNI method for tree topology improvement (**Supplementary Figure 5**).

Validation using 96 well plates.

To obtain CFCF from individual isolates, each isolate was cultured (28ºC, 3000 rpm) in 2mL of R2A liquid media overnight, and then cells were removed from the media by centrifugation (2000g, 10 min). To obtain CFCF from combinatorial mixtures, isolate panels were instead inoculated together in R2A media and cultured overnight, followed by cell removal by centrifugation. To obtain conditioned media, separate CFCF was mixed with Sp7-GFP in corresponding media at a 1:1 volumetric ratio to reach an initial OD_{600} value of 0.2 (final volume = 100 µL), at which point growth was quantified with a Biotek Epoch 2 Multi-Mode Microplate Reader (28ºC, 300rpm). Unconditioned media was obtained following the same procedure, except 1X PBS was added to fresh R2A media instead of isolating CFCF. To verify, the OD_{600} measurement was due to Sp7-FGP growth, CFCF from selected isolates without inoculation of Sp7-GFP was also measured. A total of n=3 independent replicates were calculated for each culture condition. Growth rates and carrying capacities of each condition were quantified using Growthcurver [192] (**Supplementary Figure 6**) and compared using the Wilcoxon two-sample test (**Supplementary Table 3 and 4**).

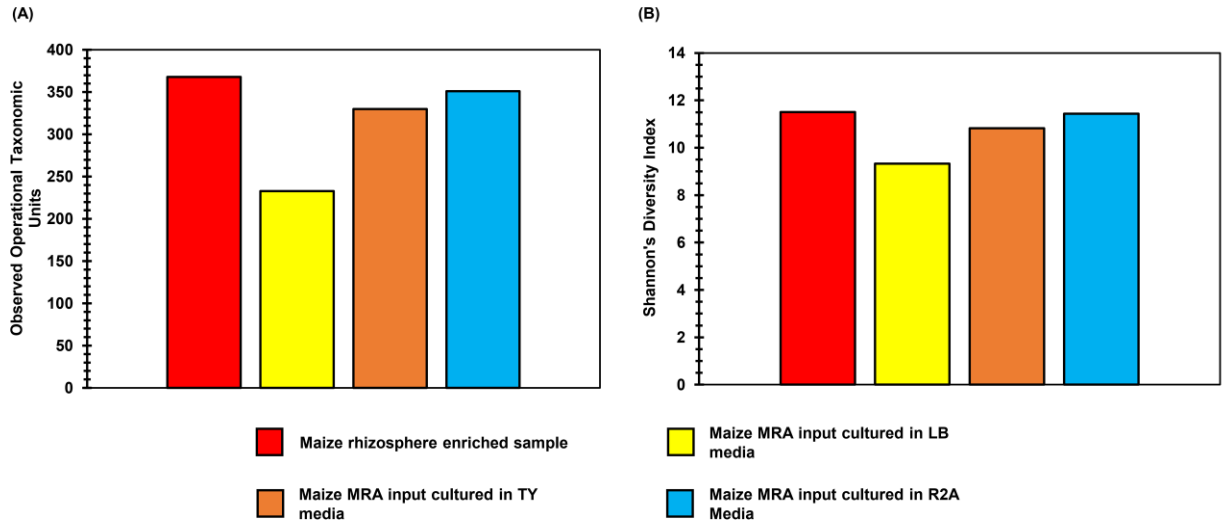

Supplementary Figure 1*:* Qiime2 output for the 16S diversity analysis for media selection for the *Zea mays* rhizosphere isolate MRA input. (A) Number of operational taxonomic units were calculated for maize rhizosphere enriched samples and MRA inputs cultured in LB, TY and R2A media. (B) Shannon's Diversity Indexes were calculated for maize rhizosphere enriched samples and MRA inputs cultured in LB, TY and R2A media.

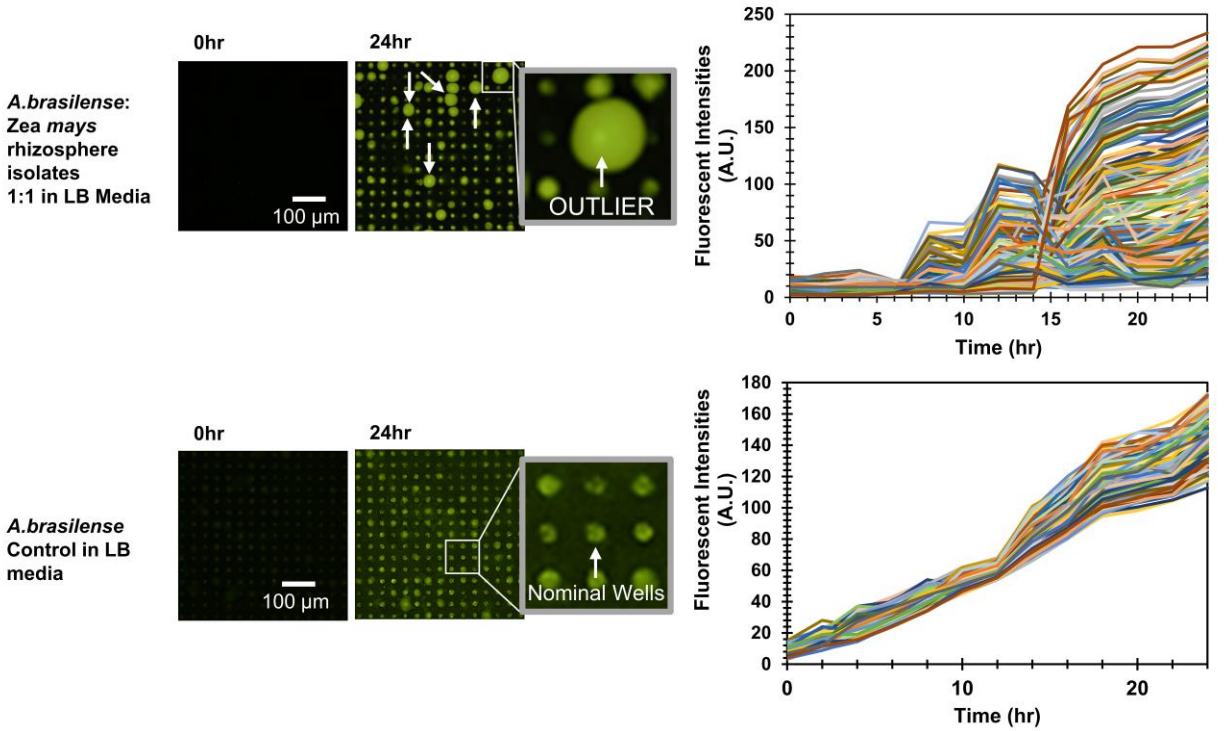

upplementary Figure 2: Inoculation and parallel tracking of A. brasilense Sp7-GFP in microwell arrays seeded with Sp7-GFP and maize root isolates in co-culture in LB media

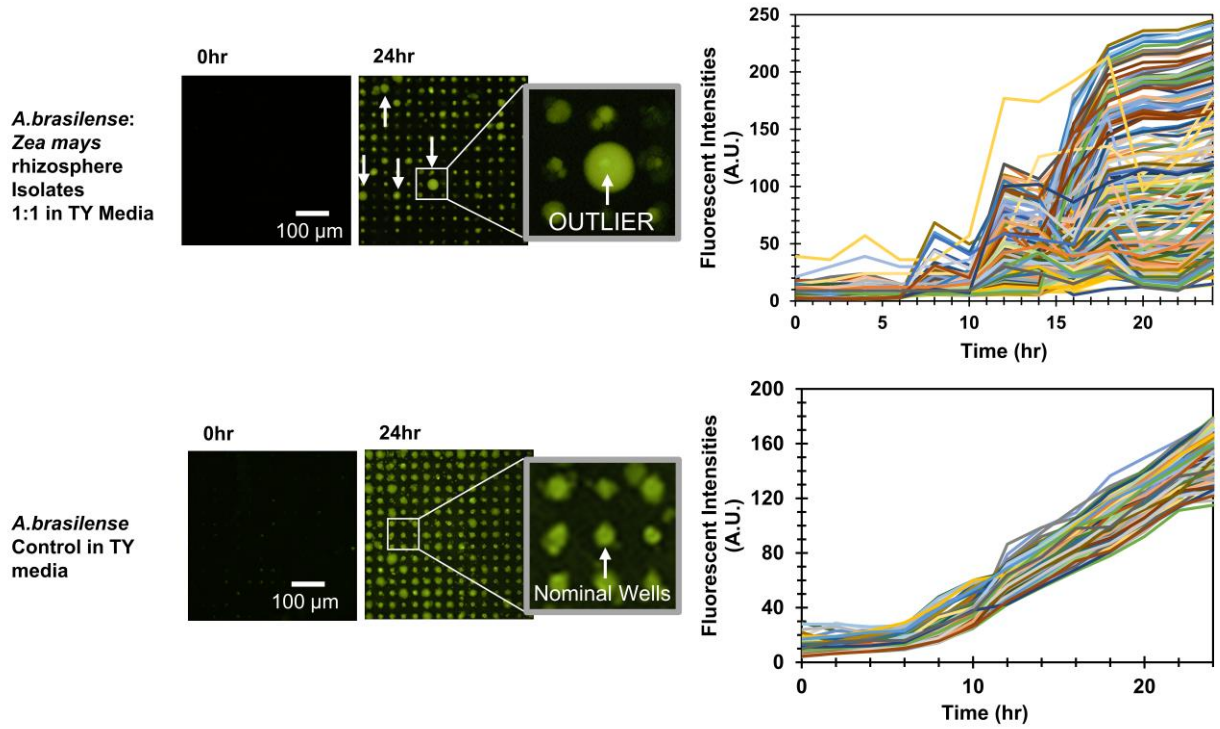

Supplementary Figure 3: Inoculation and parallel tracking of A. brasilense Sp7-GFP in microwell arrays seeded with Sp7-GFP and maize root isolates in co-culture in TY media

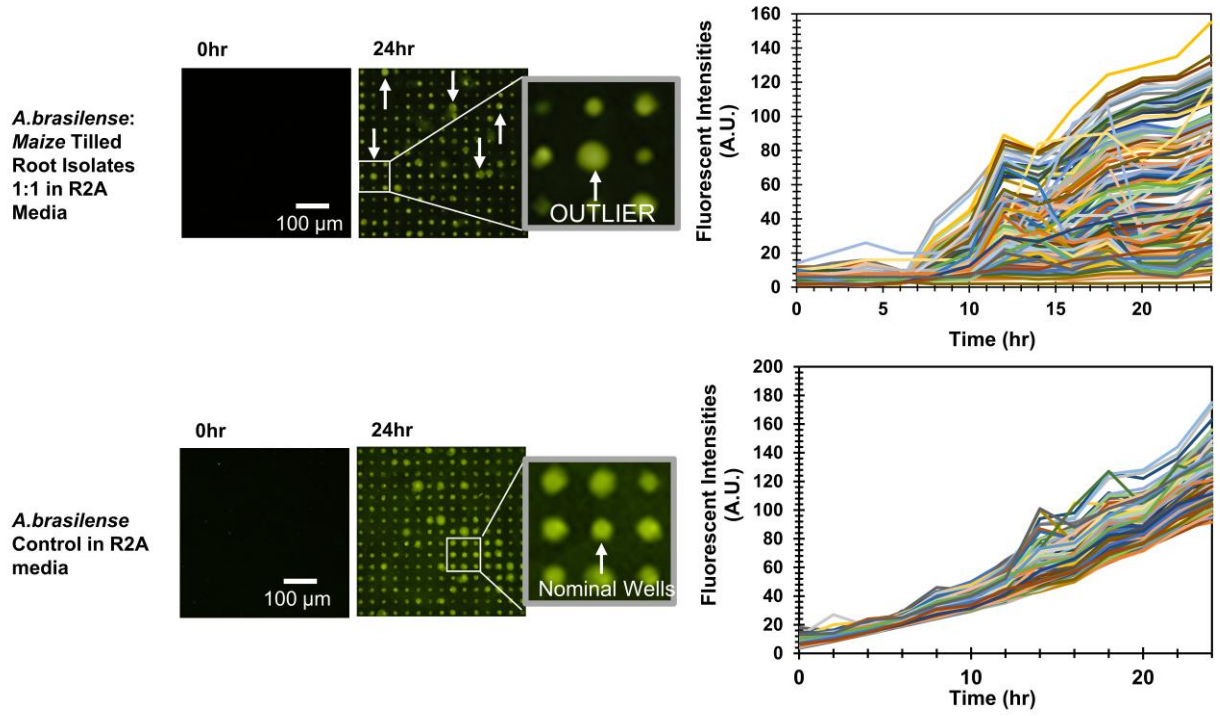

Supplementary Figure 4: Inoculation and parallel tracking of *A. brasilense* Sp7-GFP in microwell arrays seeded with Sp7-GFP and maize root isolates in co-culture in R2A media

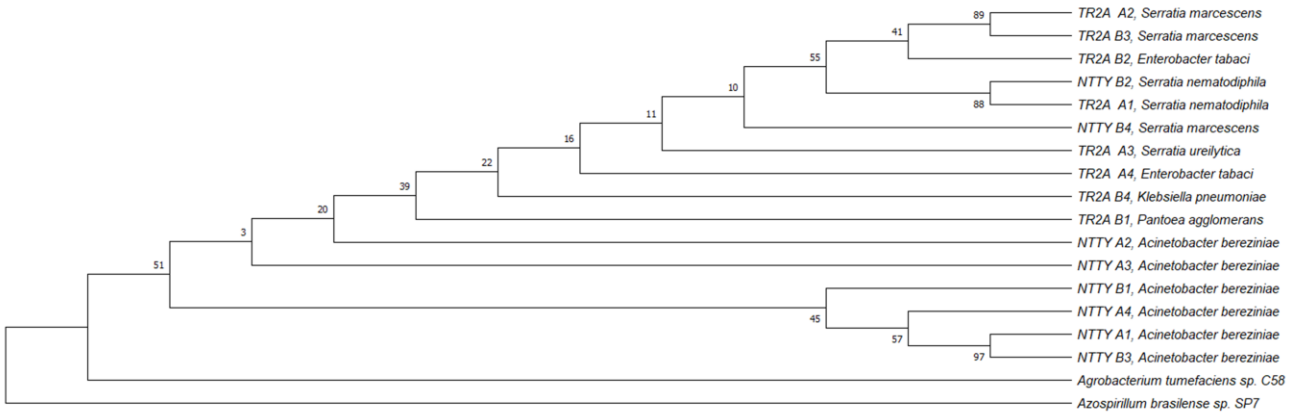

Supplementary Figure 5: Maximum likelihood phylogenetic tree based on 16S ribosomal RNA (rRNA) Sanger sequencing of the V1 to V9 regions from isolates obtained from Sp7-GFP symbiotic microwells as well as *A. tumefaciens* sp. C58 as reference strains. Smart Model Selection [191] was used to select the general time reversible substitution model [267] with a gamma distribution (GTR + G) in PhyML 3.3.20190909 [190] and bootstrap values (expressed as a percentage of 1000 replications) higher than 70% shown at nodes to construct the tree. The 16S sequences of the isolates are accessible in GenBank with unique accession numbers (Accession numbers: MZ363881.1, MZ363880.1, MZ363877.1, MZ363879.1, MZ363878.1, MZ363871.1)

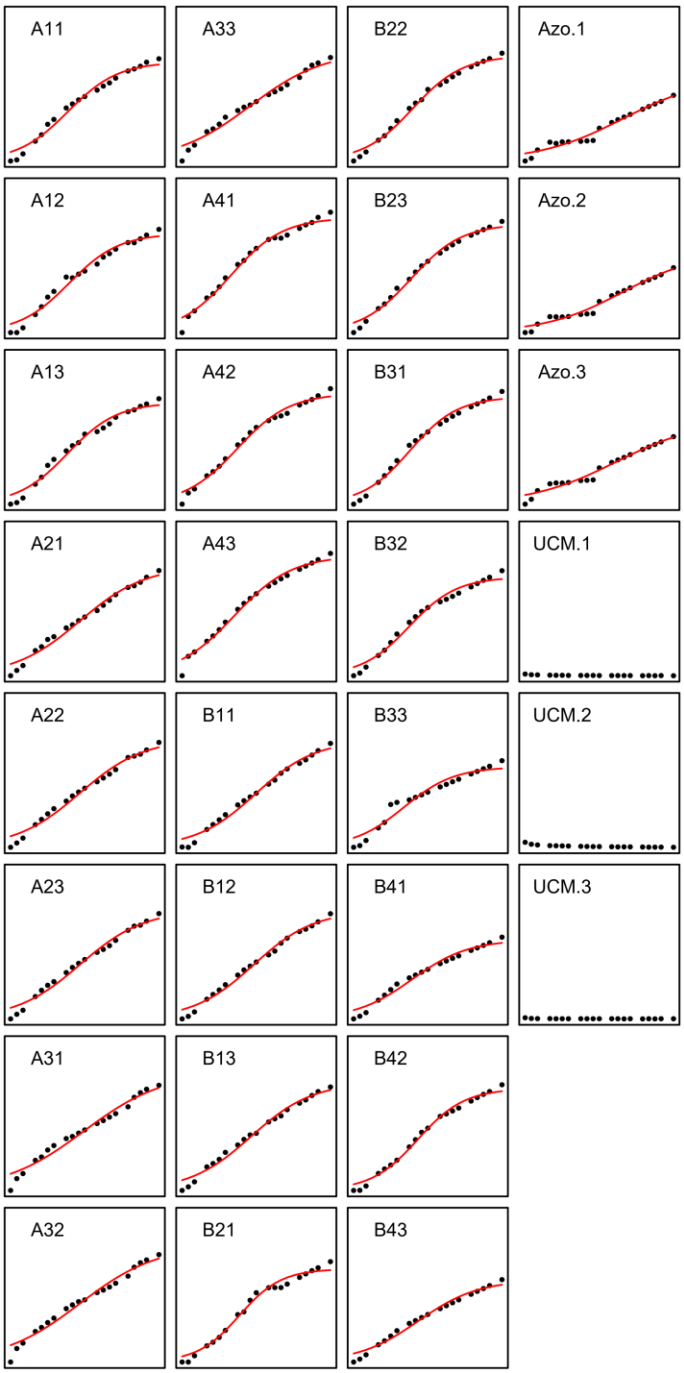

Supplementary Figure 6: Growthcurver output for analysis of growth curves generated from 96 well-plate validation assays using conventionally tilled soil isolates from microwells within which Sp7-GFP growth was promoted. For each condition, Sp7-GFP culture was measured for a total of n=6 independent replicates. Carrying capacity, k (OD_{600}) and growth rate, r (h^{-1}) for each isolate, isolate combination and control and were quantified [192].

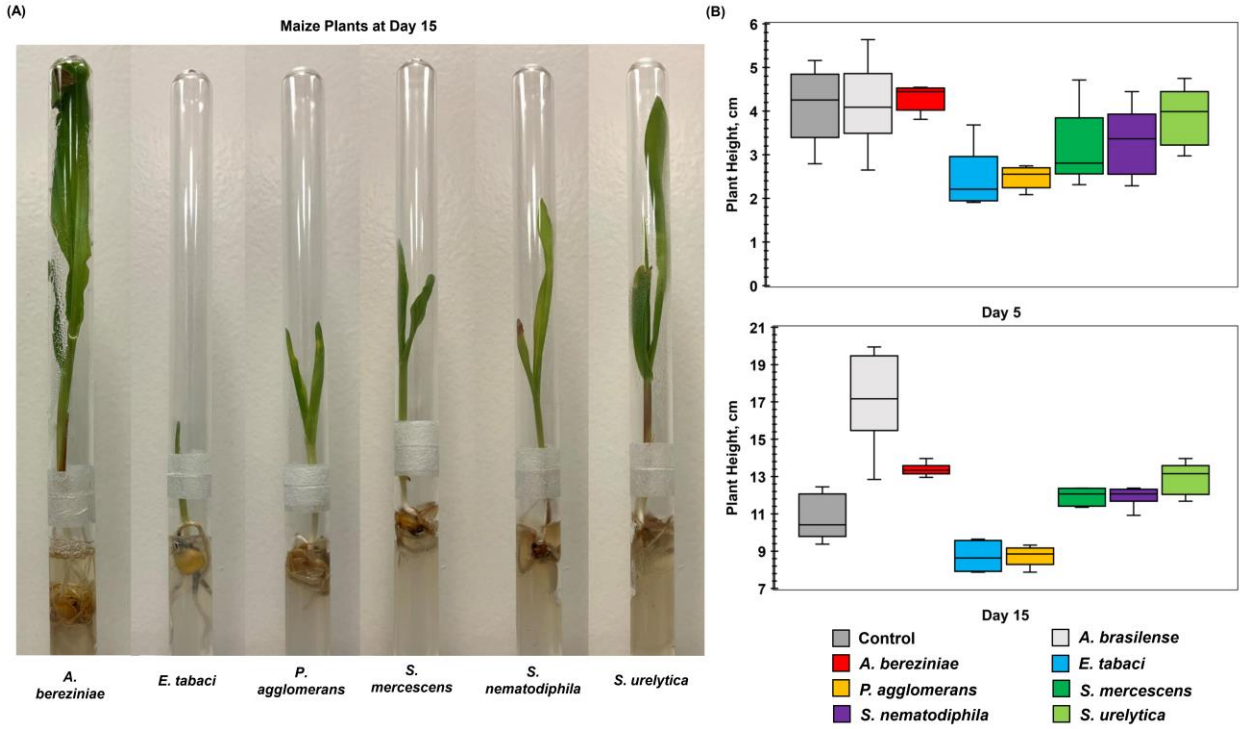

Supplementary Figure 7: Effect of isolate inoculation on the growth of axenic maize seedlings in growth chamber environment. (A) Growth of the axenic maize seedlings in the double-tube growth chamber at day 15. (B) Comparison of plant height between the treatments with Sp7-GFP symbiotic isolates with Sp7-GFP monoculture and no inoculation.

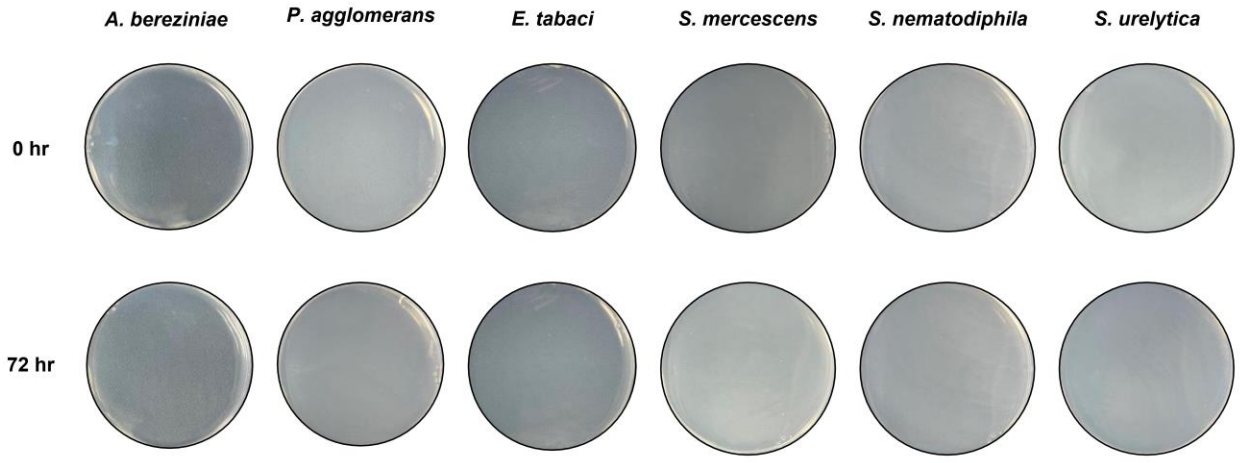

Supplementary Figure 8: Verification of antibiotic resistance of extracted isolates in R2A agar plates. The plates were supplemented with 100 µg/ml ampicillin and tetracycline. The isolates were cultured in three columns in each plate. After observing the growth for 72 hrs, no microbial colonies were observed in all plates.

Sample Name	Cover crops	Carbon content		Nitrogen content			Phosphorous content		pH	Physiological properties		
		Total C %	TOC %	Total N %	NO_3-N ppm	NH_4-N ppm	Total P ppm	P-M ppm	Sikora pH	Sand %	Silt %	Clay %
Boyde Fields	None	3.32	3.15	0.31	9.3	7.6	676	104	6.8	14	56	30
Budke Field	Millett/Sunflower in late summer. Grazed with cattle	2.31	2.28	0.23	10.6	3.9	583	65	7.8	14	60	26

Supplementary Table 1: Soil analysis report for the soil samples used in this study

Supplementary Table 2: Bacterial strains used in this study.

Strain or Plasmid	Characteristics	Source or reference
Strains		
A. brasilense Sp7-GFP	Wild-type strain carrying pHRGFPTC	[215]
A. tumefaciens C58 pSRKKm-sfGFP	Wild-type strain carrying pSRKKm-sfGFP	[214]
NTTY A1	Isolate from microwell A within which Sp7-GFP exhibited promoted growth	This study
NTTY A2	Isolate from microwell A	This study
NTTY A3	Isolate from microwell A	This study
NTTY A4	Isolate from microwell A	This study
NTTY B1	Isolate from microwell B within which Sp7-GFP exhibited promoted growth	This study
NTTY B2	Isolate from microwell B	This study
NTTY B3	Isolate from microwell B	This study
NTTY B4	Isolate from microwell B	This study
TR2A A1	Isolate from microwell A within which Sp7-GFP exhibited promoted growth	This study
TR2A A2	Isolate from microwell A	This study
TR2A A3	Isolate from microwell A	This study
TR2A A4	Isolate from microwell A	This study
TR2A B1	Isolate from microwell B within which Sp7-GFP exhibited promoted growth	This study
TR2A B2	Isolate from microwell B	This study
TR2A B3	Isolate from microwell B	This study
TR2A B4	Isolate from microwell B	This study
A4B	Isolate from microwell A4	This study
A4C	Isolate from microwell A4	This study
A4D	Isolate from microwell A4	This study
A4E	Isolate from microwell A4	This study
Plasmids		
pHRGFPTC		[215]
pSRKKm	Broad-host-range P_{lac} expression vector; KmR	[157]
pSRKKm-sfGFP	IPTG-inducible GFP expression vector derived from pSRKKm; KmR	[268]

Isolate ID	p-value for Wilcoxon two-sample test	Significance of difference
Isolate A1	<0.01	Significant
Isolate A2	<0.01	Significant
Isolate A3	<0.01	Significant
Isolate A4	<0.01	Significant
Isolate B1	<0.01	Significant
Isolate B2	<0.01	Significant
Isolate B3	<0.01	Significant
Isolate B4	<0.01	Significant

Supplementary Table 3: Wilcoxon two-sample tests for differences in carrying capacities between Sp7-GFP culture in conditioned versus unconditioned media from individual symbiotic isolates from *Zea mays* rhizobiome.

Isolate ID	p-value for Wilcoxon two-sample test	Significance of difference
Isolate A1	<0.01	Significant
Isolate A2	<0.01	Significant
Isolate A3	<0.01	Significant
Isolate A4	<0.01	Significant
Isolate B1	<0.01	Significant
Isolate B2	<0.01	Significant
Isolate B3	<0.01	Significant
Isolate B4	<0.01	Significant

Supplementary Table 4: Wilcoxon two-sample tests for differences in growth rates between Sp7-GFP culture in conditioned versus unconditioned media from individual symbiotic isolates from *Zea mays* rhizobiome.

Isolate ID	p-value for Wilcoxon two-sample test	Significance of difference
Sp7	<0.01	Significant
Sp7 + *A. bereziniae*	<0.01	Significant
Sp7 + *E. tabaci*	<0.01	Significant
Sp7 + *P. agglomerans*	<0.01	Significant
Sp7 + *S. marcescens*	<0.01	Significant
Sp7 + *S. nematodiphila*	<0.01	Significant
Sp7 + *S. urelytica*	<0.01	Significant

Supplementary Table 5: Wilcoxon two-sample tests for the comparison of plant heights for each co-inoculation treatment at Day 15.

Isolate ID	p-value for Wilcoxon two-sample test	Significance of difference
Sp7	<0.01	Significant
A. bereziniae	<0.01	Significant
E. tabaci	<0.01	Significant
P. agglomerans	<0.01	Significant
S. marcescens	<0.01	Significant
S. nematodiphila	<0.05	Significant
S. urelytica	<0.01	Significant

Supplementary Table 6: Wilcoxon two-sample tests for the comparison of CFU/ml of Sp7 between each co-inoculation treatment and Sp7 control treatment.

Isolate ID	p-value for Wilcoxon two-sample test	Significance of difference
Sp7	<0.01	Significant
A. bereziniae	<0.01	Significant
E. tabaci	<0.05	Significant
P. agglomerans	<0.01	Significant
S. marcescens	<0.01	Significant
S. nematodiphila	<0.05	Significant
S. urelytica	<0.01	Significant

Supplementary Table 7: Wilcoxon two-sample tests for the comparison of the abundance of Sp7 between each co-inoculation treatment and Sp7 control treatment.

Appendix D: Supporting information from Chapter 6

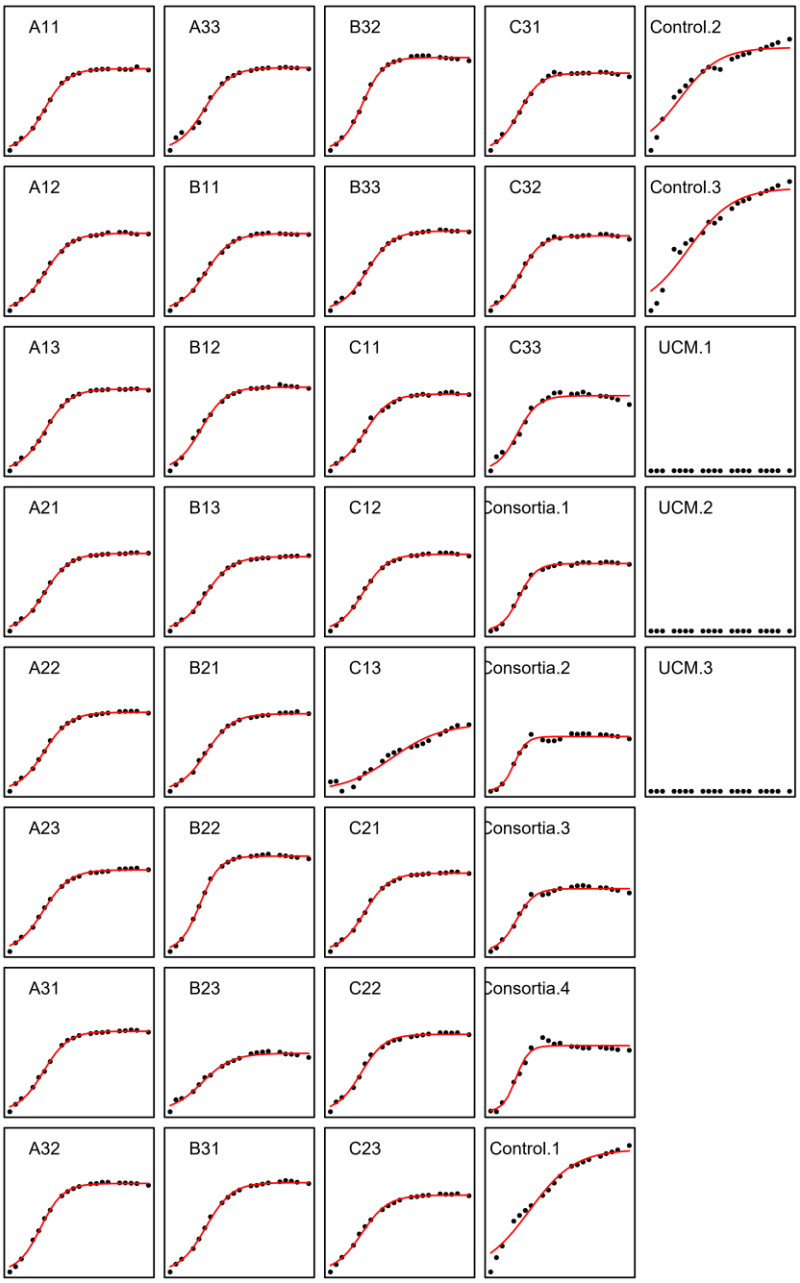

Figure S1: Growthcurver output for analysis of growth curves generated from 96 well-plate validation assays using isolates from microwells within which YR343-GFP growth was antagonized. For each condition, YR343-GFP culture was measured for a total of n=6 independent replicates. Carrying capacity, k (OD_{600}) and growth rate, r (h^{-1}) for each isolate, isolate combination and control and were quantified.[192]

Table S1: Bacterial strains used in this study.

Strain or Plasmid	Characteristics	Source or reference
Strains		
Agrobacterium tumefaciens 15955	Wild-type strain	C. Fuqua
A. tumefaciens 15955 pSRKKm-sfGFP	Wild-type strain carrying pSRKKm-sfGFP	This study
Escherichia coli S17-1 λpir	λpir, Tra+, cloning strain	[269]
E. coli S17-1 λpir pSRKKm-sfGFP	Donor strain carrying pSRKKm-sfGFP	This study
E. coli S17-1 λpir pSRKKm-mCherry	Donor strain carrying pSRKKm-mCherry	This study
A1	Isolate from microwell 1 within which *A.tumefaciens* sp. 15955 exhibited inhibited growth	This study
A2	Isolate from microwell 1	This study
A3	Isolate from microwell 1	This study
B1	Isolate from microwell 2 within which *A.tumefaciens* sp. 15955 exhibited inhibited growth	This study
B2	Isolate from microwell 2	This study
B3	Isolate from microwell 2	This study
C1	Isolate from microwell 3 within which *A.tumefaciens* sp. 15955 exhibited inhibited growth	This study
C2	Isolate from microwell 3	This study

C3	Isolate from microwell 3	This study
Plasmids		
pSRKKm	Broad-host-range P_{lac} expression vector; KmR	[157]
pSRKKm-sfGFP	IPTG-inducible GFP expression vector derived from pSRKKm; KmR	[268]

Table S2: Wilcoxon two-sample tests for differences in carrying capacities between A.tumefaciens sp. 15955 culture in conditioned versus unconditioned media from individual antagonistic isolates or from the 9-membered consortia.

Isolate ID	**p-value for Wilcoxon two-sample test**	**Significance of difference**
A1	<0.01	Significant
A2	<0.01	Significant
A3	<0.01	Significant
B1	<0.01	Significant
B2	0.0139	Significant
B3	0.0134	Significant
C1	<0.01	Significant
C2	0.0109	Significant
C3	<0.01	Significant
9-member consortia	<0.01	Significant

Table S3: Wilcoxon two-sample tests for differences in growth rates between *A.tumefaciens* sp. 15955 culture in conditioned versus unconditioned media from individual antagonistic isolates or from the 4-membered consortia.

Isolate ID	p-value for Wilcoxon two-sample test	Significance of difference
A1	<0.01	Significant
A2	<0.01	Significant
A3	<0.01	Significant
B1	<0.01	Significant
B2		Significant
B3		Significant
C1	<0.01	Significant
C2		Significant
C3	<0.01	Significant
9-member consortia	<0.01	Significant